SYNTHESIS, CHARACTERIZATION AND PROPERTIES OF SOME XENONIUM(II) SALTS CONTAINING Xe-O AND Xe-N BONDS

By

Joseph Marc Whalen

A Thesis

Submitted to the School of Graduate Studies

in Partial Fulfillment of the Requirements

for the Degree

Doctor of Philosophy

McMaster University

December 1994

SYNTHESIS, CHARACTERIZATION AND PROPERTIES OF SOME XENONIUM(II) SALTS CONTAINING Xe-O AND Xe-N BONDS

DOCTOR OF PHILOSOPHY (1994) McMASTER UNIVERSITY

(Chemistry) Hamilton, Ontario

TITLE: Synthesis, Characterization and Properties of Some Xenonium(II) Salts Containing Xe-O and Xe-N Bonds

AUTHOR: Joseph Marc Whalen, B.Sc. (Dalhousie University)

SUPERVISOR: Professor G.J. Schrobilgen

NUMBER OF PAGES: xxiv, 364

ABSTRACT

This Thesis describes the syntheses and spectroscopic characterization of noble-gas compounds containing xenon(II)-nitrogen and xenon(II)-oxygen bonds in solution by multinuclear magnetic resonance (multi-NMR) and in the solid state by low-temperature Raman spectroscopy.

The key synthetic approach for the preparation of novel xenon(II) compounds containing xenon-nitrogen and xenon-oxygen bonds involved the HF elimination reactions of XeF_2 with the AsF_6^- salts of several protonated oxygen and nitrogen bases in HF and BrF_5 solvents at low temperatures. In particular, $CF_3C(OH)NH_2^+AsF_6^-$, $F_5TeNH_3^+AsF_6^-$, and $FO_2SNH_3^+AsF_6^-$ reacted with XeF_2 by HF elimination to give $CF_3C(OXeF)NH_2^+AsF_6^-$, $F_5TeN(H)\text{-}Xe^+AsF_6^-$ and $FO_2SN(H)\text{-}Xe^+AsF_6^-$. The latter two salts are examples of a rare class of compounds in which xenon(II) is directly bonded to formally sp^3-hybridized nitrogen atoms. Their characterization in solution by multi-NMR was facilitated by preparing the xenon compounds with ^{15}N-enriched (99.5 atom %) starting materials, i.e., $F_5TeNH_3^+AsF_6^-$ and $FO_2SNH_3^+AsF_6^-$. This allowed for the observation of the one-bond $^{129}Xe\text{-}^{15}N$ scalar couplings in the ^{129}Xe and ^{15}N NMR spectra.

The salts, $CF_3C(OH)NH_2^+AsF_6^-$, $F_5TeNH_3^+AsF_6^-$, and $FO_2SNH_3^+AsF_6^-$, were prepared for the first time, and were characterized in the solid state by Raman spectroscopy, and in solution by ^{13}C, ^{19}F, ^{1}H and ^{125}Te NMR spectroscopy. The assignments of the Raman spectra of $F_5TeNH_3^+AsF_6^-$ and $FO_2SNH_3^+AsF_6^-$ were facilitated by recording the spectra of the natural abundance and 99.5 atom % ^{15}N-enriched salts, resulting in $^{14/15}N$ isotopic shifts for bands that involved vibrational motions of the nitrogen centers.

The compounds, $F_5TeN(H)\text{-}Xe^+AsF_6^-$ and $CF_3C(OXeF)NH_2^+AsF_6^-$, were isolated in the solid state and characterized by low-temperature Raman spectroscopy. Assignment of the Raman

bands associated with the vibrational motions of the nitrogen atom in $F_5TeN(H)\text{-}Xe^+AsF_6^-$ were facilitated by recording the Raman spectrum of the ^{15}N-enriched compound and observing the $^{14/15}N$ isotopic shifts. The compound, $FO_2SN(H)\text{-}Xe^+AsF_6^-$, was too unstable to be isolated from solution and therefore was not characterized by Raman spectroscopy.

The compounds, $CF_3C(OXeF)NH_2^+AsF_6^-$, $F_5TeN(H)\text{-}Xe^+AsF_6^-$ and $FO_2SN(H)\text{-}Xe^+AsF_6^-$, were characterized in solution by use of ^{129}Xe, ^{125}Te, ^{15}N, ^{19}F, ^{1}H and ^{13}C NMR spectroscopy. The assignment of the ^{1}H NMR resonances for $CF_3C(OH)NH_2^+$ and $CF_3C(OXeF)NH_2^+$ were facilitated by performing two dimensional heteronuclear (^{1}H-^{19}F) NOESY experiments, providing the first use of this technique in noble-gas chemistry.

The decomposition of $F_5TeN(H)\text{-}Xe^+AsF_6^-$ in HF and BrF_5 solvents has been studied in detail, primarily by ^{19}F NMR spectroscopy. The primary decomposition product, F_5TeNF_2, results from nucleophilic fluorination of $F_5TeN(H)\text{-}Xe^+$, and has been characterized for the first time by use of ^{15}N and ^{19}F NMR spectroscopy. The compound, F_5TeNF_2, was shown to react with $F_5TeNH_3^+AsF_6^-$ in AsF_5-acidified HF to give $FN{\equiv}N^+AsF_6^-$ and TeF_6 by ^{19}F NMR spectroscopy.

LIST OF ABBREVIATIONS AND SYMBOLS

eV	electron volt
FEP	perfluoroethylene / perfluoropropylene copolymer
INEPT	insensitive nuclei enhanced by polarization transfer
IP	ionization potential
Kel-F	chlorotrifluoroethylene polymer
LCAO	linear combination of atomic orbitals
NOESY	nuclear Overhauser effect spectroscopy
NMR	nuclear magnetic resonance
PFA	perfluoroalkoxy polymers
ppm	parts per million
SA	shielding anisotropy
Teflon (PTFE)	tetrafluoroethylene polymer
γ	rocking motion (vibrational spectroscopy)
δ	in-plane bend (vibrational spectroscopy)
δ	chemical shift in ppm from a reference compound (NMR spectroscopy)
π	out-of-plane bend (vibrational spectroscopy)
ρ_r	rocking motion (vibrational spectroscopy)
τ	torsional motion (vibrational spectroscopy)
ν	stretching motion (vibrational spectroscopy)
ϖ	wagging motion (vibrational spectroscopy)

ACKNOWLEDGEMENTS

I wish to thank Dr. G.J. Schrobilgen for his guidance and invaluable lessons in perseverence, scientific writing, the importance of paying attention to experimental details, and the value of hard work.

The interest and help offerred by Dr. J.S. Hartman and Dr. C.J.L. Lock, who both served on my Ph.D. supervisory committee, is gratefully acknowledged.

I gratefully acknowledge Dr. D.W. Hughes and Mr. B. Sawyer for their assistance with the operation of the NMR spectrometers.

I am also grateful tc the many people who have offerred their friendship and emotional support during my stay at McMaster. In particular, I wish to thank Dr. Bill Casteel, Linda Simpson and my sister, Karen Whalen, for their special friendship.

An extra special thanks is due to my parents, Joe and Ethel Whalen, who gave of themselves without reservation so that I could grow and develop. Their love is the foundation upon which my life has been built.

To realize that our knowledge is ignorance,

This is a noble insight.

To regard our ignorance as knowledge,

This is mental sickness.

Only when we are sick of our sickness

Shall we cease to be sick.

The Sage is not sick, being sick of sickness;

This is the secret of health.

——— Tao Teh Ching

TABLE OF CONTENTS

LIST OF TABLES

LIST OF FIGURES

CHAPTER 1

INTRODUCTION

GENERAL BACKGROUND

The potential for the Group VIII (18) elements of the Periodic Table to form compounds with other elements had been debated since the discovery of argon in 1894 by Ramsay and Rayleigh.[1] Early attempts to isolate compounds of Group VIII elements, also known as the noble gases and "inert" gases, were unsuccessful. In particular, shortly after the discovery of argon, Moissan[2] attempted to form a noble-gas compound by reaction of argon and elemental fluorine without success. Berthelot[3] claimed to have formed a compound of helium with carbon disulfide and benzene by combining these materials in an electric discharge. However, R.J. Strutt[4] was unable to repeat this result. Researchers such as Oddo[5] and von Antropoff[6] were proponents of noble-gas reactivity, and argued on the basis of periodic trends in valence and ionization potentials, that krypton and xenon should form compounds with the most electronegative element, fluorine. Kossel[7] also predicted the existence of a xenon and a krypton fluoride. Pauling[8] noted that main-group oxoacids could be seen as consisting of a central atom surrounded by as many oxygens as could fit around it. From the consideration of ionic radii, he reliably predicted coordination numbers of the central atom of a series of main-group oxoacids, including that of antimonic acid, $HSb(OH)_6$, with which the paper dealt obstensibly. On the basis of this simple argument, Pauling predicted coordination numbers of four and six for krypton and xenon, respectively, proposed the formula H_4XeO_6 for xenic acid, and predicted that salts of the form

Ag_4XeO_6 and AgH_3XeO_6 might be isolable. With the encouragement of Pauling, Yost and Kaye[1] attempted in 1932 and 1933 to react xenon and fluorine in an electric discharge, but no xenon fluorides were isolated.[9] By the mid-1930's, the electronic theory of valence, particularly as first proposed by Lewis[10] and Kossel,[7] was recognized for rationalizing much of the chemical behavior of the elements. A key principle of this theory was that the noble-gas valence-electron configuration was the configuration to which most elements tended in their chemical bonding. Since the theory proposed by Lewis and Kossel rationalized most of the known chemical behavior of the elements, examples of chemical species which violated the noble-gas configuration by having more than an octet of valence electrons, so-called hypervalent species, such as $Te(OH)_6$ and $IO(OH)_6$, were considered as exceptions to the theory. This theory predicted unreactivity of the noble-gases resulting from the stability of the noble-gas valence-electron configuration. This concept was reinforced by the repeated failures to combine the noble-gases chemically with other elements, particularly those of Yost and Kaye;[1,9] no further attempts to form compounds with the noble-gases were made until the 1960's.

In 1962, Bartlett[11,12] successfully oxidized xenon gas with PtF_6, resulting in a salt, then formulated as "$Xe^+PtF_6^-$", demonstrating for the first time that it was possible to form noble-gas compounds. Shortly after the isolation of "$Xe^+PtF_6^-$", the first covalent derivatives of xenon were isolated and characterized, namely XeF_2,[13] XeF_4[14] and XeF_6,[15] from the reactions of xenon and elemental fluorine. There are several synthetic routes to oxides and oxofluorides of xenon. Examples are XeO_3[16] (Xe (VI)), $XeOF_4$[17] and XeO_2F_2[18] (Xe(VI)), and $XeOF_2$[19] (Xe(IV)). No xenon(II) oxides have been isolated and characterized. Several excellent reviews detailing the developments in the chemistry of the noble gases up to 1992 are available.[20-26]

The bulk of synthetic xenon chemistry to date involves xenon in the +2 oxidation state, and

the present Thesis is involved primarily with the chemistry of xenon(II) as well.

(A) REPLACEMENT OF F^- IN XeF_2 WITH ELECTRONEGATIVE POLYATOMIC ANIONS

The thermodynamic stability of the xenon fluorides with respect to the elements is derived from the high electron affinity (-333 ± 0.4 kJ mol^{-1})[27] and small size of the fluorine atom, as can be seen in a thermochemical cycle for XeF_2 in the gas phase.[28] The experimentally determined exothermicity of equation (1.1)[29] can be rationized by summing equations (1.2) through (1.6), where I(Xe) is the first ionization potential of xenon,[28] EP is the electron pair energy for

$$Xe(g) + 2\,F(g) \longrightarrow F\text{-}Xe\text{-}F\,(g) \qquad \Delta H = -272 \text{ kJ mol}^{-1} \qquad (1.1)$$

$$Xe(g) \longrightarrow Xe^+ \qquad I(Xe) = 1176 \text{ kJ mol}^{-1} \qquad (1.2)$$

$$Xe^+(g) + F(g) \longrightarrow Xe\text{-}F^+(g) \qquad EP = -201 \text{ kJ mol}^{-1} \qquad (1.3)$$

$$F(g) \longrightarrow F^-(g) \qquad E(F) = -335 \text{ kJ mol}^{-1} \qquad (1.4)$$

$$Xe\text{-}F^+(g) + F^- \longrightarrow F\text{-}Xe^+F^- \qquad \Delta H(\text{electrostatic}) \qquad (1.5)$$

$$F\text{-}Xe^+F^- \longleftrightarrow F\text{-}Xe\text{-}F^+ \qquad \text{resonance energy} \qquad (1.6)$$

XeF^+ [30] and E(F) is the electron affinity of fluorine. The reaction represented by equation (1.1)

is exothermic because the large ionization potential of xenon is countered by the large electron affinity of fluorine and the sum of the EP, ΔH(electrostatic) and resonance energy terms, which all favor a chemically bound species. The sum of the last two terms is -912 kJ mol^{-1} since all other values are known. The small size of the fluorine atom contributes to a large value of ΔH(electrostatic), and the electronegativity of fluorine also ensures that $F\text{-}Xe^{+}F^{-}$ is stable with respect to F-Xe and F, and that $Xe\text{-}F^{+}$ is stable with respect to Xe and F^{+}.

The thermochemical data above indicate that ligands which are capable of replacing fluorine in XeF_2 must be highly electronegative. It should be noted that ΔH (electrostatic) will be less favorable for any atom or ligand group which replaces fluorine, because of the increase in size and the 1/r dependence of the electrostatic energy. Electron pair bonds [cf., EP above] involving fluorine are among the most energetically favorable bonds known, and replacement of fluorine with another ligand group is expected to lower the exothermicity of the electron pair energy (EP). These factors are well illustrated for $XeCl_2(g)$, which is an unstable species that has been observed only at low temperatures by Mössbauer[31,32] and matrix isolation infrared spectrocopy.[33,34] The lower expected EP value for $XeCl^{+}$ than XeF^{+} is reflected in the bond energies for ICl and IF (240 and 280 kJ mol^{-1}, respectively).[35,36] Further, the chlorine atom and chloride ion are much bigger than their fluorine counterparts,[36] so that ΔH(electrostatic) is less exothermic than in the fluoride case. Although the electron affinity of chlorine is 12 kJ mol^{-1} greater than for fluorine,[35] all other terms are less favorable for chlorine than fluorine. Bartlett[28] has shown that the chlorine analog of equation (1.1) is approximately 142 kJ mol^{-1} less favorable than for fluorine, in agreement with the instability of $XeCl_2$.

In the context of the above argument it is apparent that a polyatomic ligand, L, which is capable of replacing fluorine in XeF_2 to give isolable derivatives, FXeL and XeL_2, must be highly

electronegative. The conjugate bases of several strong oxygen and nitrogen acids are capable of replacing fluoride in XeF_2. Although the large electron affinities of these polyatomic groups favor stable species, their large sizes significantly reduce ΔH(electrostatic); for this reason, the ligand derivatives of XeF_2 are kinetically stable rather than thermodynamically stable. Decomposition, which is often explosive, occurs near room temperature in most cases.[20]

Several strong oxoacids are capable of replacing F^- in XeF_2 in HF elimination reactions represented by equations (1.7) and (1.8). In general, isolation of pure products requires low reaction temperatures and removal of the evolved HF under vacuum.

$$XeF_2 + HL \longrightarrow F\text{-}Xe\text{-}L + HF \tag{1.7}$$

$$XeF_2 + 2\,HL \longrightarrow L\text{-}Xe\text{-}L + 2\,HF \tag{1.8}$$

The fluorosulfate anion, FSO_3^-, is highly electronegative and is capable of stabilizing xenon(II). The mono- and bis-fluorosulfate derivatives of xenon(II) were synthesized[28,37,38] from the reaction of fluorosulfuric acid with XeF_2 as shown in equations (1.9) and (1.10).

$$XeF_2 + HSO_3F \xrightarrow{-75\,^\circ C} FXeOSO_2F + HF \tag{1.9}$$

$$XeF_2 + 2\,HSO_3F \xrightarrow{-75\,^\circ C} Xe(OSO_2F)_2 + HF \tag{1.10}$$

Other strong oxoacids which have yielded covalent derivatives of xenon(II) are HNO_3,[23] $HClO_4$,[28,37] HSO_3CF_3[28] and $HOC(O)CF_3$.[39-41] Xenon(II) derivatives containing the ligands, -

$OIOF_4$[42] and $-OPOF_2$[43] are not isolated from the reactions of XeF_2 with the parent acids. The mono- and bis- derivatives are formed according to equations (1.11) and (1.12).

$$XeF_2 + x\ P_2O_3F_4 \xrightarrow[-22\ ^\circ C]{CFCl_3} x\ P(O)F_3 + F_{2-x}Xe(OPOF_2)_x \qquad (1.11)$$

(x = 1 or 2)

$$XeF_2 + (IO_2F_3)_2 \xrightarrow[\text{or } CFCl_3]{SO_2ClF} F_{2-x}Xe(OIOF_4)_x + IOF_3 + x/2\ O_2 \qquad (1.12)$$

(x = 1 or 2)

Mono- and bis- xenon(II) derivatives of the ligands $-OSeF_5$[44,45] and $-OTeF_5$[41,46-51] have been studied extensively. The $-OTeF_5$ group is exceeded only by fluorine and oxygen in its ability to stabilize the various oxidation states of xenon. This is attributed to its high effective group electronegativity resulting from the inductive effect of five fluorines on tellurium,[52] and is demonstrated by the existence of moderately stable $-OTeF_5$ analogues of XeF_4,[51] $XeOF_4$[53] and XeF_6.[53] Salts of $Xe\text{-}OTeF_5^+$ with AsF_6^- [54,55] and $Sb_2F_{11}^-$ [54] anions are known; $XeOTeF_5^+AsF_6^-$ is prepared from the fluoride abstraction reaction of $FXeOTeF_5$ with AsF_5, and $XeOTeF_5^+Sb_2F_{11}^-$ is prepared by displacement of AsF_6^- upon dissolving $XeOTeF_5^+AsF_6^-$ in SbF_5,[54] followed by removal of SbF_5 and AsF_5 under vacuum. The salt, $XeOSeF_5^+AsF_6^-$,[26] has also been prepared by fluoride abstraction from $FXeOSeF_5$ using the strong Lewis fluoroacid, AsF_5. Owing to the high electronegativities of the F_5TeO- and F_5SeO- groups, which approach that of fluorine, the Lewis acidities of the $Xe\text{-}L^+$ cations (L = F_5TeO- and F_5SeO-) also approach that of XeF^+ [see Section (B)]. This has been demonstrated by the formation of adduct cations upon reaction of oxidatively

resistant nitrogen bases with $XeOMF_5^+AsF_6^-$ (M = Te, Se)[26] as shown in equation (1.13). All of the adducts are unstable at room temperature except *s*-$C_3F_3N_2N$-$XeOMF_5^+AsF_6^-$ (M = Se, Te).

$$XeOMF_5^+AsF_6^- + D \longrightarrow D\text{-}XeOMF_5^+AsF_6^- \qquad (1.13)$$

$$(D = s\text{-}C_3F_3N_2N,\ F_3S{\equiv}N,\ CH_3C{\equiv}N,\ C_5F_5N)$$

The number of nitrogen acids which undergo HF elimination reactions with XeF_2 is far less than the number of oxygen acids. The strong nitrogen acid, $HN(SO_2F)_2$, reacts with XeF_2 in a fashion which is analogous to that of the oxygen acids discussed above. The first Xe-N bonded species,[56] $FXeN(SO_2F)_2$, was synthesized and partially characterized in 1974 by LeBlond and DesMarteau. Complete characterization by use of X-ray crystallography by Sawyer *et al.*[57] followed. Since then the bis- compound $Xe[N(SO_2F)_2]_2$,[58,59] and the cations $XeN(SO_2F)_2^+$[60] and $F[XeN(SO_2F)_2]_2^+$[58,59,60] have been characterized. The utility of the $-N(SO_2F)_2$ ligand to form stable bonds to xenon arises from the highly electron withdrawing groups bonded to nitrogen, resulting in a ligand which is resistant to oxidative fluorination. The compounds $FXeN(SO_2F)_2$ and $Xe[N(SO_2F)_2]_2$ were synthesised according to equation (1.14). The ligand transfer reagent, $(CH_3)_3SiN(SO_2CF_3)_2$, prepared as in equation (1.15), was used to prepare $Xe[N(SO_2CF_3)_2]_2$ in a $(CH_3)_3SiF$ elimination reaction with XeF_2 [equation (1.16)].[61] The first reported xenon-nitrogen

$$x\ HN(SO_2F)_2 + XeF_2 \xrightarrow[0\ ^\circ C]{CF_2Cl_2} x\ HF + F_{(2-x)}Xe[N(SO_2F)_2]_x \qquad (1.14)$$

$$(x = 1 \text{ or } 2)$$

$$(CH_3)_3SiH + (CF_3SO_2)_2NH \xrightarrow{-196 \text{ to } 22\ ^\circ C} (CH_3)_3SiN(SO_2CF_3)_2 + H_2 \qquad (1.15)$$

$$2\ (CH_3)_3SiN(SO_2CF_3)_2 + XeF_2 \xrightarrow[CF_2Cl_2]{-22 \text{ to } 10\ ^\circ C} Xe[N(SO_2CF_3)_2]_2 + 2\ (CH_3)_3SiF \qquad (1.16)$$

adduct with a Lewis acid possessed the stoichiometry $FXeN(SO_2F)_2 \cdot AsF_5$ and was postulated to have the ionic formulation $XeN(SO_2F)_2^+AsF_6^-$ [see equation (1.17)], although it was not isolated.[58] Subjecting the salt to dynamic vacuum at room temperature resulted in the isolation

$$FXeN(SO_2F)_2 + AsF_5 \xrightarrow{-78\ ^\circ C} XeN(SO_2F)_2^+AsF_6^- \qquad (1.17)$$

of the AsF_6^- salt of the bridging cation, $F[XeN(SO_2F)_2]_2^+$,[60] according to equation (1.18). The species $XeN(SO_2F)_2^+AsF_6^-$ was later isolated, although it is thermally unstable at room temperature.[60] A crystal structure of $XeN(SO_2F)_2^+Sb_3F_{16}^-$ was obtained[60] using crystals grown after dissolving $F[XeN(SO_2F)_2]_2^+AsF_6^-$ in SbF_5 solvent [equation (1.19)].

$$2\ XeN(SO_2F)_2^+AsF_6^- \xrightarrow[\text{vacuum}]{23\ ^\circ C} F[XeN(SO_2F)_2]_2^+AsF_6^- + AsF_5 \qquad (1.18)$$

$$F[XeN(SO_2F)_2]_2^+AsF_6^- + 3\ SbF_5 \xrightarrow[0\ ^\circ C]{SbF_5} 2\ XeN(SO_2F)_2^+Sb_3F_{16}^- + AsF_5 \qquad (1.19)$$

(B) LEWIS ACIDITY AND OXIDATIVE FLUORINATING ABILITY OF THE XeF^+ CATION

The valence bond[62] and molecular orbital[63] descriptions of XeF_2 indicate semi-ionic Xe-F bonds, with considerable negative charge on the fluorine atoms; the charge distribution may be described as $F^{-1/2}Xe^{+1}F^{-1/2}$.[25] The valence-bond description of XeF_2 incorporates the notion of Xe-F bond polarity through the resonance contributions $F\text{-}Xe^+F^- \longleftrightarrow F^-Xe\text{-}F^+$. Owing to the Xe-F bond polarity, XeF_2 behaves as a fluoride ion donor towards many strong Lewis acids, yielding compounds of the form $XeF_2 \cdot xMF_5$ (x = 1/2, 1, or 2; MF_5 = Lewis acid).[21] The compounds cannot be given a purely ionic formulation (i.e., $XeF^+M_xF_{5x+1}^-$) since fluorine bridges between xenon and a fluorine of the "anion" indicate covalent character in the bonding. Single crystal X-ray diffraction studies of these adducts reveal that the bridging Xe···F bond lengths increase with decreasing lengths of the terminal Xe-F bonds and increasing fluoride ion acceptor ability of MF_5, indicating increased ionic character. For example, in $XeF_2 \cdot RuF_5$, the terminal Xe-F and bridging Xe···F bond lengths are 1.87(2) and 2.18(2) Å, respectively.[64] The corresponding bond lengths in $XeF_2 \cdot 2SbF_5$ are 1.84 and 2.35 Å.[65,66] The latter has the shortest terminal Xe-F bond length for an adduct of XeF_2, providing the closest approximation to a salt of XeF^+. This is a result of the very weak basicity of the $Sb_2F_{11}^-$ anion.

The Raman and infrared spectra of solid adducts of XeF_2 with Lewis acids complement the crystal data. They are best interpreted in terms of ionic formulations $XeF^+MF_6^-$ and $XeF^+M_2F_{11}^-$, but modes associated with the bridging Xe···F and M···F stretches and F-Xe···F bends confirm the presence of fluorine bridges.[21] In the case of $XeF^+MF_6^-$, the number of bands and selection rules for the infrared and Raman spectra indicate a symmetry lower than O_h, resulting in part from the fluorine bridge interaction with XeF^+.[21,67-69]

Fluorine bridging of the XeF^+ cation, to a fluorine of a weakly basic fluoroanion indicates that XeF^+ has substantial Lewis acid character. Schrobilgen *et al.*[26] have exploited the Lewis acid character of XeF^+ by reacting $XeF^+AsF_6^-$ with various oxidatively resistant nitrogen bases (D), resulting in Xe-N bonds [see equation (1.20)]. Because of the strong oxidizing power of XeF^+

$$D + XeF^+AsF_6^- \longrightarrow D\text{-}XeF^+AsF_6^- \qquad (1.20)$$

(estimated electron affinity 10.9 eV),[26] only oxidatively resistant bases form stable adduct cations with XeF^+. Nitrogen bases whose first adiabatic ionization potentials are greater than or equal to the electron affinity of XeF^+ are often resistant to oxidation by XeF^+, allowing the isolation of $D\text{-}XeF^+AsF_6^-$ at low temperatures. The first example of a nitrogen base to form an adduct with XeF^+ was HC≡N, whose first adiabatic ionization potential has been determined to be 13.80 eV from photoionization studies.[70] In addition, a series of nitriles RC≡N form the adducts $RC{\equiv}N\text{-}XeF^+AsF_6^-$, which have been characterized in solution (R = H, CH_3, CH_2F, C_2H_5, C_2F_5, C_3F_7 and C_6F_5)[71-73] and in the solid state (R = H, Me).[71-73] A detailed study which expands the ligand series has been carried out.[74] The general synthesis for these adducts involves the reaction of $XeF^+AsF_6^-$ or $Xe_2F_3^+AsF_6^-$ with the appropriate nitrile as shown in equations (1.21) and (1.22), resulting in the first examples of xenon bonded to an *sp*-hybridized nitrogen atom.

$$XeF^+AsF_6^- + RC{\equiv}N: \xrightarrow[\text{-20 to -10 °C}]{HF} RC{\equiv}N\text{-}XeF^+AsF_6^- \qquad (1.21)$$

$$Xe_2F_3^+AsF_6^- + RC{\equiv}N: \xrightarrow[\text{-20 to -10 °C}]{HF} RC{\equiv}N\text{-}XeF^+AsF_6^- + XeF_2 \qquad (1.22)$$

The fluoro(perfluoropyridine)xenon(II) cations, $4\text{-}RC_5F_4N\text{-}XeF^+$ (R = F or CF_3)[75] have been formed in HF solvent according to equation (1.23) and equilibria (1.24) and (1.25) at -30 to -20 °C. An alternative synthesis involves the reaction of $4\text{-}RC_5F_4NH^+AsF_6^-$ with XeF_2 in BrF_5 and HF solvents at -30 °C as in equation (1.25). As expected, the equilibrium favors a larger

$$4\text{-}RC_5F_4N \xrightarrow{HF} 4\text{-}RC_5F_4NH^+(HF)_n^- \tag{1.23}$$

$$4\text{-}RC_5F_4NH^+(HF)_n^- + XeF^+AsF_6^- \rightleftharpoons RC_5F_4NH^+AsF_6^- + XeF_2 + n\,HF \tag{1.24}$$

$$4\text{-}RC_5F_4NH^+AsF_6^- + XeF_2 \rightleftharpoons 4\text{-}RC_5F_4N\text{-}XeF^+AsF_6^- + HF \tag{1.25}$$

proportion of the xenon(II) cation in BrF_5 solvent, enabling the salts to be isolated by removal of the BrF_5 solvent under vacuum at -30 °C. The first adiabatic ionization potential of C_5F_5N (10.08 ± 0.05 eV)[76] is approximately the same as that of the electron affinity of XeF^+, in accordance with the criterion for a stable adduct. The first ionization potential (11.50 eV)[76] of *s*-trifluorotriazine, *s*-$C_3F_3N_3$ and the existence of $C_5F_5N\text{-}XeF^+AsF_6^-$ suggested that the adduct *s*-$C_3F_3N_2N\text{-}XeF^+$ should also exist. This compound has been synthesized according to equation (1.26) by the reaction of $XeF^+AsF_6^-$ with excess *s*-trifluorotriazine at room temperature for three hours followed by removal of excess *s*-$C_3F_3N_3$ under vacuum.[75] The resulting salt is unique in that it is the only salt of the series which is stable indefinitely at room temperature.

$$XeF^+AsF_6^- + s\text{-}C_3F_3N_3 \longrightarrow s\text{-}C_3F_3N_2N\text{-}XeF^+AsF_6^- \tag{1.26}$$

The ligand, $F_3S{\equiv}N$ (first IP, 12.50 eV),[77] was also allowed to react with $XeF^+AsF_6^-$ in BrF_5 solvent at -60 °C giving the adduct $F_3S{\equiv}N\text{-}XeF^+$,[26] which has been characterized by ^{19}F and ^{129}Xe NMR spectroscopy at -60 °C [equation (1.27)]. Solvolysis of $F_3S{\equiv}N\text{-}XeF^+AsF_6^-$ occurs at -20 °C in HF solvent and results in addition of HF across the S-N triple bond, followed by HF elimination to give $F_4S{=}N\text{-}Xe^+$ [equation (1.28)]. The expected intermediate cation, $F_4S{=}N(H)\text{-}XeF^+$, that results from HF addition to $F_3S{\equiv}N\text{-}XeF^+$, is not observed. Addition of HF across the S-N double bond of $F_4S{=}N\text{-}Xe^+$ results in the $F_5SN(H)\text{-}Xe^+$ cation, which is the first example of an sp^3-hybridized nitrogen bonded to xenon [equation (1.29)].

$$F_3S{\equiv}N + XeF^+AsF_6^- \xrightarrow[-60\ ^\circ C]{BrF_5} F_3S{\equiv}N\text{-}XeF^+AsF_6^- \qquad (1.27)$$

$$F_3S{\equiv}N\text{-}XeF^+ + HF \longrightarrow [F_4S{=}N(H)\text{-}Xe\text{-}F^+] \xrightarrow{-\ HF} F_4S{=}N\text{-}Xe^+ \qquad (1.28)$$

$$F_4S{=}N\text{-}Xe^+ + HF \longrightarrow F_5S\text{-}N(H)\text{-}Xe^+ \qquad (1.29)$$

The only known examples of krypton-nitrogen bonds arise from the reaction of $HC{\equiv}NH^+AsF_6^-$ with KrF_2 in BrF_5 solvent at *ca.* -60 °C, resulting in $HC{\equiv}N\text{-}KrF^+AsF_6^-$,[78] and from the reaction of the adducts $R_FC{\equiv}N\text{-}AsF_5$ (R_F = CF_3, C_2F_5, $n\text{-}C_3F_7$) with KrF_2 in BrF_5 solvent at *ca.* -60 °C, resulting in $R_FC{\equiv}N\text{-}KrF^+AsF_6^-$.[71] The krypton cations are acid-base adducts, similar to the xenon(II) cations discussed above. The estimated electron affinity of KrF^+ (13.2 eV)[26] is greater than XeF^+ (see above), indicating that it is a stronger oxidizer. As expected, the nitrile adducts with KrF^+ are less thermally stable than the xenon(II) analogs.

The oxidative fluorinating power of XeF^+ is well established. Bartlett and Sladky[79] noted

that XeF_2 was incapable of oxidizing I_2 in acetonitrile solution, but addition of trace amounts of the Lewis acids SO_2, HF, or BF_3 resulted in the immediate oxidation of I_2 to IF_5, with formation of xenon gas. This suggested that XeF^+ was formed from the interaction of the Lewis acid with XeF_2 [equation (1.30)], and that the oxidizing ability of XeF^+ greatly surpassed that of XeF_2.

$$A + XeF_2 \rightleftharpoons AF^- + XeF^+ \qquad (1.30)$$

(A = Lewis acid)

Since the work of Bartlett and Sladky,[79] salts of XeF^+ have been used as chemical reagents to oxidatively fluorinate other species. The reaction of $XeF^+MF_6^-$ (M = As, Sb) with a variety of reagents in HF solvent at low temperatures (*ca.* -80 to -40 °C) has demonstrated the oxidative fluorinating ability of the XeF^+ cation, as well as its significant Lewis acid strength. The reaction of $XeF^+MF_6^-$ with sulfur(II) species such as the disulfides $CF_3S\text{-}SCF_3$,[80] $CF_3S\text{-}SCH_3$[80] and $CH_3S\text{-}SCH_3$,[80] resulted in MF_6^- salts of the thermally unstable fluorosulfonium cations according to equation (1.31). The sulfanes $(C_6F_5)_2S$,[81] CF_3SCH_3,[82] $(CH_3)_2S$,[82,83] CF_3SH[84] and CH_3SH[84] are likewise oxidatively fluorinated by $XeF^+MF_6^-$, resulting in thermally unstable MF_6^- salts of fluorosulfonium cations [equation (1.32)]. It is interesting that the reaction of the sulfuranes [sulfur(IV)] $(CF_3)_nSF_{4-n}$[85] (n = 0 - 2) with $XeF^+MF_6^-$ in HF solvent resulted in fluoride abstraction rather than oxidative fluorination, indicating the strong Lewis acid strength of the XeF^+ cation [equation (1.33)].[85] The fluoride transfer was attributed to the weak axial S-F bonds in the

$$R\text{-}S\text{-}S\text{-}R' \;\; XeF^+MF_6^- \longrightarrow RS\text{-}S(F)R'^{+}MF_6^- + Xe \qquad (1.31)$$

$$R\text{-}S\text{-}R' + XeF^+MF_6^- \longrightarrow R\text{-}S(F)R'^+MF_6^- + Xe \qquad (1.32)$$

$$(CF_3)_nSF_{4-n} + XeF^+MF_6^- \longrightarrow (CF_3)_nSF_{3-n}^+MF_6^- + XeF_2 \qquad (1.33)$$

sulfuranes[85] and their resulting fluoride ion donor ability. The XeF_2 produced is a substantially weaker oxidative fluorinator than XeF^+ and is incapable of oxidatively fluorinating the compounds $(CF_3)_nSF_{4-n}$ (n = 0 - 2). In the case of $CF_3S(O)F$, a labile fluoride is not present, and reaction with $XeF^+MF_6^-$ results in oxidative fluorination to give $CF_3S(O)F_2^+MF_6^-$.[85] It was postulated that the xenon-oxygen bonded species, $CF_3S(OXeF)F^+MF_6^-$, is an intermediate which decomposes by transfer of "F^+" to sulfur with elimination of xenon gas. A similar adduct cation, $Cl_2S\text{-}XeF^+$, has been proposed as an intermediate in the oxidative fluorination reaction of SCl_2 by $XeF^+MF_6^-$ [86] at low temperature [equation (1.34)]. Evidence for such an intermediate has been provided by the

$$Cl_2S + XeF^+ \longrightarrow [Cl_2S\text{-}XeF^+] \longrightarrow Cl_2S\text{-}F^+ + Xe \qquad (1.34)$$

low-temperature isolation of $(CF_3)_2SO\text{-}XeF^+SbF_6^-$ from HF solvent, which indeed contains a xenon-oxygen bond.[85] Oxidative fluorination of H_2O[87] and H_2S[88] by $XeF^+MF_6^-$ in HF at low temperatures (*ca.* -78 °C) results in the salts $H_2OF^+MF_6^-$ and $H_2SF^+MF_6^-$, respectively. The oxidative fluorination of H_2O at low temperature, in spite of its high ionization potential (12.6 eV),[89] demonstrates the powerful oxidative fluorinating ability of $XeF^+MF_6^-$. Oxidative fluorination of $AsCl_3$ with $XeF^+AsF_6^-$ in HF solvent at -78 °C also resulted in the isolation of $AsCl_3F^+AsF_6^-$.[90]

As discussed above, there is a growing number of examples of the use of XeF^+ as an

oxidative fluorinating agent, and there is now a large number of salts of adduct cations, D-XeF^+, where D is a nitrogen base.[26] Although Minkwitz[86] has postulated an adduct cation Cl_2S-XeF^+ as an intermediate in the oxidative fluorination of SCl_2 by $XeF^+MF_6^-$, there are no reported examples of an isolated and definitively characterized salt of an adduct cation, D-XeF^+, which decomposes by oxidative fluorination of the base [equation (1.35)]. Further work is required to establish the existence of D-XeF^+ cations as intermediates in the oxidative fluorination of bases.

$$\text{D-XeF}^+\text{MF}_6^- \longrightarrow \text{D-F}^+\text{MF}_6^- + \text{Xe} \qquad (1.35)$$

$$(\text{M} = \text{As, Sb})$$

(C) SPECIES CONTAINING XENON-CARBON BONDS

The first reported example of a xenon-carbon bonded species was $Xe(CF_3)_2$, which was prepared from the reaction of XeF_2 with plasma generated CF_3 radicals.[91] The resulting waxy solid, assumed to be $Xe(CF_3)_2$, decomposes with a half-life of *ca.* 30 minutes at room temperature according to equation (1.36). Characterization of the material claimed to be $Xe(CF_3)_2$ is incomplete and the synthesis has not been confirmed.

$$\text{Xe(CF}_3)_2 \longrightarrow \text{XeF}_2 + \text{C}_n\text{F}_m \qquad (1.36)$$

The stability of cations containing xenon-carbon bonds was established by determination of the xenon-carbon bond energy of CH_3-Xe^+ in the gas phase by ion cyclotron resonance. The Xe-C bond energy was determined to be 180 ± 33 kJ mol^{-1} [92] and more recently, 231 ± 10 kJ mol^{-1}.[93] These values are similar to those observed for the Xe-F bonds of XeF_2 (132 kJ mol^{-1})[94]

and XeF^+ (201 kJ mol^{-1}),[94] indicating that isolation of salts containing cations with xenon-carbon bonds is feasible.

A number of structurally well-characterized compounds containing Xe-C bonds are, in fact, now known. In all cases they occur as colorless salts of xenonium cations, R-Xe^+ (R = fluorophenyl or alkynyl group). The formation of the pentafluorophenylxenon(II) cation, $C_6F_5Xe^+$, in CH_2Cl_2 (-30 °C) and $CH_3C{\equiv}N$ (0 °C) solutions, with the anions $B(C_6F_5)_3F^-$, $B(C_6F_5)_2F_2^-$ and $B(C_6F_5)F_3^-$ has been established.[95-100] The salts are typically formed by the reaction of XeF_2 with the ligand transfer reagent, $B(C_6F_5)_3$, in methylene chloride solvent [equation (1.37)]. The X-ray crystal structure of $[CH_3C{\equiv}N\text{-}XeC_6F_5]^+$ $[(C_6F_5)_2BF_2]^-$, isolated from acetonitrile solution, shows that the xenon atom of C_6F_5-Xe^+ is weakly coordinated to the nitrogen atom of a $CH_3C{\equiv}N$

$$XeF_2 + B(C_6F_5)_3 \longrightarrow Xe\text{-}C_6F_5{}^+B(C_6F_5)_2F_2^- \qquad (1.37)$$

molecule (Xe-N, 2.681(8) Å; Xe-C, 2.092(8) Å).[100] The salt decomposes slowly at 14 °C. Reaction of $[CH_3C{\equiv}N\text{-}Xe\text{-}C_6F_5]^+[(C_6F_5)_2BF_2]^-$ with AsF_5 in $CH_3C{\equiv}N$ solution results in $[CH_3C{\equiv}N\text{-}Xe\text{-}C_6F_5]^+AsF_6^-$. Solutions of this compound in $CH_3C{\equiv}N$ are stable for up to one day at room temperature.[97] The reactions of XeF_2 with the boron ligand transfer reagents $B(m\text{-}CF_3C_6H_4)_3$ and $B(p\text{-}FC_6H_4)_3$ in CH_2Cl_2 solution at -45 to -50 °C result in the formation of the white solids $[m\text{-}CF_3C_6H_4Xe]^+[m\text{-}CF_3C_6H_4BF_3]^-$,[96] and $[p\text{-}FC_6H_4Xe]^+[(p\text{-}FC_6H_4)_2BF_2]^-$.[96] The former compound is stable for up to one hour in $CH_3C{\equiv}N$ at -41 °C, whereas the latter compound decomposes below -40 °C when attempting to dissolve it in the coordinating solvent, $CH_3C{\equiv}N$. The most stable xenonium salt presently known is $[Xe(2,4,6\text{-}F_3C_6H_2)]^+[BF_4]^-$,[98] which is prepared by the reaction of $B(C_6H_2F_3)_3 \cdot thf$ and XeF_2 in the presence of $BF_3 \cdot O(CH_3)_2$ in CH_2Cl_2 solution

at -40 °C. It is stable for up to 21 days at room temperature in dry air and hydrolyzes slowly over 7 days in aqueous $CH_3C{\equiv}N$ solution. Examples of alkynyl xenonium tetrafluoroborates are known and are prepared by reaction of lithium acetylides or triphenylsilyl acetylenes with XeF_2 and $BF_3{\cdot}O(CH_3)_2$ at low temperatures (-78 to -40 °C) in CH_2Cl_2 solvent.[101] The known alkynyl derivatives are $(CH_3)_3C{-}C{\equiv}C{-}Xe^+BF_4^-$, $(CH_3)_3Si{-}C{\equiv}C{-}Xe^+BF_4^-$, $CH_3CH_2{-}C{\equiv}C{-}Xe^+BF_4^-$ and $CH_3CH_2CH_2{-}C{\equiv}C{-}Xe^+BF_4^-$; all of these species decompose in solution or as solids below 0 °C,[101] but none have been characterized in the solid state.

It is interesting to note that, of all the known species containing xenon-carbon bonds, no neutral species of the form R-Xe-F have been characterized (R = fluorophenyl or alkynyl). This may be rationalized by considering the semi-ionic nature of the bonding in hypervalent compounds of the form R-Xe-F, which is best described in valence-bond terms by the resonance contributors $R^-\ Xe{-}F^+ \longleftrightarrow R{-}Xe^+\ F^-$;[102] the relative weightings of each contributor depends on the electronegativities of F and R. The carbon ligands used to form the cations $R{-}Xe^+$ are undoubtedly among the least electronegative ligands which have ever been used as ligands with xenon. For this reason, the resonance contribution, $R{-}Xe^+\ F^-$, essentially accounts for the bonding. Confirmation of the ionic character of the Xe-F bonds in solution is provided by the absence of observed one-bond ^{129}Xe-^{19}F scalar couplings attributable to Xe-F linkages in the ^{19}F and ^{129}Xe NMR spectra. As well, the ^{129}Xe NMR chemical shifts (*ca.* -3760 ppm for $C_6F_5{-}Xe^+$ in acetonitrile solution)[95,96] are the most shielded for chemically bound xenon.[95-100] This is consistent with an ionized Xe-F bond and an Xe-C bond of high covalent character, since the ^{129}Xe chemical shifts of xenon(II) compounds containing Xe-N, Xe-O and Xe-F bonds are known to decrease (i.e., become more shielded) with increasing ionic character of the Xe-F bond.[26,103,104]

(D) PURPOSE AND GENERAL SYNTHETIC STRATEGIES UNDERPINNING THE PRESENT WORK

The overall purpose of the present work is to extend the chemistry of the noble gases and, more specifically, to prepare and characterize compounds containing novel covalent bonds between xenon and nitrogen or oxygen. One route to Xe-N bonded species is through the interaction of $XeF^+AsF_6^-$ with selected nitrogen bases in solution. Given the oxidizing strength of XeF^+, nitrogen bases were selected on the basis of their resistance to oxidation.[26] It was found that nitrogen bases whose first adiabatic ionization potentials (IP_1), when known, were greater than or equal to the estimated electron affinity of XeF^+ (10.9 eV), were often resistant to oxidative attack by XeF^+ at low temperatures. This method of base selection preceded the successful preparation of AsF_6^- salts of the adduct cations $RC{\equiv}N\text{-}XeF^+$, (R = alkyl,[72,74] fluoroalkyl,[71,72,74] C_6F_5,[72,74] H[72-74]), $C_3F_3N_2N\text{-}XeF^+$,[71] and the pyridine adducts, $C_5F_5N\text{-}XeF^+$ [74,75] and $4\text{-}CF_3C_5F_4N\text{-}XeF^+$.[74,75] All of these cations involve ligands in which the nitrogen atoms bonded to xenon are formally *sp*- or sp^2-hybridized. Except for the partially characterized salt, $F_5SN(H)\text{-}Xe^+AsF_6^-$,[26] there are no known examples of formally sp^3-hybridized nitrogen bonded to xenon(II). In the present study, the AsF_6^- salts of several cations containing Xe-N and Xe-O bonds have been prepared and characterized; the atoms directly bonded to xenon in the novel cations are formally sp^3-hybridized, contributing significantly to the chemistry of xenon(II). The importance of ligand electronegativity in stabilizing compounds of xenon(II) was discussed in Section (A) of this Chapter. The synthesis of xenon compounds in which the ligand atom bonded to xenon is sp^3-hybridized is significant because the electronegativity of a ligand group decreases as the %s character of the valence hybrid orbitals decreases.[105] Thus the ligands studied in the present work, namely $CF_3C(O)NH_2$, F_5TeNH_2 and FO_2SNH_2, are among the least electronegative nitrogen- or

oxygen-donor ligands to ever form compounds with xenon(II). The low electronegativity of these ligands is reflected in the thermal instability of the resulting xenon(II) compounds, which are among the least stable xenon(II) derivatives known.

The ligands studied in the present work, namely, $CF_3C(O)NH_2$, F_5TeNH_2 and FO_2SNH_2, are isoelectronic with the strong oxoacids, $CF_3C(O)OH$, F_5TeOH and FO_2SOH, all of which form xenon(II) compounds [see Section (A)] which are stable at or near room temperature. Trifluoroacetamide, $CF_3C(O)NH_2$, was chosen as a potential base for adduct formation with XeF^+ on the basis of its first adiabatic ionization potential (10.77 eV),[106] which is similar to the estimated electron affinity for XeF^+ (10.9 eV),[26] so that it might be resistant to oxidative attack by the noble-gas cation. The IP_1-values of F_5TeNH_2 and FO_2SNH_2 are not known; their potential as ligands in novel xenon(II) compounds is based solely on the electronic similarity of these ligands to F_5TeOH and FO_2SOH. Although $CF_3C(O)NH_2$, F_5TeNH_2 and FO_2SNH_2 are not strong acids, it was possible to protonate these species, either *in situ* from the reaction with HF acidified with an equimolar amount of $XeF^+AsF_6^-$ [equations (1.38) and (1.39)], or from the reaction with excess AsF_5 in HF, to give the isolable salts, $CF_3C(OH)NH_2^+AsF_6^-$, $F_5TeNH_3^+AsF_6^-$ and $FO_2SNH_3^+AsF_6^-$ [equation (1.40)]. Ammonium cations generated *in situ* [equations (1.38) and (1.39)] or isolated as AsF_6^- salts [equation (1.40)], react with XeF_2 by HF elimination to give

$$XeF^+AsF_6^- + HF \rightleftharpoons XeF_2 + H_2F^+AsF_6^- \qquad (1.38)$$

$$H_2F^+AsF_6^- + D \rightleftharpoons DH^+AsF_6^- + HF \qquad (1.39)$$

$$(D = CF_3C(O)NH_2,\ F_5TeNH_2,\ FO_2SNH_2)$$

$$D \xrightarrow{HF\ /\ AsF_5} DH^+AsF_6^- \qquad (1.40)$$

$$(D = CF_3C(O)NH_2,\ F_5TeNH_2,\ FO_2SNH_2)$$

Xe-N and Xe-O bonded cations, and are analogous to the reactions of strong oxoacids with XeF_2 [equation (1.7)]. The oxygen ligands $CF_3C(O)O$-, F_5TeO- and FO_2SO- are more electronegative than the analogous nitrogen ligands $CF_3C(O)NH_2$, $F_5TeN(H)$- and $FO_2SN(H)$-, which have been used as ligands in compounds of xenon(II) in the present work. A comparison of the xenon(II)-oxygen derivatives with the novel xenon(II) compounds prepared in this Thesis provides the material for a systematic study of the effect of ligand electronegativity on the bonding and stability of compounds containing Xe(II)-O and Xe(II)-N bonds.

CHAPTER 2

EXPERIMENTAL SECTION

(A) VACUUM TECHNIQUES

(i) Vacuum Systems and Inert Atmosphere Systems

The compounds used in the course of this work are moisture sensitive or were used as precursors for moisture sensitive materials. It was therefore necessary to rigorously dry all precursors and apparatus. All manipulations were carried out under rigorously anhydrous conditions in glass or metal vacuum systems or in the oxygen and moisture free (< 0.1 ppm) inert nitrogen atmosphere of a Vacuum Atmospheres Model DLX drybox. The drybox was equipped with a cryogenic well which was cooled to -196 °C for the manipulation of thermally unstable materials under anhydrous conditions. Volatile reagents and solvents were manipulated by vacuum transfer using two vacuum lines. Volatile materials which were noncorrosive towards glass in the absence of water such as organic solvents [e.g., CH_2Cl_2, $CHCl_3$, $(CH_3CH_2)_2O$], F_5TeOH and $S_2O_5F_2$ were manipulated using a vacuum line constructed of Pyrex with grease-free 6-mm J. Young glass stopcocks equipped with FEP barrels (Figure 2.1). Volatile materials which attack glass, such as HF and BrF_5 solvents, were manipulated by vacuum transfer on a vacuum line constructed from nickel and 316 stainless steel valves and fittings (Autoclave Engineers, Inc.), Teflon, FEP, and Kel-F (Figure 2.2). Pressures were measured at ambient temperature using an

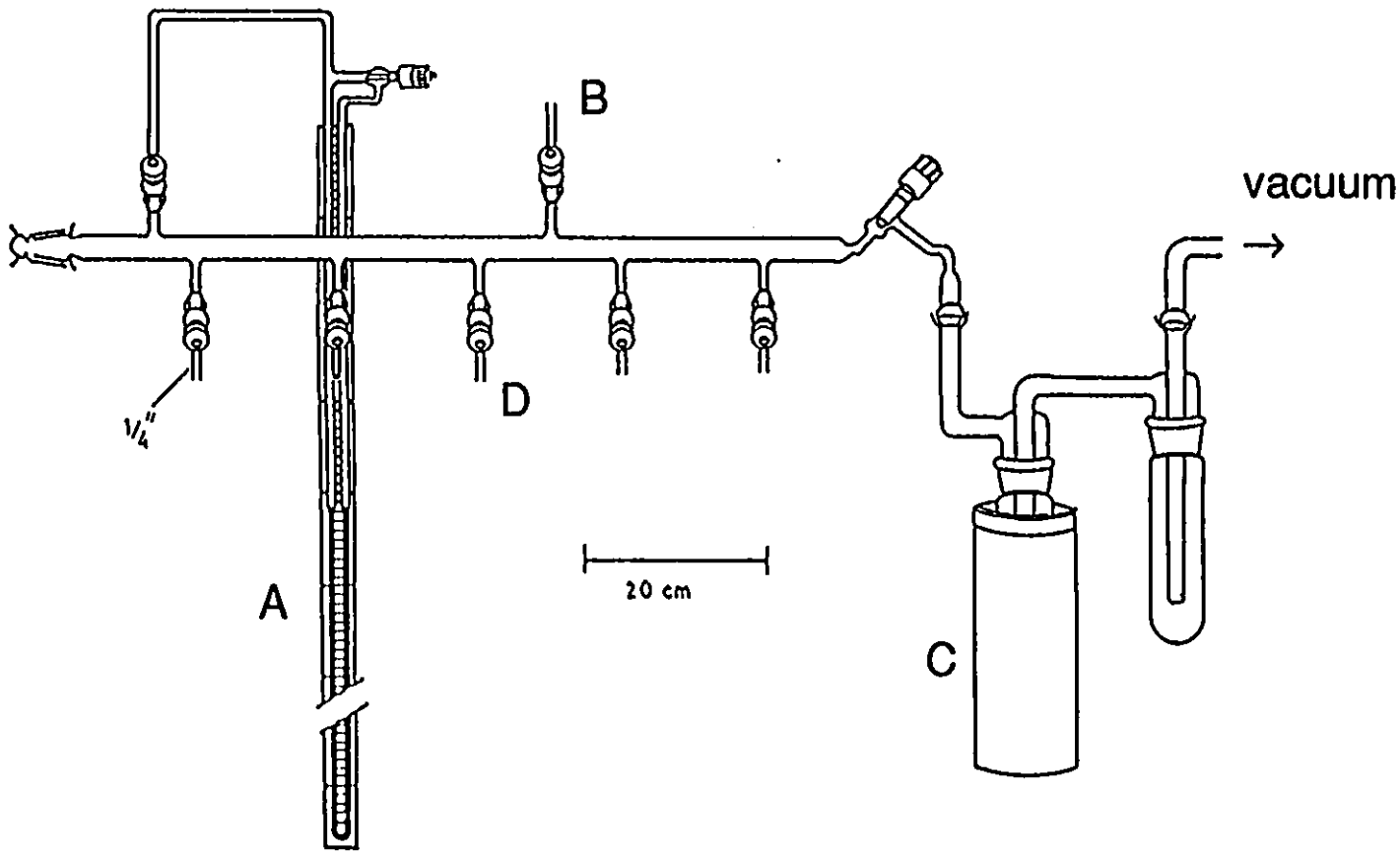

Figure 2.1 Glass vacuum line; (A) mercury manometer, (B) dry nitrogen inlet, (C) liquid nitrogen trap, (D) grease-free glass 6-mm J. Young stopcock with FEP barrel.

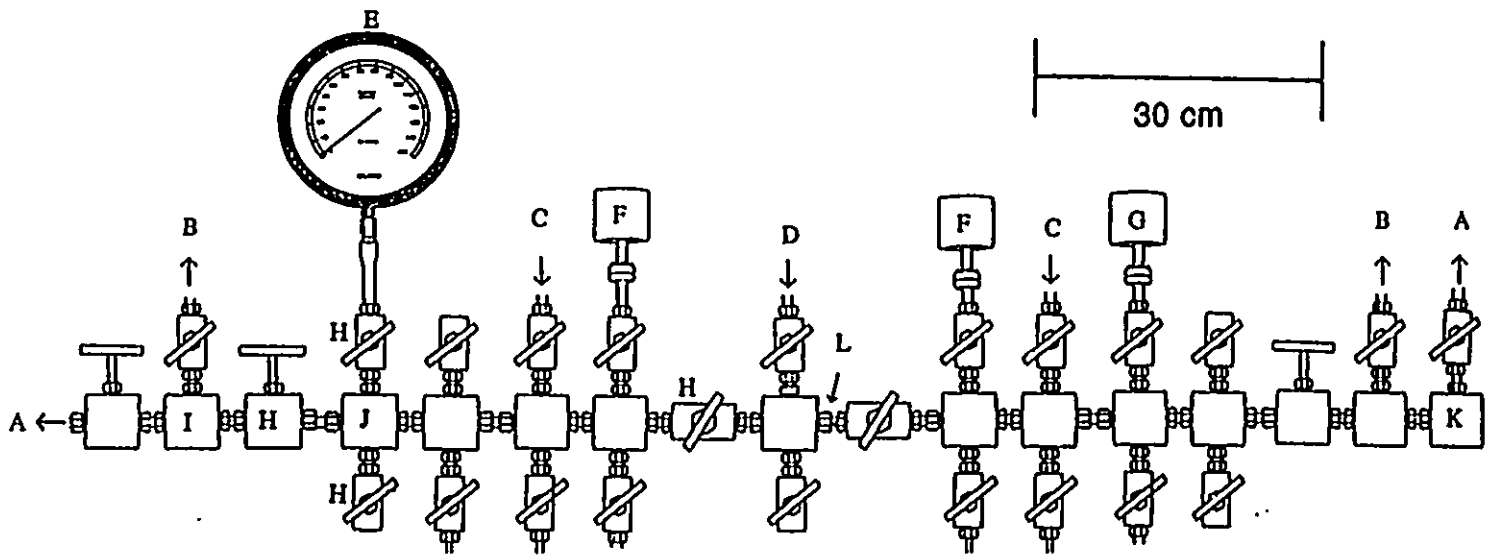

Figure 2.2 Metal vacuum line; (A) outlet to liquid nitrogen and charcoal traps followed by a two stage direct drive rotary vacuum pump (Edwards, E2M8) - hard vacuum, (B) outlet to soda lime and liquid nitrogen traps followed by a two stage direct drive rotary vacuum pump (Edwards, E2M8) - rough vacuum, (C) dry nitrogen inlet, (D) fluorine inlet, (E) 0 - 1500 Torr Bourdon gauge (F) MKS Model PDR-5B pressure transducers (0 - 1100 Torr), (G) MKS Model PDR-5B pressure transducer (0 - 1 Torr), (H) 3/8-in. 316 SS high pressure valve (Autoclave Engineers, 30VM6071), (I) 316 SS tee, (J) 316 SS cross, (K) 316 SS L, (L) nickel connectors

MKS Model PDR-5B power supply and digital readout in conjunction with pressure transducers having inert wetted surfaces constructed of Inconel. Two transducers of different dynamic pressure ranges were used, 0 to 1100 Torr and 0 to 1 Torr. The pressures were accurate to ± 0.5% of scale.

Vacuum on the glass line and metal line was attained by using Edwards two stage E2M8 direct drive high vacuum pumps. Two vacuum pumps were used on the metal vacuum line; one, a roughing pump, was used for the removal and disposal of volatile reactive fluorinated compounds by pumping through and entrapment on a bed of soda lime, which consisted of a copper tube (*ca.* 60 cm length, 15 cm dia.) packed with soda lime absorbent (Fisher Scientific, 4-8 mesh). The second vacuum pump provided the high vacuum source for the manifold (*ca.* 10^{-4} Torr). In the construction of the glass and metal vacuum lines, traps cooled to -196 °C were attached immediately before the vacuum pumps to prevent the passage of condensible volatile materials into the pumps.

(ii) Preparative Apparatus and Sample Vessels for Raman and NMR Spectroscopy

All synthetic procedures were performed in apparatus constructed from 304 and 316 stainless steel, glass, Kel-F or FEP. Stainless steel cylinders (Whitey) of 40 mL volume equipped with 316 stainless steel valves (Whitey ORM 2) were used in preparations requiring high pressures. Prior to use, these vessels were passivated by treatment with *ca.* 800 Torr of fluorine gas overnight, followed by vacuum removal of all volatiles at room temperature. Vessels constructed from glass were dried under vacuum on a glass vacuum line for at least 12 h prior to use. Sample preparations involving materials which attack glass were carried out in tubes fashioned from lengths of ¼-in. (7 mm), ½-in. (14 mm), and ¾" (21 mm) o.d. FEP tubing (Furon) which were heat sealed at one end and heat-flared (45° SAE) at the other. The tubes were then

attached to Kel-F valves encased in aluminum housings by flare fittings. All vessels constructed in this way were dried by first pumping on a glass vacuum line for at least 5 h followed by passivation on a metal vacuum line with *ca.* 800 Torr of fluorine gas overnight. All volatiles were then removed under vacuum, and the vessel pressurized with 760 Torr of dry N_2 gas.

Nuclear magnetic resonance (NMR) spectra were recorded on samples prepared in FEP tubes (9-mm and 4-mm o.d.). The 9-mm o.d. FEP NMR tubes were fabricated from lengths of 3/8-in. (9.5-mm) o.d. FEP tubing by reducing their diameter to 9-mm o.d. in a heated brass cylindrical form with mechanical pressure. One end of the tube was heat-sealed by pushing it into the end of a thin-walled 10-mm o.d. glass NMR tube previously heated in a Bunsen flame. The other end was heat flared (45° SAE) for direct attachment to a Kel-F valve. The 4-mm o.d. FEP tubing had one end heat sealed by pushing the tube into the end of a thin-walled 5-mm o.d. NMR tube and the other end was heat flared (45° SAE) for direct attachment to a Kel-F valve. The sample tubes used for recording the NMR spectra were heat sealed using a small diameter nichrome wire resistance furnace.

Raman spectra at room temperature were recorded on samples in Pyrex melting point capillaries. Before use, the melting pointing capillaries were heated under dynamic vacuum for 24 h at 200 °C and then stored in a dry nitrogen-filled drybox where they were loaded with the appropriate materials. The ends of the loaded melting point capillaries were filled with Kel-F grease before removal from the drybox. The capillaries were then immediately sealed using a miniature oxygen-natural gas torch. Raman spectra at low temperatures were recorded on samples in FEP or glass tubes. FEP tubes of 7-mm or 4-mm o.d. were heat-sealed at one end and heat flared at the other end (45° SAE) for direct attachment to Kel-F valves. The tubes were fluorinated as above prior to addition of solid materials. Glass tubes for low temperature Raman spectroscopy

were constructed from medium wall 3-mm o.d. glass tubes that were heat sealed at one end and glassblown onto *ca.* 5-cm lengths of ¼-in. o.d. glass tubing on the other end. The ¼-in. o.d. end of each glass tube was attached to a 4-mm J. Young glass stopcock with a Teflon barrel and dried overnight under high vacuum. The appropriate materials were loaded into each tube in a drybox, followed by heat sealing below the stopcock using an oxygen-natural gas torch.

Vessels were attached to vacuum lines using Teflon, FEP and/or Kel-F adaptors. All tubing was connected using ¼-in. Teflon unions (Swagelok) and Teflon compression fittings (back and front ferrules, Hoke Controls). The fluoroplastic valves and connectors have been described in greater detail elsewhere.[107]

(B) PREPARATION AND PURIFICATION OF STARTING MATERIALS

(i) HF, BrF_5 and SO_2ClF Solvents

Hydrogen fluoride and BrF_5 solvents were transferred on a metal vacuum line through all fluoroplastic connections. Anhydrous hydrogen fluoride (Harshaw Chemical Co.) was purified by treatment with 5 atm. of F_2 gas in a nickel can for a period of 1 month, converting residual water to HF and O_2 gas. The anhydrous HF was then vacuum distilled into a dry Kel-F storage vessel equipped with a Kel-F valve and stored at room temperature until used. Hydrogen fluoride was transferred into reaction vessels by vacuum distillation on a metal vacuum line through connections constructed of Teflon, Kel-F and FEP as shown in Figure 2.3.

Bromine pentafluoride (Ozark-Mahoning Co.) was purified as described earlier,[107] and stored over dry KF in a ¾-in. o.d. Kel-F storage tube equipped with a Kel-F valve. Bromine pentafluoride solvent was transferred into reaction vessels by vacuum distillation on a metal line

through connections constructed of Teflon, Kel-F and FEP as shown in Figure 2.4.

Sulfuryl chloride fluoride, SO_2ClF (Aldrich) was purified according to the literature method[108] and stored over KF in a glass vessel equipped with a 6-mm glass J. Young stopcock equipped with a glass barrel. Transfers of SO_2ClF were performed under vacuum using a vacuum line and tubing constructed of glass as shown in Figure 2.5. Fluorine-19 NMR indicated the presence of a trace of SO_2F_2 impurity [$\delta(^{19}F)$ = 32.4 ppm] in the solvent.

(ii) <u>$CHCl_3$, CH_2Cl_2, $(CH_3CH_2)_2O$, $CH_3C{\equiv}N$ and CF_2ClCF_2Cl Solvents</u>

Chloroform, $CHCl_3$ (Caledon Reagent Grade), CH_2Cl_2 (Caledon Reagent Grade) and CD_2Cl_2 (Isotech Inc.) were dried by combining the solvent with Davison Type 3A molecular sieves (Fisher Scientific) for 3 days followed by vacuum distillation into a dry glass bulb equipped with a 4-mm glass J. Young stopcock equipped with a Teflon barrel. The molecular sieves were dried under dynamic vacuum for 24 h at 120 °C prior to use as a drying agent.

Acetonitrile, $CH_3C{\equiv}N$ (Caledon HPLC Grade) was purified according to the literature procedure.[109]

Diethyl ether (Fisher Scientific) was refluxed over sodium wire with benzophenone indicator under a dry nitrogen atmosphere until the solution turned blue (*ca.* 2 h). Refluxing was continued for an additional 10 h, and the ether was then distilled under atmospheric pressure onto fresh sodium wire in a glass vessel equipped with a greaseless 6-mm glass J. Young stopcock equipped with a Teflon barrel. After several days, the ether was vacuum distilled into a similar vessel which had been previously dried under vacuum.

Freon-114, CF_2ClCF_2Cl (Aldrich), was purified according to the literature method[110] and was transferred under vacuum using all glass apparatus.

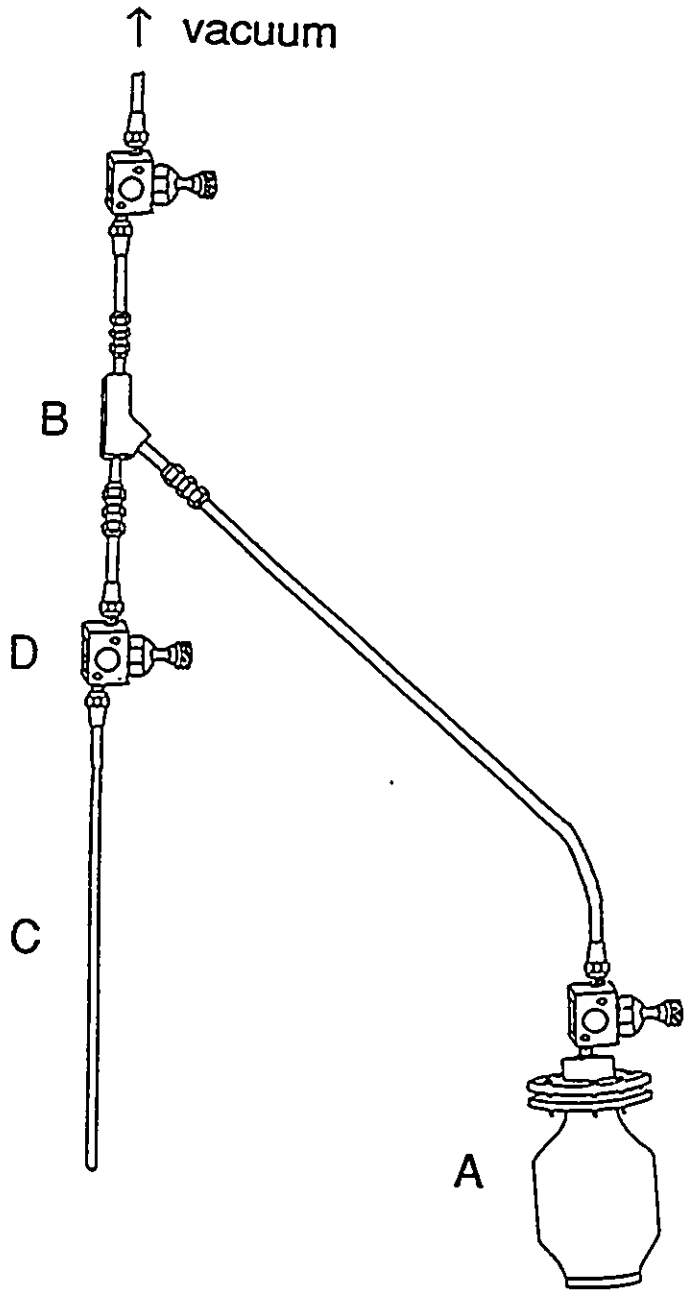

Figure 2.3 Apparatus for the storage and vacuum transfer of anhydrous HF solvent; (A) 250 mL Kel-F HF container equipped with a Kel-F valve, (B) Kel-F Y-connector, (C) FEP tube reactor, (D) Kel-F valve with aluminum casing.

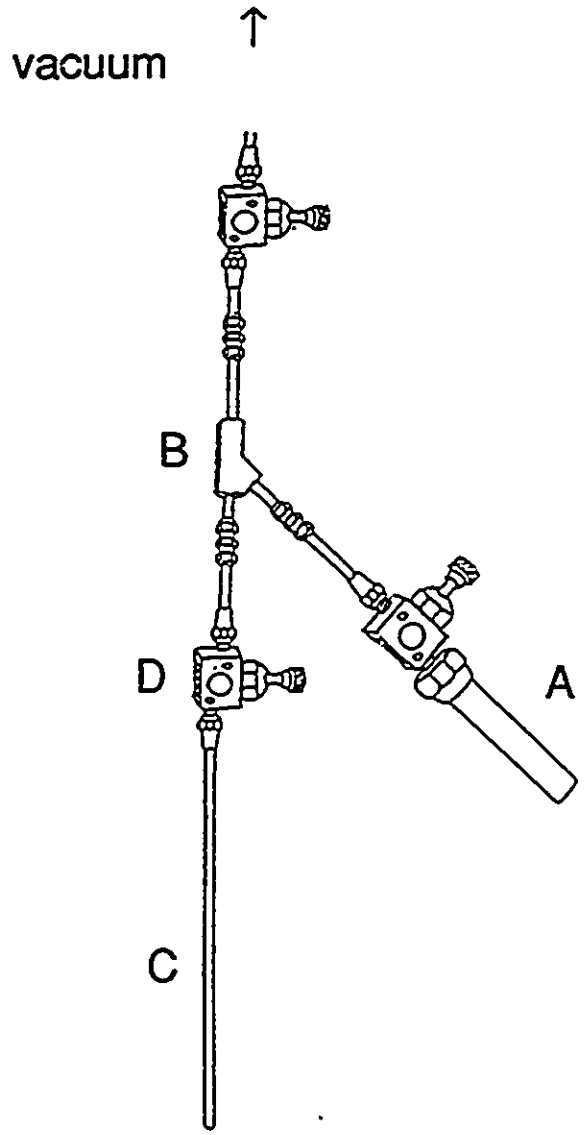

Figure 2.4 Apparatus for the storage and vacuum transfer of BrF_5 solvent; (A) ¾-in. o.d. Kel-F storage vessel containing BrF_5 over KF, (B) Kel-F Y-connector, (C) FEP tube reactor, (D) Kel-F valve in aluminum casing.

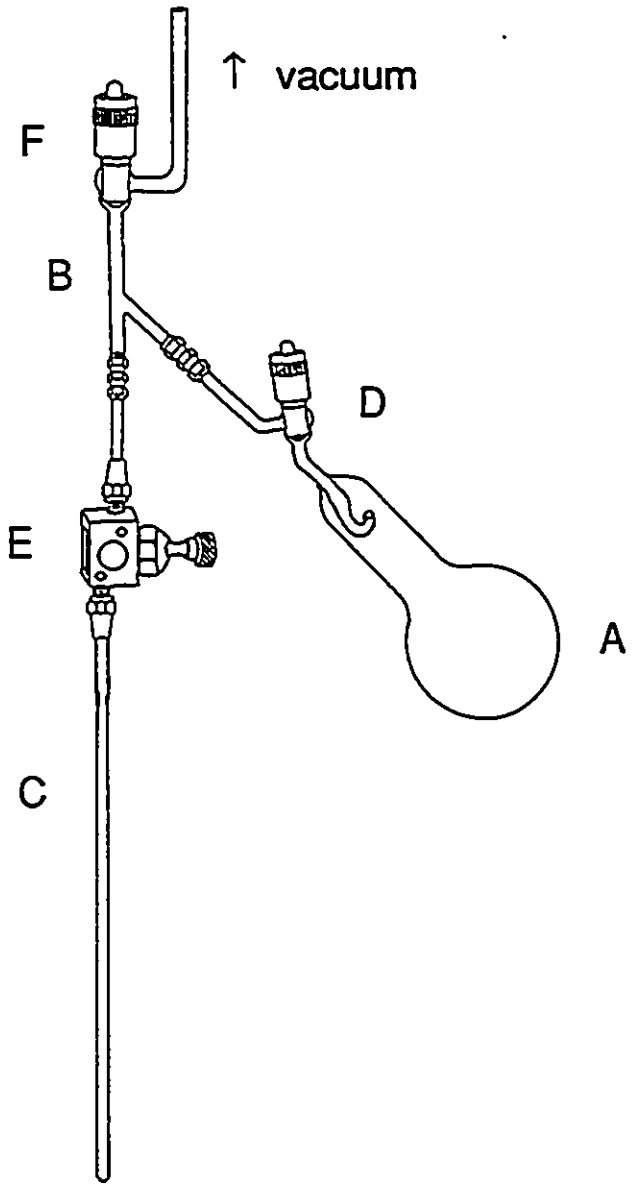

Figure 2.5 Apparatus for the storage and vacuum transfer of SO_2ClF solvent; (A) 250 mL glass bulb equipped with a 6-mm glass J. Young stopcock with glass barrel containing SO_2ClF over KF, (B) glass Y-connector, (C) FEP tube reactor, (D) 6-mm J. Young glass stopcock with FEP barrel, (E) Kel-F valve with aluminum casing.

(iii) Purification of SbF_5 and Preparation of AsF_5 and TeF_6

Antimony pentafluoride, SbF_5 (Ozark-Mahoning Co.) was purified by the literature method[111] and stored in a glass vessel. Subsequent transfers of SbF_5 were performed using an all glass syringe in the inert atmosphere of a glove bag which had been previously purged with dry nitrogen for 12 h.

Arsenic pentafluoride was prepared according to the literature method[112] by the fluorination of AsF_3[113] in a nickel can. The AsF_5 was distilled into a nickel storage cylinder from which it was used without further purification.

Tellurium hexafluoride was prepared from the fluorination of TeF_4, which was prepared according to the literature method,[114] in a monel reactor using a 50 mol% excess of elemental fluorine under autogeneous pressure at 250 °C for 4 h. Crude TeF_6 was purified by condensation onto a dry sample of NaF in a stainless steel Whitey cylinder at -196 °C and stored at room temperature for several days prior to use.

(iv) Preparation of XeF_2 and $XeF^+AsF_6^-$

Xenon difluoride was prepared from elemental xenon and fluorine by the thermal method described in the literature.[112] The salt $XeF^+AsF_6^-$ was prepared from the reaction of XeF_2 and AsF_5 in HF solvent as described earlier.[74] Both reagents were stored in Kel-F tubes in the inert nitrogen atmosphere of a dry box. All transfers of the solids $XeF^+AsF_6^-$ and XeF_2 were made from their Kel-F storage vessels inside the drybox.

(v) Preparation of F_5TeOH, $B(OTeF_5)_3$, $As(OTeF_5)_5$, and $Xe(OTeF_5)_2$

Pentafluoroorthotelluric acid, F_5TeOH,[115] $B(OTeF_5)_3$,[116] $As(OTeF_5)_5$,[117] and

$Xe(OTeF_5)_2$[48] were prepared and purified according to the literature procedures. The compounds, $B(OTeF_5)_3$ and $As(OTeF_5)_5$, were stored in an FEP tube and a PFA jar, respectively, in the inert nitrogen atmosphere of a drybox, and transfers of the solids were performed inside the drybox. The compound, $Xe(OTeF_5)_2$, was stored at -78 °C in a ½-in. o.d. FEP vessel equipped with a Kel-F valve under *ca.* 1300 Torr of dry nitrogen gas. Transfers of $Xe(OTeF_5)_2$ into reaction vessels was done in the inert nitrogen atmosphere of a drybox. The compound, F_5TeOH, was stored in a ¾-in. o.d. FEP vessel equipped with a Kel-F valve back-filled with *ca.* 1300 Torr of dry nitrogen gas at room temperature. Transfers of F_5TeOH were carried out by vacuum sublimation in an all glass apparatus.

(vi) Preparation of $CF_3C(OH)NH_2^+AsF_6^-$

In a typical purification procedure, 1.2860 g (11.377 mmol) of 2,2,2-trifluoroacetamide (Aldrich) was purified by recrystallization from 224 g of anhydrous $CHCl_3$ in one arm of an H-vessel (Figure 2.6). The arms of the H-vessel were constructed from 2.5-cm o.d. medium wall glass tubing. The arms of the H-vessel were separated by a medium porosity sintered glass frit. The crystals were isolated by filtration through the frit followed by drying under dynamic vacuum for 12 h at room temperature; 0.6255 g (48.6% yield) of $CF_3C(O)NH_2$ was isolated, indicating some degree of volatility of the compound at room temperature.

The salt, $CF_3C(OH)NH_2^+AsF_6^-$, was prepared from the reaction of $CF_3C(O)NH_2$ and AsF_5 in HF solvent according to equations (2.1) and (2.2)

$$CF_3C(O)NH_2 + (x + 1)\,HF \longrightarrow CF_3C(OH)NH_2^+F(HF)_x^- \qquad (2.1)$$

$$CF_3C(OH)NH_2^+F(HF)_x^- + AsF_5 \longrightarrow CF_3C(OH)NH_2^+AsF_6^- + x\ HF \qquad (2.2)$$

In a typical preparation of $CF_3C(OH)NH_2^+AsF_6^-$, $CF_3C(O)NH_2$ (1.2708 g, 11.242 mmol) was loaded into a ½-in. o.d. FEP tube attached to a Kel-F valve and dissolved in 4 mL of anhydrous HF at -78 °C, giving a yellow solution. Arsenic pentafluoride was metered from a nickel storage can into a dry 0.4005 L preweighed glass bulb. The AsF_5 was condensed onto the $CF_3C(O)NH_2$ solution at -196 °C. Weighing of the glass bulb before and after the transfer indicated that 2.5086 g (14.764 mmol) of AsF_5 was condensed onto the frozen solution. Warming to -78 °C resulted in a dark orange precipitate and a yellow supernatant. The precipitate dissolved on warming to -50 °C, resulting in a colorless solution. The solvent was removed *in vacuo* at -42 °C leaving a white microcrystalline material. After pumping for 0.5 h at -42 °C and 3.5 h at -10 °C, 3.3820 g of $CF_3C(OH)NH_2^+AsF_6^-$ (99.3% yield) was recovered. Decomposition with liquefaction was observed after one month at room temperature, however indefinite storage without decomposition was possible at -78 °C. The salt was stored in the reaction vessel at -78 °C under *ca.* 1300 Torr of dry nitrogen gas. Transfers of $CF_3C(OH)NH_2^+AsF_6^-$ were carried out directly from the storage vessel inside a nitrogen-filled drybox.

(vii) Preparation of the First-Stage Graphite Intercalate $C_{10}AsF_5$

Graphite powder was intercalated with AsF_5 using a modified version of the method described by Chun-Hsu *et al.*[118] Graphite rod (Ultra Carbon; Spectrographic analysis grade) was ground to a fine powder with a mortar and pestle and dried by heating under vacuum at 150 °C for 24 h. In a nitrogen-filled glove bag, 0.9003 g (74.96 mmol carbon) of the graphite powder was

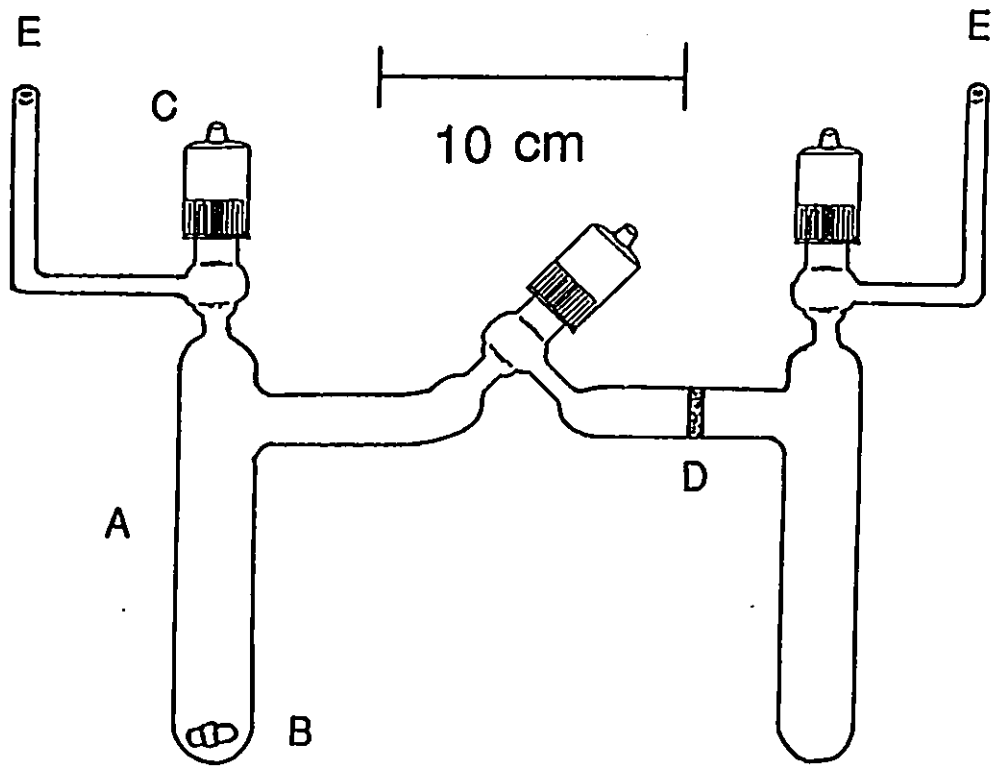

Figure 2.6 Glass H-vessel; (A) arm of H-vessel connstructed from 2.5-cm o.d. medium wall Pyrex glass, (B) Teflon-coated magnetic stir bar, (C) 6-mm J. Young glass stopcock with FEP barrel, (D) medium porosity sintered glass frit, (E) ¼-in. o.d. glass tubing.

loaded into a passivated ½-in. o.d. FEP tube equipped with a Kel-F valve. Approximately 1500 Torr of AsF_5 gas was expanded from its nickel storage container into the manifold of the metal vacuum line and the reaction vessel containing the graphite powder (-196 °C). With constant agitation of the reaction vessel, the absorption of AsF_5 by the graphite was monitored by observing the pressure in the manifold. Complete absorption of the AsF_5 was observed upon warming the sample to ambient temperature after *ca.* 10 min. The partially intercalated graphite was blue in color and the volume had increased. This procedure was repeated until no more AsF_5 was absorbed by the graphite. The blue powder was pumped for *ca.* 1 min. at room temperature to remove any unreacted AsF_5. The sample was then placed under static vacuum and the pressure was monitored. No increase in pressure was observed, indicating the absence of a significant amount of unreacted AsF_5. The mass of the resulting blue powder (2.1398 g) corresponded closely to that expected for a quantitative preparation of $C_{10}AsF_5$ (2.1740 g). The $C_{10}AsF_5$ was stored under *ca.* 1000 Torr of dry nitrogen gas and was used without further characterization.

(viii) Preparation of *trans*-N_2F_2 and Investigation of *cis*-/*trans*-N_2F_2 Isomerization at Low Temperature in AsF_5-Acidified HF Solvent

The *trans*-isomer of difluorodiazene, N_2F_2 was selectively prepared without the formation of a detectable amount of the *cis*-isomer from the reaction of N_2F_4 and the first stage graphite intercalate $C_{10}AsF_5$ using the method of Munch and Selig[119] according to equation (2.3). In a nitrogen-filled glove bag, 0.3969 g (1.368 mmol) of $C_{10}AsF_5$ was transferred to a vessel constructed from a fluorinated ½-in. o.d. FEP tube equipped with a Kel-F valve.

$$C_{10}AsF_5 + N_2F_4 \longrightarrow C_{10}AsF_7 + \textit{trans}\text{-}N_2F_2 \qquad (2.3)$$

Tetrafluorohydrazine, N_2F_4[120] (1.312 mmol) was expanded into the manifold of a metal vacuum line and condensed onto the $C_{10}AsF_5$ at -196 °C. The reaction vessel was slowly warmed to room temperature with periodic agitation. The vessel was allowed to sit for 2 days with periodic shaking. The vessel was pumped under dynamic vacuum at -196 °C. The *trans*-N_2F_2 produced in this manner was allowed to remain over the AsF_5 intercalated graphite at room temperature. Transfers of *trans*-N_2F_2 were carried out by allowing the gas to expand from the reaction vessel at room temperature into the manifold of a metal vacuum line. The *trans*-N_2F_2 was then condensed into the appropriate reaction vessel at -196 °C. The purity of the *trans*-N_2F_2 was confirmed from the ^{19}F NMR spectrum at room temperature in Freon-114 solvent (*ca.* 0.5 M), and consisted of the characteristic AA'XX' spectrum centered at $\delta(^{19}F) = 92.2$ ppm, as expected.[121] The ^{19}F NMR resonance of the *cis*- isomer of N_2F_2 was not observed at *ca.* $\delta(^{19}F) = 133.7$ ppm,[121] indicating the selectivity of the reaction.

The possibility of AsF_5-assisted isomerization of *trans*-N_2F_2 in HF was investigated at low temperature. The *trans*-isomer of N_2F_2 was expanded into the volume calibrated manifold (0.019 L) of a metal vacuum line at ambient temperature. Using the ideal gas approximation and the measured pressure, the quantity of *trans*-N_2F_2 in the manifold was determined to be 0.0882 mmol. The contents of the manifold was condensed into a 4-mm FEP tube containing approximately 0.4 mL of HF at -196 °C. Arsenic pentafluoride (0.808 mmol) was likewise expanded into the manifold and condensed into the FEP sample tube at -196 °C. The tube was warmed to -20 °C, whereupon a clear colorless solution was formed. The sample was kept at -20 °C for 5 min., and was then heat sealed at -196 °C under dynamic vacuum. Only *trans*-N_2F_2, HF and AsF_6^- were observed in the ^{19}F NMR spectrum at -37 °C, indicating that *cis*/*trans*-N_2F_2 isomerization did not occur under these conditions.

(ix) Purification of Ammonia

Ammonia gas, NH_3 (Canadian Liquid Air, Ltd. or Matheson) was condensed from a gas cylinder into an ammonia drying tube at -78 °C containing freshly cut sodium metal (0.3 - 0.4 g; BDH Chemicals). Liquid ammonia (100 - 200 mL) was stored at -78 °C in a dry ice-acetone bath for at least one week prior to use. Transfers of ammonia gas directly from the storage vessel were performed under vacuum using all glass apparatus.

(x) Preparation of ^{15}N-Enriched (99.5 atom %) Ammonia

The apparatus shown in Figure 2.7, which was modified from the literature,[122] was dried under vacuum for 12 h and back-filled with nitrogen gas. Nitrogen-15 enriched NH_3 was prepared according to equation (2.4). A solution of 99.5 atom % $^{15}NH_4Cl$ (1.2083 g; MSD Isotopes or

$$^{15}NH_4Cl + \text{xs KOH} \xrightarrow{H_2O} KCl + {}^{15}NH_3 \qquad (2.4)$$

Isotech, Inc.) in 10 mL of distilled water was prepared and pipetted into the round bottom flask of the apparatus. The apparatus was sealed using ½-in. Teflon unions (Swagelok) as shown in Figure 2.7 and the pressure above the solution was decreased to 450 Torr of dry nitrogen with the U-trap immediately following the reflux column cooled to -196 °C. The stopcock immediately following the -196 °C U-trap was closed and the aqueous solution was gently heated with a heat gun to initiate gentle reflux, which slowly leached the KOH pellets (13.47 g) situated on platform B directly above the reaction flask into the solution, whereupon $^{15}NH_3$ gas was evolved from the aqueous solution and collected in the U-trap at -196 °C. After the reflux subsided, additional NH_3

Figure 2.7 Glass ammonia generator; (A) Approximately 50 mL round bottom flask, (B) platforms with 3 - 3.5 mm diameter holes to support KOH pellets, (C) condenser, (D) 3/8-in. Teflon unions (Swagelok) equipped with 3/8-in. Teflon compression fittings (Swagelok), (E) sections of 3/8-in. o.d. glass tubing, sealed at one end, (F) 6-mm glass J. Young stopcock with FEP barrel, (G) ¼-in. Teflon unions (Swagelok) equipped with ¼-in. Teflon compression fittings (Swagelok), (H) 120 or 300 mL glass flask.

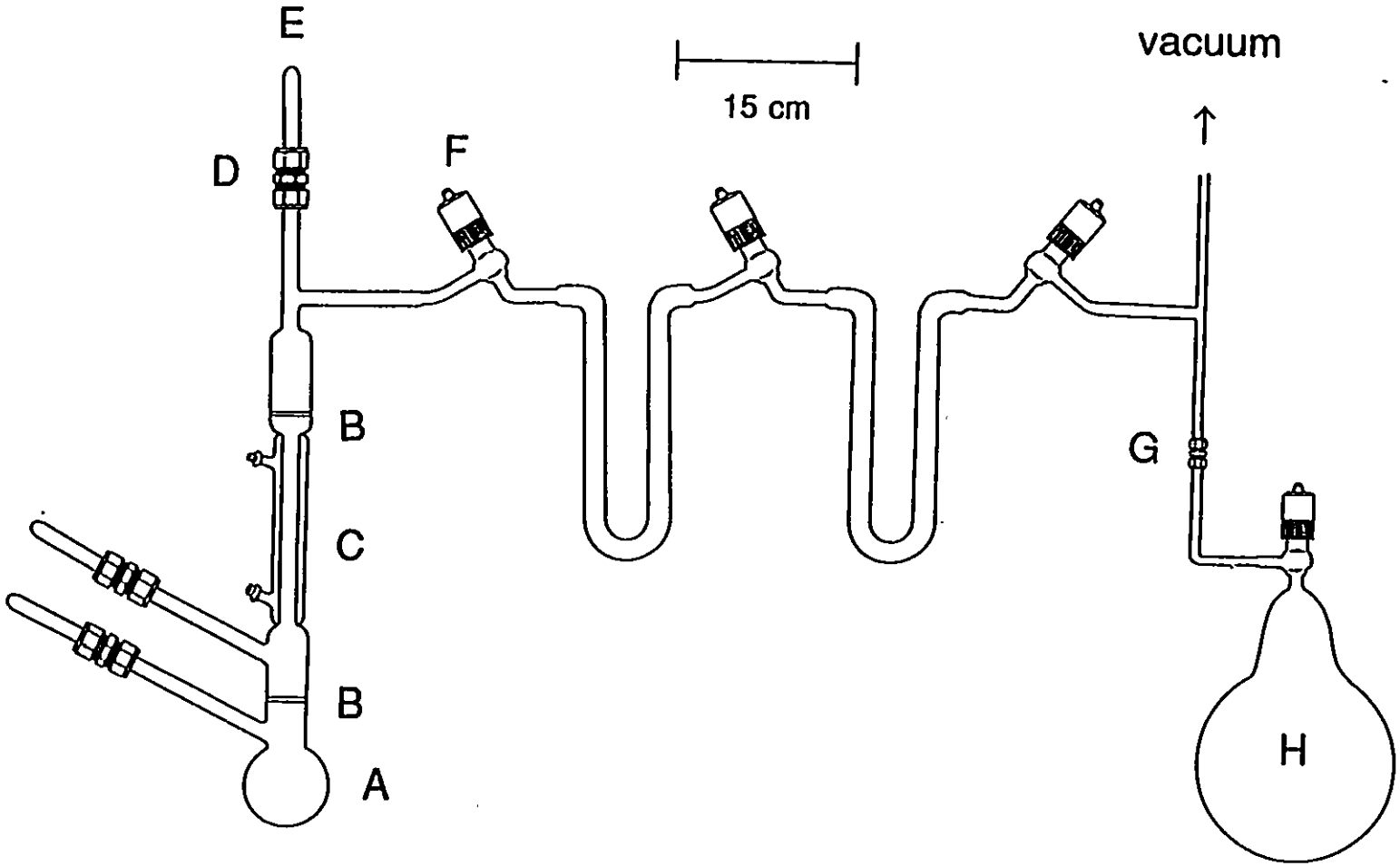
E
D
F
15 cm
vacuum
B
C
B
A
G
H

gas was liberated from the aqueous solution by cooling the solution to -78 °C and evacuating the vessel by quickly opening and closing the stopcock immediately following the 196 °C U-trap. Warming the solution until liquefaction resulted in condensation of additional $^{15}NH_3$ gas into the -196 °C U-trap. This was repeated until condensation of additional $^{15}NH_3$ was no longer observed in the -196 °C U-trap. The U-trap was warmed to -78 °C and the $^{15}NH_3$ was slowly condensed over *ca.* 3 h under static vacuum into a second U-trap at -196 °C. The second trap was warmed to -78 °C and the $^{15}NH_3$ was condensed under static vacuum into a preweighed 120 mL glass bulb at -196 °C. The glass bulb was warmed to room temperature and weighed; 0.3949 g of $^{15}NH_3$ was isolated (98.83 % yield).

(xi) Preparation of 99.5 atom % ^{15}N Enriched $[(CH_3)_3Si]_2NH$

The method of Sauer,[123] was modified for the synthesis of $[(CH_3)_3Si]_2{}^{15}NH$ from $^{15}NH_3$ gas and $(CH_3)_3SiCl$ using Freon-114 as solvent, according to equation (2.5)

$$3\ {}^{15}NH_3 + 2\ (CH_3)_3SiCl \longrightarrow [(CH_3)_3Si]_2{}^{15}NH + 2\ {}^{15}NH_4Cl \qquad (2.5)$$

Chlorotrimethylsilane (Aldrich) was purified by vacuum distillation into a dry glass bulb equipped with a grease-free 4-mm glass J. Young stopcock equipped with a Teflon barrel. By vacuum distillation, 1.6144 g (14.86 mmol) of $(CH_3)_3SiCl$ was transferred into a dry glass H-vessel equipped with a medium porosity sintered glass frit between the two arms of the vessel (Figure 2.6). Freon-114 (16.3 g) was distilled onto the $(CH_3)_3SiCl$ at -196 °C. A clear colorless solution resulted on warming to room temperature. Nitrogen-15 enriched NH_3 (0.3949 g, 21.92 mmol) was vacuum transferred onto the frozen solution of $(CH_3)_3SiCl$ and Freon-114 (-196 °C). The vessel

was allowed to warm slowly to ambient temperature with stirring. Upon liquefaction of the solvent, a white precipitate formed. After stirring for 7 days, the contents of the arm containing the white precipitate was cooled to -60 °C. With the other arm at -60 °C, the mixture was filtered, giving a clear colorless filtrate. The white precipitate was washed three times by repeated back-distilling of solvent (with the appropriate arms of the vessel at -40 and -60 °C) followed by filtration as above. The bulk of the solvent was back-distilled onto the residue after the last filtration, and the resulting clear liquid was distilled through a one-piece glass dual-trap apparatus (Figure 2.8), with the U-traps cooled to -40 and -196 °C. Pure $[(CH_3)_3Si]_2{}^{15}NH$ was collected in the -40 °C U-trap (1.0345 g, 87.2 % yield). The ^1H NMR parameters are similar to those reported by Cowley *et al.*[124] (neat liquid at 25 °C): $\delta(^1H)$ = -0.61 ppm (CH_3), $^2J(^1H\text{-}^{29}Si)$ = 6.6 Hz; $\delta(^1H)$ = 0.52 ppm (NH), $^1J(^1H\text{-}^{15}N)$ = 63.1 Hz. The -196 °C trap contained freon-114 (CF_2ClCF_2Cl), $(CH_3)_3SiCl$, and a trace of $[(CH_3)_3Si]_2{}^{15}NH$.

(xii) <u>Preparation of $F_5TeNHSi(CH_3)_3$</u>

The compound, $F_5TeNHSi(CH_3)_3$, was prepared using the method of Seppelt *et al.*[125] with modifications, according to equation (2.6). In a typical preparation, $[(CH_3)_3Si]_2NH$

$$TeF_6 + [(CH_3)_3Si]_2NH \longrightarrow F_5TeNHSi(CH_3)_3 + (CH_3)_3SiF \qquad (2.6)$$

(1.79946 g, 11.149 mmol; Aldrich) was vacuum distilled into a 40 mL Whitey 304 stainless steel cylinder equipped with a Whitey ORM 2 valve, cooled to -196 °C. The cylinder was passivated with fluorine gas (*ca.* 1000 Torr) prior to use. Tellurium hexafluoride was expanded into the volume calibrated (0.019 L) manifold of a metal vacuum line equipped with a 1.976 L nickel

Figure 2.8 Glass dual U-trap apparatus; (A) glass H-vessel (see Figure 2.6), (B) ¼-in. Teflon unions (Swagelok) equipped with ¼-in. Teflon compression fittings (Swagelok), (C) 6-mm glass J. Young stopcock with FEP barrel, (D) 304 SS 40 mL cylinder (Whitey) equipped with a 316 SS valve (Whitey ORM 2).

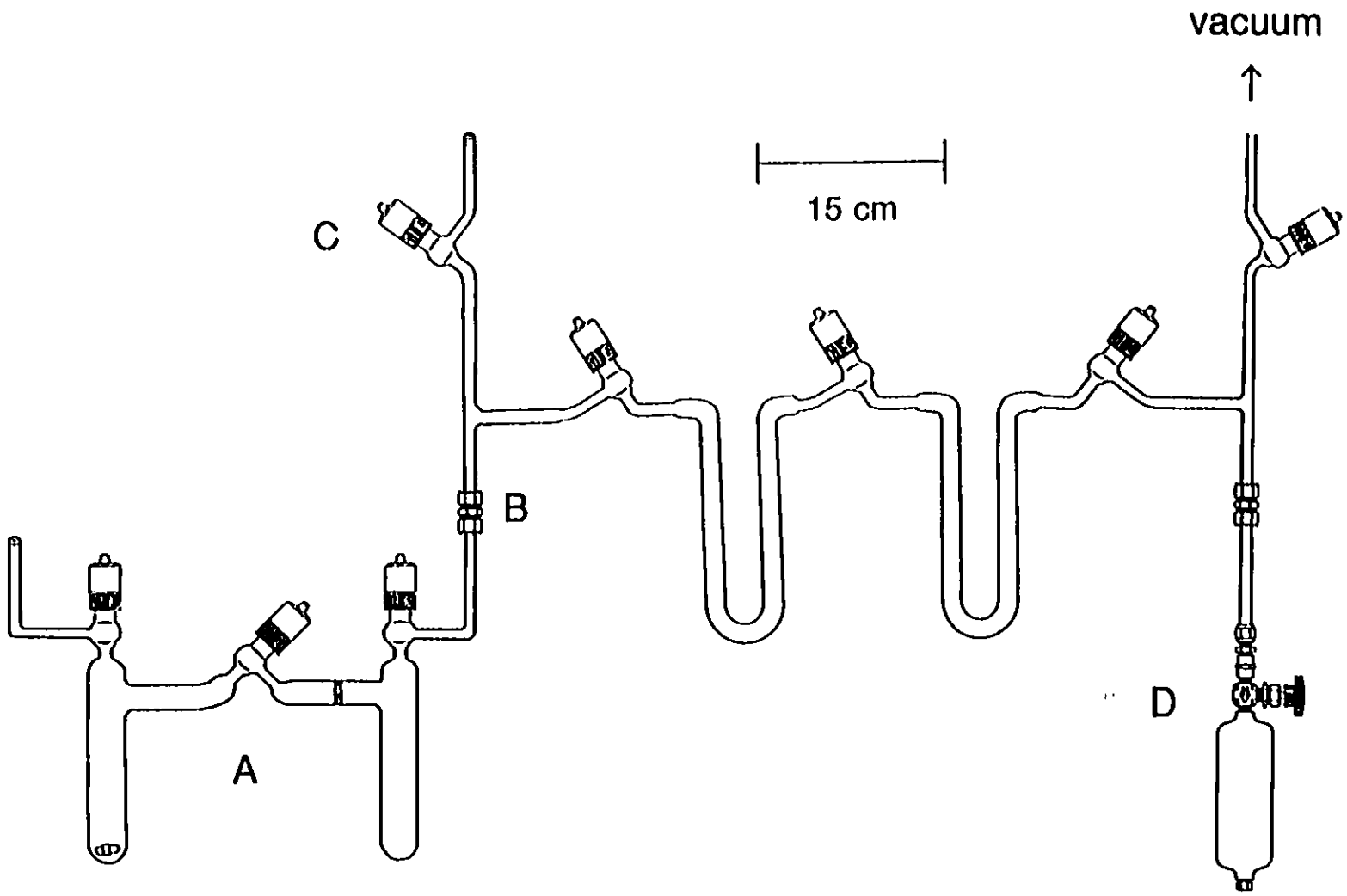
vacuum
15 cm
C
B
A
D

ballast can at ambient temperature (total volume, 1.995 L). The pressure of TeF_6 was converted to moles using the ideal gas approximation. A total pressure of 134 Torr (14.4 mmol) of TeF_6 was transferred into the cylinder, which was cooled to -196 °C. The cylinder was allowed to warm slowly to ambient temperature and then shaken mechanically for 1 week. Excess TeF_6 and $(CH_3)_3SiF$ were pumped off at -50 °C. After no vapor pressure was detected, the cylinder was warmed to room temperature and subjected to vacuum distillation using a one-piece glass dual U-trap apparatus (Figure 2.8); the first trap (-30 °C) contained 2.365 g (68.2 % yield) of pure $F_5TeNHSi(CH_3)_3$ (checked by ^{19}F and ^{1}H NMR). The explosive *cis*-$F_4Te[N(H)Si(CH_3)_3]_2$,[125] which is often a minor product in the synthesis, was not observed in the ^{19}F NMR spectra. The second trap (-196 °C) contained $(CH_3)_3SiF$, $[(CH_3)_3Si]_2NH$, and some products which were not identified.

Seppelt[125] noted that the successful synthesis of $F_5TeNHSi(CH_3)_3$ free from significant amounts of explosive *cis*-$F_4Te[N(H)Si(CH_3)_3]_2$ required that the stainless steel reaction vessel be rinsed with concentrated nitric acid between runs and the reaction be carried out at room temperature. In the present work, concentrated hydrochloric acid was substituted for nitric acid as the rinsing agent.

(xiii) <u>Preparation of F_5TeNH_2 and $F_5Te^{15}NH_2$</u>

The compounds, F_5TeNH_2 and $F_5Te^{15}NH_2$, were prepared by a modificaton of the published synthesis.[125] Typically $[(CH_3)_3Si]_2NH$ (0.7485 g, 4.637 mmol; Aldrich) and TeF_6 (6.056 mmol) were combined in a 40 mL Whitey 304 stainless steel cylinder for 1 week followed by vacuum distillation of all volatiles at -50 °C, as outlined above for the preparation of $F_5TeNHSi(CH_3)_3$. The compound, $F_5TeNHSi(CH_3)_3$, was allowed to react with HF in an

$(CH_3)_3SiF$ elimination reaction according to equation (2.7). Anhydrous HF (0.1705 g, 8.505

$$F_5TeNHSi(CH_3)_3 + HF \longrightarrow F_5TeNH_2 + (CH_3)_3SiF \qquad (2.7)$$

mmol) was transferred by vacuum distillation into the cylinder at -196 °C. The cylinder was allowed to warm to ambient temperature and was mechanically agitated overnight. Volatiles were removed under vacuum at -78 and at -40 °C. The cylinder was warmed to 40 °C and the remaining material was sublimed under vacuum into a ¼-in. o.d. FEP vessel cooled to -196 °C. A sticky white solid was isolated, identified by ^{19}F NMR spectroscopy as F_5TeNH_2 (0.5688 g; 51.41% yield).[125]

The synthesis of $F_5Te^{15}NH_2$ was identical to that of F_5TeNH_2, except that 99.5 atom % ^{15}N enriched $[(CH_3)_3Si]_2NH$ was used in the preparation of the former. The ^{15}N enriched $[(CH_3)_3Si]_2NH$ isolated in the -40 °C U-trap [see Section (B), Part (xi)] was condensed into the 40 mL stainless steel vessel attached to the dual trap apparatus depicted in Figure 2.8. The remainder of the procedure for the preparation of $[^{15}N]F_5TeNH_2$ was identical to that for F_5TeNH_2. The compounds, F_5TeNH_2 and $F_5Te^{15}NH_2$, were stored in FEP tubes inside the drybox. Transfers of the reagents were made from the FEP storage vessels inside the drybox.

(xiv) <u>Preparation of $F_5TeNH_3^+AsF_6^-$ and $F_5Te^{15}NH_3^+AsF_6^-$</u>

The salt, $F_5TeNH_3^+AsF_6^-$, was prepared from the reaction of F_5TeNH_2 with excess AsF_5 in anhydrous HF solvent according to equations (2.8) and (2.9). In a typical preparation,

$$F_5TeNH_2 + (x + 1)\,HF \longrightarrow F_5TeNH_3^+F(HF)_x^- \qquad (2.8)$$

$$F_5TeNH_3^+F(HF)_x^- + AsF_5 \longrightarrow F_5TeNH_3^+AsF_6^- + x\ HF \qquad (2.9)$$

1.1873 g (4.9758 mmol) of F_5TeNH_2 was placed in a ½-in. o.d. FEP tube which was flared (45° SAE) and connected by means of compression fittings to a Whitey ORM 2 316 stainless steel valve. Anhydrous HF (4 mL) was distilled onto the F_5TeNH_2 (-196 °C). Warming to -78 °C resulted in a colorless solution. Arsenic pentafluoride (6.1 mmol) was condensed onto the frozen solution at -196 °C. Warming to -55 °C resulted in a colorless solution. Excess AsF_5 was removed under vacuum at -78 °C. The HF solvent was removed under vacuum at -40 °C until 2.0442 g of a white powder remained (96% yield), with no detectable vapor pressure at this temperature. The salt, $F_5TeNH_3^+AsF_6^-$, is stable indefinitely under anhydrous conditions at room temperature and hydrolyzes rapidly in the presence of water.

The preparation of $F_5Te^{15}NH_3^+AsF_6^-$ was identical to that described for $F_5TeNH_3^+AsF_6^-$ using $F_5Te^{15}NH_2$ as the starting material. The salts were stored at room temperature in ½-in. or ¼-in. o.d. FEP tubes inside a nitrogen-filled drybox. Tranfers of the salts were made directly from the storage vessels inside the drybox.

(xv) <u>Preparation of $F_5TeNH_3^+As(OTeF_5)_6^-$</u>

In a ¼-in. o.d. FEP tube equipped with a Kel-F valve, F_5TeOH (0.09635 g, 0.4021 mmol) was combined with $As(OTeF_5)_5$ (0.49494 g, 0.39037 mmol) and F_5TeNH_2 (0.10858 g, 0.45504 mmol) at -196 °C. The solvent, SO_2ClF, was vacuum distilled onto the reagents at -196 °C, giving a clear colorless solution on warming to -78 °C. (*ca.* 0.7 M). The SO_2ClF solvent was removed at -32 °C under vacuum, leaving a sticky white precipitate. A finely divided white powder resulted on further vacuum pumping at -45 °C for 2 h.

(xvi) Sulfur trioxide

Sulfur trioxide, SO_3 (Sulfan B; Allied Chemical) was heated to *ca.* 65 °C for 2 h to effect depolymerization.[126] The liquified SO_3 was then poured into a dry evacuated round bottom flask equipped with a greaseless 6-mm glass J. Young stopcock equipped with a Teflon barrel and used without further purification.

(xvii) Preparation of $S_2O_5F_2$

The anhydride of fluorosulfuric acid, $S_2O_5F_2$, was prepared, with modification, using the method of Gillespie and Rothenbury,[127] by the reaction of excess SO_3 with SbF_5. The reactions were conducted in the vessel depicted in Figure 2.9. Two 3/8-in. o.d. FEP tubes were sealed at one end and fused to lengths of ½-in. o.d. FEP tubing. The tubes were joined using a ½-in. Teflon T-piece union (Swagelok) with Teflon compression fittings (Swagelok). A Kel-F valve was attached as shown in Figure 2.9. In a typical preparation, SbF_5 (12.0880 g, 0.0557713 mol) was syringed into the FEP tube to be attached at 90° to the Kel-F valve inside a dry nitrogen-filled glove bag. Sulfur trioxide (*ca.* 16 mL) was vacuum sublimed through an all glass apparatus into the FEP tube to be attached at 180° to the Kel-F valve. The SbF_5 was gently heated with a heat gun and poured onto the SO_3 at 50 °C. After 5 h at 50 °C with intermittent shaking, a clear liquid below a white solid resulted. The liquid was vacuum distilled into a dry ½-in. o.d. FEP tube equipped with a Kel-F valve containing approximately an equal volume of H_2SO_4 (>99%, Fisher Scientific) to remove excess SO_3. The white solid, reported to consist mainly of antimony oxides,[127] did not

Figure 2.9 FEP T-vessel for preparation of $S_2O_5F_2$; (A) 3/8-in. o.d. FEP tubing, heat-sealed at one end, (B) 3/8-in. Teflon T (Swagelok) equipped with Teflon 3/8-in. compression fittings (Swagelok), (C) 3/8-in. FEP tubing drawn down to ¼-in. o.d. using a Bunsen flame for attachment by a flare fitting (45° SAE) to a Kel-F valve, (D) Kel-F valve in aluminum casing.

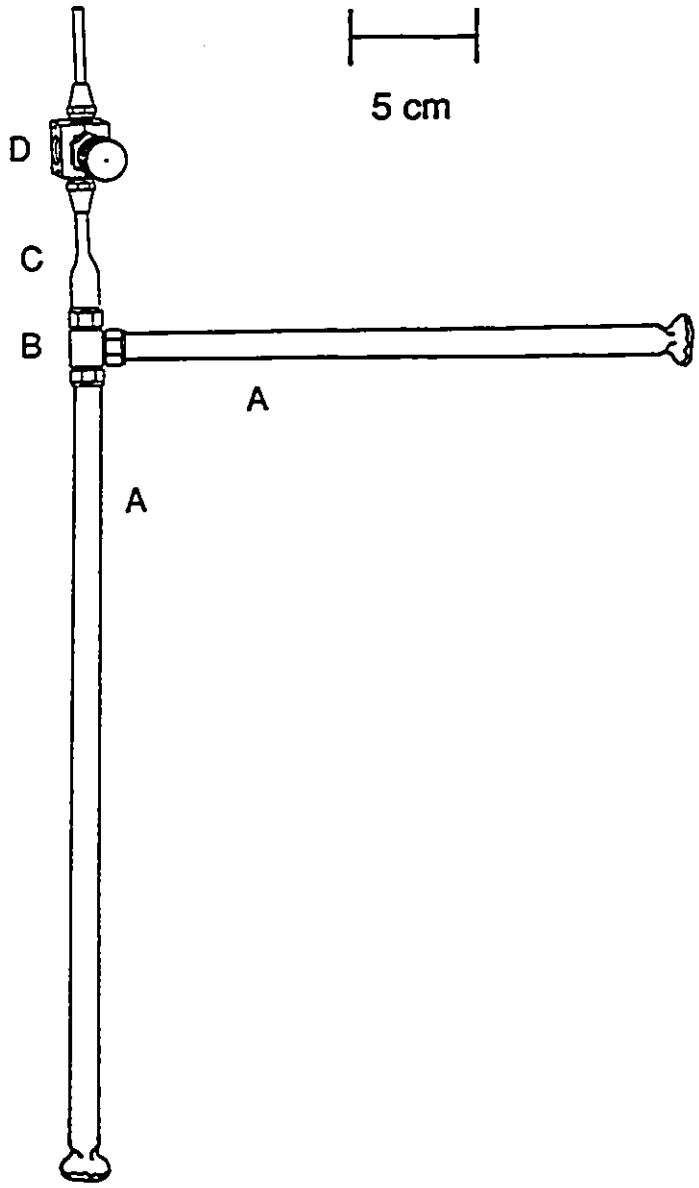
5 cm
D
C
B
A
A

transfer under vacuum. Two liquid phases resulted after 1 h at 55 °C. Some white solid (assumed to be SO_3) was observed at the interface of the two liquids. After mixing intermittently at 55 °C for several hours, the volatile contents of the tube were vacuum distilled onto a second approximately equal volume of >99% H_2SO_4. After mixing at 55 °C for several hours, the white solid at the liquid interface had dissolved, leaving two liquid phases. The volatile layer (low density phase) was vacuum distilled into a dry ½-in. o.d. FEP tube equipped with a Kel-F valve and shown to be pure $S_2O_5F_2$ (8.3798 g; 33% yield based on SbF_5) from the gas phase infrared spectrum[128] (3 Torr pressure, 1 dm pathlength, AgCl windows).

(xviii) Preparation of 99.5 atom% ^{15}N Enriched FO_2SNH_2

The compound, $FO_2S^{15}NH_2$, was prepared by the reaction of $^{15}NH_3$ and $S_2O_5F_2$[129] at low temperature in diethyl ether solvent according to equation (2.10). In a typical preparation,

$$2\ ^{15}NH_3 + S_2O_5F_2 \longrightarrow FO_2S^{15}NH_2 + {}^{15}NH_4^+SO_3F^- \qquad (2.10)$$

$S_2O_5F_2$ (3.9559 g, 21.722 mmol) was vacuum distilled into an arm of a glass H-vessel (Figure 2.6). Diethyl ether (34 mL) was vacuum distilled onto the $S_2O_5F_2$ at -196 °C. A colorless solution resulted on warming to room temperature. Under static vacuum, 99.5 atom % ^{15}N enriched NH_3 (0.7890 g, 43.80 mmol) was condensed into the empty arm of the H-vessel at -196 °C. Both arms of the H-vessel were cooled to -78 °C for 3 days. The arm containing the ether/$S_2O_5F_2$ solution was warmed to -60 °C and the arm containing the $^{15}NH_3$ was warmed to -45 °C. The middle stopcock was opened and with constant stirring by means of a magnetic stir bar and intermittent opening and closing of the middle stopcock, the $^{15}NH_3$ had essentially completely reacted after

ca. 0.5 h, as indicated by the almost complete consumption of the pool of liquid $^{15}NH_3$ in the -45 °C arm. This was accompanied by the development of a white precipitate in the ether solution. The ether solution was then frozen at -196 °C to condense any unreacted $^{15}NH_3$ gas into the arm containing the frozen ether solution, and the middle stopcock was closed. The ether solution was warmed to -60 °C for an additional 0.5 h with constant stirring. The empty arm of the H-vessel was cooled to -78 °C, and with the arm containing the ether solution at room temperature, the middle stopcock was opened and the ether solution was filtered through the medium porosity sintered glass frit; however, filtration was slow. It was necessary to slightly warm the frit with a heat gun to prevent freezing of the $FO_2S^{15}NH_2$ (m.p., 8 °C)[129] upon evaporation of the diethyl ether from the frit. Filtration required *ca.* 2 h to complete. The white precipitate was washed by back-distilling diethyl ether into the arm. This was facilitated with a -78 / 25 °C temperature gradient. After washing the precipitate, four additional filtrations and washings were performed using the conditions described above. After an additional filtration, the ether solution was pipetted into a one-piece glass distillation vessel (Figure 2.10) in a dry nitrogen-filled glove bag. Most of the diethyl ether was removed under vacuum at 0 °C, leaving a yellow viscous liquid. The liquid was distilled under static vacuum while heating the liquid gently with a heat gun and cooling the distillate receptacle to -196 °C. A clear liquid distillate was isolated, leaving behind a solid yellow residue. The distillate was then pumped at 0 °C for 2 h under dynamic vacuum, and redistilled at room temperature under dynamic vacuum in a micro-distillation apparatus (Figure 2.11); 0.6859 g of a colorless liquid was isolated. ^{1}H NMR ($CD_3C{\equiv}N$ solution): doublet of doublets, $\delta(^1H)$ = 6.79 ppm, $^1J(^1H\text{-}^{15}N)$ = 86.7 Hz, $^3J(^1H\text{-}^{19}F)$ = 6.1 Hz. Multiplets at $\delta(^1H)$ = 1 - 5 ppm indicated the presence of residual organic material (*ca.* 5 - 10%). ^{19}F NMR: triplet of doublets, $\delta(^{19}F)$ = 56.78 ppm, $^2J(^{19}F\text{-}^{15}N)$ = 2.7 Hz, $^3J(^{19}F\text{-}^1H)$ = 6.3 Hz. The Raman spectrum (neat

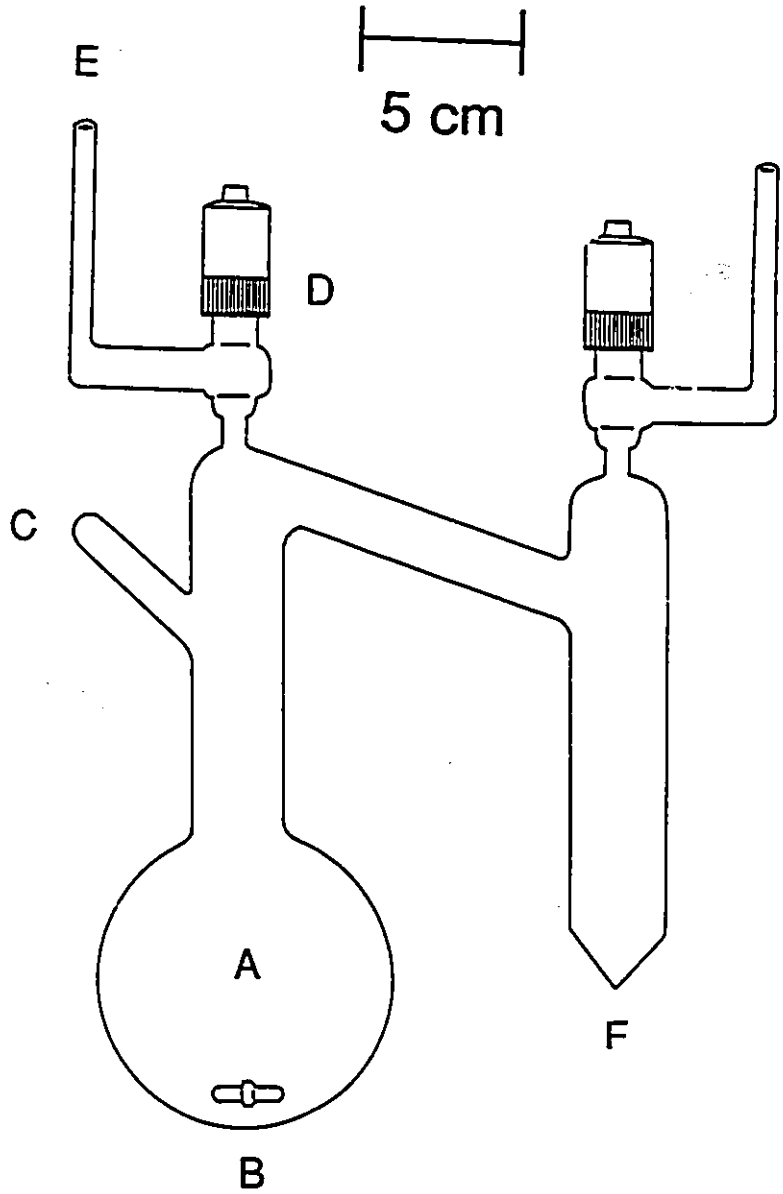

Figure 2.10 Glass distillation apparatus used to fractionate FO_2SNH_2 and ^{15}N-enriched FO_2SNH_2; (A) 250 mL round bottom flask, (B) Teflon-coated magnetic stir bar, (C) entrance for stir bar after annealing of glass apparatus (now sealed), (D) 6-mm glass J. Young stopcock with FEP barrel, (E) ¼-in. o.d. glass tubing, (F) receptacle arm tapered to allow removal of distillate by pipet.

liquid) was similar to the infrared spectrum of FO_2SNH_2[130] with residual organic impurities containing ether groups.[131,132] Raman bands of impurity (relative intensities): 2991.9 (5.2), 2952.4 (10.0), 2941.8 (6.2), 2910.6 (2.3), 2885.7 (2.3), 2735.0 (0.4), 1458.1 (1.7), 1449.2 (1.6), 1104.2 (1.6), 1074.8 (1.2), 1061.4 (0.6), 1050.3 (0.3), 689.0 (0.6), 658.9 (0.4), 594.8 (0.7), 577.3 (0.9), 408.1 (1.5), 395.0 (2.1), 336.3 cm^{-1} (3.1). Multiple distillations did not remove the residual organic impurity.

(xix) Preparation of FO_2SNH_2

Natural abundance FO_2SNH_2[133,134] was prepared according to equations (2.11) and (2.12)

$$ClO_2SNCO + NaF \longrightarrow NaCl + FO_2SNCO \qquad (2.11)$$

$$FO_2SNCO + H_2O \longrightarrow [FO_2SN(H)C(O)OH] \xrightarrow{\Delta} FO_2SNH_2 + CO_2 \qquad (2.12)$$

In a typical preparation, chlorosulfuryl isocyanate, ClO_2SNCO (14.0027 g; Aldrich) was pipetted into a 250 mL glass distillation vessel (Figure 2.10) in a dry nitrogen-filled glove bag. Dry acetonitrile (50 mL) was vacuum distilled onto the ClO_2SNCO at -196 °C. A clear solution resulted at room temperature, which turned pale yellow after 1 h. Dry NaF (4.4496 g; J.T. Baker) was added to the solution under a dry nitrogen atmosphere with stirring by means of a magnetic stir bar. The solution immediately became intense yellow. The vessel was closed and the reaction mixture was heated at 70 °C for 2.5 h. The contents of the vessel were frozen at -78 °C and 1.782 g of distilled water was added to the empty arm of the reaction vessel with a pipet.

Figure 2.11 Glass micro-distillation apparatus used to fractionate FO_2SNH_2; (A) 50 mL round bottom flask, (B) Teflon coated stir bar, (C) 4-mm glass J. Young stopcock with FEP barrel, (D) ¼-in. o.d. glass tubing, (E) condenser, (F) thermocouple inlet for temperature determination, (G) B19 ground glass joint, lubricated with Apiezon "N" grease, (H) ¼-in. Teflon unions (Swagelok) equipped with ¼-in. Teflon compression fittings (Swagelok), (I) glass tapered receiving tubes.

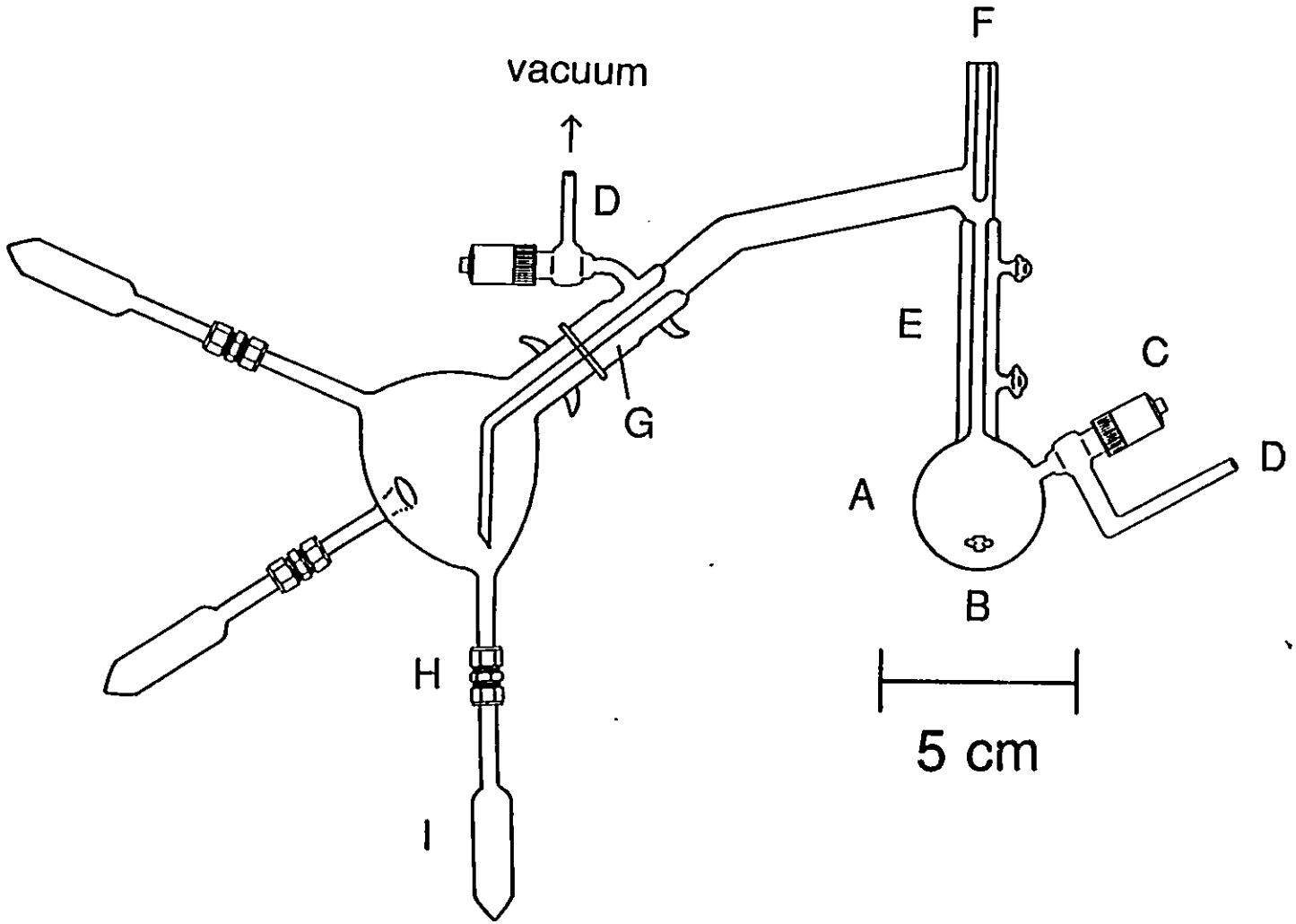
vacuum
D
F
E
C
D
A
B
G
H
I
5 cm

With both arms of the vessel cooled to -78 °C, the reaction vessel was evacuated. The acetonitrile solution was cooled to -196 °C and the arm containing the water was warmed to room temperature. The water sublimed to the walls immediately above the frozen acetonitrile solution, where it immediately froze. The vessel was back-filled with approximately 760 Torr of nitrogen gas and the arm of the vessel containing the reagents was allowed to slowly warm to room temperature. The pressure of the system was monitored by leaving the vessel open to the mercury manometer of a glass vacuum line. As the water melted, immediate bubbling with an increase in pressure of 10 Torr occurred each time a drop of water was added to the stirred yellow reaction mixture. The pressure increase resulting from the evolution of CO_2 gas upon decomposition of the unstable carbamic acid, $FO_2SN(H)C(O)OH$, according to equation (2.12), was released by opening the stopcock to the vacuum line until the total pressure of the reaction vessel was reduced to *ca.* 760 Torr. Shortly after the addition of the water was complete, the large increases in pressure ceased. The pressure was monitored and occasionally adjusted to *ca.* 760 Torr while the solution was heated to 70 °C with constant stirring for 2 h. No significant increase in pressure was observed during this time. The vessel was cooled to 0 °C and most of the $CH_3C{\equiv}N$ solvent was removed under dynamic vacuum. After *ca.* 1 h, a yellow mixture of liquid and solid material remained. The empty arm of the vessel was cooled to -196 °C while under static vacuum and the yellow material was gently warmed with a heat gun. A colorless liquid distillate was collected, leaving behind a yellow powder. The colorless distillate was redistilled under dynamic vacuum at room temperature using the micro-distillation apparatus depicted in Figure 2.11. Pure FO_2SNH_2 (4.3908 g, 45% yield based on FO_2SNCO) was obtained. ^1H NMR (neat liquid): $\delta(^1H)$ = 5.41 ppm (singlet). ^{19}F NMR (neat liquid): 56.52 ppm (singlet). The FO_2SNH_2 was stored in a ¾-in. o.d. FEP vessel in the drybox. Transfers of FO_2SNH_2 were carried out by pipetting the colorless

liquid directly from the FEP storage vessel inside the drybox.

(xx) Preparation of Natural Abundance and 99.5 % ^{15}N-Enriched $FO_2SNH_3^+AsF_6^-$

The natural abundance and 99.5 % ^{15}N-enriched salts, $FO_2SNH_3^+AsF_6^-$, were prepared from the reaction of AsF_5 with FO_2SNH_2 or $FO_2S^{15}NH_2$ in HF solvent at -40 °C [equation (2.13)]

$$FO_2SNH_2 + HF + AsF_5 \longrightarrow FO_2SNH_3^+AsF_6^- \qquad (2.13)$$

In a typical preparation, natural abundance FO_2SNH_2 (0.3056 g, 3.084 mmol) was pipetted into a ¼-in. o.d. FEP tube equipped with a Kel-F valve. Approximately 0.6 mL of anhydrous HF was condensed onto the FO_2SNH_2 at -196 °C. Warming to -78 °C resulted in a clear colorless solution. The contents of the tube were cooled to -196 °C and 3700 Torr of AsF_5 was expanded into the manifold of a metal vacuum line (manifold volume = *ca.* 19 mL). The AsF_5 was condensed into the tube at -196 °C (3.8 mmol AsF_5 transferred using the ideal gas approximation). Upon warming to -78 °C with constant agitation of the reaction tube, a white precipitate formed with a colorless supernatant. The HF was pumped off at -40 °C over 2 h, resulting in a finely divided white powder (0.7923 g; 88.91% yield).

(C) PREPARATION OF THERMALLY UNSTABLE XENON-NITROGEN AND XENON-OXYGEN BONDED CATIONS

The xenon-nitrogen bonded cations $FO_2SN(H)\text{-}Xe^+$ and $F_5TeN(H)\text{-}Xe^+$ were prepared by combining stoichiometric amounts of FO_2SNH_2 or F_5TeNH_2 with $XeF^+AsF_6^-$ in HF solvent at -196 °C followed by warming to -50 to -30 °C to effect reaction and dissolution. Alternatively,

the xenon-nitrogen bonded cations $FO_2SN(H)\text{-}Xe^+$ and $F_5TeN(H)\text{-}Xe^+$ and the xenon-oxygen bonded cation $CF_3C(OXeF)NH_2^+$ were prepared by combining the hexafluoroarsenate salts of the protonated ligands, namely $FO_2SNH_3^+AsF_6^-$, $F_5TeNH_3^+AsF_6^-$ and $CF_3C(OH)NH_2^+AsF_6^-$ with stoichiometric amounts of XeF_2 in BrF_5 solvent at -196 °C followed by warming to -65 to -50 °C to effect reaction and dissolution. The cation $F_5TeN(H)\text{-}Xe^+$ was also prepared by combining stoichiometric amounts of $F_5TeNH_3^+As(OTeF_5)_6^-$ and $Xe(OTeF_5)_2$ in SO_2ClF solvent at -196 °C followed by warming to -60 °C to effect reaction and dissolution. The xenon-nitrogen and xenon-oxygen bonded cations were characterized in solution by ^{129}Xe, ^{15}N, ^{19}F, ^{1}H, ^{125}Te and ^{13}C NMR spectroscopy and in the solid state by Raman spectroscopy.

(i) <u>Preparation and Isolation of $CF_3C(OXeF)NH_2^+AsF_6^-$</u>

Solid samples of $CF_3C(OXeF)NH_2^+AsF_6^-$ were prepared and characterized by low-temperature Raman spectroscopy. In a typical preparation, 0.1987 g (1.758 mmol) $CF_3C(O)NH_2$ was dissolved in ca. 1 mL of anhydrous HF at -50 °C in a prefluorinated reaction vessel constructed from a ¼-in. o.d. FEP tube equipped with a Kel-F valve. The tube was cooled to -196 °C and 0.5970 g (1.760 mmol) of $XeF^+AsF_6^-$ was added. The sample was warmed to -50 °C with agitation, whereupon approximately 95% of the white solid material dissolved. The supernatant was pale yellow. It was necessary to remove the HF solvent under vacuum very slowly to prevent precipitation of the $CF_3C(OH)NH_2^+AsF_6^-\cdot XeF_2\cdot xHF$ adduct [see Part (iii) of this Section]. The sample was slowly pumped under dynamic vacuum, reducing the solvent volume by *ca.* 75% after 3 h. At this point all of the solid dissolved, and the solution was pale yellow. After a further 3 h of pumping under dynamic vacuum, a free flowing white powder remained. The Raman spectrum indicated the presence of solvated HF from the broad peaks at

3150, 3175, and 3299 cm^{-1}, assignable to HF hydrogen bonded to the amido group. This assignment was made by analogy with bands at 3250, 3393 and 3526 cm^{-1} observed in the infrared spectrum of $CF_3C(O)NH_2$ and HF condensed on a CsI window at 12 K.[135] The HF was removed by pumping at -50 °C for 14.5 h using a glass vacuum line and an intermediate copper U-trap (-196 °C) for HF trapping. Removal of HF was confirmed by the absence of the peaks attributable to hydrogen bonded HF in the low temperature Raman spectrum.

(ii) Preparation of NMR Samples of $CF_3C(OXeF)NH_2^+AsF_6^-$

The $CF_3C(OXeF)NH_2^+$ cation was characterized in BrF_5 solution by ^1H, ^{13}C, ^{19}F and ^{129}Xe NMR spectroscopy. The salt, $CF_3C(OH)NH_2^+AsF_6^-$, (0.01668 g, 0.05504 mmol) was transferred into a 4-mm o.d. FEP tube; the tube was cooled to -196 °C and XeF_2 (0.00985 g, 0.0582 mmol) was added. Bromine pentafluoride (0.3 mL) was condensed onto the walls of the tube above the reagents at -196 °C. The BrF_5 slowly melted upon warming the tube to -60 °C. After agitating for approximately 10 min. at -55 °C, a pale yellow solution resulted. A similar procedure was followed using a 9-mm o.d. FEP tube, and the amounts of reagents were 0.13405 g (0.44250 mmol) $CF_3C(OH)NH_2^+AsF_6^-$, 0.0840 g (0.496 mmol) XeF_2 and 1.7 mL of BrF_5. The tubes were heat sealed under dynamic vacuum at -196 °C and stored at this temperature prior to recording their NMR spectra at -60 to -50 °C.

(iii) Preparation and Isolation of $CF_3C(OH)NH_2^+AsF_6^-\cdot XeF_2\cdot xHF$

In a typical preparation, $CF_3C(OH)NH_2^+AsF_6^-$ (0.0919 g, 0.303 mmol) and XeF_2 (0.0516 g, 0.305 mmol) were combined in a 4-mm o.d. FEP tube at -196 °C and dissolved in ca. 0.4 mL of anhydrous HF at -50 °C, following the same procedure as was used in the preparation of

$CF_3C(OXeF)NH_2^+AsF_6^-$ [see Part (i) of this Section]. Alternatively, the reaction of equimolar amounts of $CF_3C(O)NH_2$ and $XeF^+AsF_6^-$ resulted in the isolation of the same product. The solvent was rapidly pumped off at -50 °C, resulting in the isolation of a free flowing white powder after 1 h. The Raman spectrum (-160 °C) was consistent with the formulation $CF_3C(OH)NH_2^+AsF_6^-\cdot XeF_2\cdot xHF$. The sample was further pumped for 28 h at -50 °C using a glass vacuum line with an intermediate copper U-trap (-196 °C). The Raman spectrum (-160 °C) was still consistent with the formulation, $CF_3C(OH)NH_2^+AsF_6^-\cdot XeF_2\cdot xHF$. Anhydrous HF was then condensed onto the white solid at -196 °C, giving a pale yellow solution after periodic agitation for 15 min at -50 °C (0.55 mL volume). After slow removal of the solvent under dynamic vacuum for 4 h, a white free flowing powder was isolated. The low temperature Raman spectrum was consistent with the formulation $CF_3(OXeF)NH_2^+AsF_6^-$.

(iv) <u>Preparation and Isolation of $F_5TeN(H)\text{-}Xe^+AsF_6^-$ and $[^{15}N]F_5TeN(H)\text{-}Xe^+AsF_6^-$</u>

A typical preparation involved combining XeF_2 (0.0660 g, 0.390 mmol) and $F_5TeNH_3^+AsF_6^-$ (0.1716 g, 0.3995 mmol) in a 4-mm o.d. FEP tube fused to a ¼-in. (7-mm) o.d. T-piece with a Kel-F valve (Figure 2.12). The 4-mm o.d. tube was maintained at -196 °C to prevent reaction of the solids. Anhydrous HF (0.5 mL) was vacuum distilled onto the reagents, resulting in a colorless solution at -40 °C. The solution was warmed to -36 °C, resulting in a pale yellow solution after 5 minutes. The yellow color is attributed to the formation of the $F_5TeN(H)\text{-}Xe^+$ cation in solution. Alternatively, stoichiometric amounts of $XeF^+AsF_6^-$ and F_5TeNH_2 combined in HF solvent as described above result in the generation of the $F_5TeN(H)\text{-}Xe^+$ cation in solution. After 40 minutes, a deposit of orange crystals with a pale yellow supernatant was present. The sample was cooled to -40 °C, resulting in the precipitation of more crystals of the

Figure 2.12 FEP vessel for isolation of $F_5TeN(H)\text{-}Xe^+AsF_6^-$; (A) 4-mm o.d. FEP tube sealed at one and heat-fused to ¼-in. (7-mm) o.d. FEP tubing at the other, (B) ¼-in. (7-mm) o.d. FEP tubing, (C) T connection formed by heat-fusing three ¼-in. o.d. FEP tubes, (D) end heat-sealed, (E) Kel-F valve in aluminum casing.

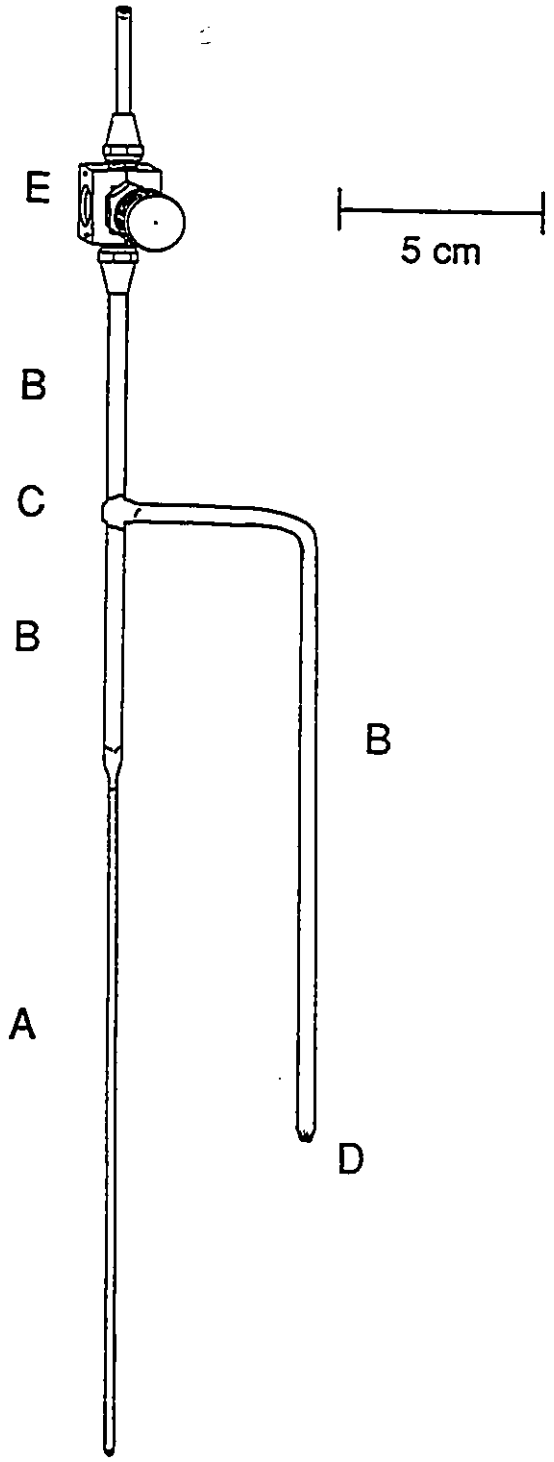
E
5 cm
B
C
B
B
A
D

same morphology and color after 10 minutes. Samples were not cooled below -40 °C since pale yellow and white crystalline materials began to precipitate. The ¼-in. o.d. FEP T-piece was cooled to -78 °C, and the yellow supernatant was decanted into the ¼-in. o.d. tube. Care was taken to prevent warming of the orange crystals above -40 °C, since decomposition occurred. Both ends of the FEP apparatus were cooled to -196 °C, and the tube containing the supernatant was separated from the apparatus using a heat seal. The crystalline precipitate was pumped on at -50 °C for 20 h using a glass vacuum line with an intermediate copper U-trap cooled to -196 °C to remove any remaining HF solvent. Raman spectra were obtained by insertion of the 4-mm o.d. reaction vessel containing the yellow-orange solid directly into the laser beam at low temperature. Violent photodegradation occurred on a sample using a 514.5-nm laser power of 250 mW with the sample at -140 °C. Routine spectra were obtained without decomposition at -160 to -165 °C using laser powers of ≤ 210 mW.

Attempts to mount crystals of $F_5TeN(H)\text{-}Xe^+AsF_6^-$ in glass or quartz capillaries at low temperature failed due to their thermal instability; rapid decomposition occurred above -30 °C.

Identical procedures were used for the preparation and characterization of the $F_5TeN(H)\text{-}Xe^+AsF_6^-$ and $[^{15}N]F_5TeN(H)\text{-}Xe^+AsF_6^-$ salts.

(v) <u>Preparation of NMR Samples of $F_5TeN(H)Xe^+AsF_6^-$ and $[^{15}N]F_5TeN(H)Xe^+AsF_6^-$</u>

Identical conditions were used to prepare NMR samples of $F_5TeN(H)\text{-}Xe^+AsF_6^-$ and $[^{15}N]F_5TeN(H)\text{-}Xe^+AsF_6^-$ for characterization by ^{19}F, ^{1}H, ^{125}Te, ^{129}Xe and ^{15}N NMR spectroscopy. Samples for NMR in HF solvent typically were prepared by combining stoichiometric amounts of F_5TeNH_2 (0.02567 g, 0.1076 mmol) with $XeF^+AsF_6^-$ (0.03630 g, 0.1070 mmol) in a 4-mm o.d. FEP tube at -196 °C, followed by vacuum distillation of HF (ca.

0.2 mL) into the tube. A sample prepared in a 9-mm o.d. FEP tube typically contained 0.1428 g (0.5984 mmol) of F_5TeNH_2 and 0.2010 g (0.5926 mmol) of $XeF^+AsF_6^-$ combined with *ca.* 1.5 mL of HF solvent. The tubes were sealed under vacuum at -196 °C, and warming to -35 °C for *ca.* 50 minutes effected reaction and dissolution, resulting in pale yellow solutions which often contained white and yellow crystalline precipitates. Spectra were typically run at temperatures between -45 and -32 °C. Samples of identical composition were prepared by combining similar molar quantities of $F_5TeNH_3^+AsF_6^-$ and XeF_2 in HF solvent under the same conditions.

Samples for NMR spectroscopy in BrF_5 solvent were prepared by combining at -196 °C similar molar amounts of $F_5TeNH_3^+AsF_6^-$ and XeF_2 as used in the preparations of the 4- and 9-mm o.d. FEP samples in HF solvent (see above, this Section). Approximately 0.3 and 1.5 mL volumes of BrF_5 solvent were then vacuum distilled into the 4-mm and 9-mm o.d. FEP tubes, respectively, at -196°C. After sealing under dynamic vacuum at -196 °C, the tubes were warmed to -40 °C for 10 min., resulting in pale yellow solutions. NMR spectra were run at temperatures between -58 and -44 °C. Complete decomposition of the BrF_5 solutions of $F_5TeN(H)\text{-}Xe^+$ had occurred after several hours at -44 °C, as determined by ^{19}F NMR spectroscopy, resulting in pale purple colored solutions.

(vi) <u>Attempted Preparation of NMR Samples of $F_5TeN(H)\text{-}Xe\text{-}F$</u>

(a) *Reaction of XeF_2 and F_5TeNH_2.* Xenon difluoride (0.01570 g, 0.09274 mmol) and F_5TeNH_2 (0.02074 g, 0.08692 mmol) were combined at -196 °C in a 4-mm. o.d. FEP tube equipped with a Kel-F valve. Sulfuryl chlorofluoride solvent was distilled in at -196 °C and the tube was heat sealed under dynamic vacuum. The sample was warmed to -25 °C, whereupon the XeF_2 remained undissolved, and ^{19}F NMR indicated no F_5Te- group present except that of

F_5TeNH_2. Warming to -12 °C resulted in dissolution of the XeF_2 to give a colorless solution. Fluorine-19 NMR indicated the presence of unreacted F_5TeNH_2 and XeF_2. No change in the ^{19}F NMR spectrum was observed after warming the sample to 0 °C for 10 minutes. The absence of TeF_6 in the ^{19}F NMR indicated that no fluorination of the F_5TeNH_2 by the solvent or XeF_2 occurred in this temperature range. Further warming of the sample was not attempted.

(b) *Reaction of $F_5TeNHSi(CH_3)_3$ and XeF_2.* The compound $F_5TeNHSi(CH_3)_3$ (0.05346 g, 0.1076 mmol) was pipetted into a 4-mm o.d. FEP tube equipped with a Kel-F valve. The tube was cooled to -196 °C and XeF_2 (0.01898 g, 0.1121 mmol) was added. Sulfuryl chlorofluoride solvent was distilled into the tube at -196 °C, and the tube was heat sealed under vacuum as above. The ^{19}F NMR spectrum indicated no reaction upon warming to -12 °C, and resulted in a colorless solution. The absence of TeF_6 and $(CH_3)_3SiF$ in the ^{19}F NMR spectrum indicated that $F_5TeNHSi(CH_3)_3$ was stable to fluorination by XeF_2 and the solvent at -12 °C. Further warming of the sample was not attempted.

(vii) <u>Preparation of NMR Samples of $F_5TeN(H)Xe^+As(OTeF_5)_6^-$ in SO_2ClF Solvent</u>

In a typical preparation, 0.11810 g (0.067637 mmol) of $F_5TeNH_3^+As(OTeF_5)_6^-$ was loaded into a 4-mm o.d. FEP tube equipped with a Kel-F valve. The vessel was cooled to -196 °C and 0.03902 g (0.06413 mmol) of $Xe(OTeF_5)_2$ was added. Sulfuryl chloride fluoride solvent was vacuum distilled into the vessel at -196 °C. The FEP tube was heat sealed under dynamic vacuum at -196 °C followed by warming to -78 °C, which resulted in a clear colorless solution (*ca.* 0.2 M). The ^{19}F, ^{1}H, and ^{129}Xe NMR spectra were initially obtained at -61 °C. Although the solution was initially colorless at this temperature, after 2 h the solution became pale yellow in color. Exchange in the F-on-Te(VI) region complicated the interpretation of the ^{19}F NMR spectra;

however, cooling to -115 °C substantially slowed the exchange without precipitation of the reagents, allowing the assignment of most of the resonances.

(viii) Preparation of NMR Samples of $FO_2SN(H)\text{-}Xe^+AsF_6^-$ and $[^{15}N]FO_2SN(H)\text{-}Xe^+AsF_6^-$

The $FO_2SN(H)\text{-}Xe^+$ cation was generated in BrF_5 solvent and characterized by ^{129}Xe, ^{19}F, and ^1H NMR spectroscopy. Samples were typically prepared by combining 0.0563 g (0.195 mmol) of $FO_2SNH_3^+AsF_6^-$ and 0.0377 g (0.223 mmol) of XeF_2 at -196 °C in a 4-mm o.d. FEP tube equipped with a Kel-F valve. Bromine pentafluoride was vacuum distilled onto the reagents at -196 °C and the sample tube was sealed under vacuum at -196 °C. Warming to -56 °C resulted in the formation of a pale yellow solution (*ca.* 1 M). Dissolution of the XeF_2 crystals required agitation for *ca.* 10 min. at this temperature. NMR spectra were recorded at -58 to -60 °C. Samples in 9-mm o.d. FEP tubes were prepared by combining 0.1219 g (0.4218 mmol) of $FO_2SNH_3^+AsF_6^-$ and 0.0713 g (0.421 mmol) of XeF_2 in BrF_5 solvent (*ca.* 0.27 M) under identical conditions.

(D) NUCLEAR MAGNETIC RESONANCE SPECTROSCOPY

(i) Instrumentation

All NMR spectra were recorded unlocked (field drift < 0.1 Hz h^{-1}) with the use of Bruker AC-200 (4.6975 T), AC-300 (7.0463 T), and AM-500 (11.7440 T) spectrometers equipped with Aspect 2000 or 3000 computers.

Spectra were recorded on samples in heat sealed 9-mm o.d. or 4-mm o.d. FEP NMR tubes as described below. The FEP sample tubes were placed inside 10-mm o.d. or 5-mm o.d. Wilmad

precision thin wall glass NMR tubes before being placed in the probe of the NMR spectrometer.

The ^{129}Xe, ^{15}N, ^{125}Te and ^{13}C NMR spectra were recorded at 11.7440 T in 9-mm o.d. FEP sample tubes (HF, BrF_5 and SO_2ClF solvents) using a 10-mm VSP probe (broad-banded over the frequency range 23 - 202 MHz) tuned to 139.051 (^{129}Xe), 50.698 (^{15}N), 157.795 (^{125}Te) or 125.760 (^{13}C) MHz, respectively. Xenon-129 and ^{1}H NMR spectra of the $FO_2SN(H)$-Xe^+ and $F_5TeN(H)$-Xe^+ cations were also recorded at 7.0463 T in 9-mm FEP tubes (HF solvent) on a 10-mm VSP probe (broad-banded over the frequency range 14 - 121 MHz) tuned to 83.445 (^{129}Xe) and 300.144 MHz (^{1}H) to reduce SA broadening effects which are observed at 11.7440 T. Fluorine-19 (470.599 MHz) and proton (500.138 MHz) spectra were generally recorded at 11.7440 T in 4-mm o.d. FEP tubes (HF, BrF_5 and SO_2ClF solvents) using a 5-mm dual $^{1}H/^{19}F$ probe, except for the ^{1}H NMR spectra of F_5TeNH_2 and $[^{15}N]F_5TeNH_2$, which were recorded at 4.6975 T (200.133 MHz) in 4-mm o.d. FEP sample tubes (CD_2Cl_2 solvent) using a 5-mm ^{1}H probe.

Xenon-129 NMR spectra at 11.7440 T were recorded using 16 - 64 K data points with a spectral width of 50 - 100 kHz and with acquisition times of 0.333 - 0.164 s and data point resolutions of 3.0 - 6.1 Hz/pt (1500 - 21,000 scans). Xenon-129 NMR spectra recorded at 7.0463 T were acquired using 8 K data points with a spectral width of 8474 Hz, an aquisition time of 0.483 s and a data point resolution of 2.1 Hz/pt (19,573 scans). Fluorine-19 NMR spectra were recorded using 1 - 64 K data points with spectral width settings of 2 - 125 kHz, acquisition times of 0.256 - 0.262 s, and data point resolutions of 3.8 - 3.9 Hz/pt (4500 - 11,000 scans). Carbon-13 NMR spectra were recorded using 32 K data points, a spectral width of 50 kHz, an acquisition time of 0.328 s, and a data point resolution of 3.1 Hz/pt (11,475 - 57,000 scans). Proton spectra at 11.7440 T were recorded using 16 - 32 K data points, spectral widths of 10 kHz, acquisition times of 1.638 - 0.820 s and data point resolutions of 0.61 - 1.22 Hz/pt (200 - 400 scans). Proton

NMR spectra at 4.6975 T were recorded using 4 - 32 K data points, spectral widths of 3 - 5 kHz, acquisition times of 0.684 - 1.638 s and data point resolutions of 0.3 - 1.5 Hz/pt (140 - 230 scans). Nitrogen-15 NMR spectra were recorded using 32 K data points, a spectral width of 25 kHz, an acquisition time of 0.655 s and a data point resolution of 1.52 Hz/pt (300 - 500 scans). Tellurium-125 NMR spectra were recorded using 32 - 64 K data points, a spectral width range 25 - 50 kHz, an acquisition time of 0.333 - 0.655 s, and a data point resolution of 1.5 - 3.0 Hz/pt (7000 - 40,850 scans).

Proton-fluorine heteronuclear 2D NOESY spectra of $CF_3C(OH)NH_2^+AsF_6^-$ and $CF_3C(OXeF)NH_2^+AsF_6^-$ in BrF_5 solvent were recorded in the absolute value mode using the pulse sequence reported by Yu and Levy.[136] Spectra were acquired in 16 scans for each of the 128 free induction decays that contained 2K data points in F2 (^{19}F dimension) over a 5 kHz spectral width. The ^{19}F 90° pulse width was 14.3 μs while the ^1H 90° pulse width through the decoupler channel was 9.0 μs. A 1.0 s relaxation delay was employed between aquisitions. A mixing time of 0.25 s was used. Zero-filling in the F1 (^1H) dimension produced a 1K x 2K data matrix with a digital resolution of 7.1 Hz/pt in F2 and 3.5 Hz/pt in F1. During 2D Fourier transformation, a sine-bell squared window function shifted by $\pi/2$ was applied to both dimensions. The transformed data were not symmetrized.

Xenon-129 INEPT spectra of $[^{15}N]F_5TeN(H)\text{-}Xe^+AsF_6^-$ in HF solvent were recorded at 83.468 MHz using a 10 mm VSP probe (broad-banded over the frequency range 14 - 121 MHz). The spectra were acquired over a 15 kHz spectral width in 2K data points (0.682 s acquisition time and a data point resolution of 1.5 Hz/pt). Spectra were obtained using the INEPT pulse sequence with a ^{129}Xe 90° pulse width of 14.0 μs. The ^1H 90° pulse width through the decoupler channel was 20.0 μs. The fixed delay in the INEPT pulse sequence ($0.25\{1/[^2J(^{129}Xe\text{-}^1H)]\}$) was

0.01086 s with a relaxation delay of 1.0 s. The free induction decays were zero-filled to 8K data points and processed using Gaussian multiplication for resolution enhancement (line broadening, -2.5; Gaussian broadening, 0.35) before Fourier transformation.

Pulse widths corresponding to bulk magnetization tip angles of ~90 ° were 18 (11.7440 T) and 14 (7.0463 T) (^{129}Xe), 1 (^{19}F), 6 (^{13}C) and 5 (11.7440 T) and 7 μs (4.6975 T) (^{1}H). Line broadening parameters used in exponential multiplication of the free induction decays were set equal to or less than their respective data point resolutions or the natural line widths of the resonances. All line shape functions were Lorentzian unless specified, where the free induction decays were multiplied by Gaussian functions for resolution enhancement on Fourier transformation. No relaxation delays were applied except for ^{15}N, where relaxation delays of 20 - 120 s were applied.

The respective nuclei were referenced externally to neat samples of $XeOF_4$ (^{129}Xe), $CFCl_3$ (^{19}F), natural abundance CH_3NO_2 (^{15}N), $Te(CH_3)_2$ (^{125}Te) and $(CH_3)_4Si$ (^{13}C and ^{1}H) at 30 °C. Positive chemical shifts were assigned to resonances occurring to high frequency of the reference substance.

For variable temperature measurements, samples were kept cold (-196 or -78 °C) until immediately prior to their placement in the NMR probe. They were generally warmed only enough to liquify and solubilize the contents and were then quickly placed in the precooled probe. Prior to data accumulation, the tubes were allowed to equilibrate in the probe for periods of several minutes while spinning. Temperatures were periodically checked by placing a copper constantan thermocouple into the sampling region of the probe. Temperatures were considered to be accurate to within ±1 °C.

(ii) NMR Sample Preparation

All NMR samples were prepared in sample tubes constructed from 4-mm and 9-mm o.d. FEP tubes. Low volatility compounds such as XeF_2, $XeF^+AsF_6^-$, F_5TeNH_2, $F_5TeNH_3^+AsF_6^-$, FO_2SNH_2, $FO_2SNH_3^+AsF_6^-$ $CF_3C(O)NH_2$ and $CF_3C(OH)NH_2^+AsF_6^-$ were transferred into preweighed FEP sample tubes inside the dry box. The FEP sample tubes were cooled to -196 °C inside the drybox using a cryowell cooled with liquid nitrogen from the outside of the drybox prior to combining reactive reagents. The FEP sample tubes were rapidly removed from the drybox and placed inside a -78 °C temperature bath prior to addition of solvent. The solvents HF and BrF_5 were vacuum distilled into the FEP sample tubes through all fluoroplastic connections using a metal vacuum line. Solvents which do not attack glass in the absence of water vacuum distilled into the reaction tubes using all glass connections.

FEP sample tubes were sealed by immersing the sample in liquid nitrogen and causing the tube to collapse under dynamic vacuum by heating with a small cylindrical electrical tube furnace near the top of the sample tube. The FEP tubes were inserted into thin-walled glass Wilmad NMR tubes prior to placement in the probe of the NMR spectrometer.

(E) RAMAN SPECTROSCOPY

(i) Instrumentation

Raman spectra were recorded on a Jobin-Yvon Mole S-3000 triple spectrograph system equipped with a 0.32-m prefilter, adjustable 25-mm entrance slit, and a 1.00-m monochromator. Holographic gratings were used for the prefilter (600 grooves mm^{-1}, blazed at 500 nm) and monochromator (1800 grooves mm^{-1}, blazed at 550 nm) stages. The 514.5-nm line of an Ar^+ ion

laser was used for excitation of the samples. The spectra of microcrystalline samples of $CF_3C(O)NH_2$, $F_5TeNH_3^+AsF_6^-$, $[^{15}N]F_5TeNH_3^+AsF_6^-$ FO_2SNH_2 and $[^{15}N]FO_2SNH_2$, which were sealed in a baked-out Pyrex melting point capillaries, were recorded at ambient temperature. The Raman spectra of the microcrystalline salts $CF_3C(OH)NH_2^+AsF_6^-$, $CF_3C(OXeF)NH_2^+AsF_6^-$, $CF_3C(OH)NH_2^+AsF_6^-\cdot XeF_2\cdot xHF$ (in 9-mm or 6-mm o.d. FEP tubes), $F_5TeN(H)Xe^+AsF_6^-$ and $[^{15}N]F_5TeN(H)Xe^+AsF_6^-$ (in 4-mm o.d. FEP tubes), $FO_2SNH_3^+AsF_6^-$ and $[^{15}N]FO_2SNH_3^+AsF_6^-$ (in 3-mm medium wall glass tubes) were recorded at -160 to -165 °C in the macro-sample chamber of the instrument. The low temperatures were achieved by flowing dry nitrogen gas, chilled by passing through a 50 L tank of liquid nitrogen, along the outside of the sample tube, which was mounted vertically in an open-ended unsilvered glass Dewar jacket [Figure (2.13)]. The angle between the sample tube and the laser beam was 90° and Raman scattered radiation was observed at 90° to the incident laser beam and at 90° to the sample tube. The temperature was measured using a copper-constantan thermocouple (error ± 0.8 °C). The spectra were recorded by signal averaging using a Spectraview-2D CCD detector equipped with a 25-mm chip (1152 x 298 pixels). The laser powers measured at the samples were 90 ($CF_3C(OXeF)NH_2^+AsF_6^-$ and $CF_3C(O)NH_2$), 190 ($CF_3C(OH)NH_2^+AsF_6^-$), 120 ($CF_3C(OH)NH_2^+AsF_6^-\cdot XeF_2\cdot xHF$), 240 ($F_5TeNH_2$ and $[^{15}N]F_5TeNH_2$), 260 ($F_5TeNH_3^+AsF_6^-$ and $[^{15}N]F_5TeNH_3^+AsF_6^-$, 210 ($F_5TeN(H)Xe^+AsF_6^-$ and $[^{15}N]F_5TeN(H)Xe^+AsF_6^-$), 240 ($FO_2SNH_2$ and $[^{15}N]FO_2SNH_2$) and 260 mW ($FO_2SNH_3^+AsF_6^-$ and $[^{15}N]FO_2SNH_3^+AsF_6^-$). Slit settings corresponded to a resolution of 0.5 - 1 cm^{-1}. A total of 20 - 30 reads having 10 - 40 s integration times were summed for each of the Raman spectra.

Unless otherwise specified, Raman frequencies involving $^{14/15}N$ isotopic studies are estimated to be accurate to ± 0.5 cm^{-1}. As a result $^{14/15}N$ isotopic shifts less than 0.5 cm^{-1} in the

Figure 2.13 Apparatus for low temperature Raman spectroscopy; (A) Kel-F valve flare-sealed (45° SAE) onto FEP tube, (B) rubber septum, (C) unsilvered glass vacuum jacket, (D) copper-constantan thermocouple, (E) glass ball and socket joint, (F) steel mount for adjustment of the sample tube in the laser beam, (G) cold nitrogen gas stream (≥ -170 °C) generated by passing room temperature nitrogen gas into a 50 L tank of liquid nitrogen.

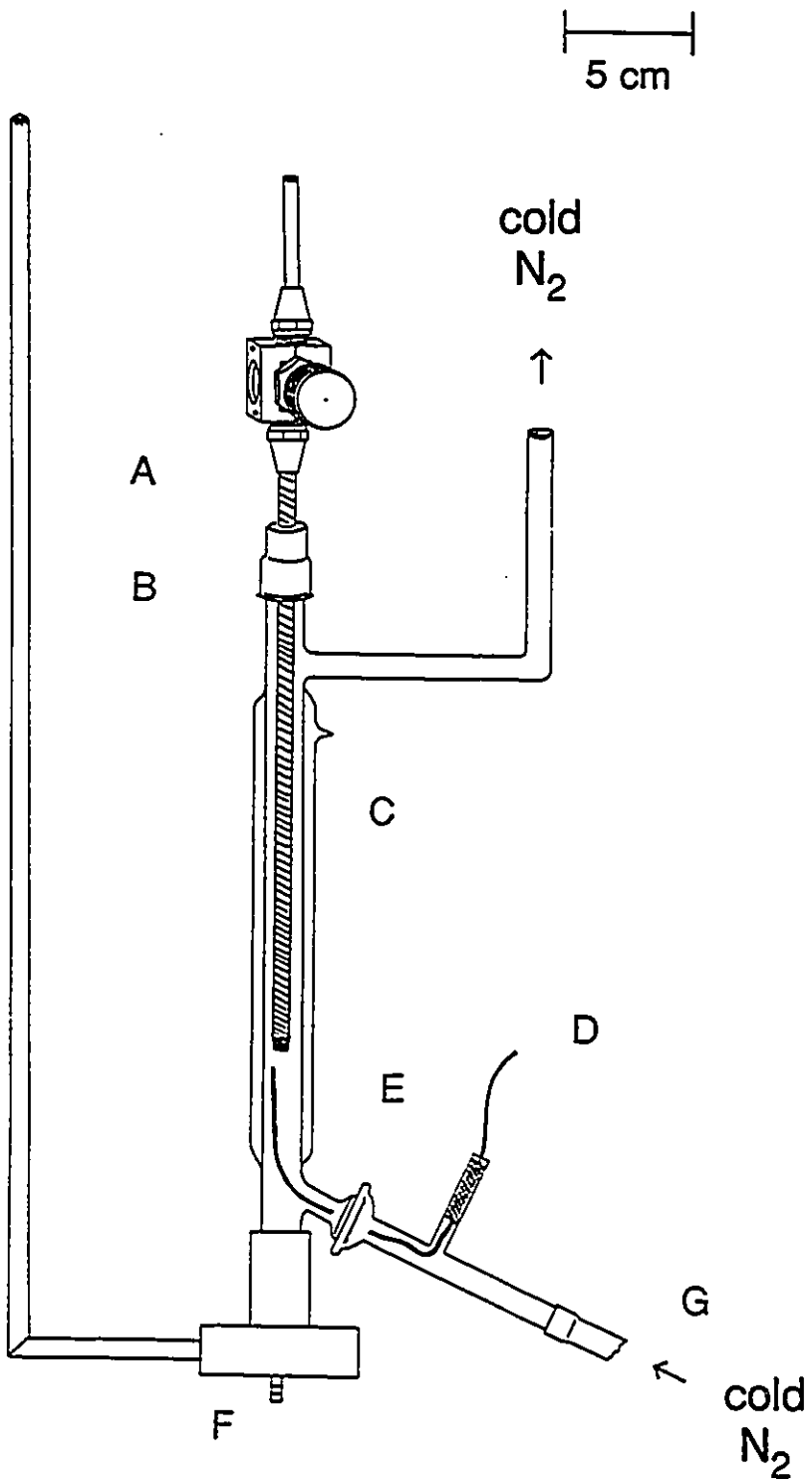
5 cm
cold
N_2
A
B
C
D
E
G
cold
N_2
F

Raman spectra of the natural abundance and 99.5 atom % ^{15}N enriched samples of F_5TeNH_2, $F_5TeNH_3^+AsF_6^-$, $F_5TeN(H)Xe^+AsF_6^-$, FO_2SNH_2 and $FO_2SNH_3^+AsF_6^-$ were considered to be insignificant. The Raman spectra of natural abundance and 99.5% ^{15}N-enriched samples of a givencompound were recorded on the same day using identical conditions in order to minimize systematic errors.

Raman spectra obtained in FEP sample tubes contained lines resulting from the FEP sample tube. The frequencies and intensities of the Raman lines at -154 °C are: 203 (0.2), 278 (0.6), 294 (4.5), 309 (0.9), 381 (3.6), 387 (2.6), 579 (1.3), 598 (0.3), 734 (10.0), 752 (0.9), 1217 (1.2), 1310 (1.6) and 1385 (3.3) cm^{-1}. The prominence of these lines in the Raman spectra depended on the scattering efficiency of the sample and where the laser beam was focussed. In the present work, lines arising from FEP have been subtracted out of the spectra reported in the Tables but not in the Figures.

The Raman spectrometer was calibrated using the 1018.3 cm^{-1} line of vacuum distilled neat liquid indene in a sealed glass melting point capillary at ambient temperature.[137]

(ii) Raman Sample Preparation

The Raman sample vessels constructed from ¼-in. (7-mm) o.d. FEP tubing were heat sealed at one end by pushing the tube into the end of a flame heated piece of glass tubing that had been previously stretched to approximately 0.5-mm at one end using an oxygen torch. Vessels constructed from 4-mm o.d. tubing were heat sealed similarly at one end by pushing the end into a flame heated 5-mm thin-walled glass NMR tube. The other ends of the Raman vessels were heat flared (45° SAE) for direct attachment to a Kel-F valve. All Raman sample vessels were pressurized with dry nitrogen gas (*ca.* 1300 Torr) at -78 °C prior to obtaining the Raman spectrum

at -160 to -165 °C. Low-temperature Raman samples of materials which do not attack glass were run in vessels constructed of 3-mm o.d. medium wall glass tubing. The tubing was flame sealed at one end and attached to a length of ¼-in. o.d. glass tubing at the other. The tubing was then attached using a ¼-in. Teflon union (Swagelok) with Teflon compression fittings (Swagelok) to a glass 4-mm J. Young stopcock equipped with a Teflon barrel. The vessel was vacuum dried and flamed out. Samples were loaded into the tube inside the dry box. The loaded 3-mm o.d. vessels were then flame sealed under vacuum while cooling the sample to -78 or -196 °C. The Raman spectra were obtained directly on the samples contained in the sealed glass tubes at -160 to -165 °C. Samples run at room temperature were loaded into glass melting point capillaries in the drybox and plugged with Kel-F grease. The capillaries were then removed from the drybox and immediately sealed with an oxygen-natural gas microtorch. The sample tubes were stored at -78 °C prior to running the Raman spectra.

CHAPTER 3

SYNTHESIS AND CHARACTERIZATION OF $CF_3C(OXeF)NH_2^+$ AND $CF_3C(OH)NH_2^+AsF_6^-$ AND $CF_3C(OH)NH_2^+AsF_6^-\cdot XeF_2\cdot xHF$ SALTS USING MULTI-NMR AND RAMAN SPECTROSCOPY

INTRODUCTION

The noble-gas cations NgF^+ (Ng = Xe, Kr) have long been known to exhibit Lewis acid character in their salts with weakly fluorobasic anions such as AsF_6^-, SbF_6^- and $Sb_2F_{11}^-$ where the NgF^+ cation interacts with the fluoroanion in the solid state by means of a fluorine bridge.[21] Recently, the Lewis acidities of NgF^+ (Ng = Kr, Xe) cations have been exploited to synthesize novel adduct cations containing Xe-N and Kr-N bonds.[26,71-73,75,78] A variety of oxidatively resistant organic nitrogen bases have now been shown to form adducts with XeF^+, including hydrogen cyanide,[72,73] alkylnitriles,[72] perfluorobenzenenitrile,[72] perfluoroalkylnitriles,[71,72] perfluoropyridines[75] and *s*-trifluorotriazine.[71] Adducts of the strong oxidant cation, KrF^+, with hydrogen cyanide[78] and perfluoroalkyl nitriles,[71] have also been stabilized at low temperatures to give the $R_FC{\equiv}N\text{-}KrF^+$ ($R_F = CF_3$, C_2F_5, $n\text{-}C_3F_7$) and $HC{\equiv}N\text{-}KrF^+$ cations, and provide the only examples of Kr-N bonds presently known. The Ng-N bonds in the cations have been shown by ^{19}F and ^{129}Xe NMR spectroscopy to have high degrees of ionic character.[26,73] The ability of a base to resist oxidation by the strongly oxidizing NgF^+ cations correlates well with the first adiabatic ionization potential (IP_1) of the nitrogen base. It has

been shown that a base having an IP_1-value that is similar to or greater than the estimated electron affinities of XeF^+ (10.9 eV) and KrF^+ (13.2 eV) may be sufficiently resistant to oxidation by NgF^+ to form kinetically stable Ng-N bonds at low temperatures.[26]

Where possible, the general preparative strategy has been straight forward and has entailed the interaction of the appropriate base with an NgF^+ salt in HF solvent. In instances where the protonated form of the base predominates in HF solvent, or when the base is readily oxidized by the noble-gas cation, NgF_2 is allowed to react with the oxidatively more resistant protonated nitrogen base cation in the strongly oxidizing solvent, BrF_5. Equilibrium displacement of HF from the protonated base by the difluoride occurs to a significant extent in BrF_5 solvent at the low temperatures usually required to stabilize the adduct cations. These synthetic approaches are illustrated by the NgF^+ adducts of HC≡N. Hydrogen cyanide (IP_1 = 13.80 eV)[138] forms the adduct cation $HC{\equiv}N\text{-}XeF^+$ upon reaction of HC≡N with $XeF^+AsF_6^-$ or $Xe_2F_3^+AsF_6^-$ in HF solution at -20 to -10 °C,[72,73] whereas the powerful oxidizing ability of KrF^+ requires the reaction of $HC{\equiv}NH^+AsF_6^-$ with KrF_2 in BrF_5 solvent near the melting point of the solvent to prepare the krypton analog, $HC{\equiv}N\text{-}KrF^+AsF_6^-$.[78] A third synthetic approach, which also avoids the use of the strong oxidant NgF^+ cations, is exemplified by the perfluoroalkyl nitriles $R_FC{\equiv}N$ ($R_F = CF_3$, C_2F_5, $n\text{-}C_3F_7$) and relies upon the reaction of the adducts $R_FC{\equiv}N\text{-}AsF_5$ and KrF_2 to form the $R_FC{\equiv}N\text{-}NgF^+$ (Ng = Kr, Xe) adduct cations at low temperatures in BrF_5 solvent.[71]

Oxygen electron-pair donors have not been investigated to any significant extent as bases towards NgF^+ cations. Only one example of a cation containing the O-Xe-F linkage, namely $(CF_3)_2S{=}O\text{-}XeF^+$, has been reported.[85] This cation was prepared by reaction of the sulfurane, $(CF_3)_2S{=}O$, with $XeF^+SbF_6^-$ in HF at -65 °C over a 12 h period; the solid decomposes explosively above -78 °C if mechanically shocked. The present work describes the second example of an

adduct cation containing the O-Xe-F linkage, namely, $CF_3C(OXeF)NH_2^+$ and its characterization in the solid state by low-temperature Raman spectroscopy and in solution by ^{19}F, ^{1}H, ^{13}C and ^{129}Xe NMR spectroscopy.

RESULTS AND DISCUSSION

(A) SYNTHESES AND ISOLATION OF $CF_3C(OH)NH_2^+AsF_6^-\cdot XeF_2\cdot xHF$, $CF_3C(OXeF)NH_2^+AsF_6^-$ AND $CF_3C(OH)NH_2^+AsF_6^-$

The first adiabatic ionization potential of 2,2,2-trifluoroacetamide (10.77 eV)[106] is similar to the estimated electron affinity of the XeF^+ cation (10.9 eV),[73] suggesting that it is potentially resistant to oxidation by XeF^+ under suitable solvent conditions and at low temperature, enabling an Xe-O bonded adduct cation to be formed.

The $CF_3C(OXeF)NH_2^+$ cation results from the HF elimination reaction of the conjugate acid of $CF_3C(O)NH_2$, namely $CF_3C(OH)NH_2^+$, with XeF_2. The strong electrophilic characters of XeF^+ and BrF_5 solvent and nucleophilicities of the oxygen and nitrogen base sites were mitigated by protonation of $CF_3C(O)NH_2$ under superacid conditions by reaction of the amide with excess AsF_5 in HF solvent. Upon removal of the solvent, $CF_3C(OH)NH_2^+AsF_6^-$ was isolated as a white microcrystalline powder in quantitative yield according to equation (3.1), and underwent slow decomposition at room temperature.

$$CF_3C(O)NH_2 + AsF_5 \xrightarrow[-50\ ^\circ C]{HF} CF_3C(OH)NH_2^+AsF_6^- \qquad (3.1)$$

$$CF_3C(OH)NH_2^+AsF_6^- + XeF_2 \xrightleftharpoons[\text{-62 to -55 °C}]{BrF_5} CF_3C(OXeF)NH_2^+AsF_6^- + HF \qquad (3.2)$$

$$CF_3C(O)NH_2 + XeF^+AsF_6^- \xrightleftharpoons[\text{-50 °C}]{HF} CF_3C(OH)NH_2^+AsF_6^- + XeF_2 \qquad (3.3)$$

The salt $CF_3C(OH)NH_2^+AsF_6^-$ was characterized in solution by multi-NMR using BrF_5 as solvent at low temperature. The slow reaction of the $CF_3C(OH)NH_2^+$ cation with BrF_5 solvent at -55 °C is indicated by the presence of broad resonances at $\delta(^1H)$ = 5.2, 3.3 and 2.6 ppm in the ^1H NMR spectrum, which likely result from the rapidly exchanging H-on-N environments of NH_4^+, N_2H_4 and HN_3. A doublet at $\delta(^1H)$ = 5.1 ppm [$^1J(^1H\text{-}^{19}F)$ = 535 Hz] indicated the presence of HF.

Combining stoichiometric amounts of $CF_3C(OH)NH_2^+AsF_6^-$ with XeF_2 in BrF_5 solvent at -62 to -55 °C [equation (3.2)] resulted in the formation of the xenon cation, $CF_3C(OXeF)NH_2^+$. The HF elimination reaction represented by equation (3.2) is directly analogous to the reaction of $CF_3C(O)OH$ and XeF_2 to give the neutral species $CF_3C(O)OXeF$.[39,41,139] The ^{19}F and ^{129}Xe NMR spectra show that the reaction between $CF_3C(O)NH_2$ and $XeF^+AsF_6^-$ does not proceed to any measurable extent in anhydrous HF solvent owing to solvolysis of the reagents; XeF^+ is a strong fluoride ion acceptor in HF solvent and $CF_3C(O)NH_2$ is protonated according to equation (3.3). However, slow removal of HF solvent at -50 °C under dynamic vacuum displaces equation (3.2) toward the right, yielding a pale yellow viscous solution which, after continued pumping, yielded $CF_3C(OXeF)NH_2^+AsF_6^-$ as a white microcrystalline solid. The ^{129}Xe and ^{19}F NMR spectra of solutions of this material in BrF_5 solvent (-60 °C) confirm the presence of the

$CF_3C(OXeF)NH_2^+$ cation. In the solid state, $CF_3C(OXeF)NH_2^+AsF_6^-$ decomposes rapidly with gas evolution and liquefaction at temperatures approaching 0 °C. In contrast, rapid removal of HF solvent from a solution of $XeF^+AsF_6^-$ and $CF_3C(O)NH_2$ under dynamic vacuum at -50 °C results in immediate precipitation of the solvated adduct, $CF_3C(OH)NH_2^+AsF_6^-\cdot XeF_2\cdot xHF$, as a white powder [equation (3.4)]; no $CF_3C(OXeF)NH_2^+AsF_6^-$ was observed in the solid by Raman

$$CF_3C(OH)NH_2^+AsF_6^-{}_{(HF)} + XeF_{2(HF)} \xrightarrow[-50\ ^\circ C]{-\ HF} CF_3C(OH)NH_2^+AsF_6^-\cdot XeF_2\cdot xHF_{(s)} \qquad (3.4)$$

spectroscopy. Elimination of HF from $CF_3C(OH)NH_2^+AsF_6^-\cdot XeF_2\cdot xHF$ did not occur after pumping under dynamic vacuum for 28 h at -50 °C; however, redissolution of the adduct in HF at -50 °C followed by slow removal of the solvent under vacuum resulted in the isolation of pure $CF_3C(OXeF)NH_2^+AsF_6^-$ [see Section (D), below]. The adduct, $CF_3C(OH)NH_2^+AsF_6^-\cdot XeF_2\cdot xHF$, is considered to be an intermediate in the HF elimination reaction of $CF_3C(OH)NH_2^+$ and XeF_2. Although several examples of HF elimination reactions involving XeF_2 and acids, HL, are known (L = FO_2SO-,[37-39,140] CF_3O_2SO-,[140] CH_3O_2SO-,[140] F_5TeO-,[41,46-48,115,141,142] F_5SeO-,[44] ClO_3O-,[140] $CF_3C(O)O$-,[39,41] and $(FSO_2)_2N$-,[56-60]), $CF_3C(OH)NH_2^+AsF_6^-\cdot XeF_2\cdot xHF$, represents the first reported instance of the isolation of an intermediate in an HF elimination reaction involving XeF_2.

(B) <u>CHARACTERIZATION OF $CF_3C(OH)NH_2^+AsF_6^-$ BY ^1H, ^{13}C AND ^{19}F NMR SPECTROSCOPY AND BY TWO DIMENSIONAL (^1H-^{19}F) NOESY EXPERIMENTS</u>

Since the $CF_3C(OXeF)NH_2^+$ cation is in equilibrium with $CF_3C(OH)NH_2^+$ in BrF_5 solvent

[equation (3.2)], unambiguous NMR characterization of the $CF_3C(OXeF)NH_2^+$ cation required a detailed NMR study of $CF_3C(OH)NH_2^+AsF_6^-$ in BrF_5 solution. Although $CF_3C(O)NH_2$ is potentially an ambident base, the ^1H NMR spectrum of $CF_3C(OH)NH_2^+$ AsF_6^- in BrF_5 solvent at -55.4 °C (Figure 3.1) confirms that protonation occurs exclusively at the oxygen and that the oxygen site is more basic (cf. resonance Structures 3.1 and 3.2).

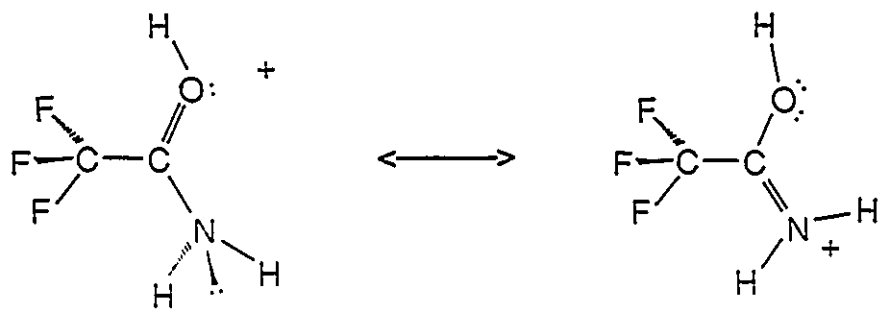

3.1 3.2

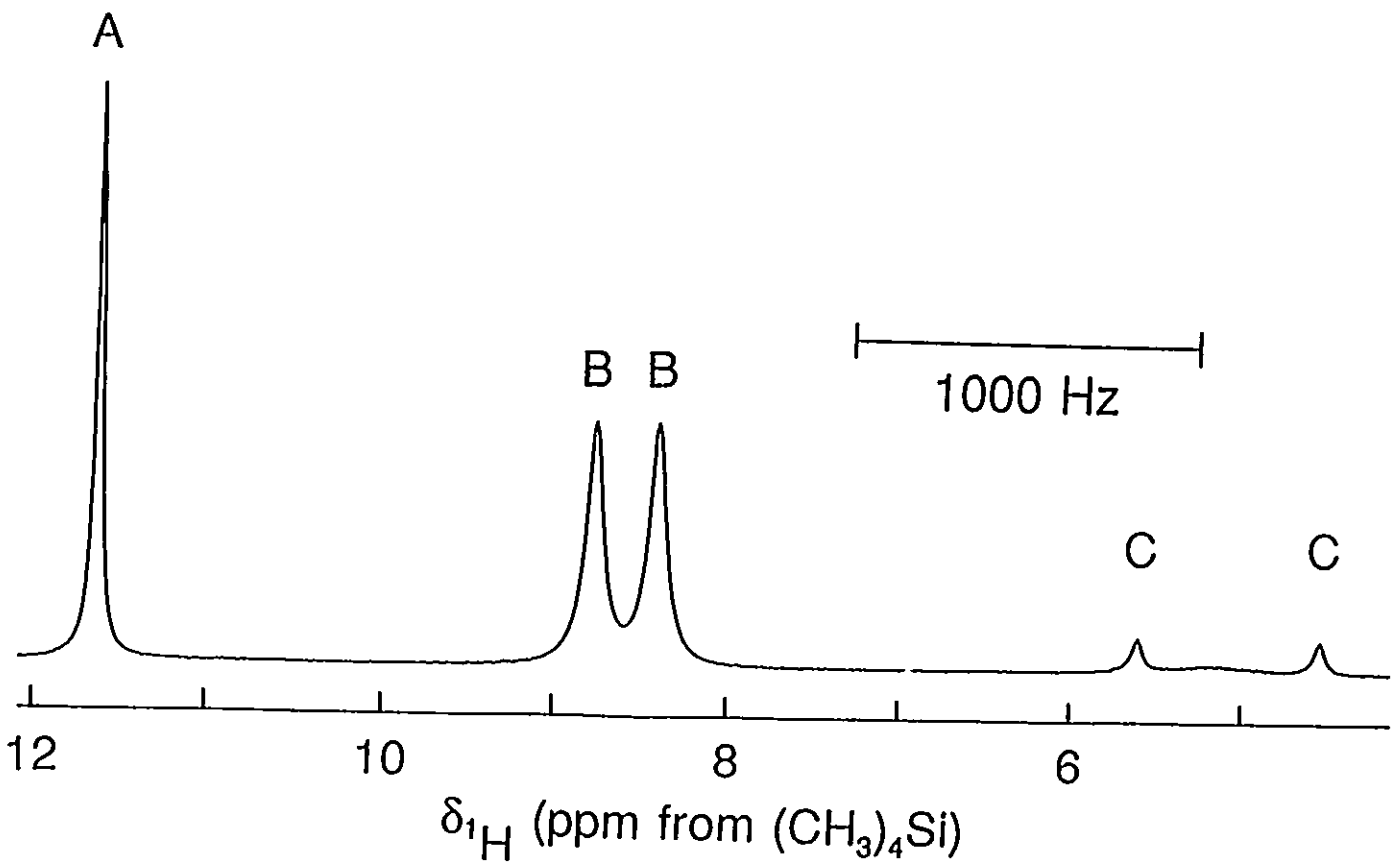

Figure 3.1 ^1H NMR spectrum (500.138 MHz) at -55.4 °C of $CF_3C(OH)NH_2^+AsF_6^-$ (0.25 M) in BrF_5 solvent; (A) proton on oxygen of the protonated carbonyl group, (B) two singlets of equal intensity arising from the chemically inequivalent amido protons, (C) HF.

Previous work has shown that amides are protonated at oxygen in strong acid and superacid media.[143-149] The ^1H NMR resonance of the protonated carbonyl group of the $CF_3C(OH)NH_2^+$ cation is a singlet at $\delta(^1H) = 11.61$ ppm, $\Delta\nu_{1/2} = 20$ Hz, in agreement with the value reported for the protonated carbonyl group of the $FC(OH)NH_2^+$ cation [$\delta(^1H) = 11.07$ ppm, HSO_3F/SO_2 solution at -80 °C].[149] Similar ^1H chemical shifts have been reported for O-protonated acetamide [$\delta(^1H) = 10.72$ ppm, -80 °C],[145] formamide [$\delta(^1H) = 10.81$ ppm, -85 °C],[145] and benzamide [$\delta(^1H) = 10.14$ ppm, -85 °C][144] in HSO_3F solvent. The NH protons of the $CF_3C(OH)NH_2^+$ cation are inequivalent on the NMR time scale (Figure 3.1), giving two broad singlets ($\Delta\nu_{1/2} = 61$ Hz) of equal intensity at 8.75 and 8.38 ppm. The large line widths are primarily attributed to residual one-bond scalar coupling between the protons and ^{14}N (I = 1). The chemical inequivalence of the NH protons is attributed to hindered rotation about the C-N bond, and is consistent with the large barriers to C-N bond rotation found for neutral $[^{15}N]CF_3C(O)NH_2$ in dioxan ($E^{\ddagger} = 76.5 \pm 2.9$ kJ mol^{-1}) and methyl propyl ketone ($E^{\ddagger} = 77.8 \pm 2.5$ kJ mol^{-1}) solvents.[150] Oxygen coordination of amides has been shown to substantially increase the barrier to rotation about the C-N bond by increasing the C-N double bond character relative to that of the free amide.[143] Examples of increases in C-N bond rotational barriers resulting from O-coordination have been extensively studied by NMR spectroscopy and include O-protonation of dimethyl formamide, *N*-methyl formamide and *N*-methyl acetamide in 100% H_2SO_4[146] and O-coordination of BF_3 in *sym*- and *unsym*-dimethylureas[151] and of BX_3 in tetramethylurea (X = Br, Cl, F).[152] In all cases, resonance structures can be drawn, representing "amide-like" linkages containing C-N double bonds which dominate the bonding when oxygen is coordinated to a Lewis acid. Resonance Structure 3.2 represents π-donation from nitrogen to carbon, and is expected to be the dominant contributing structure for the $CF_3C(OH)NH_2^+$ cation [see Section (E) below]. Hindered rotation in protonated

primary amides in acidic solution has been observed in a variety of acidic media and at different temperatures by ^1H NMR spectroscopy. The relative shieldings of the amido proton resonances in the $CF_3C(OH)NH_2^+$ cation cannot be unambiguously assigned by comparison with previously reported examples.[153] However, definitive assignments of the amido protons in the $CF_3C(OH)NH_2^+$ cation were obtained from a two-dimensional heteronuclear (^1H-^{19}F) NOESY experiment performed on a sample of $CF_3C(OH)NH_2^+$ AsF_6^- dissolved in BrF_5 solvent at -58.9 °C (Figure 3.2). A correlation was observed between the ^{19}F NMR resonance of the CF_3 group and both the low-frequency proton-on-nitrogen resonance and the proton-on-oxygen resonance. This experiment utilizes the nuclear Overhauser effect (nOe), which results from a through-space dipolar interaction between nuclei.[154] This effect rapidly diminishes with internuclear distance, so that correlations are only observed for nuclei which are close to one another. The presence of a correlation between the CF_3 group and the low-frequency proton-on-nitrogen resonance indicates that this ^1H resonance arises from the proton cis to the CF_3 group (cf. resonance Structures 3.1 and 3.2). A correlation is also observed between the proton-on-oxygen resonance and the fluorine resonance of the CF_3 group, indicating that intermolecular exchange involving the proton on oxygen is slow relative to dipolar relaxation induced by the fluorine atoms of the CF_3 group. The ^{19}F NMR spectrum of the $CF_3C(OH)NH_2^+$ cation in BrF_5 solvent at -55.4 °C consisted of a singlet at -75.6 ppm assigned to the CF_3 resonance. A value of $^4J(^{19}F\text{-}^1H) = 1.8$ Hz was observed by Akiyama *et al.*[155] for the scalar coupling between the NH proton trans to the carbonyl group and the fluorines of the CF_3 group in $CF_3C(O)NH_2$ at -40 °C in tetrahydrofuran, using ^{19}F NMR spectroscopy. The large line width ($\Delta\nu_{1/2} = 32$ Hz) observed in the ^{19}F NMR spectrum of the $CF_3C(OH)NH_2^+$ cation precluded resolution of the $^4J(^{19}F\text{-}^1H)$ scalar coupling. The quadrupole collapsed ^{19}F NMR resonance of the AsF_6^- anion occurs at -60.7 ppm ($\Delta\nu_{1/2} = 284$ Hz), as

Figure 3.2 Heteronuclear [^{1}H (500.138 MHz)-^{19}F (470.599 MHz)] NOESY spectrum at -58.9 °C of $CF_3C(OH)NH_2^+AsF_6^-$ (0.48 M) in BrF_5 solvent; one-dimensional ^{1}H and ^{19}F NMR spectra are displayed along the vertical and horizontal axes, respectively; (A) proton on oxygen environment of the protonated carbonyl group, (B) amido proton trans to the CF_3 group, (C) amido proton cis to the CF_3 group, (D) fluorine on carbon environment of the $CF_3C(OH)NH_2^+$ cation. The continuous horizontal line of peaks running through the two-dimensional plot is an axial peak artifact along F1 = 0.[182]

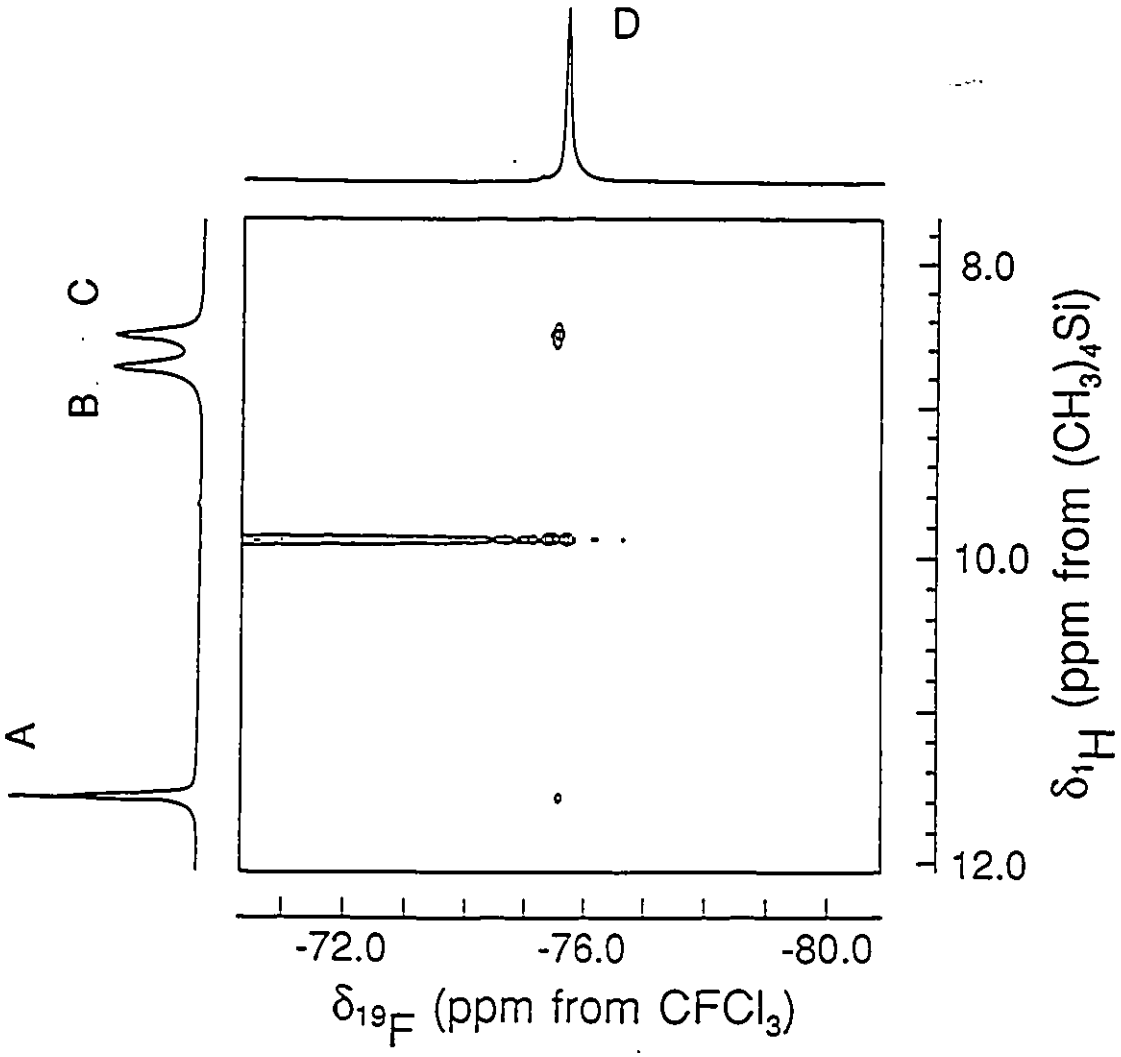
D
C
B
A
8.0
10.0
12.0
$\delta_{^1H}$ (ppm from $(CH_3)_4Si$)
-72.0
-76.0
-80.0
$\delta_{^{19}F}$ (ppm from $CFCl_3$)

previously observed for AsF_6^- in BrF_5 solvent at low temperature.[73] The carbon-13 spectrum of $CF_3C(OH)NH_2^+AsF_6^-$ (-56.2 °C) in BrF_5 solvent consists of two binomial quartets at $\delta(^{13}C)$ = 166.2 [$^2J(^{13}C\text{-}^{19}F)$ = 46 Hz] and at 114.0 ppm [$^1J(^{13}C\text{-}^{19}F)$ = -284 Hz], which are assigned to the COH and CF_3 resonances, respectively, and are similar to those reported for related compounds containing the $CF_3C(O)$- moiety.[156]

(C) CHARACTERIZATION OF $CF_3C(OXeF)NH_2^+AsF_6^-$ BY ^1H, ^{13}C, ^{19}F AND ^{129}Xe NMR SPECTROSCOPY AND BY TWO-DIMENSIONAL ($^1H\text{-}^{19}F$) NOESY EXPERIMENTS

The structure of the $CF_3C(OXeF)NH_2^+$ cation was established in solution by ^1H, ^{13}C, ^{19}F and ^{129}Xe NMR spectroscopy, and is consistent with resonance Structures 3.3 and 3.4.

The ^{129}Xe NMR spectrum of the $CF_3C(OXeF)NH_2^+$ cation consists of a doublet centered at -1578 ppm (-53.0 °C, BrF_5 solvent) arising from $^1J(^{129}Xe\text{-}^{19}F)$ = 5991 Hz, in the region expected for xenon(II) covalently bonded to fluorine (Figure 3.3). The magnitude of $^1J(^{129}Xe\text{-}^{19}F)$ is comparable to other directly bonded $^{129}Xe\text{-}^{19}F$ couplings.[103,104,108] The XeF_2 triplet is also present [$\delta(^{129}Xe)$ = -1572 ppm; $^1J(^{129}Xe\text{-}^{19}F)$ = 5651 Hz] and is consistent with equation (3.2).

In the ^{19}F NMR spectrum, a singlet at $\delta(^{19}F)$ = -183.1 ppm with a satellite doublet [$^1J(^{19}F\text{-}^{129}Xe)$ = 6012 Hz] is assigned to the F-on-Xe(II) of the $CF_3C(OXeF)NH_2^+$ cation (Figure 3.4). The ^{19}F resonance centered at -187.5 ppm with accompanying ^{129}Xe satellites [$^1J(^{129}Xe\text{-}^{19}F)$ = 5650 Hz] is assigned to XeF_2. A doublet centered at -193.1 ppm [$^1J(^{19}F\text{-}^1H)$ = 534 Hz] is assigned to HF formed according to equation (3.2). The ^{19}F NMR resonance of the CF_3 group of the $CF_3C(OXeF)NH_2^+$ cation consists of a singlet at $\delta(^{19}F)$ = -74.4 ppm (-54.0 °C, BrF_5 solvent). The CF_3 group of the $CF_3C(OH)NH_2^+$ cation occurs at $\delta(^{19}F)$ = -75.6 ppm. Integration of the

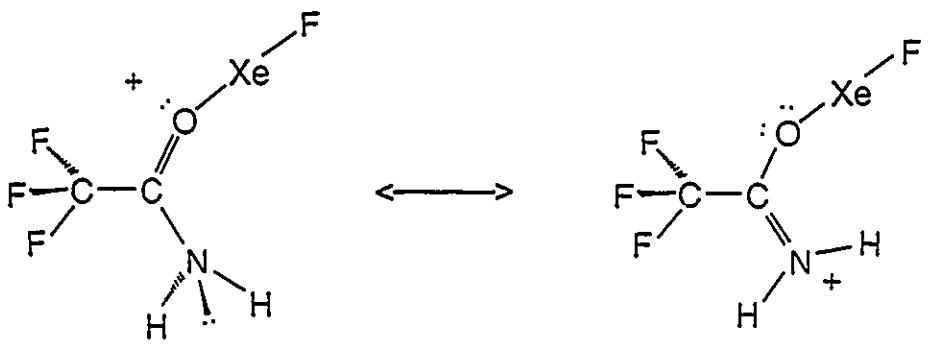

3.3 3.4

^{129}Xe NMR spectrum and F-on-Xe(II) region of the ^{19}F NMR spectrum gave values of 0.29 and 0.30[157] for the ratio $[CF_3C(OXeF)NH_2^+]/[XeF_2]$ (initial molar ratios were $CF_3C(OH)NH_2^+AsF_6^-/XeF_2$ = 0.892 and 0.946; initial $[XeF_2]$ = 0.29 and 0.20 M), respectively. Integration of the CF_3 group resonances gave a value of 0.32[157] for the ratio $[CF_3C(OXeF)NH_2^+]/[CF_3C(OH)NH_2^+]$ (initial molar ratio $CF_3C(OH)NH_2^+AsF_6^-/XeF_2$ = 0.946; initial $[XeF_2]$ = 0.20 M), in good

Figure 3.3 ^{129}Xe NMR spectrum (139.051 MHz) at -53.0 °C of $CF_3C(OXeF)NH_2^+AsF_6^-$ (0.26 M) and XeF_2 (0.29 M) dissolved in BrF_5 solvent; (A) doublet arising from the one-bond coupling $^1J(^{129}Xe\text{-}^{19}F)$ in the $CF_3C(OXeF)NH_2^+$ cation, (B) triplet arising from the one-bond coupling $^1J(^{129}Xe\text{-}^{19}F)$ in XeF_2.

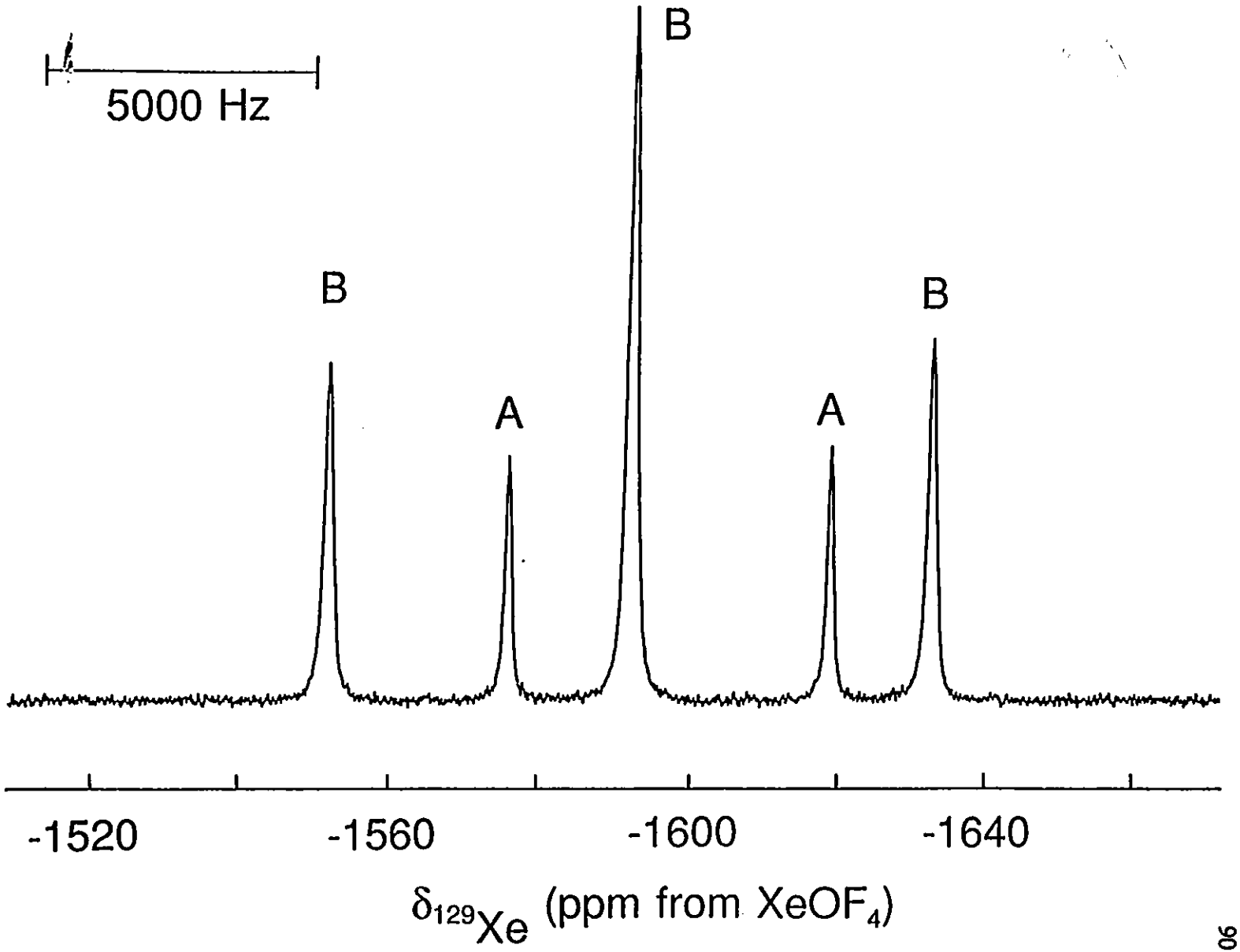
5000 Hz
B
B
A
A
B
-1520
-1560
-1600
-1640
$\delta_{^{129}Xe}$ (ppm from $XeOF_4$)

Figure 3.4 ^{19}F NMR spectrum (470.599 MHz) at -54.0 °C of $CF_3C(OXeF)NH_2^+AsF_6^-$ (0.18 M) and XeF_2 (0.19 M) dissolved in BrF_5 solvent; only the F-on-Xe(II) region is shown; (A) $CF_3C(OXeF)NH_2^+$ cation, (B) singlet arising from the fluorine environment of XeF_2, (C) HF. Lower case letters denote ^{129}Xe satellites.

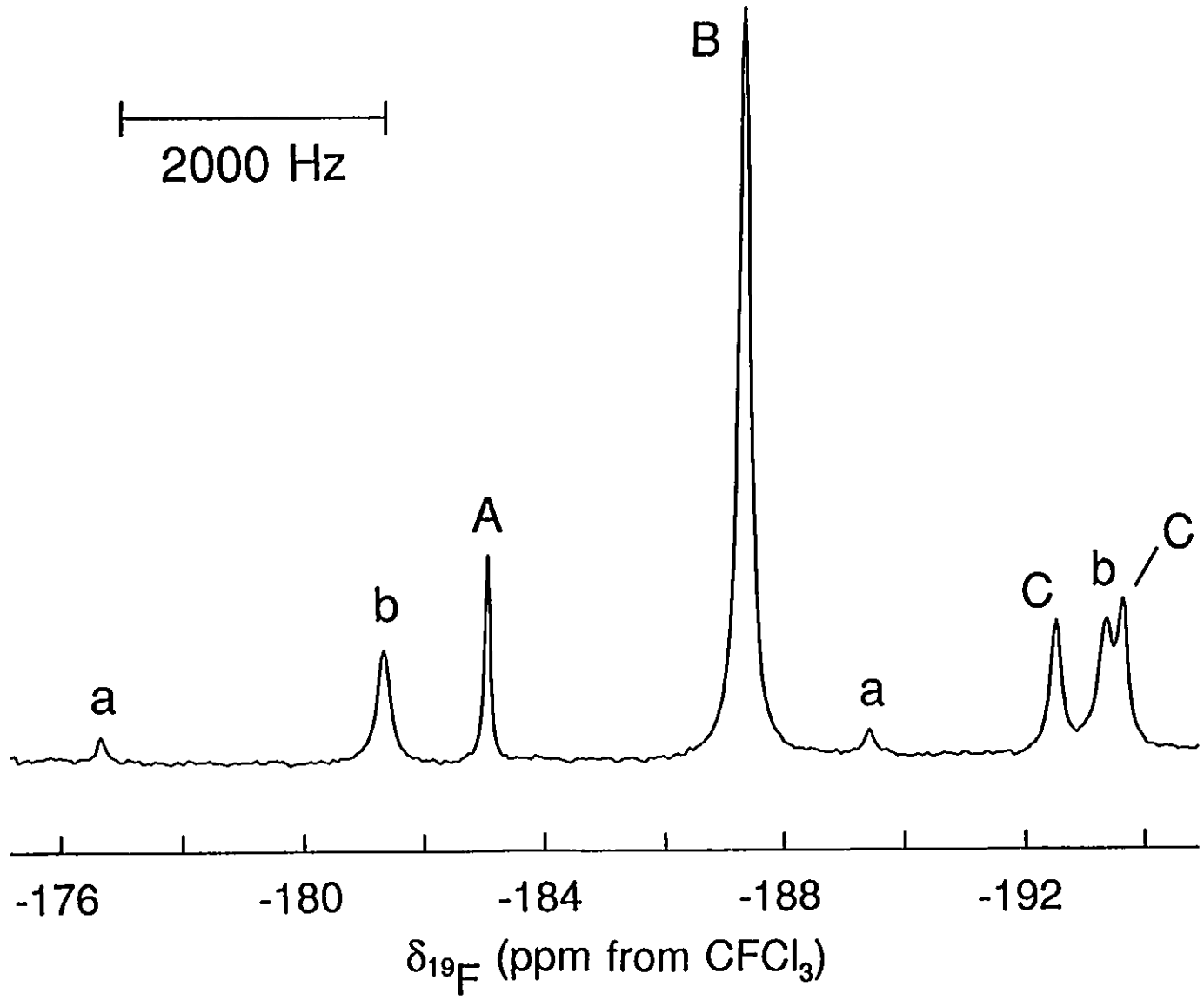
2000 Hz
B
A
b
a
a
C
b
C
-176
-180
-184
-188
-192
$\delta_{^{19}F}$ (ppm from $CFCl_3$)

agreement with values obtained from the ^{129}Xe NMR spectrum and from the ^{19}F NMR spectrum of the F-on-Xe(II) region.

The ^{13}C NMR spectrum of the $CF_3C(OXeF)NH_2^+$ cation (-59.4 °C, BrF_5 solvent) consisted of two binomial quartets at -165.7 ppm [$^2J(^{13}C\text{-}^{19}F)$ = 42 Hz] and at -113.7 ppm [$^1J(^{13}C\text{-}^{19}F)$ = 285 Hz], which were assigned to the CO and CF_3 carbons, respectively. Satellites arising from $^2J(^{13}C\text{-}^{129}Xe)$, were not observed in the ^{13}C NMR spectrum due to a low signal-to-noise ratio.

The ^1H NMR spectrum of an equimolar mixture of $CF_3C(OXeF)NH_2^+AsF_6^-$ and XeF_2 in BrF_5 solvent at -55.0 °C (Figure 3.5) was consistent with equation (3.2). The two broad peaks of equal intensity at 7.88 and 7.71 ppm were assigned to the chemically inequivalent proton-on-nitrogen resonances of the $CF_3C(OXeF)NH_2^+$ cation arising from hindered rotation about the C-N bond. This is consistent with an O-Xe-F linkage, since an N-Xe-F linkage would result in free rotation about the C-N bond, and the observation of only one proton-on-nitrogen resonance in the ^1H NMR spectrum. The proton-on-oxygen resonance of the $CF_3C(OH)NH_2^+$ cation was observed at 12.04 ppm, and was deshielded by 0.41 ppm relative to that of $CF_3C(OH)NH_2^+AsF_6^-$ in BrF_5 solvent at the same temperature (Figure 3.1). The two equal-intensity singlets at 8.48 and 8.39 ppm were assigned to the amido protons of the $CF_3C(OH)NH_2^+$ cation (Figure 3.5); the separation of the peaks is 135 Hz less than that observed for pure $CF_3C(OH)NH_2^+AsF_6^-$ in BrF_5 solvent (Figure 3.1), and is consistent with partial coalescence of the amido protons of the $CF_3C(OH)NH_2^+$ cation arising from proton exchange between the $CF_3C(OH)NH_2^+$ cation and HF, which is present in the system according to equation (3.2). Exchange was confirmed by recording the ^1H NMR spectrum of $CF_3C(OH)NH_2^+AsF_6^-$ in the presence of HF (1.83 molar equivalents of anhydrous HF in BrF_5 solvent at -57.6 °C). Complete collapse of the proton-on-nitrogen resonance to a broadened singlet resulted [$\delta(^1H)$ = 8.59 ppm,

Figure 3.5 ^1H NMR spectrum (500.138 MHz) at -55.0 °C of $CF_3C(OH)NH_2^+$ AsF_6^- (0.18 M) and XeF_2 (0.19 M) dissolved in BrF_5 solvent; (A) proton on oxygen of $CF_3C(OH)NH_2^+$, (B) protons on nitrogen of $CF_3C(OH)NH_2^+$,(C) protons on nitrogen of $CF_3C(OXeF)NH_2^+$, (D) HF.

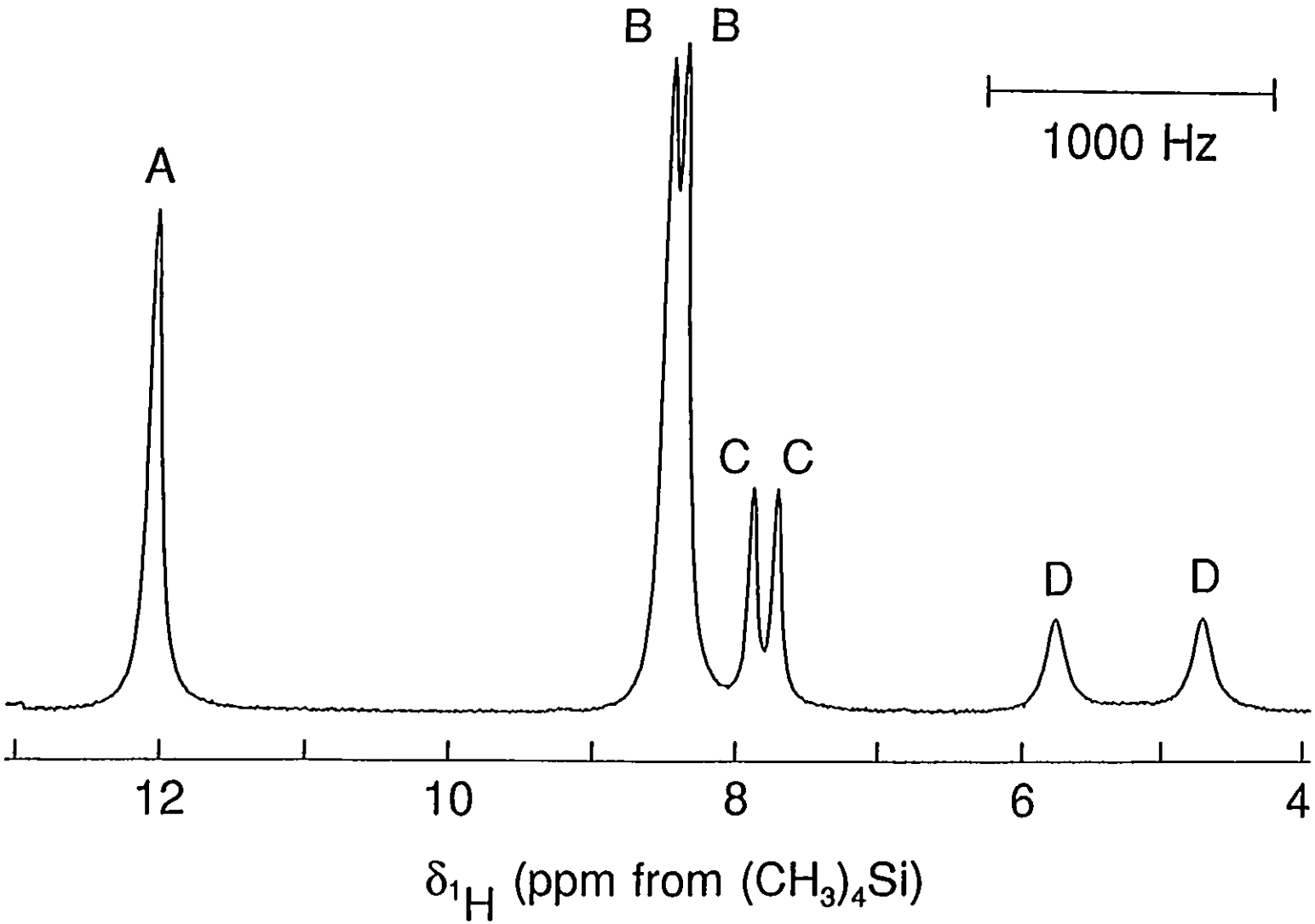
A
B
B
C
C
D
D
1000 Hz
12
10
8
6
4
$\delta_{^1H}$ (ppm from $(CH_3)_4Si$)

Figure 3.6 Heteronuclear [^{1}H (500.138 MHz)-^{19}F(470.599) MHz)] NOESY spectrum at -57.6 ^{o}C of $CF_3C(OH)NH_2^+AsF_6^-$ (0.35 M) and XeF_2 (0.38 M) dissolved in BrF_5 solvent; portions of the one-dimensional ^{1}H and ^{19}F NMR spectra are displayed along the vertical and horizontal axes, respectively; (A) and (B) are the proton on nitrogen resonances of $CF_3C(OH)NH_2^+$, (C) and (D) are the protons on nitrogen which are cis and trans to the CF_3 group, respectively, in $CF_3C(OXeF)NH_2^+$, (E) CF_3 group resonance of $CF_3C(OXeF)NH_2^+$, (F) CF_3 group resonance of $CF_3C(OH)NH_2^+$.

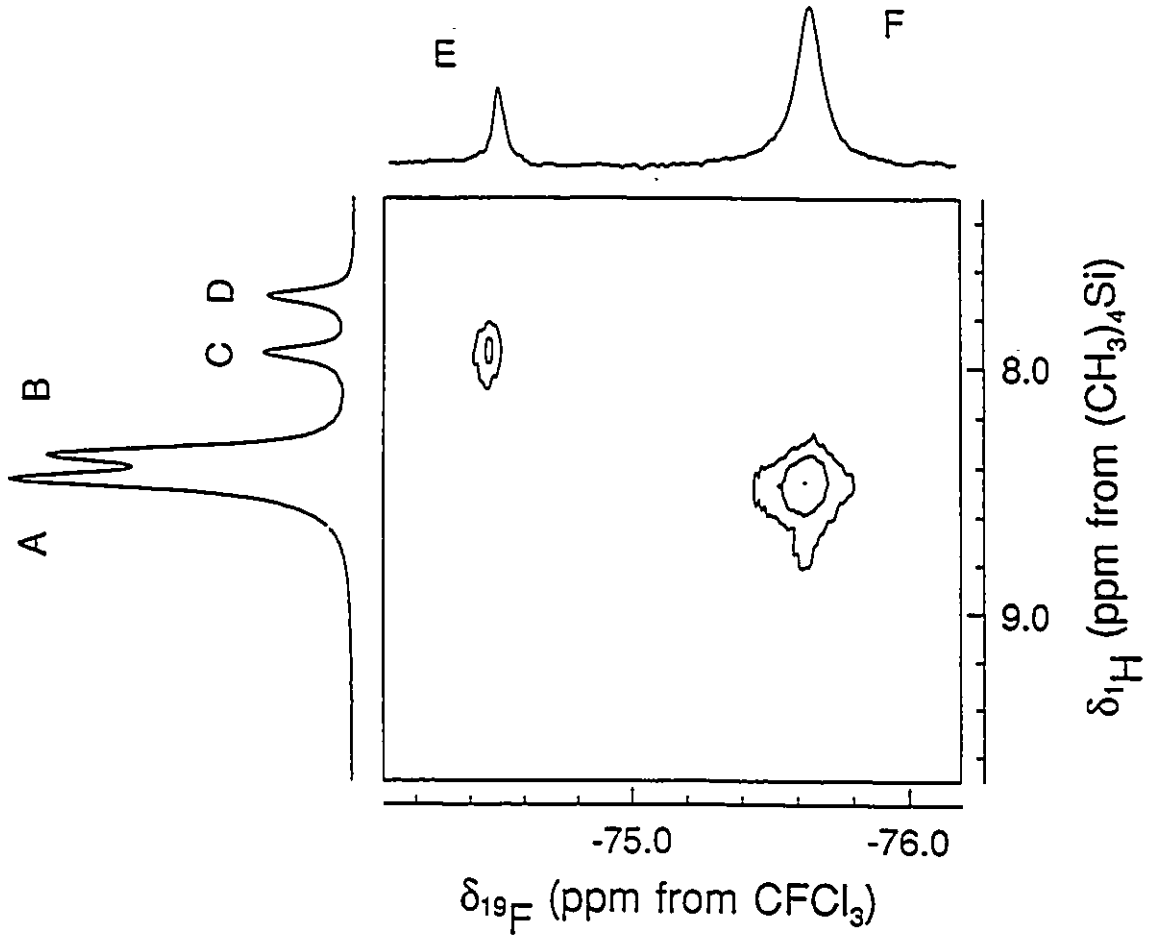
A
B
C
D
E
F
8.0
9.0
$\delta_{^1H}$ (ppm from $(CH_3)_4Si$)
-75.0
-76.0
$\delta_{^{19}F}$ (ppm from $CFCl_3$)

$\Delta\nu_{1/2}$ = 88 Hz] with retention of the proton-on-oxygen resonance [$\delta(^1H)$ = 11.68 ppm]. Coalescence of the amido proton peaks can arise from two possible mechanisms: deprotonation to give the amidic acid, $CF_3C(OH)=NH$, [equation (3.5)], and N-protonation to give the $CF_3C(OH)NH_3^{2+}$ dication [equation (3.6)]. Both equilibria would account for retention of the

$$CF_3C(OH)=NH_2^+ + HF \rightleftharpoons CF_3C(OH)=NH + H_2F^+ \qquad (3.5)$$

$$CF_3C(OH)=NH_2^+ + 2\,HF \rightleftharpoons CF_3C(OH)\text{-}NH_3^{2+} + HF_2^- \qquad (3.6)$$

proton-on-oxygen resonance. Equation (3.5) can be discounted since the amidic acid mechanism has been shown to be inhibited by strong acid (H_2SO_4), and contributes to proton exchange only in dilute aqueous acid.[147] The transient diprotonated cation, $CF_3C(OH)\text{-}NH_3^{2+}$ [equation (3.6)], could undergo free rotation about the C-N bond, resulting in partial collapse of the amido proton doublet with retention of the proton on oxygen resonance.

The protons on nitrogen of $CF_3C(OXeF)NH_2^+$ were assigned by performing a two-dimensional heteronuclear (^1H-^{19}F) NOESY experiment in BrF_5 solvent at -57.6 °C (Figure 3.6). A correlation was observed between the ^{19}F NMR resonance of the CF_3 group and the high-frequency [$\delta(^1H)$ = 7.88 ppm] proton on nitrogen resonance of the $CF_3C(OXeF)NH_2^+$ cation, implying that the high-frequency ^1H NMR resonance arises from the proton cis to the CF_3 group (trans to the OXeF group). It is interesting that the relative shieldings of the proton-on-nitrogen resonances for the $CF_3C(OXeF)NH_2^+$ cation are opposite to those observed for the $CF_3C(OH)NH_2^+$ cation. The change in relative shieldings may result from differences in electronic anisotropy resulting from the different moieties bonded to oxygen in the $CF_3C(OXeF)NH_2^+$ and

$CF_3C(OH)NH_2^+$ cations. The CF_3 group in the $CF_3C(OH)NH_2^+$ cation correlates with both the cis and trans protons of the amido group (Figure 3.6). This is attributed to insufficient resolution of the partially coalesced proton on nitrogen resonances for the $CF_3C(OH)NH_2^+$ cation resulting from exchange with HF (see above).

(D) CHARACTERIZATION OF $CF_3C(OXeF)NH_2^+AsF_6^-$ BY LOW-TEMPERATURE RAMAN SPECTROSCOPY

Assignments for the $CF_3C(OXeF)NH_2^+$ cation (Table 3.1 and Figure 3.7) were based on the Raman spectra of $CF_3C(O)NH_2$[161] and related compounds containing the O-Xe-F linkage.[41,42,85,140,158] Assignments for the AsF_6^- anion were made by comparison with those of $XeF^+AsF_6^-$,[158] $HC{\equiv}NXeF^+AsF_6^-$,[73] and $O_2^+AsF_6^-$.[159]

Evidence for the O-Xe-F linkage is provided by the characteristic bands arising from O-Xe-F stretching and bending fundamentals. Five bands are observed in the ν(Xe-O) and ν(Xe-F) regions. The intense bands at 543 and 530 cm^{-1} are assigned to ν(Xe-F) by comparison with the assigned Xe-F stretches in related xenon(II) compounds: FO_2SOXeF (539, 532, 527, 521 cm^{-1}),[158] *cis*- and *trans*-$F_4OIOXeF$ (527 cm^{-1}),[42] $F_5TeOXeF$ (520 cm^{-1}),[41] CF_3O_2SOXeF (534 cm^{-1}),[140] and $(CF_3)_2S{=}OXeF^+SbF_6^-$ (552 cm^{-1}).[85] The bands at 508, 502 and 476 cm^{-1} are assigned to ν(Xe-O) by comparison with the assigned Xe-O stretches in FO_2SOXeF (434 cm^{-1}),[158] *cis*- and *trans*-$F_4OIOXeF$ (488, 438 cm^{-1}),[42] $F_5TeOXeF$ (457 cm^{-1}),[41] CF_3O_2SOXeF (369 cm^{-1}),[140] and $(CF_3)_2S{=}OXeF^+SbF_6^-$ (494 cm^{-1}).[85] The splitting of the ν(Xe-F) and ν(Xe-O) bands may result from vibrational coupling of two or more cations in the unit cell (factor-group splitting), but cannot be confirmed without knowledge of the crystal structure of $CF_3C(OXeF)NH_2^+AsF_6^-$. Site-symmetry effects can be eliminated as the source of the splitting since the highest possible point-

Figure 3.7 Raman spectrum of microcrystalline $CF_3C(OXeF)NH_2^+AsF_6^-$ (-165 °C) recorded in an FEP sample tube using 514.5-nm excitation. Asterisks (*) denote FEP sample tube lines.

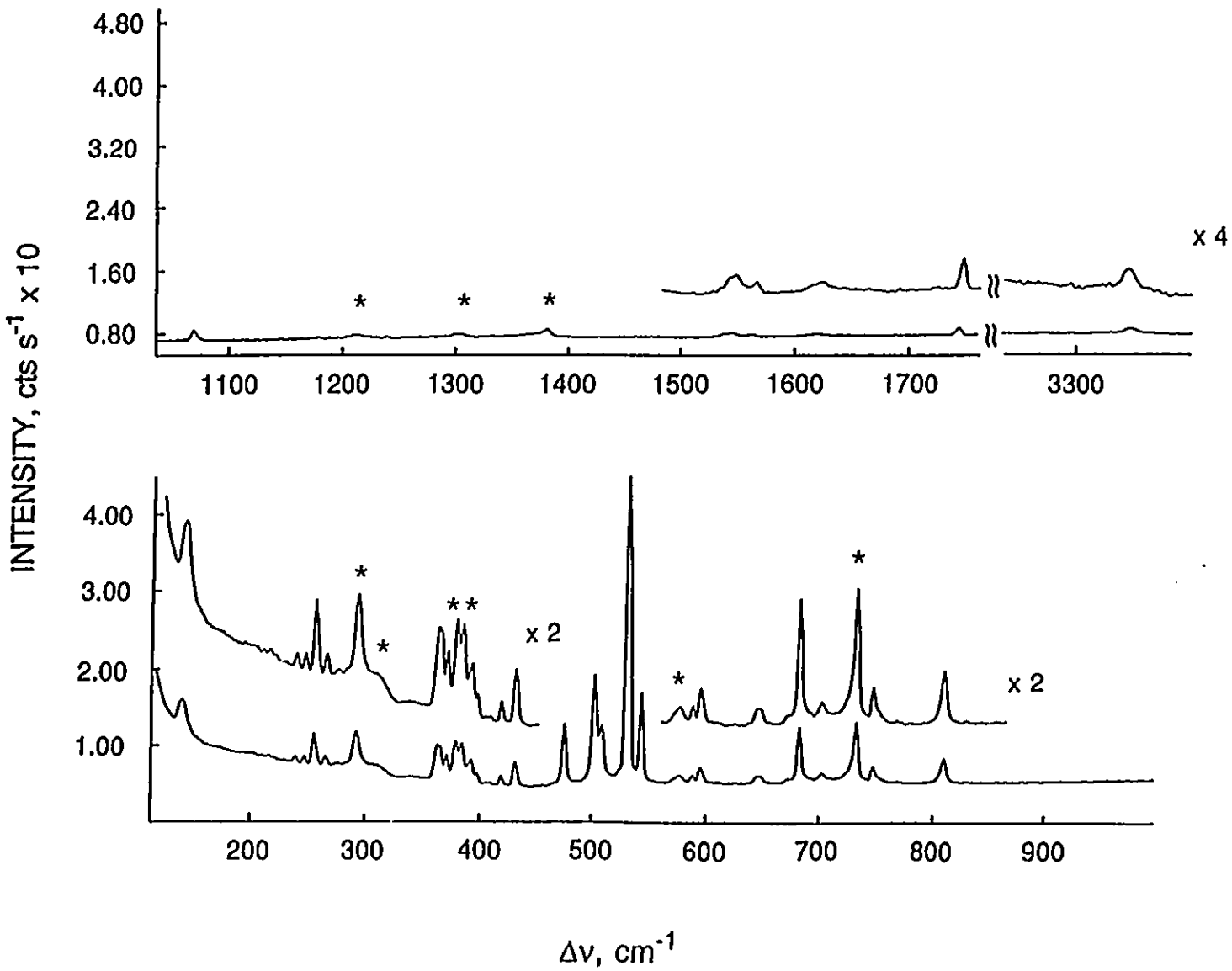
INTENSITY, cts s-1 x 10
4.80
4.00
3.20
2.40
1.60
0.80
1100
1200
1300
1400
1500
1600
1700
3300
x 4
4.00
3.00
2.00
1.00
200
300
400
500
600
700
800
900
x 2
x 2
Δν, cm-1

group symmetry for the $CF_3C(OXeF)NH_2^+$ cation is C_s, which does not possess any degenerate irreducible representations. Similar band splittings for modes assigned to ν(Xe-F) are observed in the Raman spectra of $HC{\equiv}N\text{-}XeF^+AsF_6^-$,[73] FO_2SOXeF,[158] and $XeF^+MF_6^-$ salts (M = Ru, Pt, Ir).[67] It is interesting to compare the ν(Xe-O) and ν(Xe-F) stretching modes of the $CF_3C(OXeF)NH_2^+$ cation with those of the $(CF_3)_2S{=}OXeF^+$ cation, since these are the only reported examples of cations containing the O-Xe-F linkage. The ν(Xe-F) and ν(Xe-O) Raman bands in the structurally related $(CF_3)_2S{=}O\text{-}XeF^+$ cation were observed at 552 and 494 cm^{-1}, respectively.[85] The average of the bands assigned to ν(Xe-O) for the $CF_3C(OXeF)NH_2^+$ cation, 495 cm^{-1}, is very similar to ν(Xe-O) in the $(CF_3)_2S{=}O\text{-}XeF^+$ cation, and the average of the bands assigned to ν(Xe-F) for the $CF_3C(OXeF)NH_2^+$ cation, 536 cm^{-1}, is 16 cm^{-1} lower than ν(Xe-F) for the $(CF_3)_2S{=}O\text{-}XeF^+$ cation. Raman spectroscopic trends in the terminal Xe-F stretches of xenon(II) compounds indicate a more ionic Xe-F bond in the $CF_3C(OXeF)NH_2^+$ cation than in the $(CF_3)_2S{=}O\text{-}XeF^+$ cation [see Section (G) of this Chapter]. The bands at 141 and 292 cm^{-1} are assigned to the O-Xe-F and C-O-Xe bending modes, respectively. Comparable values for δ(O-Xe-F) and δ(X-O-Xe) are observed in structurally related xenon(II) compounds containing the O-Xe-F linkage.[41,42,85,140,158]

The band at 3335 cm^{-1} in the Raman spectrum of $CF_3C(OXeF)NH_2^+AsF_6^-$ is assigned to an NH stretching mode. Two bands are usually observed in the vibrational spectra of primary amides arising from the symmetric and asymmetric NH_2 stretches.[160] Although peaks observed at 3174 and 3337 cm^{-1} can be assigned to $\nu_{sym}(NH_2)$ and $\nu_{asym}(NH_2)$, respectively, in the Raman spectrum of solid trifluoroacetamide,[161] it is not possible to assign the NH stretch of $CF_3C(OXeF)NH_2^+AsF_6^-$ to a particular symmetry species since the bands observed in this region for O-complexed amides are often not directly comparable to the bands of the free amide.[162,163] The out-of-plane wag of the NH_2 group, $\omega(NH_2)$, is assigned to the band at 672 cm^{-1} by

comparison with $CF_3C(O)NH_2$ (666 cm^{-1}),[161] and the frequency increase (6 cm^{-1}) is attributed to O-coordination of $CF_3C(O)NH_2$ to the XeF^+ cation and an attendant increase in C-N double bond character. This mode is observed at 639 cm^{-1} in matrix isolated $CF_3C(O)NH_2$, and complexation with HF by bridging of the HF molecule between oxygen and an NH proton results in an increase of 17 cm^{-1}.[164] The fundamental arising from the torsional motion of the NH_2 group, $\tau(NH_2)$, is tentatively assigned to the band at 810 cm^{-1} by analogy with solid $CF_3C(O)NH_2$ (796 cm^{-1}).[161] The increase in $\tau(NH_2)$ (14 cm^{-1}) is attributed to an increase in C-N double bond character resulting from O-coordination. The rocking motion fundamental, $\gamma(NH_2)$, is not observed in the Raman spectrum of $CF_3C(OXeF)NH_2^+AsF_6^-$, but is observed as a weak band at 1199 cm^{-1} in the Raman spectrum of solid $CF_3C(O)NH_2$.[161] The band at 1623 cm^{-1} has been assigned primarily to the in-plane bending mode, $\delta(NH_2)$, which is 6 cm^{-1} lower than that observed for $CF_3C(O)NH_2$. This mode is relatively insensitive to complexation, as observed for several primary amides and their HF complexes.[164]

The bands at 1543, 1562 and 1745 cm^{-1} result from the $\nu(CO)$ and $\nu(CN)$ stretching modes. Although vibrational coupling of these modes is likely, $\nu(CO)$ is formally assigned to the bands at 1543 and 1562 cm^{-1} (Table 3.1) following the method of assignment for amidium salts,[165] which are electronically similar to the $CF_3C(OXeF)NH_2^+$ cation. The CO stretching frequency is expected to be lower than that of uncomplexed $CF_3C(O)NH_2$ because the double-bond character of the C-O linkage is significantly reduced upon O-coordination. This implies dominance of resonance Structure 3.4 in the bonding of the $CF_3C(OXeF)NH_2^+$ cation. Correspondingly, the C-N stretch is expected to increase significantly and is assigned to the band at 1745 cm^{-1}, which is close to the observed range for $\nu(CN)$ in the infrared spectra of O-protonated and O-alkylated amides[166] (ca. 1600 - 1730 cm^{-1}). Unambiguous evidence for the reversal of $\nu(CO)$ and $\nu(CN)$

frequencies upon O-protonation of amides has been provided by Cook,[167] who compared the infrared spectra of *N*-acyltrialkylammonium halides and O-protonated *N,N*-dicyclohexylacetamide hydrohalide salts. Since the former are isoelectronic with the hypothetical N-protonated amides, a direct comparison of the infrared spectra of these salts with those of the neutral compounds aided in the assignment of the ν(CO) and ν(CN) bands. Following previously published assignments,[161] the bands at 1706 and 1460 cm^{-1} in the Raman spectrum of $CF_3C(O)NH_2$ are assigned to ν(CO) and ν(CN), respectively. When compared to $CF_3C(OXeF)NH_2^+AsF_6^-$, these values show a decrease in ν(CO) of 154 cm^{-1} and an increase in ν(CN) of 285 cm^{-1} in the xenon cation. Similar values of ν(CO) and ν(CN) have been reported from the infrared spectra of protonated amides; for example, ν(CO) for the O-protonated salt of *N,N*-dimethylacetamide, $CH_3C(OH)N(CH_3)_2^+SbCl_6^-$,[165] is observed at 1401 cm^{-1} and that of *N,N*-dimethylacetamide vapor is observed at 1651 cm^{-1} [Δν(CO) = 250 cm^{-1}],[168] whereas the value of ν(CN) increases to 1680 cm^{-1} (average of three bands) upon O-protonation of *N,N*-dimethylacetamide,[165] compared to 1492 cm^{-1} for the amide vapor [Δν(CO) = 188 cm^{-1}].[168] An incomplete report of the infrared spectrum of $CF_3(O)NH_2{\cdot}BF_3$ provides a value of 1760 cm^{-1} for ν(CO).[169] If $CF_3(O)NH_2{\cdot}BF_3$ is indeed O-bonded, it is likely that ν(CO) has been misassigned in light of the well established trends noted above for ν(CO) and ν(CN).

The in-plane (δ) and out-of-plane (π) OCN bends are tentatively assigned to the peak at 596 cm^{-1} by analogy with $CF_3C(O)NH_2$,[161] assuming that they are similar in the $CF_3C(OXeF)NH_2^+$ cation.

The CF_3 group modes of $CF_3C(OXeF)NH_2^+$ are assigned by analogy with those in Raman spectrum of solid $CF_3C(O)NH_2$: 1073 [$\nu_{asym}(CF_3)$], 747 [$\delta_{sym}(CF_3)$], 523 [$\delta_{asym}(CF_3)$] and 432, 419 cm^{-1} [$\gamma(CF_3)$]. The symmetric stretch, $\nu_{sym}(CF_3)$, is not observed in the Raman spectra of

$CF_3C(O)NH_2$ and $CF_3C(OXeF)NH_2^+$, but is observed at 1340 cm^{-1} in the infrared spectrum of $CF_3C(O)NH_2$.[161] The symmetric stretch of the CF_3 group is not observed in the Raman spectrum of the $CF_3C(OXeF)NH_2^+$ cation, because it is too weak and/or because it coincides with an FEP sample tube band at 1384 cm^{-1}.

A total of 21 bands are assigned to the AsF_6^- anion, and are derived from the six normal modes for AsF_6^- under O_h point symmetry.[170] Since only three bands [$\nu_1(A_{1g})$, $\nu_2(E_g)$, and $\nu_5(F_{2g})$] are Raman active for O_h symmetry, a reduction of anion symmetry is apparent. A symmetry of C_{2v} or C_s would account for the observation of 15 normal modes, since all mode degeneracies would then be removed. The apparent reduction in anion symmetry may result in part from a low site symmetry for the AsF_6^- anion in the unit cell, or from a true distortion of the molecular geometry of the anion due to hydrogen bonding interactions with the protons of the cation, as observed in the SbF_6^- and AsF_6^- salts of OH_3^+,[171] SH_3^+,[172] and $NF_2H_2^+$.[173] The observation of more than 15 bands is attributed to intermolecular vibrational coupling within the crystallographic unit cell. This is likely since low site symmetry alone cannot account for the splitting of the non-degenerate $\nu_1(A_{1g})$ mode for AsF_6^- (647, 683 cm^{-1}). A crystal structure is required, however, to confirm these assignments (factor group analysis).

(E) CHARACTERIZATION OF $CF_3C(OH)NH_2^+AsF_6^-$ BY LOW-TEMPERATURE RAMAN SPECTROSCOPY

The assignments for the Raman spectrum of $CF_3C(OH)NH_2^+AsF_6^-$ were made by analogy with those of $CF_3C(O)NH_2$[161] and $CF_3C(OXeF)NH_2^+AsF_6^-$ (Table 3.1 and Figure 3.8). The ν(CO) and ν(CN) modes are assigned to the bands at 1519 and 1767 cm^{-1}, indicating greater double-bond character for the C-N bond than for the C-O bond and are similar to those of $CF_3C(OXeF)NH_2^+$.

Table 3.1. Raman Frequencies[a] and Assignments for $CF_3C(O)NH_2$, $CF_3C(OH)NH_2^+AsF_6^-$, $CF_3C(OH)NH_2^+AsF_6^-\cdot XeF_2 \cdot xHF$, and $CF_3C(OXeF)NH_2^+AsF_6^-$.

$CF_3C(O)NH_2$[b]	$CF_3C(OH)NH_2^+$ AsF_6^-[c]	$CF_3C(OH)NH_2^+AsF_6^-$ $\cdot XeF_2 \cdot xHF$[c]	$CF_3C(OXeF)NH_2^+$ AsF_6^-[c]	Assignments
3337 (7)		3336 (0.2)[e]		$\nu_{asym}(NH_2)$
	3227 (3)[d]		3355 (1)[d]	
	3211 (3)[d]			
3174 (11)		3205 (0.9)[f]		$\nu_{sym}(NH_2)$
		3090 (1.5)		$\nu_{sym}(HF)$
1706 (40)	1519 (3)	1549 (2)	1562 (1)	$\nu(CO)$
			1543 (1)	
1629 (5)	f	1631 (0.4)	1623 (0.5)	$\delta(NH_2)$
1460 (31)	1767 (5)	1750 (1.5)	1745 (2)	$\nu(CN)$
	1276 (5)	1262 (3)		$\delta(OH)$
		1232 (4)		
1199 (4)	1197 (3)	1202 (1)	d	$\gamma(NH_2)$
		1182 (2)		
f	1314 (11) or	1308 (0.5) or	1304 (1) or	$\nu_{sym}(CF_3)$
	1384 (19)[g]	1385 (1)[g]	1384 (4)[g]	
1135 (100)	1218 (7)[g]	1064 (6)	1073 (3)	$\nu_{asym}(CF_3)$
796 (45)	806 (3)	827 (0.6)	810 (8)	$\tau(NH_2)$
806 (7)				
f	734 (8)[g]	742 (0.7)	747 (5)	$\delta_{sym}(CF_3)$
	720 (23)	719 (2)	724 (sh)	$\nu_3(AsF_6)$[h]
		714 (sh)	702 (3)	
		703 (0.7)	693 (2)	
	691 (100)	688 (13)	683 (19)	$\nu_1(AsF_6^-)$[h]
		680 (2)	647 (6)	
		646 (2)		
666 (11)	670 (15)	674 (6)	672 (1)	$\varpi(NH_2)$
		669 (2)		
591 (10)	600 (23)	610 (1)	596 (5)	$\delta(OCN)$ +
		605 (1)		$\pi(OCN)$
		600 (3)		
	578 (15)	589 (2)	589 (2)	$\nu_2(AsF_6)$[h]
		583 (5)	577 (2)[g]	
		578 (1)		
		571 (0.8)		
		560 (3)		

			543 (29)	ν_{asym}(OXeF)
			530 (100)	
			508 (18)	ν_{sym}(OXeF)
			502 (34)	
			476 (23)	
513 (2)	547 (13)	f	523 (4)	$\delta_{asym}(CF_3)$
	513 (8)			
		515 (100)		ν_{sym}(FXeF)
		511 (79)		
430 (30)	434 (13)	436 (2)	432 (8)	$\gamma(CF_3)$
415 (39)	412 (13)	409 (2)	419 (3)	
	389 (25)[g]	f	409 (0.3)	$\nu_4(AsF_6^-)$[h]
		f	405 (0.3)	
	372 (18)	398 (0.8)	398 (3)	$\nu_5(AsF_6^-)$[h]
	363 (15)	394 (0.8)	393 (8)	
		363 (0.4)	390 (6)	
		343 (0.4)	385 (14)[g]	
			379 (14)[g]	
			371 (9)	
			366 (12)	
			363 (12)	
			292 (12)[i]	δ(COXe)
291 (8)	273 (6)	274 (0.8)	255 (10)	γ(C-C)
266 (23)		261 (1)		
	251 (9)	248 (0.1)	277 (1)	$\nu_6(AsF_6^-)$[h]
		242 (0.3)	265 (3)	
			247 (2)	
			239 (2)	
168 (9)	167 (1)	f	f	τ(C-C)
			141 (9)	δ(OXeF)
	139 (50)	157 (3)		H-bonding and
100 (3)		152 (5)		lattice modes
	78 (4)	141 (2)		
119 (6)				
		112 (6)		
		97 (2)		
		81 (7)		
		70 (4)		
		58 (3)		

Table 3.1 (contiued)

[a]Values in parentheses denote relative intensities; sh denotes a shoulder. [b]Recorded at room temperature in a glass sample tube; this work. Assignments have been taken from ref. (161). [c]Raman spectra were recorded in FEP sample tubes at -165 °C. Raman lines due to the FEP sample tube have been omitted from the table unless overlap with a sample tube band is likely. Data are given for the spectra depicted in Figures 3.7 - 3.9. [d]The symmetries of the N-H stretches cannot be assigned from the available data. [e]The broadness of the $\nu_{asym}(NH_2)$ and $\nu_{sym}(NH_2)$ bands is attributed, in part, to hydrogen bonding involving solvated HF. [f]Bands not observed in the Raman spectrum. [g]Band may overlap with an FEP sample tube band. [h]Notation provided for the fundamental modes of the AsF_6^- anion is that for O_h symmetry. The splitting of degenerate modes may be attributable to low site symmetry in the solid state or vibrational coupling within the unit cell. [i]The band assigned to the δ(COXe) bend in the $CF_3C(OXeF)NH_2^+$ cation is coincident with an FEP band at 292 cm^{-1}. This is indicated by the increased intensity of this band relative to the most intense FEP band at 734 cm^{-1}.

Figure 3.8 Raman spectrum of microcrystalline $CF_3C(OH)NH_2^+AsF_6^-$ (-165 °C) recorded in an FEP sample tube using 514.5-nm excitation. Asterisks (*) denote FEP sample tube lines. A dagger (†) denotes an artifact characteristic of the instrument.

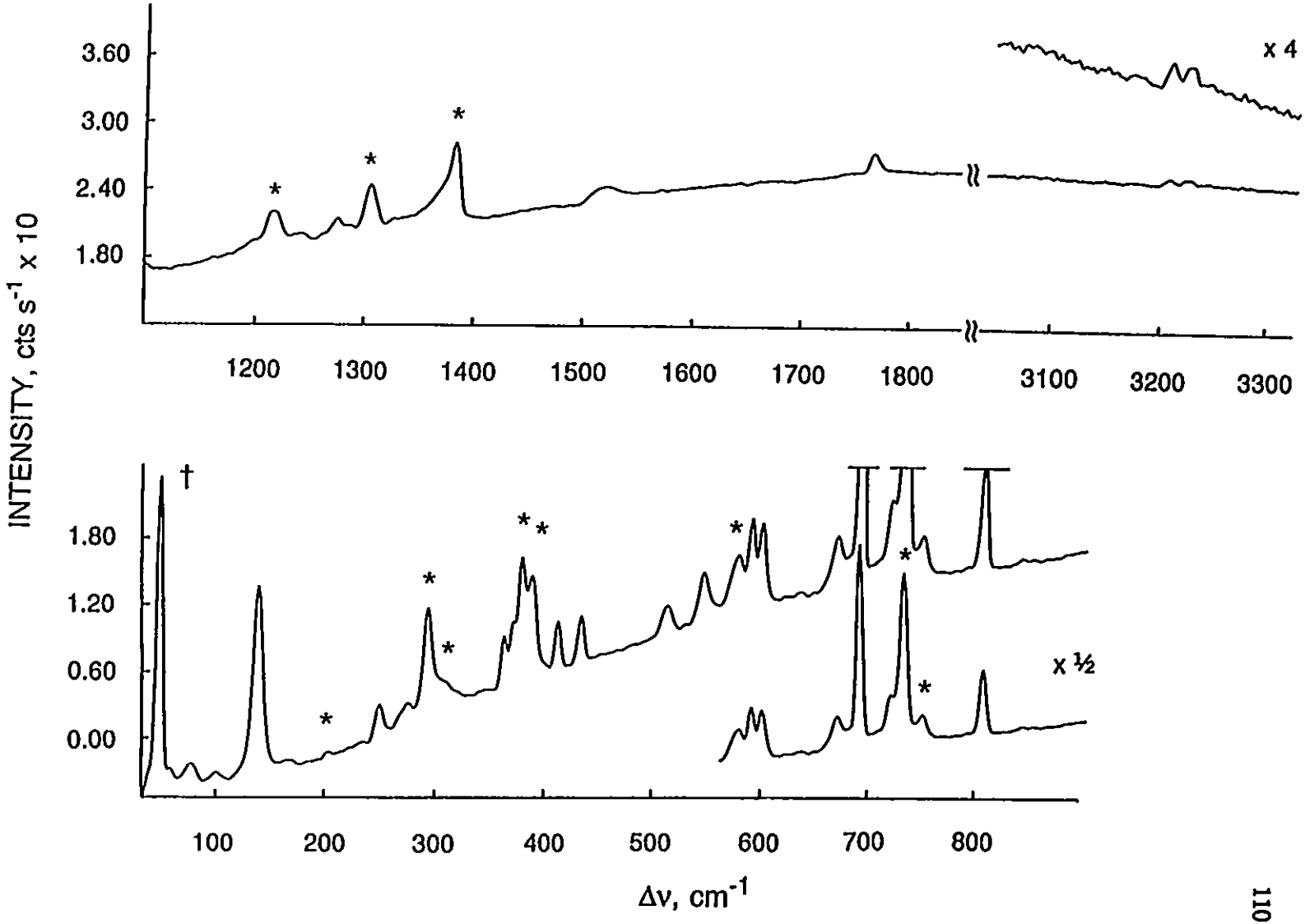
INTENSITY, cts s-1 x 10
3.60
3.00
2.40
1.80
x 4
1200
1300
1400
1500
1600
1700
1800
3100
3200
3300
†
1.80
1.20
0.60
0.00
x ½
100
200
300
400
500
600
700
800
Δν, cm-1

The bands attributed to $\omega(NH_2)$ (670 cm^{-1}), $\tau(NH_2)$ (806 cm^{-1}) and $\gamma(NH_2)$ (1197 cm^{-1}) are also similar to those observed in the Raman spectra of $CF_3C(O)NH_2$ and $CF_3C(OXeF)NH_2^+AsF_6^-$. A band attributable to $\delta(NH_2)$ was not observed, and is likely the result of the inherent low Raman intensity of this band.[174]

The band at 1276 cm^{-1} has been tentatively assigned to $\delta(OH)$ of the protonated carbonyl group. Infrared spectra of the related salts $CH_3C(OH)NH_2^+X^-$ (X = $SbCl_6$, NO_3, Cl),[162] $[CH_3C(OH)NH_2^+]_2X^{2-}$ (X = $SnCl_6$, $PtCl_6$)[162] and $CH_3C(OH)N(CH_3)_2^+X^-$ (X = Cl, Br, I, $SbCl_6$)[165] exhibit bands at 1333-1368 and 1040-1192 cm^{-1}, respectively, which are assigned to $\delta(OH)$. Bands attributable to $\gamma(OH)$ and $\nu(OH)$, which, like $\delta(NH_2)$, usually have very low Raman intensities,[174] and were too weak to be observed.

Seven bands have been assigned to the AsF_6^- anion, as opposed to three bands expected for AsF_6^- with O_h symmetry. Again, hydrogen bonding between cation and anion, as in the salt, $CF_3C(OXeF)NH_2^+AsF_6^-$, may contribute to symmetry lowering of the anion. Low site symmetry in the solid may also give rise to the splitting of the ν_5 band and observation of ν_3 (720 cm^{-1}) and ν_6 (251 cm^{-1}), both of which are formally Raman forbidden for octahedral XY_6 species.[170] All bands are assigned except ν_4 (ca. 420 cm^{-1}). This can be accounted for by considering the low intensity of this band in the Raman spectrum of $HC{\equiv}NXeF^+AsF_6^-$,[73] combined with the presence of bands in this region due to the FEP sample tube.

(F) CHARACTERIZATION OF $CF_3C(OH)NH_2^+AsF_6^-{\cdot}XeF_2{\cdot}xHF$ BY LOW-TEMPERATURE RAMAN SPECTROSCOPY

A white microcrystalline powder precipitates upon rapid removal of the HF solvent under vacuum from a solution containing stoichiometric amounts of $CF_3C(O)NH_2$ and $XeF^+AsF_6^-$, or

Figure 3.9 Raman spectrum of microcrystalline $CF_3C(OH)NH_2^+AsF_6 \cdot XeF_2 \cdot xHF$ (-165 °C) recorded in an FEP sample tube using 514.5-nm excitation. Asterisks (*) denote FEP sample tube lines. A dagger (†) denotes an artifact characteristic of the instrument.

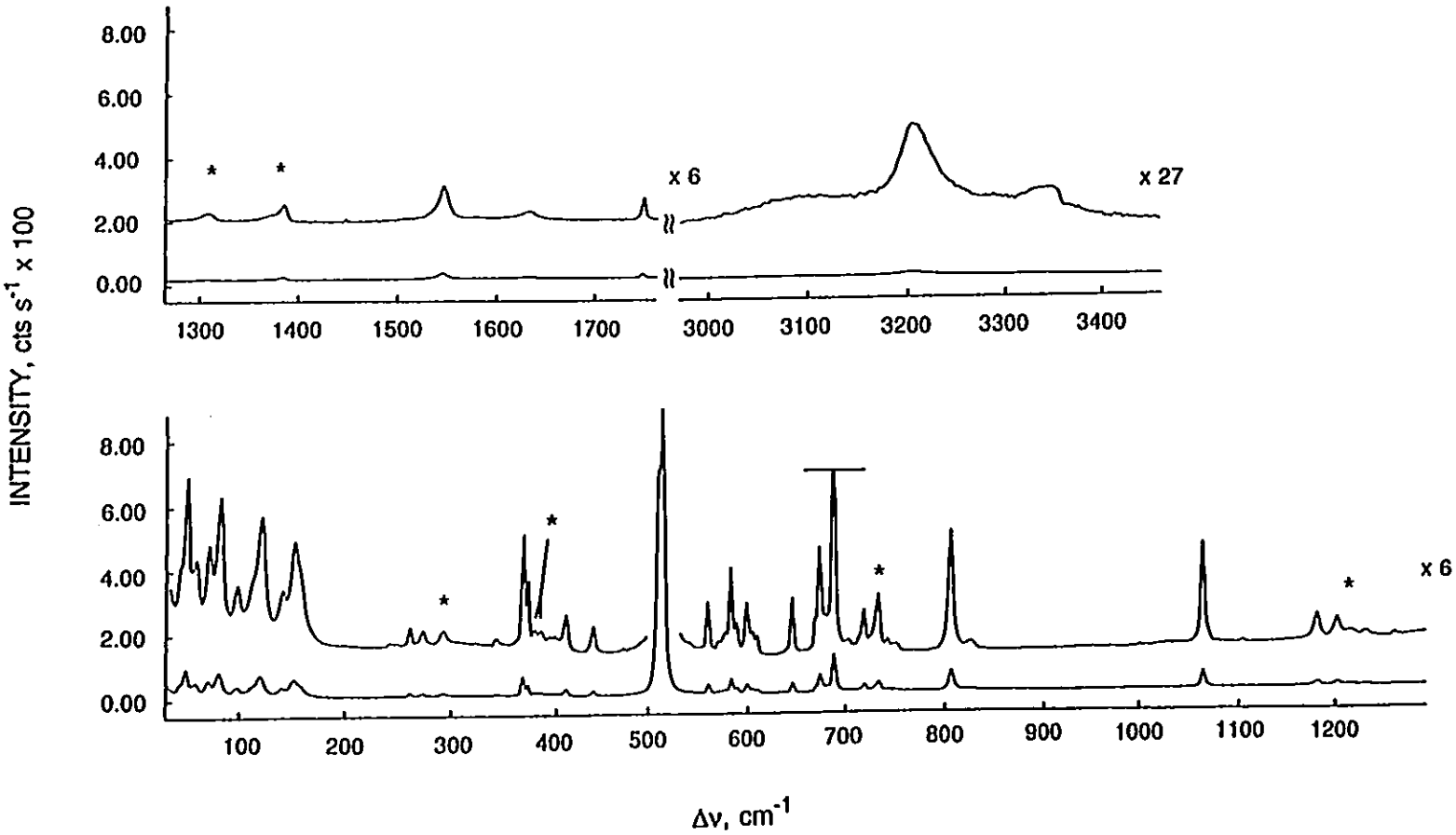
INTENSITY, cts s-1 x 100
8.00
6.00
4.00
2.00
0.00
x 6
x 27
1300
1400
1500
1600
1700
3000
3100
3200
3300
3400
x 6
100
200
300
400
500
600
700
800
900
1000
1100
1200
Δν, cm-1

$CF_3C(OH)NH_2^+AsF_6^-$ and XeF_2. The Raman spectroscopic results (Table 3.1 and Figure 3.9) are consistent with the formulation $CF_3C(OH)NH_2^+AsF_6^-\cdot XeF_2\cdot xHF$. The Raman spectrum resembles that expected for a mixture of polycrystalline XeF_2 and $CF_3C(OH)NH_2^+AsF_6^-$. However, the average of the very intense peaks at 511 and 515 cm^{-1}, assigned to ν_{sym}(Xe-F) of XeF_2 incorporated in the adduct, is 17 cm^{-1} higher in frequency than the symmetric Xe-F stretch for polycrystalline XeF_2 (495 cm^{-1}).[175a] The interaction of XeF_2 with fluoroacids as in $XeF^+AsF_6^-$,[176] $XeF^+Sb_2F_{11}^-$ [69] and $XeF_2\cdot XeF_5^+AsF_6^-$ [177] results in elongation of one Xe-F bond (Xe···F bridge bond) in complexed XeF_2, accompanied by a shortening of the remaining (terminal) Xe-F bond. This results in bands which are assignable to a bridging Xe···F stretch and a terminal Xe-F stretch, that are lower and higher in frequency, respectively, than ν_{sym}(Xe-F) [496 cm^{-1}][175b] and ν_{asym}(Xe-F) [547 cm^{-1}][175c] in uncoordinated XeF_2, from which they are formally derived. The latter mode is Raman forbidden for XeF_2 under $D_{\infty h}$ point symmetry. The absence of a relatively intense band assignable to ν_{asym}(Xe-F) at approximately 550 cm^{-1} in the Raman spectrum of $CF_3C(OH)NH_2^+AsF_6^-\cdot XeF_2\cdot xHF$ indicates that the Xe-F bonds in coordinated XeF_2 are essentially symmetric. The frequency of ν_{sym}(Xe-F) is also inconsistent with an XeF_2 molecule containing significantly different Xe-F bond lengths (see above). The observation of two peaks for ν_{sym}(Xe-F) is attributed to vibrational coupling of XeF_2 molecules within the unit cell of $CF_3C(OH)NH_2^+AsF_6^-\cdot XeF_2\cdot xHF$. By analogy with known adducts containing symmetric XeF_2,[178] it is probable that the fluorine ligands of XeF_2 interact with the positive centers of the $CF_3C(OH)NH_2^+$ cation in the adduct $CF_3C(OH)NH_2^+AsF_6^-\cdot XeF_2\cdot xHF$, namely the hydroxyl and amido protons, through hydrogen bonding. Structures 3.5 - 3.7 illustrate possible hydrogen bonding interactions of XeF_2 and $CF_3C(OH)NH_2^+$ in which the local molecular point symmetry of XeF_2 does not deviate significantly from $D_{\infty h}$.

3.5

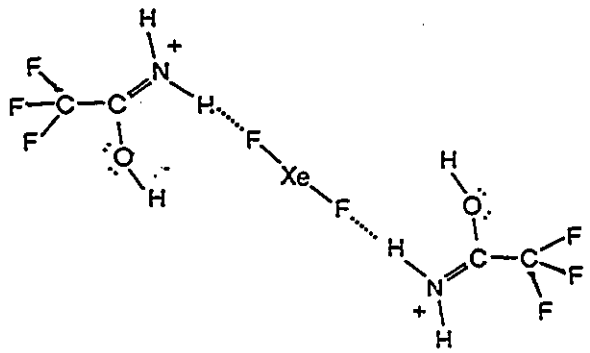

3.6

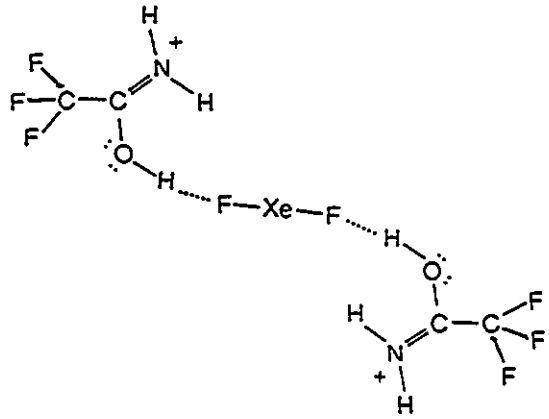

3.7

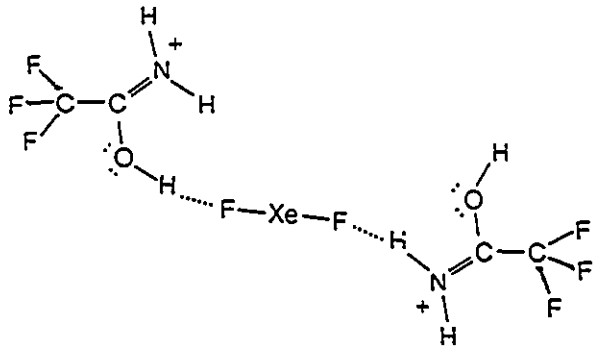

Further evidence for the assigned structure of the solvate $CF_3C(OH)NH_2^+AsF_6^-\cdot XeF_2\cdot xHF$ was obtained by comparing bands in the amide region of the Raman spectrum with those of $CF_3C(O)NH_2$ and $CF_3C(OH)NH_2^+AsF_6^-$. The bands at 1767 and 1549 cm^{-1} are assigned to ν(CN) and ν(CO), respectively. This is consistent with an increase of 262 cm^{-1} for ν(CN) and a decrease of 157 cm^{-1} for ν(CO) relative to $CF_3C(O)NH_2$ and with the changes in C-N and C-O bond order anticipated upon O-protonation of amides. The bands at 1262 and 1232 cm^{-1} are assigned to the bending mode, δ(OH), and are similar to the value assigned for $CF_3C(OH)NH_2^+AsF_6^-$ (1276 cm^{-1}). As in the Raman spectrum of $CF_3C(OH)NH_2^+AsF_6^-$, modes arising from ν(OH) and γ(OH) are presumably too weak to be observed. Evidence for solvation by HF is provided by the presence of a broad band at 3090 cm^{-1} which is assigned to ν_{sym}(HF), and is similar to that observed in the infrared spectra of hydrogen-bonded complexes of HF with $CF_3C(O)NH_2$.[164]

A total of 17 bands are attributed to the AsF_6^- anion, and have been assigned using arguments similar to those already presented for $CF_3C(OH)NH_2^+AsF_6^-$ and $CF_3C(OXeF)NH_2^+$ AsF_6^-.

(G) NATURE OF THE BONDING IN $CF_3C(OXeF)NH_2^+$

The bonding in the $CF_3C(OXeF)NH_2^+$ cation can be assessed using trends for xenon(II) compounds that are well established from Raman and NMR spectroscopy. Previous NMR studies of xenon(II) derivatives containing XeF groups bonded to oxygen or fluorine have shown that the ^{19}F and ^{129}Xe NMR parameters can be used to assess the relative covalent characters of the Xe-O, Xe---F bridge and terminal Xe-F bonds in compounds of the type F-Xe-L (L = ligand atom).[26,103,104,108] In general, as the ionic character of the Xe-L bond increases, the covalent character of the terminal Xe-F bond increases, increasing the formal charge on xenon. This trend

is paralleled by increasing values of $\delta(^{129}Xe)$ and $^{1}J(^{129}Xe\text{-}^{19}F)$, and decreasing values of $\delta(^{19}F)$ for the terminal Xe-F group. The pattern observed in the ^{19}F and ^{129}Xe NMR spectra is complemented by measurements of ν(Xe-F) provided by Raman spectroscopy, which signify increased covalent character of the Xe-F bond with shifts to higher frequency, and *vice versa*.[26]

Table 3.2 lists the relevant NMR and Raman spectroscopic data for the $CF_3C(OXeF)NH_2^+$ cation and some related Xe-O, Xe-N and Xe---F bonded compounds of Xe(II) arranged in approximate order of increasing ionic character of the Xe-F bond. Xenon difluoride and $XeF^+Sb_2F_{11}^-$, in which the XeF^+ cation is fluorine bridged to the weakly fluorobasic $Sb_2F_{11}^-$ anion,[69] provide the upper and lower limits, respectively, of the terminal Xe-F bond ionic character. The charge distribution for XeF_2 may be represented as $F^{-1/2}Xe^+F^{-1/2}$, indicating a high degree of Xe-F bond ionic character.[179] The low basicity of the $Sb_2F_{11}^-$ anion in $XeF^+Sb_2F_{11}^-$ provides the closest approximation to a free XeF^+ cation, where the Xe-F bond order approaches one. Consistent with the valence bond Structures 3.8 and 3.9, the degree of Xe-F bond ionic character in L-Xe-F depends upon the basicity of the ligand L.[26] As can be inferred from

$$\underset{3.8}{L\text{-}Xe^+F^-} \longleftrightarrow \underset{3.9}{L^-Xe\text{-}F^+} \longleftrightarrow \underset{3.10}{L^-\,Xe^{2+}\,F^-}$$

$$\underset{3.11}{L\text{-}Xe^{2+}\,F^-} \longleftrightarrow \underset{3.12}{L\,Xe\text{-}F^+} \longleftrightarrow \underset{3.13}{L\,Xe^{2+}\,F^-}$$

^{19}F and ^{129}Xe NMR shielding trends, the magnitude of $^{1}J(^{19}F\text{-}^{129}Xe)$ and terminal Xe-F stretching frequencies (Table 3.2), the Xe-O bond in the $CF_3C(OXeF)NH_2^+$ cation is significantly more

Table 3.2. Comparison of Chemical Shifts, One Bond Xe-F Coupling Constants and ν(Xe-F) of Some L-Xe-F Derivatives

Species	ν(Xe-F),[b] cm^{-1}	NMR Parameters[a] $^1J(^{129}Xe-^{19}F)$, Hz	$\delta(^{129}Xe)$,[c] ppm	$\delta(^{19}F)$,[d] ppm	T, °C	ref
$F_{10}Sb_2F^-$---XeF^+ [e]	619	7230	-574	-290.2	23	66,69,108,111
F-Xe---F---Xe-F^+	593	6740	-1051	-252.0	-62	69,108,111
$(CF_3)_2S{=}OXeF^+SbF_6^-$	552	6343	-1679		-70	85
$F_3S{\equiv}NXeF^+AsF_6^-$	554	6248	-1661	-180.5	-60	180
$HC{\equiv}NXeF^+AsF_6^-$	564	6181	-1569	-198.4[f]	-58	72,73
$CH_3C{\equiv}NXeF^+AsF_6^-$ [g]	560	6020	-1708	-185.5	-10	72
$CF_3C(OXeF)NH_2^+AsF_6^-$	536	5991	-1578	-183.1	-54	h
4-$(CF_3)C_5F_4NXeF^+AsF_6^-$	524	5963	-1853	-144.6	-50	75
$C_5F_5NXeF^+AsF_6^-$	528	5926	-1922	-139.6	-30	75
s-$C_3F_3N_2NXeF^+AsF_6^-$	548	5932	-1862	-145.6	-50	71
cis-$F_4OIOXeF$	527	5803	-1824	-161.7[i]	0	42
trans-$F_4OIOXeF$	527	5910	-1720	-170.1[i]	0	42
FO_2SOXeF	528	5830	-1666		-40	108,111,140,158
$F_5TeOXeF$[j]	520	5670	-2051	-151.0[k]	26	180,181
$(FO_2S)_2NXeF$	506	5586	-1977	-126.1	-58	57,59
$CF_3C(O)OXeF$[l]	510	5550	-2176		-30	39,139
XeF_2	495	5621	-1685	-184.3	-52	71,175a

Table 3.2 (continued)

[a]Spectra were recorded in BrF_5 solvent unless otherwise indicated. The NMR parameters of the XeF group, in particular $\delta(^{129}Xe)$, are very sensitive to solvent and temperature conditions; it is therefore important to make comparisons in the same solvent medium and at the same or nearly the same temperature. Table entries refer to the terminal fluorine on the xenon atom. [b]Vibrational data refers to terminal Xe-F stretches. [c]Referenced with respect to the neat liquid $XeOF_4$ at 30 °C. [d]Referenced with respect to the neat liquid $CFCl_3$ at 30 °C. [e]NMR parameters recorded in SbF_5 solvent. [f]$\delta(^{19}F)$ measured in anhydrous HF solvent at -10 °C. [g]NMR parameters measured in HF solvent. [h]This work. [i]$\delta(^{19}F)$ measured in SO_2ClF solvent at -40 °C. [j]NMR parameters measured in SO_2ClF solvent. [k]NMR parameters measured in SO_2ClF solvent at -50 °C. [l]Vibrational spectrum obtained using infrared spectroscopy in acetonitrile solvent at ambient temperature. NMR parameters obtained in $CD_3C{\equiv}N$ solvent at -30 °C.

covalent than those of the Xe-N bonded cations $F_3S{\equiv}N\text{-}XeF^+$, $HC{\equiv}N\text{-}XeF^+$ and $CH_3C{\equiv}N\text{-}XeF^+$, which have been shown to have highly ionic Xe-N bonds.[26] Based on $^1J(^{129}Xe\text{-}^{19}F)$ and $\nu(XeF)$, the Xe-F bond in the $CF_3C(OXeF)NH_2^+$ cation is more ionic than the Xe-F bond in $(CF_3)_2S{=}O\text{-}XeF^+$, implying a more covalent Xe-O bond in the former cation. The $\delta(^{129}Xe)$ values are, however, opposite in direction to the trend established above, but the difference in the solvents and temperatures used, and the large influence that these factors are known to have on the ^{129}Xe NMR chemical shifts of Xe(II) compounds,[103,108] renders this parameter unreliable for assessing Xe-F bond ionicity in the present case. One possible factor contributing to the ionic character of the Xe-O bonds in the $(CF_3)_2S{=}O\text{-}XeF^+$ and $CF_3C(OXeF)NH_2^+$ cations is the formal hybridization on oxygen. In general, a greater *s*-contribution to the hybridization of the ligand donor atom is expected to increase its effective electronegativity,[105] resulting in a more ionic Xe-L bond. This is illustrated in the series of cations containing Xe-N bonds, where the Xe-N bonds in cations containing formally *sp*-hybridized nitrogen (e.g., $F_3S{\equiv}N\text{-}XeF^+$, $RC{\equiv}N\text{-}XeF^+$) are consistently more ionic than the Xe-N bonds in the cations containing formally sp^2-hybridized nitrogen (e.g., 4-$CF_3C_5F_4N\text{-}XeF^+$, $C_5F_5N\text{-}XeF^+$, *s*-$C_3F_3N_2N\text{-}XeF^+$). The oxygen of the $(CF_3)_2S{=}OXeF^+$ cation is formally sp^2-hybridized, whereas resonance Structure 3.4 for the $CF_3C(OXeF)NH_2^+$ cation indicates π-donation from nitrogen to carbon, which effectively lowers the *s*-contribution to hybridization on oxygen so that it is intermediate between sp^2 and sp^3, resulting in a more covalent Xe-O bond in the $CF_3C(OXeF)NH_2^+$ cation. It is also apparent from Table 3.2 that cationic $L\text{-}Xe\text{-}F^+$ compounds exhibit spectroscopic properties which are consistent with more ionic Xe-L bonds than the structurally analogous neutral compounds. This can be rationalized using a simple valence bond description. Resonance Structures 3.8 - 3.10 represent the bonding in the neutral molecules L-Xe-F, whereas 3.11 - 3.13 represent the corresponding cationic species L-Xe-

F^+. For the neutral species L-Xe-F, resonance Structure 3.10 contributes least to the bonding as a result of the dipositive charge on xenon. The relative weights of 3.8 and 3.9 depend on the group electronegativity of the ligand L, with a greater contribution from Structure 3.8 for lower electronegativity of L. For the L-Xe-F^+ cations, resonance Structures 3.11 and 3.13 have reduced weights relative to 3.12 as a result of the high charge localization. Thus, resonance Structure 3.12, which represents a purely ionic interaction of the ligand L and XeF^+, is expected to dominate the bonding in $CF_3C(OXeF)NH_2^+$ and related O- and N-bonded xenon(II) cations.

CHAPTER 4

CHARACTERIZATION AND COMPARISON OF THE BONDING IN F_5TeNH_2 AND $F_5TeNH_3^+AsF_6^-$ USING ^{19}F NMR AND RAMAN SPECTROSCOPY

INTRODUCTION

(A) REVIEW OF THE SYNTHESIS, CHARACTERIZATION AND BONDING OF THE ACIDS F_5XOH AND THE SALTS $M^+OXF_5^-$ (X = S, Se, Te)

The ligands F_5XO- (X = S, Se, Te) are bulky, highly electronegative and are second only to fluorine in their ability to stabilize high oxidation states of metals and nonmetals.[52,183,184] The first compounds containing the F_5XO- group were prepared from the direct fluorination of the chalcogens in the elemental state or the oxides, yielding hypofluorites F_5XOF (X = S,[185] Se[186]), peroxides $F_5XO\text{-}OXF_5$ (X = S,[187] Se[186]) and $F_5TeOTeF_5$.[188] The synthetic potential of the F_5XO- group increased dramatically in 1964 with the discovery of the acid, $HOTeF_5$[189] from the reaction of $BaTeO_4$ with HSO_3F in an attempt to prepare TeC_2F_2 by analogy with the preparation of SeO_2F_2 from $BaSeO_4$ and HSO_3F.[190] Failure to prepare TeO_2F_2 in this way reflects the propensity of hexavalent tellurium to adopt coordination number six.[52] The compound $HOTeF_5$ is best prepared according to equation (4.1)

$$Te(OH)_6 + 5\ HSO_3F \longrightarrow 5\ H_2SO_4 + HOTeF_5 \qquad (4.1)$$

The preparation of $HOSeF_5$, first reported in 1972 by Seppelt,[142,191] involves the reaction of SeO_2F_2 and HF with an increase in coordination number of selenium(VI) according to equation (4.2), which illustrates the tendency for coordination numbers four and six to exist in the same system for hexavalent selenium.

$$3\ SeO_2F_2 + 4\ HF \rightleftharpoons 2\ HOSeF_5 + H_2SeO_4 \qquad (4.2)$$

In contrast to SeO_2F_2, SO_2F_2 is extremely inert showing no tendency to increase its coordination number to six. The preparation of $HOSF_5$ therefore requires a more indirect route, involving the reaction of SOF_4 with ClF to give the hypochlorite $ClOSF_5$ as an intermediate, followed by reaction with HCl (equation 4.3).[192,193]

$$SOF_4 + ClF \xrightarrow{CsF} ClOSF_5 \xrightarrow[-Cl_2]{HCl} HOSF_5 \qquad (4.3)$$

The thermal stabilities of $HOSF_5$, $HOSeF_5$ and $HOTeF_5$ vary considerably:[193]

$$HOSF_5 \xrightarrow{-60\ °C} HF + SOF_4 \qquad (4.4)$$

$$HOSeF_5 \xrightarrow{290\ °C} HF + 1/2\ O_2 + SeF_4 \qquad (4.5)$$

$$HOTeF_5 \xrightarrow{>310\ °C} HF + (TeOF_4)_n + TeF_4 + TeF_6 + \ldots \qquad (4.6)$$

Below -60 °C, $HOSF_5$ is only kinetically stable with respect to reduction of coordination number, limiting its use as a synthetic reagent. The selenium analog, $HOSeF_5$, decomposes at 290 °C with reduction of selenium from the +6 to the +4 oxidation state. The tendency to undergo reduction is reflected in the powerful oxidizing power of $HOSeF_5$. As a result, $HOSeF_5$ is the strongest oxidizer among the three $HOXF_5$ compounds. The high thermal decomposition temperature of $HOTeF_5$ and the uncharacteristic distribution of products indicates the stability of hexacoordinate tellurium (VI) with respect to reduction of coordination number and oxidation state. Thus, most of the chemistry of the F_5XO- ligand has involved $HOTeF_5$ as the starting material. The chemistry of the F_5SeO- ligand is less extensive, and few examples of the F_5SO- ligand are known owing to the instability of $HOSF_5$.

The inductive effect resulting from the accumulation of fluorine atoms results in high group electronegativities for the F_5XO- ligands, enabling them to stabilize high oxidation states that are only otherwise stabilized by the most electronegative element, fluorine. Examples include $W(OTeF_5)_6$,[194] $U(OTeF_5)_6$,[195,196] $O{=}Xe(OTeF_5)_4$,[51,53,181] $Br(OSeF_5)_3$,[45] and $Kr(OTeF_5)_2$.[197] Several methods have been used to establish the electronegativities of the F_5TeO- and F_5SeO- groups relative to fluorine and the other halogens. The ^1H NMR chemical shift of the methyl protons of CH_3OSeF_5 relative to those of CH_3X (X = F, Cl, Br, I) has indicated that the F_5SeO- group has an electronegativity which is greater than that of fluorine.[198] Although the electronegativity of the F_5TeO- group relative to fluorine has been debated,[52] the weight of evidence indicates that fluorine is more electronegative. Using the difference in the ^1H NMR chemical shifts of the methyl and methylene protons in the compounds CH_3CH_2X (X = $OTeF_5$, F, Cl, Br, I),[181] a value of 3.88 has been obtained for the electronegativity of the F_5TeO- group, as compared to 3.98 for fluorine (Pauling scale). A study involving ^{127}I and ^{129}Xe Mössbauer and

^{129}Xe and ^{125}Te NMR spectroscopic measurements on a series of xenon and iodine compounds containing F and F_5TeO- as ligands also indicate that the electronegativity of the F_5TeO- group is less than that of fluorine.[181]

As expected from the high electronegativity of the F_5TeO- and F_5SeO- groups, the compounds $HOTeF_5$ and $HOSeF_5$ are strong acids. The acid strength of $HOTeF_5$ has been found to lie between those of HNO_3 and HCl by spectrophotometric measurements in acetic acid solution.[200] The high acidity is also reflected in the large variety of known F_5XO^- salts.[52] Salts of the F_5XO^- anions (X = Te, Se) may be obtained directly from $HOTeF_5$ and $HOSeF_5$ by reaction with nitrogen bases [equations (4.7) and (4.8)]:[201-204]

$$HOTeF_5 + D \longrightarrow DH^+OTeF_5^- \quad (4.7)$$

$$(D = C_5H_5N,\ NH_3,\ C_{14}H_{18}N_2,\ N(CH_2CH_3)_3)$$

$$HOSeF_5 + D \longrightarrow DH^+OSeF_5^- \ (D = NH_3) \quad (4.8)$$

The salts $NR_4^+OTeF_5^-$ (R = CH_3,[205] $CH_3CH_2CH_2CH_2$-[203]) have been prepared from the HCl elimination reaction of $HOTeF_5$ with NR_4Cl. Alkali metal derivatives of F_5TeO^- may be prepared from $HOTeF_5$ and MCl (M = K, Rb, Cs) with the evolution of HCl.[201,206] Syntheses of the analogous $M^+OSeF_5^-$ salts requires the use of MF (M = Li, Na, K, Rb, Cs) producing HF,[204] since chloride is oxidized by selenium(VI), giving chlorine gas. The salts, $Na^+OXF_5^-$, (X = Se, Te)[207] may be prepared from the reaction of a siloxane R_3OSi-OXF_5 with $NaOSiR_3$ [equation (4.9)] and $Li^+OTeF_5^-$ [207] is prepared from the reaction of $LiOCH_3$ and $HOTeF_5$ [equation (4.10)]. Other derivatives include $NO_2^+OSeF_5^-$ [208] and $NO^+OTeF_5^-$,[209] which both have covalent formulations

$$R_3Si\text{-}OXF_5 + NaOSiR_3 \longrightarrow Na^+OXF_5^- + R_3SiOSiR_3 \quad (X = Se, Te) \tag{4.9}$$

$$HOTeF_5 + LiOCH_3 \longrightarrow HOCH_3 + Li^+OTeF_5^- \tag{4.10}$$

in the gas phase, and the salt $Ag^+OTeF_5^-$,[206] for which a partially covalent interaction between the cation and anion has been observed in acetonitrile solution. Because of the instability of $HOSF_5$ above -60 °C,[192,193] salts of the OSF_5^- anion can not be prepared from the parent acid. The salt, $Cs^+OSF_5^-$, is prepared from the addition reaction of CsF and SOF_4.[210,211]

The OXF_5^- anions all exhibit molecular geometries having C_{4v} point symmetry in solution and in the solid state. Structural characterization of these anions has been obtained by ^{19}F NMR spectroscopy, which exhibits typical AB_4 spectra, and infrared and Raman spectroscopy. Because of orientational disorder resulting from the essentially spherical shape of the OXF_5^- anions and the similarities of the covalent and van der Waals radii of oxygen and fluorine atoms, the salts are not suitable for detailed single crystal X-ray analysis. Only one salt F_5XO^- salt, namely [1,8-bis(dimethylamino) naphthalenium]$^+OTeF_5^-$, has been published in which the oxygen and fluorine atoms are not disordered.[202]

The wealth of vibrational and ^{19}F NMR spectroscopic data on compounds containing F_5XO- groups has made it possible to compare the bonding in F_5XO-M (X = S, Se, Te) compounds as M is varied.[52,83,84] It has been noted that increasing ionic character of the O-M bond results in a strengthening of the O-X bond, and a weakening of the X-F bonds. Further, the axial X-F bond is weakened more than the equatorial X-F bonds, a well established "trans effect". This is adequately illustrated by comparing the acids $HOXF_5$ (M = H) with salts of the form

$M^+OXF_5^-$, where the ionic characters of the M-O bonds in the latter compounds are significantly greater than in the former. Table 4.1 lists the ^{19}F NMR and vibrational data for $HOXF_5$ and the OXF_5^- anions (X = S, Se, Te). As shown in the vibrational data, deprotonation of the acids $HOXF_5$ to give OXF_5^- results in a lowering of the $\nu(X\text{-}F_{ax.})$ and $\nu_{sym}(X\text{-}F_{eq.})$ stretching frequencies and an increase in the $\nu(XO)$ stretching frequencies. The axial X-F stretches are decreased more than the equatorial X-F stretching frequencies, consistent with the expected changes in bond strengths described above. The X-O bond orders in the F_5XO^- anions have been estimated from the force constants obtained from normal coordinate calculations to lie between one and two for X = Se[206] and Te;[206] an S-O bond order of 1.5 has been calculated for the F_5SO^- anion.[210] Structural evidence for partial double bond in the F_5TeO^- is present in the single crystal X-ray structure of [1,8-(dimethylamino)naphthalenium]$^+OTeF_5^-$,[202] where the Te-O bond length [1.803(3) Å] is significantly shorter than a Te-O single bond [cf., $Te(OH)_6$, Te-O = 1.908(1) Å].[211] The X-O bond orders are indicative of partial double bonds resulting from π-donation from oxygen to the F_5X- group. Valence bond theory has been used by several authors (c.f., resonance Structures 4.1 - 4.3) to represent the bonding in the OXF_5^- anions (X = S, Se, Te)[206,210,213,214] without explicitly identifying the orbitals on the hypervalent chalcogen center which accept π-electron density from oxygen. The weaker axial X-F bonds are represented by greater weighting of resonance Structure 4.3. Strauss *et al.* have stated that vacant *d*-orbitals on the chalcogen center function as acceptor orbitals for the π-electron density from oxygen (d_π-p_π bonding).[203] Oberhammer and Seppelt[215] also provide evidence for d_π-p_π bonding in the oxides F_5XOXF_5 (X = S, Se, Te) from the energetically unfavorable eclipsed geometries of the equatorial fluorine ligands, the nearly constant X-O-X bond angles (*ca.* 140°) and the short X-O bond lengths. With regard to the bonding in the OXF_5^- anions, Seppelt[215] has stated that resonance Structures 4.1 -

Table 4.1. Comparison of Raman and ^{19}F NMR Spectroscopic Data for the Acids F_5XOH and Some of the Salts, $[M]^+[F_5XO]^-$ (X = S, Se, Te).

Compound	Raman Frequencies, cm^{-1} [a]			^{19}F NMR Chemical Shifts, ppm[b]		Ref
	$\nu(X\text{-}F_{ax.})$	$\nu_{sym}(X\text{-}F_{eq.})$	$\nu(X\text{-}O)$	δ_A [c]	δ_B [c]	
F_5TeOH	735	685	735	-44.3	-46.6	214,220
$[N(n\text{-}Bu)_4]^+OTeF_5^-$ [d]	576	645	867	-19.0	-36.8	202,203
$N(CH_3)_4^+OTeF_5^-$ [e]	583, 650	583, 650	868	-19.1	-36.9	205
F_5SeOH [f]	625	685	753	82.7	64.8	214,215
$K^+OSeF_5^-$ [g]	559	649	919	121.1	78.4	204,214,215
F_5SOH [h,i]	610, 635	761	-	71.8	67.0	192,193
$Cs^+OSF_5^-$ [j]	722	697	1153	138.3	94.9	211

Table 4.1 (continued)

[a] Raman spectra were performed on the neat compounds at ambient temperatures unless otherwise specified. [b] ^{19}F NMR spectra were recorded at ambient temperatures unless otherwise specified and positive (negative) chemical shifts are deshielded (shielded) relative to $CFCl_3$ standard. [c] δ_A and δ_B refer to the axial and equatorial ^{19}F NMR resonances, respectively. [d] ^{19}F NMR spectra recorded in CH_2Cl_2 solvent. [e] ^{19}F NMR spectra recorded in $CH_3C{\equiv}N$ solvent at -10 °C. [f] ^{19}F NMR spectra recorded in $CH_3C{\equiv}N$ solvent. [g] Raman spectra recorded in $CH_3C{\equiv}N$ solvent. [h] Raman spectra recorded at -160 °C. [i] ^{19}F NMR spectra recorded at -70 °C in $CHClF_2$ solvent. [j] ^{19}F NMR spectra recorded in DMSO solvent.

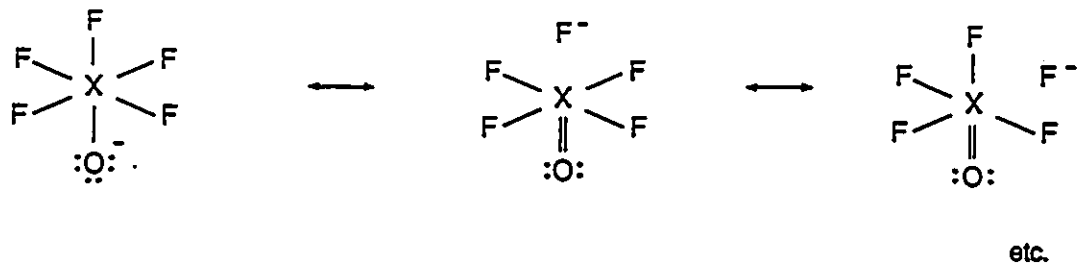

4.1 4.2 4.3

4.3 imply hyperconjugation. This is a misnomer since hyperconjugation implies donation of electron density from a σ orbital to a π^* orbital. In these anions, negative hyperconjugation[216] may contribute significantly to the bonding, where π electron density from the *p*-orbitals on oxygen donate electron density into σ^* orbitals of the F_5Te- group. Recent SCF *ab initio* calculations using natural population analysis[216] on molecules containing hypervalent main-group centers such as CH_3SO_2Cl, F_3CO^- and the hypothetical F_3TeC^- anion indicate that the primary acceptor orbitals on the hypervalent centers are σ^*, constructed mainly from valence *s* and *p* orbitals and that valence *d* orbitals play only a minor role. The lengthening of the X-F bonds (X = S, Se, Te) upon deprotonation of $HOXF_5$ to give OXF_5^- is predicted, since $\pi_O \rightarrow \sigma^*$(X-F) donation increases the population of X-F antibonding orbitals. The "trans effect" described above indicates that $\pi_O \rightarrow \sigma^*(X\text{-}F_{ax.}) > \pi_O \rightarrow \sigma^*(X\text{-}F_{eq.})$, which may be confirmed by performing the appropriate calculations.

An explanation for the observed behavior of the ^{19}F NMR chemical shifts (Table 4.1) of the $HOXF_5$ / OXF_5^- pairs (X = S, Se, Te) cannot be made with certainty, but may be related to the effect of negative hyperconjugation discussed above. Table 4.1 illustrates that both the axial and

equatorial fluorine resonances of the OXF_5^- anions are deshielded relative to those of the acids, $HOXF_5$. In particular the axial fluorine resonances are deshielded by 18 to 25 ppm (X = Te), 38 ppm (X = Se) and 66 ppm (X = S). The equatorial resonances are deshielded by 4 to 10 ppm (X = Te), 14 ppm (X = Se), and 30 ppm (X = S). This qualitatively resembles the trend observed in the X-F force constants derived from the vibrational data, where the axial X-F bond is affected more by changes in the X-O bond order, which has been attributed to $\pi_O \rightarrow \sigma^*$(X-F) negative hyperconjugation. In the presence of a magnetic field, mixing of lower energy orbitals with higher unoccupied orbitals, which are termed "excitations", results in paramagnetic currents which may deshield (negative paramagnetic contribution) or shield (positive paramagnetic contribution) the nucleus.[218,219] It is possible that the population of the σ^*(X-F) orbitals resulting from negative hyperconjugation deshields the fluorine nuclei by altering the paramagnetic circulations involving σ^*(X-F) as the higher energy orbital. Further speculation is unwarranted without a detailed knowledge of the electronic states of the OXF_5^- anions.

(B) SYNTHESIS AND CHARACTERIZATION OF F_5XNH_2 (X = S, Te)

The chemistry of the nitrogen analogues, F_5XNH_2 (X = S, Se, Te), is less developed than that of the oxygen acids $HOXF_5$ (X = S, Se, Te). Although preceded by several examples of α-fluoro secondary amines R_fNHR_f' where R_f and R_f' have been either perfluoroalkyl or pentafluorosulfur groups,[221-225] the preparation of the α-fluoro primary aminosulfur(VI) pentafluoride was first reported in 1965, by Clifford and Duncan[226] by addition of HF across the SN triple bond of $F_3S{\equiv}N$ [equation (4.11)].

$$F_3S{\equiv}N + 2\,HF \longrightarrow F_5SNH_2 \qquad (4.11)$$

The compound, F_5SNH_2, dissociates slowly at room temperature and more rapidly at 45 °C to give HF and $F_3S{\equiv}N$. However, F_5SNH_2 is much more stable than F_5SOH, which decomposes to give SOF_4 and HF at -60 °C.[192,193] As a result, the chemistry of F_5SNH_2 has been investigated to a greater extent. In spite of the electron withdrawing effect of the F_5S- group, F_5SNH_2 has some degree of basic character, since 1:1 adducts are formed with PF_5 and BF_3 that are both stable at room temperature.[227]

Of the heavier analogues, i.e., F_5SeNH_2 and F_5TeNH_2, only the latter is known. The preparation of F_5TeNH_2 was preceded by the preparation of the dialkylamino derivatives, $F_5TeN(CH_3)_2$,[228,229] $F_5TeN(CH_2CH_3)_2$,[229] and $F_5TeN(C_4H_8)$.[229] These species were prepared from the appropriate dialkylaminotrimethylsilane and TeF_6 in silicon-nitrogen cleavage reactions [equation (4.12)]. The thermodynamic driving force for the reactions is the formation of the very

$$R_2NSi(CH_3)_3 + TeF_6 \longrightarrow R_2NTeF_5 + FSi(CH_3)_3 \qquad (4.12)$$

strong Si-F bond. The primary amine, F_5TeNH_2,[230] was prepared in 1973 in a two-step silicon-nitrogen cleavage reaction [equations (4.13) and (4.14)]. Aminotellurium(VI) pentafluoride, as expected by analogy with $HOTeF_5$, exhibits no tendency to undergo HF elimination or reduce its

$$TeF_6 + (CH_3)_3SiNHSi(CH_3)_3 \longrightarrow F_5TeNHSi(CH_3)_3 + (CH_3)_3SiF \qquad (4.13)$$

$$F_5TeNHSi(CH_3)_3 + HF \longrightarrow F_5TeNH_2 + (CH_3)_3SiF \qquad (4.14)$$

coordination number at ambient temperatures,and decomposes only when heated to 150 °C.

Unlike the sulfur analogues, *cis*-disubstituted products may be produced in the preparation of the compounds F_5TeNRR' [R, R' = alkyl; R = H, R' = $Si(CH_3)_3$]. Of the alkyl derivatives studied, only the reaction of $(CH_3)_3SiN(CH_3)_2$ with TeF_6[228,229] produces a stable *cis*-disubstituted product, namely *cis*-$F_4Te[N(CH_3)_2]_2$, which is formed along with $F_5TeN(CH_3)_2$. In the preparation of $F_5TeNHSi(CH_3)_3$ cited above, reaction conditions must be carefully controlled to prevent the formation of *cis*-$F_4Te[NHSi(CH_3)_3]_2$, which is known to be explosive.[230,125] The formation of *cis*-$F_4Te[NHSi(CH_3)_3]_2$ is believed to be favored for kinetic reasons since the trans isomer, being less sterically hindered, should be thermodynamically more stable.[125]

The basicity of the nitrogen center in F_5TeNH_2 was investigated by attempting to prepare adducts with the Lewis acids AsF_5 and BF_3.[230] A 1:1 adduct is formed with AsF_5 which is stable at room temperature, whereas the 1:1 adduct formed with the weaker Lewis acid,BF_3, decomposes reversibly above -60 °C. The fact that the $F_5TeNH_2 \cdot BF_3$ adduct is less thermally stable than $F_5SNH_2 \cdot BF_3$ (stable at room temperature)[227] has been interpreted as an indication of the weaker basicity of F_5TeNH_2 relative to that of F_5SNH_2. The electron withdrawing power of the F_5Te-group results in some acid character for F_5TeNH_2, however, it is only marginally acidic. In contrast to the strong acid $HOTeF_5$,[52] no definite products result from the reaction of F_5TeNH_2 and nitrogen bases such as pyridine and triethylamine.[230] No reaction is observed between F_5TeNH_2 and CsF, rather an unstable salt assumed to be $Cs^+NHTeF_5^-$ is isolated according to equation (4.15).[230] The resulting $Cs^+HNTeF_5^-$ salt decomposes in most solvents, and has exploded

$$F_5TeNHSi(CH_3)_3 + CsF \longrightarrow Cs^+HNTeF_5^- + (CH_3)_3SiF \qquad (4.15)$$

in the laser beam of a Raman spectrometer.[230]

The weaker basicity of the nitrogen lone pair in F_5TeNH_2 relative to that in F_5SNH_2 was attributed by Seppelt[230] to result from Te-N p_π-d_π bonding. As mentioned above for the OXF_5^- anions, the acceptor orbitals may largely consist of σ^*(Te-$F_{ax.}$) and σ^*(Te-$F_{eq.}$) antibonding orbitals, with only a minor contribution from vacant *d*-orbitals. In describing the bonding in F_5TeNH_2, a direct comparison can be made with the $OTeF_5^-$ anion [Section (A) of this Chapter]. Protonation of F_5TeNH_2 to give the acid cation, $F_5TeNH_3^+$, is expected to result in a reduction in the Te-N π-bonding and a strengthening of the Te-F bonds, by analogy with the changes in bonding which occur upon protonation of the $OTeF_5^-$ anion.

The present Chapter investigates the synthesis and characterization of F_5TeNH_2 and the corresponding novel acid cation, $F_5TeNH_3^+$, as the AsF_6^- salt to investigate the effect of protonation of F_5TeNH_2 on the bonding of the F_5TeN- group, using ^{19}F and ^1H NMR and Raman spectroscopy. The salt, $F_5TeNH_3^+AsF_6^-$, has been characterized for the first time by Raman spectroscopy and ^{19}F, ^{15}N, ^1H and ^{125}Te NMR spectroscopy.

RESULTS AND DISCUSSION

(A) PREPARATION AND ISOLATION OF F_5TeNH_2, $F_5TeNH_3^+AsF_6^-$ AND THE 99.5 % ^{15}N-ENRICHED ANALOGS

Aminotellurium(VI) pentafluoride, F_5TeNH_2, was prepared according to the method of Seppelt [equations (4.13) and (4.14)].[125,230] The amine is a volatile white solid at room temperature, subliming easily under vacuum, and is consistent with the physical properties observed by Seppelt.[230] The physical properties of F_5TeNH_2 are similar to those observed for

F_5TeOH, also a volatile solid at room temperature,[52] and are consistent with the essentially spherical structures of these molecules. The 99.5% ^{15}N enriched compound was prepared using a similar procedure, however, [^{15}N]hexamethyldisilazane was prepared from ^{15}N enriched NH_4Cl [equations (4.16) and (4.17)].

$$^{15}NH_4Cl + KOH \longrightarrow {}^{15}NH_3 + KCl + H_2O \tag{4.16}$$

$$3\ {}^{15}NH_3 + 2\ (CH_3)_3SiCl \longrightarrow 2\ {}^{15}NH_4Cl + [(CH_3)_3Si]_2{}^{15}NH \tag{4.17}$$

Identical procedures were used for the preparation of the salts $F_5TeNH_3^+AsF_6^-$ and [^{15}N]$F_5TeNH_3^+AsF_6^-$ from the amines, F_5TeNH_2 and [^{15}N]F_5TeNH_2. The basicity of F_5TeNH_2 was previously demonstrated from the formation of the 1:1 adducts $F_5TeNH_2{\cdot}BF_3$ and $F_5TeNH_2{\cdot}AsF_5$ by reaction of F_5TeNH_2 and the Lewis acid in CH_2Cl_2.[230] Only the adduct with the stronger Lewis acid, namely, $F_5TeNH_2{\cdot}AsF_5$, is stable with respect to dissociation into the starting materials at room temperature. In light of the stability of this adduct, the ability of F_5TeNH_2 to behave as a protic base in HF/AsF_5 superacid solution ($H_o \approx -20$)[231] was investigated. The compound, F_5TeNH_2, was dissolved in HF solvent at -78 °C. A 20 mole % excess of AsF_5 was condensed onto the frozen solution at -196 °C. On warming to -78 °C, a white precipitate formed which was isolated after removal of the solvent and excess AsF_5 at -55 °C under vacuum. The resulting white powder has been shown by mass balance, multinuclear NMR spectroscopy in solution and Raman spectroscopy in the solid state to be $F_5TeNH_3^+AsF_6^-$, formed according to equation (4.18) in near quantitative yield (96%). The salt hydrolyses very

$$F_5TeNH_2 + HF + AsF_5 \xrightarrow{-78 \text{ to } -55\ ^\circ C} F_5TeNH_3^+AsF_6^- \quad (4.18)$$

rapidly in the presence of air, but can be stored indefinitely at room temperature under a dry nitrogen atmosphere.

(B) CHARACTERIZATION OF F_5TeNH_2 IN THE SOLID STATE BY LOW TEMPERATURE RAMAN SPECTROSCOPY

The low temperature Raman spectra of natural abundance and 99.5 atom % ^{15}N-enriched F_5TeNH_2 were obtained at -160 °C, both of which are microcrystalline solids at this temperature. Figure 4.1 illustrates the Raman spectrum of F_5TeNH_2 and the $^{14/15}N$ isotopic shifts in the Raman spectra of F_5TeNH_2 and $[^{15}N]F_5TeNH_2$ are shown in Figure 4.2, and the frequencies are listed in Table 4.2, along with those of the related F_5TeOF, F_5TeO^- and F_5TeOH compounds. Although F_5TeNH_2 was characterized by infrared and Raman spectroscopy in methylene chloride solution in the paper which reported the original synthesis,[230] a more thorough assignment of the bands is presented here. This has been facilitated by observing the $^{14/15}N$ isotopic shifts of bands which arise from modes that involve the motion of the nitrogen atom by comparison of the Raman spectra of natural abundance F_5TeNH_2 (99.63% ^{14}N) and 99.5 atom % ^{15}N-enriched F_5TeNH_2. The isotopic shifts, $\Delta\nu(^{14/15}N)$, are given as the difference in the frequencies (cm^{-1}), $\nu(^{14}N) - \nu(^{15}N)$. Isotopic shifts are often quoted as the ratio $\Delta\lambda(^{14/15}N)/\lambda(^{14}N)$ as defined in references (73) and (232), where λ refers to a normal mode. This convention has not been used here, however, since the likely occurrence of vibrational coupling prevents the direct assignment of each band in the Raman spectra to a particular vibrational mode of F_5TeNH_2 (see below).

A total of 3N - 6 = 21 normal modes are expected for F_5TeNH_2. There are several

Figure 4.1 Raman spectrum of solid natural abundance F_5TeNH_2 recorded at -160 °C by use of 514.5-nm excitation.

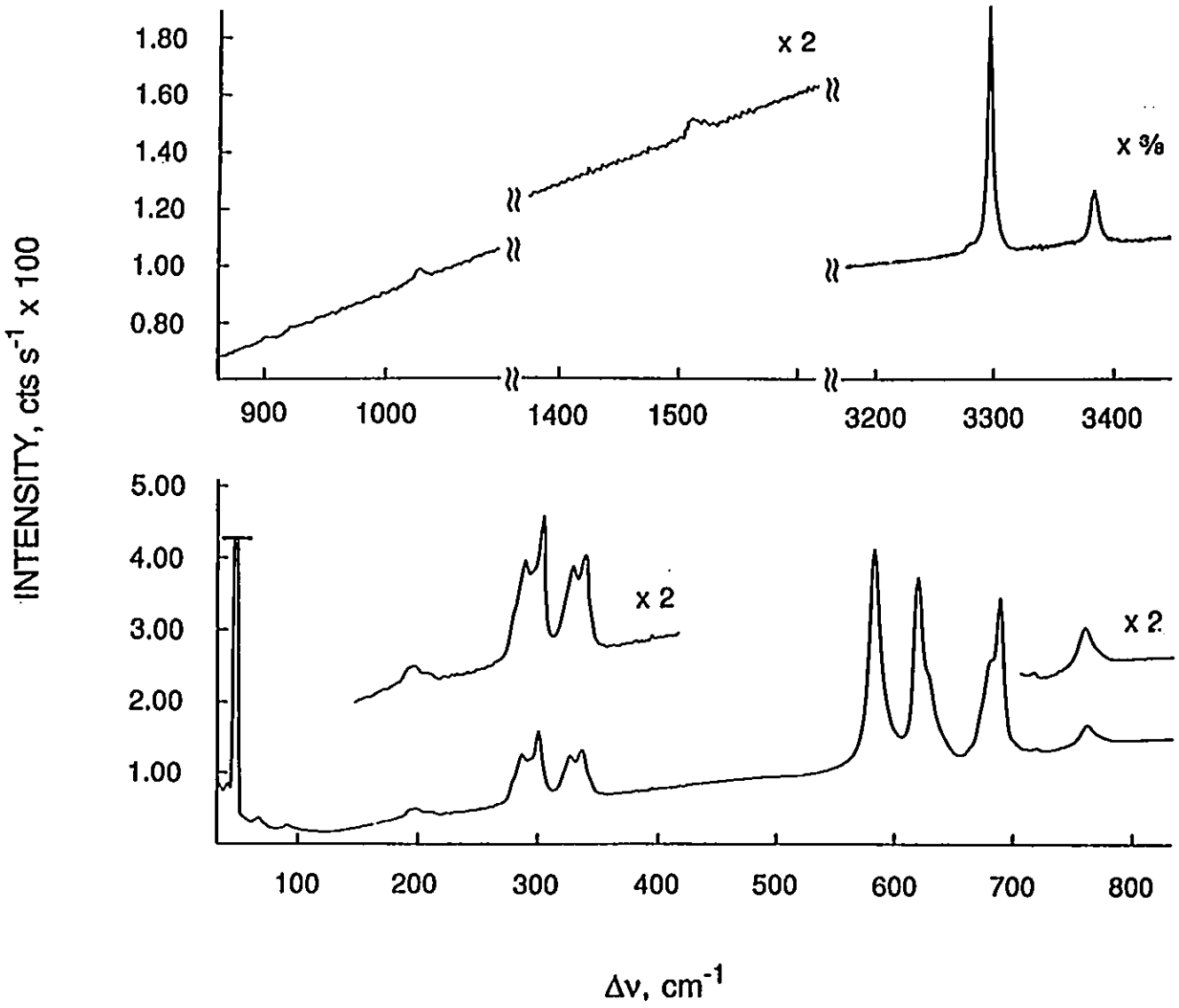
INTENSITY, cts s-1 x 100
1.80
1.60
1.40
1.20
1.00
0.80
x 2
x 3/8
900
1000
1400
1500
3200
3300
3400
5.00
4.00
3.00
2.00
1.00
x 2
x 2
100
200
300
400
500
600
700
800
Δν, cm-1

Figure 4.2 Raman spectra of solid natural abundance (lower traces) and 99.5 atom % ^{15}N-enriched (upper traces) F_5TeNH_2 recorded at -160 °C by use of 514.5-nm excitation; (a) 150 - 800 cm^{-1} region and (b) 1000 - 1050, 1450 - 1550 and 3250 - 3400 cm^{-1} regions.

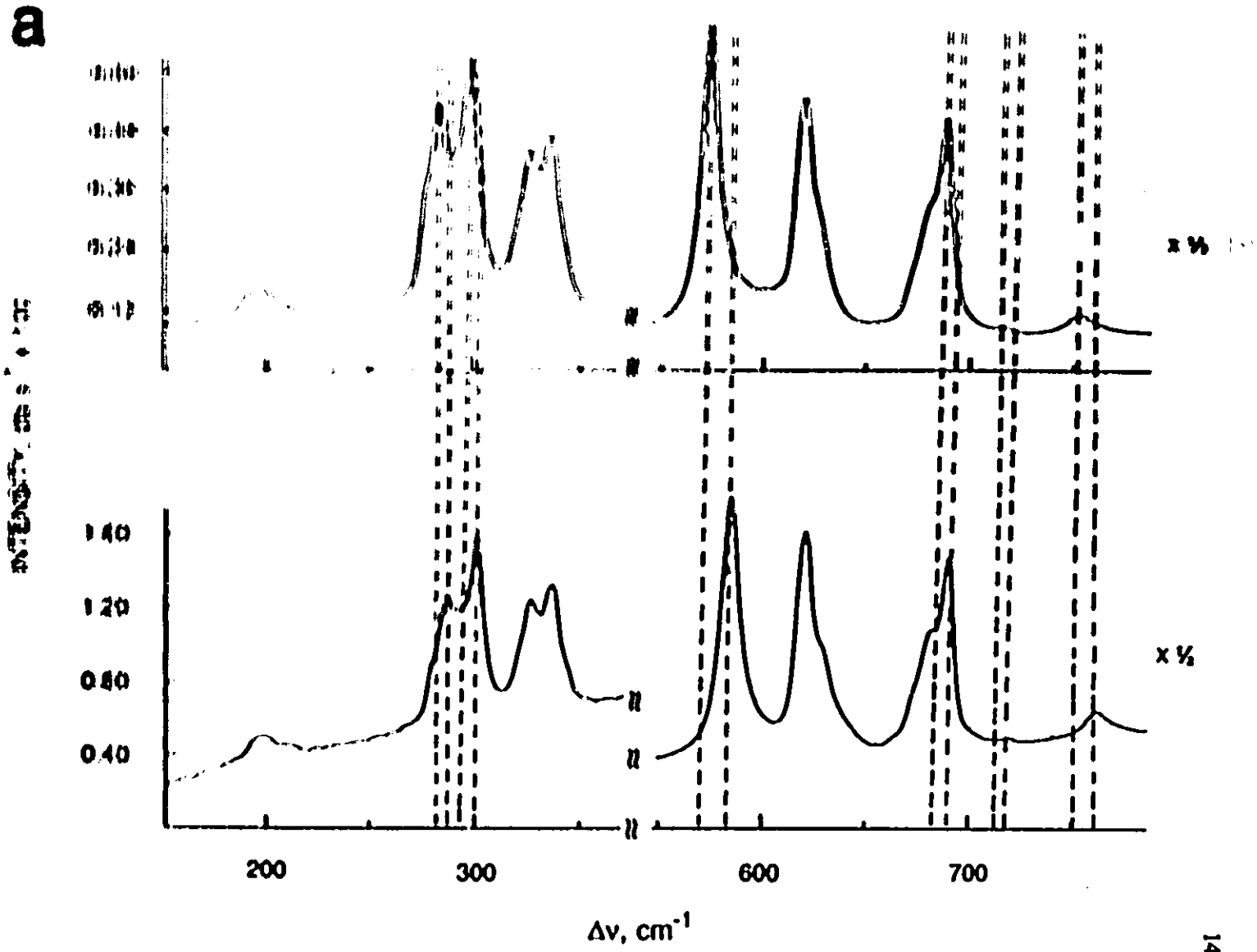
a
1.40
1.20
0.80
0.40
x ½
200
300
600
700
Δν, cm⁻¹

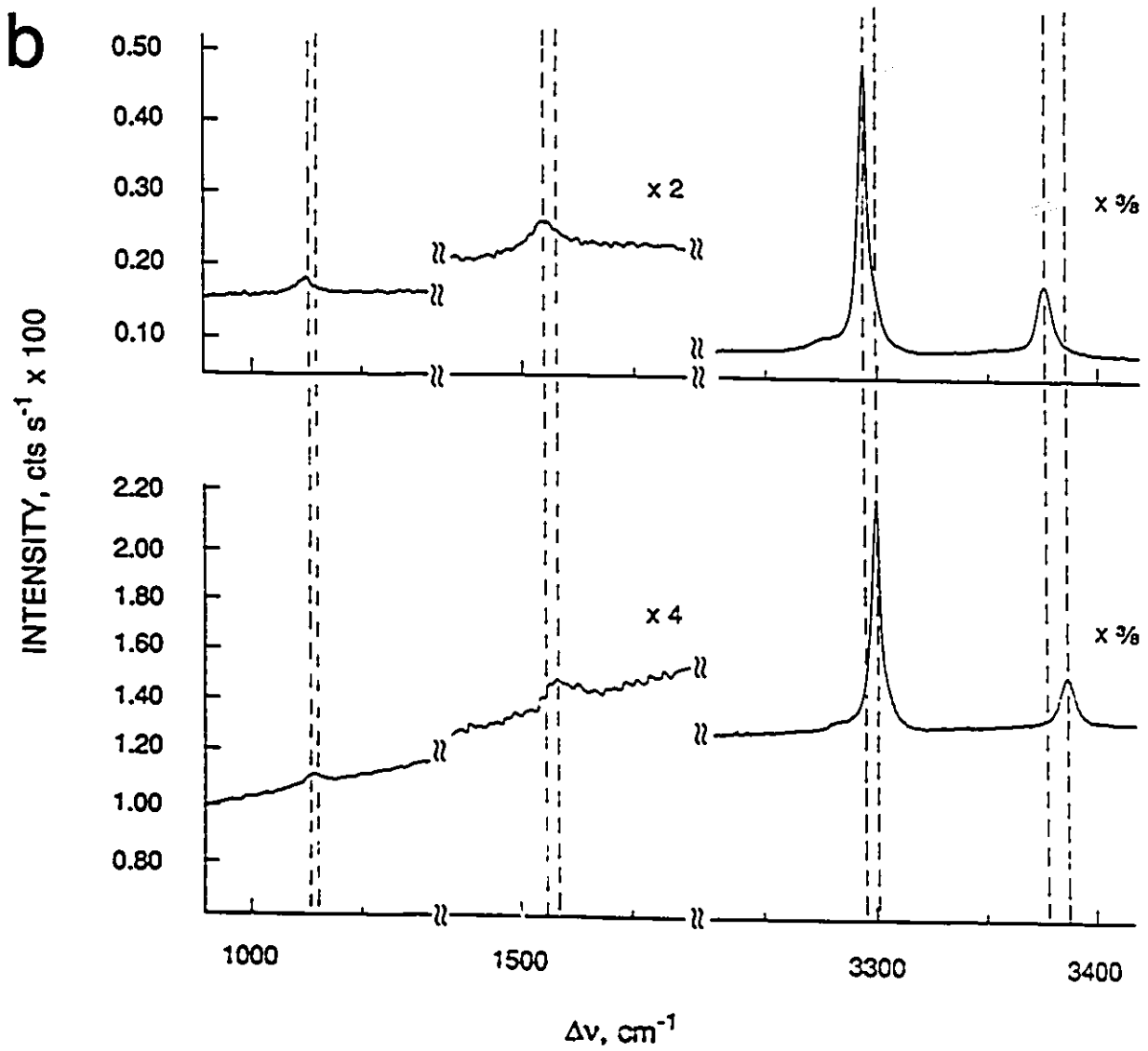
b
0.50
0.40
0.30
0.20
0.10
x 2
x 3/8
2.20
2.00
1.80
1.60
1.40
1.20
1.00
0.80
x 4
x 3/8
INTENSITY, cts s-1 x 100
1000
1500
3300
3400
Δν, cm-1

Table 4.2. Vibrational Frequencies and Assignments for F_5TeNH_2 and $[^{15}N]F_5TeNH_2$, and Comparison with F_5TeOF, F_5TeO^-, F_5TeOH[a]

F_5TeOF[b]	F_5TeO^- [c]	F_5TeOH[e]	F_5TeNH_2[g]	$[^{15}N]F_5TeNH_2$[g]	$\Delta\nu(^{14/15}N)$[h]	Assgnt and Approx Mode Description
						C_{4v}
721 (1.6)	584 (30)	735				A_1 ν_1, $\nu(Te\text{-}F_{ax.})$
			582.7 (10)	572.9 (10)	-9.8	sym $[\nu_1 + \nu_3]$
669 (10)	652 (100)	685	619.6 (8.42)	619.4 (7.62)	0	ν_2, $\nu_{sym}(TeF_4)$
613 (3.8)	868 (47)	735				ν_3, $\nu(Te\text{-}X)$
			761.0 (1.03)	752.9 (0.59)	-8.1	asym $[\nu_1 + \nu_3]$
301 (0.5)	319[d]	319	300.7 (3.36)	298.8 (2.76)	-1.9	ν_4, $\delta_{sym}(TeF_4)$ umbrella
		310				
660 (0.3)	584 (30)	652	628.6 (sh)	628.0 (sh)	-0.6	B_1 ν_5, $\nu_{sym}(TeF_4)$ out-of-phase
n.o.	n.o.	n.o.	n.o.	n.o.		ν_6, $\delta_{pucker}(TeF_4)$
309 (1.0)	283 (6)		326.8 (2.06)	326.5 (1.75)	-0.3	B_2 ν_7, $\Delta_{sciss}(TeF_4)$ in-plane
738 sh	636[d]	733.5[f]	689.1 (7.14)	688.5 (6.90)	-0.6	E ν_8, $\nu_{asym}(TeF_4)$
			680.4 (4.38)	681.0 (3.98)	-0.6	
325 sh	346 (6)		336.8 (2.29)	336.6 (1.91)	-0.2	ν_9, $\delta(FTeF_4)$
309-325	328 (40)		286.7 (2.41)	283.1 (2.27)	-3.6	ν_{10}, $\delta(XTeF_4)$
279 (0.2)	196 (3)	168	210.4 (0.21)	210.0 (0.14)	-0.4	ν_{11}, $\delta_{asym}(TeF_4)$
		145	194.6 (0.46)	194.6 (0.31)	0	
						C_s
			3280.1 (0.28)	3275.8 (0.25)	-4.3	A' ν_{12}, $\nu_{sym}(NH_2)$
			3297.2 (7.58)	3292.9 (5.72)	-4.3	

	1514.2 (0.10)	1509.3 (0.12)	-4.9	ν_{14}, $\delta(NH_2)$
	1028.4 (0.16)	1024.8 (0.13)	-3.6	ν_{13}, $\delta_{sym}(SNH)$
	3385.3 (1.65)	3376.1 (1.28)	-9.2	A" ν_{15}, $\nu_{asym}(NH_2)$
	719.3 (0.17)	717.6 (0.11)	-1.7	ν_{16}, $\delta_{asym}(SNH)$
	41.2 (0.75)	42.0 (0.35)		lattice modes and/or
	67.5 (0.23)	67.5 (0.31)		hydrogen-bonding
	91.0 (0.14)	91.0 (0.16)		interactions

Table 4.2 (continued)

[a]Data obtained from Raman spectra unless otherwise specified. Assignments for the modes of the F_5TeX groups have made assuming C_{4v} symmetry using the mode species descriptions from ref (233). All frequencies are reported in cm^{-1}. [b]Ref (233); liquid at -55 °C. [c]Ref (205); solid $N(CH_3)_4^+OTeF_5^-$ at 25 °C. ν_1 and ν_2 have been described as antisymmetric and symmetric combinations of $\nu_{sym}(TeF_4)$ and $\nu(Te\text{-}F_{ax})$, respectively. [d]Obtained from the infrared spectra at 25 °C. [e]Refs (220) and (203); Raman spectrum of the liquid, recorded at room temperature. [f]Obtained from the gas phase infrared spectrum, ref (220). [g]This work; Raman spectra recorded at -150 °C using 154.4-nm excitation. [h]Isotopic shifts $\Delta\nu(^{14/15}N) = \nu(^{15}N) - \nu(^{14}N)$, where the frequencies of the bands ν are given in cm^{-1}.

possibilities for the molecular point symmetry. In the presence of a planar nitrogen center, which may result from Te-N π bonding, C_{2v} point symmetry is expected if the NH_2 group is staggered or eclipsed with respect to the equatorial fluorines of the F_5Te- group. A pyramidal nitrogen center would result in C_s point symmetry for the staggered and eclipsed conformations. All modes are Raman active under these symmetry designations. Due to the large difference in mass of the atoms in the F_5TeN- and -NH_2 groups, the vibrational frequencies associated with these two moieties are well separated from each other. As a result, it is possible to assign the modes of each moiety separately, allowing for the comparison of the vibrational modes of each moiety with those of simpler molecules. Precedent for this approximation was established in the assignment of the vibrational spectra of F_5TeOCl and F_5TeOF.[233]

All bands attributable to the F_5TeN- group have been successfully assigned to the 3N - 6 = 15 normal modes under C_{4v} point group symmetry to provide direct comparision with the large body of published vibrational data for the F_5TeX group (X = O^-,[205,206] OH,[220] OF,[233] OCl,[233] and Cl[234]). Comparisons are made with F_5TeO^-, F_5TeOF, F_5TeOH in Table 2. Under C_{4v} symmetry, the normal modes belong to the irreducible representations 4 A_1 + 2 B_1 + B_2 + 4 E and are shown in Figure 4.3, all of which are Raman active.

The bands at 582.7 and 761.0 cm^{-1} both have large isotopic shifts, and therefore have contributions from the Te-N stretching mode. The bands are tentatively assigned to the symmetric and asymmetric ν(N-Te-$F_{ax.}$) stretching modes (ν_1 + ν_3), respectively. This assignment is in accord with the rule of thumb that an asymmetric stretch is usually higher in frequency than the associated asymmetric stretch. As expected in the Raman, the intensity of the symmetric stretch is greater than that for the asymmetric stretch (see Table 4.2). The strong coupling of the ν_1 and ν_3 modes supports Seppelt's hesitation to make a distinction between the Te-F and Te-N stretching

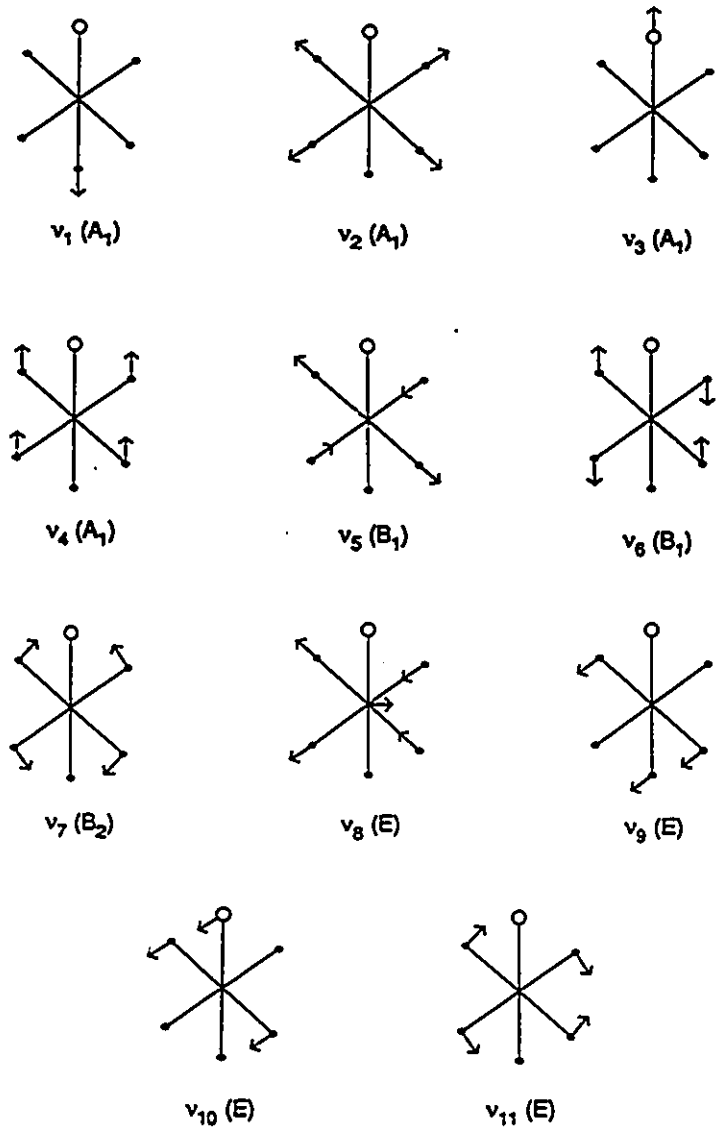

Figure 4.3 Normal modes for pseudo-octahedral species, XY_5Z, of C_{4v} point symmetry.

vibrations in the original assignment of the infrared and Raman spectra for F_5TeNH_2 in methylene chloride solution.[230] Strong coupling of ν_1 and ν_3 was observed in the calculation of a modified valence force field for the analogous F_5SO^- anion.[210] The range of frequencies assigned to Te-N stretching modes for the related dialkylamino derivatives F_5TeNR_2 (538 -629 cm^{-1})[229] is in agreement with the present study. The $^{14/15}N$ isotopic shift of the band at 300.7 cm^{-1} [$\Delta\nu(^{14/15}N$ = -1.9 cm^{-1}] indicates that this band arises from the symmetric umbrella motion (out of plane bend) of the equatorial fluorines, $\delta_{sym}(TeF_4)$, since this mode undoubtedly couples with ν(Te-N), as observed in the vibrational spectra of F_5TeOX (X = Cl, F).[233] The isotopic dependence of the band at 286.7 cm^{-1} [$\Delta\nu(^{14/15}N$ = -3.6 cm^{-1}] in the Raman spectrum of F_5TeNH_2 provides evidence for its assignment to the $\delta(NTeF_4)$ mode. The frequency is also similar to those observed for F_5TeOF (309 - 325 cm^{-1}),[233] and F_5TeO^- (328 cm^{-1}).[205,206] The assignments of bands to $\nu_{sym}(TeF_4)$ (A_1) and $\nu_{asym}(TeF_4)$ (E) have been made on the basis of intensity, since $\nu_{sym}(TeF_4)$ is consistently the most intense band in the Raman spectra of F_5TeCl,[234] F_5TeOF,[233] and F_5TeOCl,[233] and the assumption that an asymmetric stretch is in general higher in frequency than the corresponding symmetric stretch. The $\nu_{asym}(TeF_4)$ (E) band is split, and may result from vibrational coupling of adjacent molecules within the unit cell of the microcrystalline solid, or from site symmetry effects in the solid state, since the Raman spectrum for F_5TeNH_2 in CH_2Cl_2 solution,[230] where solid state interactions are alleviated, exhibits a single band at 684 cm^{-1}, the average of the solid state bands attributed to $\nu_{asym}(TeF_4)$. The small isotopic shifts of both of the bands attributed to $\nu_{asym}(TeF_4)$ [$\nu(^{14/15}N)$ = -0.6 cm^{-1}] are assumed to result from vibrational coupling with the $\delta(NTeF_4)$ mode of the same symmetry (E).

The assignment of bands to ν_7 [$\delta_{sciss}(TeF_4)$ in plane], ν_9 [$\delta(FTeF_4)$] and ν_{11} [$\delta_{asym}(TeF_4)$] is straightforward by comparison with F_5TeOF,[233] F_5TeOH,[220] and F_5TeO^-,[205,206] since these

bands are relatively constant for different substituents X in F_5TeX compounds, as shown in Table 4.2.

The band attributed to the $\nu_{sym}(TeF_4)$ mode of B_1 symmetry (ν_5) exhibits a small $^{14/15}N$ isotopic shift ($\Delta\nu^{14/15}N = -0.6\ cm^{-1}$). The accuracy of the isotopic shift is dubious, however, since the band is observed as a shoulder on the more intense band at 619.6 cm^{-1}. Under C_{4v} point group symmetry, this mode is not expected to couple with ν(Te-N) (ν_3) or $\delta(NTeF_4)$ (ν_{10}) because it does not belong to the E or A_1 irreducible representations. This selection rule for vibrational coupling of modes, and thus for the observation of isotopic dependences, may not apply since the true point group symmetry of F_5TeNH_2 is C_{2v} or C_s (see above) and the assumption of C_{4v} symmetry is only an approximation applied to the F_5TeN- group. If one considers that C_{2v} and C_s are subgroups of C_{4v}, correlation tables[235] indicate that $\nu_{sym}(TeF_4)$ may couple with ν(Te-N) or $\delta(NTeF_4)$. For example, the irreducible representation of symmetry E, assignable to $\delta(NTeF_4)$ under C_{4v} point group symmetry correlates with A' + A" under C_s. The mode $\nu_{sym}(TeF_4)$ belongs to the B_1 irreducible representation under C_{4v}, which correlates with A' under C_s, allowing it to couple with $\delta(NTeF_4)$. Similarly, ν(Te-N) belongs to the A' irreducible representation under C_s point group symmetry. Under C_{2v} point group symmetry, $\nu_{sym}(TeF_4)$ may couple with ν(Te-N) since they both belong to the A_1 irreducible representation.

As shown in Table 4.2, the frequencies of the bands attributed to Te-F stretching modes in F_5TeNH_2, in particular $\nu(Te\text{-}F_{ax.})$ [cf., symmetric combination of $\nu_1 + \nu_3$], are significantly lower than those of F_5TeOH and F_5TeOF. The Te-F stretching frequencies are, however, similar to those of the F_5TeO^- anion. The lowering of these bands relative to their equivalents in F_5TeOH has been attributed, by analogy with IOF_5,[236] to an increase in donation of electron density from oxygen to tellurium, which increases the ionic character, and thus weakens the Te-F bonds.[206] As

discussed in Section (A) of this Chapter, a more accurate model may involve donation of π-electron density from oxygen to σ^*(Te-F) orbitals in F_5TeO^-. Population of these antibonding orbitals accounts for the weakening of the Te-F bonds. The weakness of the axial Te-F bond compared to the equatorial Te-F bonds may result from the fact that $\pi_O \rightarrow \sigma^*(\text{Te-F}_{ax.}) > \pi_O \rightarrow \sigma^*(\text{Te-F}_{eq.})$. Resonance Structures 4.4 - 4.6 may be proposed for F_5TeNH_2, which are analogous to those proposed to describe the bonding in the F_5TeO^- anion[206] [see Section (A) of this Chapter]. Greater weighting of resonance Structure 4.6 reflects the weaker axial Te-F bond.

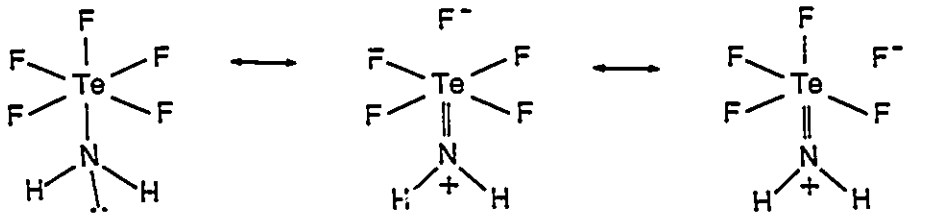

etc.

4.4 4.5 4.6

A band attributable to ν_6, $\delta(TeF_4)$ is not observed in the Raman spectrum of F_5TeNH_2, presumably owing to an inherently low intensity and is likewise too weak to be observed in the vibrational spectra of F_5TeCl,[234] F_5TeOCl,[233] F_5TeOF,[233] F_5TeOH,[220] F_5IO[236] and F_5TeO^-.[206] A value of 275 cm^{-1} has been estimated for F_5IO[236] from an infrared combination band. A value of ν_6 for F_5TeCl (199.1 cm^{-1}) has been calculated from the force constants obtained using the Wilson F/G matrix method.[234]

The 3N - 6 = 6 modes for the $TeNH_2$ group may be assigned to the irreducible representations 4 A' + 2 A" under C_s point group symmetry assuming a nonplanar nitrogen

geometry, or to 3 A_1 + B_1 + 2 B_2 under C_{2v} point group symmetry for a planar nitrogen center. The latter may result from N → Te π-donation, by analogy with amides, where substantial N → C π-donation results in a planar nitrogen center.[237] By analogy with a vibrational study of aniline,[232] it is possible to estimate the degree of the planarity of the nitrogen center from the $^{14/15}N$ isotopic frequency dependence of the bands associated with the NH_2 group on the HNH bond angle (θ). The quantitative dependence of the isotopic shift on the HNH bond angle (θ) is derived from the isotopic dependence of the **G** matrices for ^{14}N and ^{15}N aniline which are calculated for different geometries of the NH_2 group.[232] The degree of vibrational coupling of the symmetric and asymmetric stretching modes of the NH_2 group with other vibrational modes in aniline is negligibic,[232] and therefore the bands assignable to the $\nu_{sym}(NH_2)$ and $\nu_{asym}(NH_2)$ modes are more reliable than the other bands assigned to the NH_2 group for estimating θ, since these latter bands may have contributions from several modes. Assuming similar vibrational purity of the bands assigned to $\nu_{sym}(NH_2)$ and $\nu_{asym}(NH_2)$ in F_5TeNH_2, Table 4.3 compares observed values of $\Delta\lambda/\lambda^o$ for $\nu_{sym}(NH_2)$ and $\nu_{asym}(NH_2)$ with calculated values of $\Delta\lambda/\lambda^o$ as a function of θ, for $[^{14}N]F_5TeNH_2$ and $[^{15}N]F_5TeNH_2$. The results do not indicate a rigorously planar nitrogen center, where θ = 120°, since there is not a close correspondence of the calculated and observed values of $\Delta\lambda/\lambda^o$ for $\nu_{sym}(NH_2)$ and $\nu_{asym}(NH_2)$ [see Table 4.3]. This provides evidence against a pure Te-N π-bond of bond order 2, which would result in a planar nitrogen center. Possibly a Te-N bond order of less than two is present, as has been observed from calculation of X-O force constants for IOF_5, F_5TeO^- and F_5SeO^-.[206] In addition, $\pi_N \rightarrow \sigma^*$ negative hyperconjugation as a mechanism for π-donation from nitrogen to the F_5Te- group does not require a planar nitrogen geometry. This has been illustrated in geometric optimizations for FCH_2NH_2,[238] which indicate maximum negative hyperconjugation when the plane defined by the NH_2 group is 144.6° with

Table 4.3. Calculated and Observed $^{14/15}N$ isotopic shifts, $\Delta\lambda/\lambda^o$, of $\nu_{sym}(NH_2)$ and $\nu_{asym}(NH_2)$ for F_5TeNH_2.

	Calculated values of $\Delta\lambda/\lambda^o$ [a]					
Symmetry Coordinate	Planar[b] ($\theta = 120^o$)	Planar[b] ($\theta = 107^o$)	Pyramidal[b] ($\theta = 109.5^o$)	Observed $\Delta\lambda/\lambda^o$	Frequency, (cm^{-1})[c] $[^{14}N]F_5TeNH_2$	$[^{15}N]F_5TeNH_2$
$\nu_{sym}(NH_2)$	-0.00230	-0.00322	-0.00304	-0.00261	3297.2	3292.9
$\nu_{asym}(NH_2)$	-0.00645	-0.00566	-0.00582	-0.00543	3385.3	3376.1

[a] $\Delta\lambda/\lambda^o = [\lambda(^{15}N) - \lambda(^{14}N)]/\lambda^{14}N$; $\lambda = 4\pi^2c^2\nu^2$, where c = velocity of light. Values for $\Delta\lambda/\lambda^o$ were calculated from G matrices in ref (232). [b] θ = HNH bond angle. [c] This work; frequencies obtained from Raman spectra of $[^{14}N]F_5TeNH_2$ and $[^{15}N]F_5TeNH_2$ recorded at -150 °C using 514.5-nm excitation.

respect to the N-C bond axis, indicating a pyramidal nitrogen geometry.

The bands attributable to the $TeNH_2$ group have therefore been assigned under the modes of C_s symmetry as shown in Table 4.2 (ν_{12} to ν_{16}). One of the A' modes has been omitted since it is the same mode as ν_1 [ν(Te-N)] of the F_5TeN- group. All modes associated with the $TeNH_2$ group exhibit $^{14/15}N$ isotopic shifts. The band associated with δ(TeNH) has been assigned by comparison to the infrared spectrum of F_5TeOH (1023.8, 1014.8 cm^{-1}).[220] Comparison with the infrared spectrum of matrix isolated FNH_2[239] and aniline in dilute solution[232] allowed for the assignments of $\nu_{sym}(NH_2)$, $\nu_{asym}(NH_2)$, δ_{sym}(SNH), and $\delta(NH_2)$. The $^{14/15}N$ isotopic dependence and the process of elimination allowed for assignment of the band at 719.3 cm^{-1} in the Raman spectrum of F_5TeNH_2 to the wagging mode, $\omega(NH_2)$, referred to as ν_{16} [δ_{asym}(SNH)] in Table 4.4, which occurs at 700 cm^{-1} in the infrared spectrum of liquid aniline.[232]

Bands observed at 91.0, 67.5 and 41.2 cm^{-1} exhibit no measurable shifts on ^{15}N substitution and have been assigned to hydrogen bonding and/or lattice modes.

(C) CHARACTERIZATION OF F_5TeNH_2 AND [^{15}N]F_5TeNH_2 IN SOLUTION BY ^{19}F AND ^1H NMR SPECTROSCOPY

The ^{19}F NMR spectrum for F_5TeNH_2 was investigated in CD_2Cl_2 solvent at 30 °C, and is similar to that reported by Seppelt.[230] The C_{4v} point symmetry of the F_5TeN- group is apparent from the characteristic AB_4 pattern, where δ_A = -37.3, and δ_B = -41.2 ppm. The two-bond coupling constant $^2J(^{19}F_A\text{-}^{19}F_B)$ = 170 Hz. The couplings $^1J(^{19}F_B\text{-}^{125}Te)$ = 3519, $^1J(^{19}F_B\text{-}^{123}Te)$ = 2944, and $^1J(^{19}F_A\text{-}^{125}Te)$ = 3284 Hz were also resolved. The couplings $^1J(^{19}F_A\text{-}^{123}Te)$, $^2J(^{19}F_A\text{-}^{15}N)$, $^2J(^{19}F_B\text{-}^{15}N)$, $^3J(^{19}F_A\text{-}^1H)$ and $^3J(^{19}F_B\text{-}^1H)$ were not resolved in the ^{19}F NMR spectrum of [^{15}N]F_5TeNH_2. The ^{19}F NMR spectra are consistent with observations made for

dialkylaminotellurium pentafluorides F_5TeNR_2 (R = CH_3,[228,229] CH_2CH_3,[229] C_4H_8[229]) and F_5TeNH_2.[230]

The ^1H NMR spectrum of F_5TeNH_2 in CD_2Cl_2 solvent at 30 °C (Figure 4.4a) exhibits a broad singlet ($\Delta\nu_{1/2}$ = 79 Hz) centered at $\delta(^1H)$ = 4.30 ppm, arising from the protons directly bonded to nitrogen. The large line width and the absence of any resolved couplings results from fast relaxation of ^1H due to interactions with the directly bonded quadrupolar ^{14}N nucleus (I = 1). The effects of quadrupolar broadening of the proton resonance are alleviated in the ^1H NMR spectrum of $[^{15}N]F_5TeNH_2$ in CD_2Cl_2 solvent at 30 °C (Figure 4.4b), and a doublet centered at $\delta(^1H)$ = 4.29 ppm arising from $^1J(^1H\text{-}^{15}N)$ = 71 Hz is observed (reduced coupling constant $^1K(H\text{-}N) = 5.8 \times 10^{20}\ NA^{-2}m^{-3}$). Each peak of the doublet is flanked by a low intensity satellite doublet arising from $^2J(^1H\text{-}^{125}Te)$ = 42 Hz. The magnitude of $^1J(^1H\text{-}^{15}N)$ is directly comparable to that observed for related $R^{15}NH_2$ compounds where R = $(CF_3)_2P$-, $(CF_3)_2As$-, CF_3S-.[124] Several attempts have been made to arrive at an empirical relationship between the magnitude of $^1J(^1H\text{-}^{15}N)$ and the 2s character in the nitrogen bonding orbitals[240,241] with the aim of evaluating the hybridization at nitrogen. The fundamental assumption in attempting to correlate the magnitude of a directly bonded coupling constant with the nature of the bond hybridization is that the Fermi contact term is the dominant contribution to the coupling mechanism. This statement is usually assumed to be valid if one of the coupled nuclei is a proton.[242] Equation (4.19) is a simplified expression for the Fermi contact contribution to the one bond $^{15}N\text{-}^1H$ coupling constant. Here

$$^1J(^{15}N\text{-}^1H) \propto \gamma(^{15}N)\gamma(^1H)(\Delta E)^{-1}(\alpha_N)^2(\alpha_H)^2|\psi_{N(2s)}(0)|^2|\psi_{H(1s)}(0)|^2 \qquad (4.19)$$

$\gamma(^{15}N)$ and $\gamma(^1H)$ are the gyromagnetic ratios of the coupled nuclei, ΔE is the average excitation

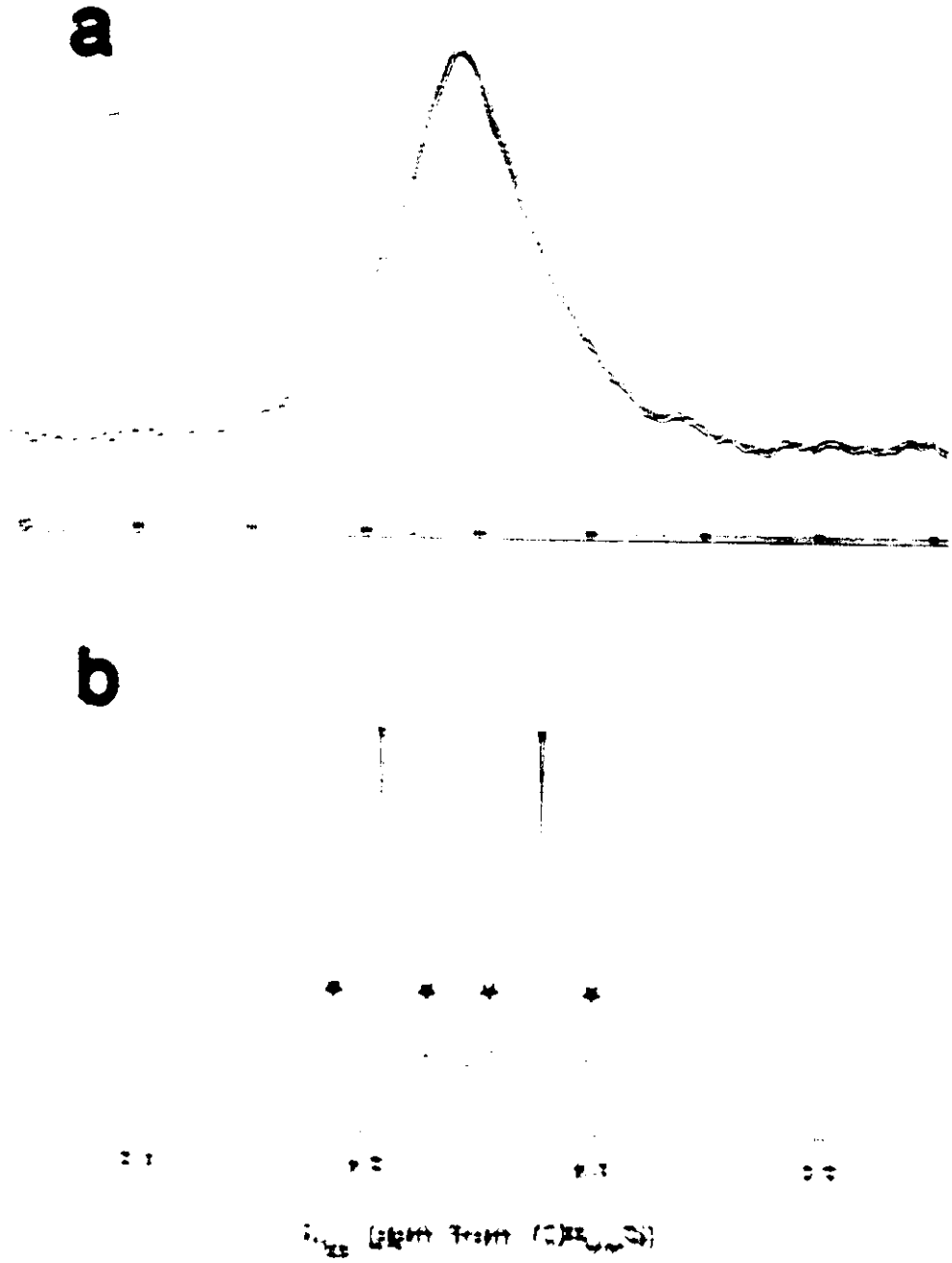

Figure [illegible] (a) [illegible] (b) [illegible]

energy; $(\alpha_N)^2$ and $(\alpha_H)^2$ are the *s* characters of the hybrid orbitals which make up the N-H bond, and the $|\psi(0)|^2$ terms represent the magnitudes of the indicated valence *s* orbitals at the appropriate nuclei. Bunch *et al.*[240] published an empirical equation (4.20) based on the

$$\%\ s = 0.43|^1J(^{15}N,^1H)| - 6 \qquad (4.20)$$

proportionality of $^1J(^{15}N,^1H)$ and the *s* characters of the hybrid orbitals which make up the N-H bond as shown in equation (4.19). This has been used to assess the hybridization at nitrogen (i.e., % *s* characters of 50.0, 33.3, and 25.0 correspond to sp, sp^2 and sp^3 nitrogen valence orbital hybridizations, respectively). This information might in turn be used to assess the nature of the nitrogen heteroatom bond. For instance, an sp^2 valence orbital hybridization for nitrogen would imply a trigonal planar geometry and the presence of a filled *p* orbital on nitrogen, with the possibility for π donation from nitrogen to the directly bonded heteroatom. Equation (4.20) was established originally from coupling constant data obtained from molecules with tetrahedral and trigonal planar nitrogen geometries,[241] but has also been shown to be valid for linear species such as $HC^{15}N^{1}H^{+}$ and $CH_3C^{15}N^{1}H^{+}$.[242] Using equation (4.20), the observed value of $^1J(^{15}N,^1H) = 71$ Hz for $F_5S^{15}N^{1}H_2$ predicts a % *s* character of 28.5 for the nitrogen valence hybrid orbitals, indicating that the nitrogen atom is sp^3 hybridized. This would imply a tetrahedral nitrogen geometry and preclude a model where there is substantial "N=S" double bond character. It is difficult to assess the applicability of equation (4.20) to the present system, since Cowley *et al.*[243] have previously published that this equation breaks down when the electronegativity of the heteroatom bonded to nitrogen is significantly different from that of carbon. Based on the data available, it is not possible to evaluate the hybridization at nitrogen in $F_5S^{15}N^{1}H_2$. From the magnitude of $^1J(^{15}N,^1H)$,

and the presence or absence of p_π-d_π bonding between nitrogen and tellurium cannot be commented upon.

(D) CHARACTERIZATION OF $F_5TeNH_3^+AsF_6^-$ AND $[^{15}N]F_5TeNH_3^+AsF_6^-$ IN SOLUTION BY ^{19}F, ^1H, ^{15}N, AND ^{125}Te NMR SPECTROSCOPY

Bromine pentafluoride and anhydrous HF solvents were found to be suitable for obtaining the NMR spectra of $F_5TeNH_3^+AsF_6^-$, and the parameters obtained from the multinuclear NMR spectra are listed in Table 4.4.

The ^1H NMR spectrum of $F_5TeNH_3^+AsF_6^-$ in BrF_5 solvent at -53 °C (Figure 4.5a) consists of a broad singlet centered at 7.45 ppm ($\Delta\nu_{1/2}$ = 28 Hz). The broadening and absence of resolved couplings results from the fast relaxation of the directly bonded quadrupolar nitrogen center (I = 1). The ^1H NMR spectrum of $[^{15}N]F_5TeNH_3^+AsF_6^-$ in BrF_5 solvent at -56 °C (Figure 4.5b) illustrates a doublet arising from $^1J(^1H\text{-}^{15}N)$ = 76 Hz (reduced coupling constant $^1K(N\text{-}H) = 6.2 \times 10^{20}$ $NA^{-2}m^{-3}$) centered at 7.43 ppm. The magnitude of the one-bond reduced N-H scalar coupling constant is comparable to that observed for similar compounds containing formally sp^3 hybridized, positively charged nitrogen centers (cf., $NH_4^+AsF_6^-$:[244] $^1K(N\text{-}H) = 6.2 \times 10^{20}$ $NA^{-2}m^{-3}$; $CH_3NH_3^+Cl^-$:[240] $^1K(N\text{-}H) = 6.2 \times 10^{20}$ $NA^{-2}m^{-3}$).

The ^{19}F NMR spectrum of the salt $F_5TeNH_3^+AsF_6^-$ at -44 °C in BrF_5 solvent (Figure 4.6) consists of a typical AB_4 pattern confirming the C_{4v} symmetry of the F_5TeN- group, where $\delta(^{19}F_A)$ = -55.6 ppm and $\delta(^{19}F_B)$ = -30.2 ppm. The parameters obtained from the ^{19}F NMR spectrum are listed in Table 4.4. Assignments of the chemical shifts and coupling constants are made by analogy with F_5TeNH_2 (see above). The peak at -53.2 ppm results from TeF_6 and the broad resonance centered at -60 ppm is assigned to the AsF_6^- anion. Broadening of this resonance

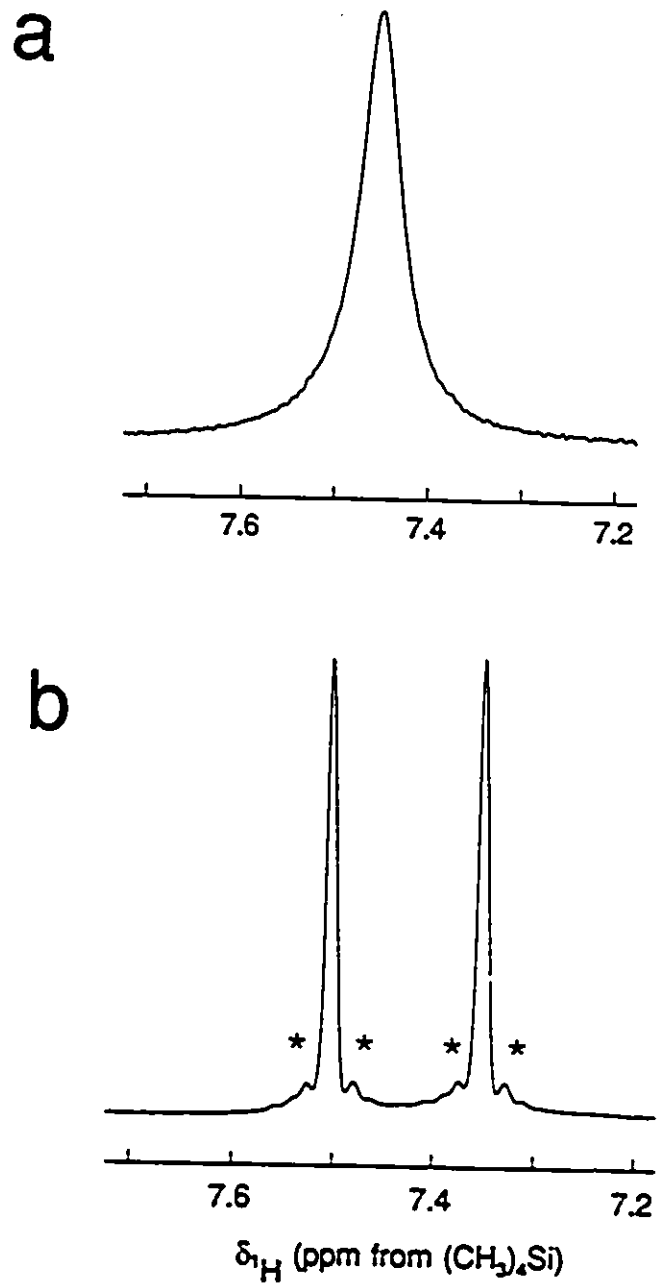

Figure 4.5 ^1H NMR spectra (500.138 MHz) of (a) natural abundance $F_5TeNH_3^+AsF_6^-$ (-53 °C: BrF_5 solvent) and (b) 99.5 atom % ^{15}N-enriched $F_5TeNH_3^+AsF_6^-$ (-56 °C: BrF_5 solvent). Asterisks (*) denote ^{125}Te satellites.

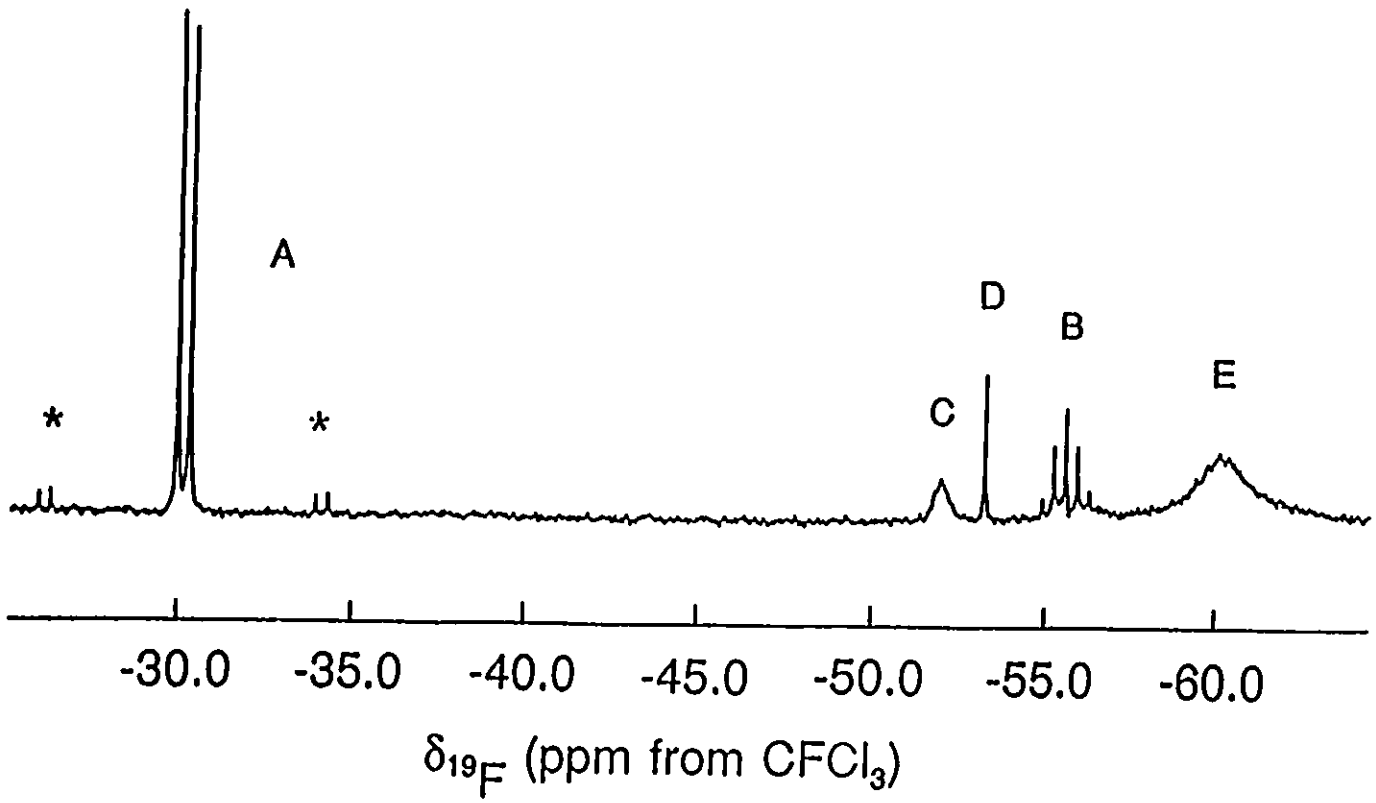

Figure 4.6 ^{19}F NMR spectrum (470.599 MHz) of natural abundance $F_5TeNH_3^+AsF_6^-$ in BrF_5 solvent (-44 °C); (A) resonance of equatorial fluorine atoms bonded to tellurium, (B) resonance of axial fluorine atom bonded to tellurium, (C) unidentified resonance, (D) TeF_6, (E) AsF_6^-. Asterisks (*) denote ^{125}Te satellites.

is due to the rapid quadrupole relaxation of ^{75}As (I = 3/2). The broad resonance at -52.0 ppm is attributed to a decomposition product, but the lack of coupling information prevents the assignment of this resonance. No additional couplings were observed in the ^{19}F NMR spectrum of $[^{15}N]F_5TeNH_3^+AsF_6^-$ in HF or BrF_5 solvents.

The ^{125}Te NMR spectrum of $[^{15}N]F_5TeNH_3^+AsF_6^-$ in HF solvent at -45.0 °C is shown in Figures 4.7a and 4.7b, and the ^{125}Te NMR chemical shift [$\delta(^{125}Te)$ = 588 ppm] is consistent with that expected for the F_5Te- group (cf., F_5TeOH, $\delta(^{125}Te)$ = 601 ppm in $CH_3C{\equiv}N$ solvent[248]). All possible scalar couplings involving ^{125}Te are observed, and are listed in Table 4.4. The ^{125}Te NMR resonance is split into a doublet from the one-bond coupling $^1J(^{125}Te\text{-}^{19}F_A)$ = 3801 Hz. Each line of the doublet is further split into a quintet from the scalar coupling of tellurium with four equivalent equatorial fluorines [$^1J(^{125}Te\text{-}^{19}F_B)$ = 3651 Hz]. These couplings are consistent with those observed in the ^{19}F NMR spectra. Each line of this multiplet is further split into a doublet of quartets from the scalar coupling of tellurium with nitrogen [$^1J(^{125}Te\text{-}^{15}N)$ = 48 Hz] and with the three equivalent protons of the $-NH_3^+$ group [$^2J(^{125}Te\text{-}^1H)$ = 25 Hz]. The magnitude of $^2J(^{125}Te\text{-}^1H)$ is consistent with that observed for the same coupling in the ^1H NMR spectrum of the $F_5TeNH_3^+$ cation. The observation of well defined quartets corresponding to the two-bond scalar coupling with the protons on nitrogen indicates that $F_5TeNH_3^+$ predominates in the highly acidic HF solvent.

The ^{15}N NMR spectrum of $[^{15}N]F_5TeNH_3^+AsF_6^-$ (Figure 4.8) at -40 °C in HF solvent consists of a quartet centered at -317.1 ppm. The quartet structure arises from the one-bond scalar coupling of nitrogen and the three equivalent protons [$^1J(^{15}N\text{-}^1H)$ = 76 Hz]. The magnitude of the coupling is consistent with $^1J(^1H\text{-}^{15}N)$ observed in the proton ^1H NMR spectrum. Each line of the quartet is flanked by low intensity satellites arising from $^2J(^{15}N\text{-}^{125}Te)$ = 48 Hz, which is

Figure 4.7 ^{125}Te NMR spectrum (157.795 MHz) of 99.5 atom % ^{15}N-enriched $F_5TeNH_3^+AsF_6^-$ in HF solvent (-45 °C); (a) entire multiplet, dagger (†) denotes a peak of the TeF_6 multiplet (not shown in full), and (b) expansion of the central region of the multiplet attributed to $F_5TeNH_3^+$.

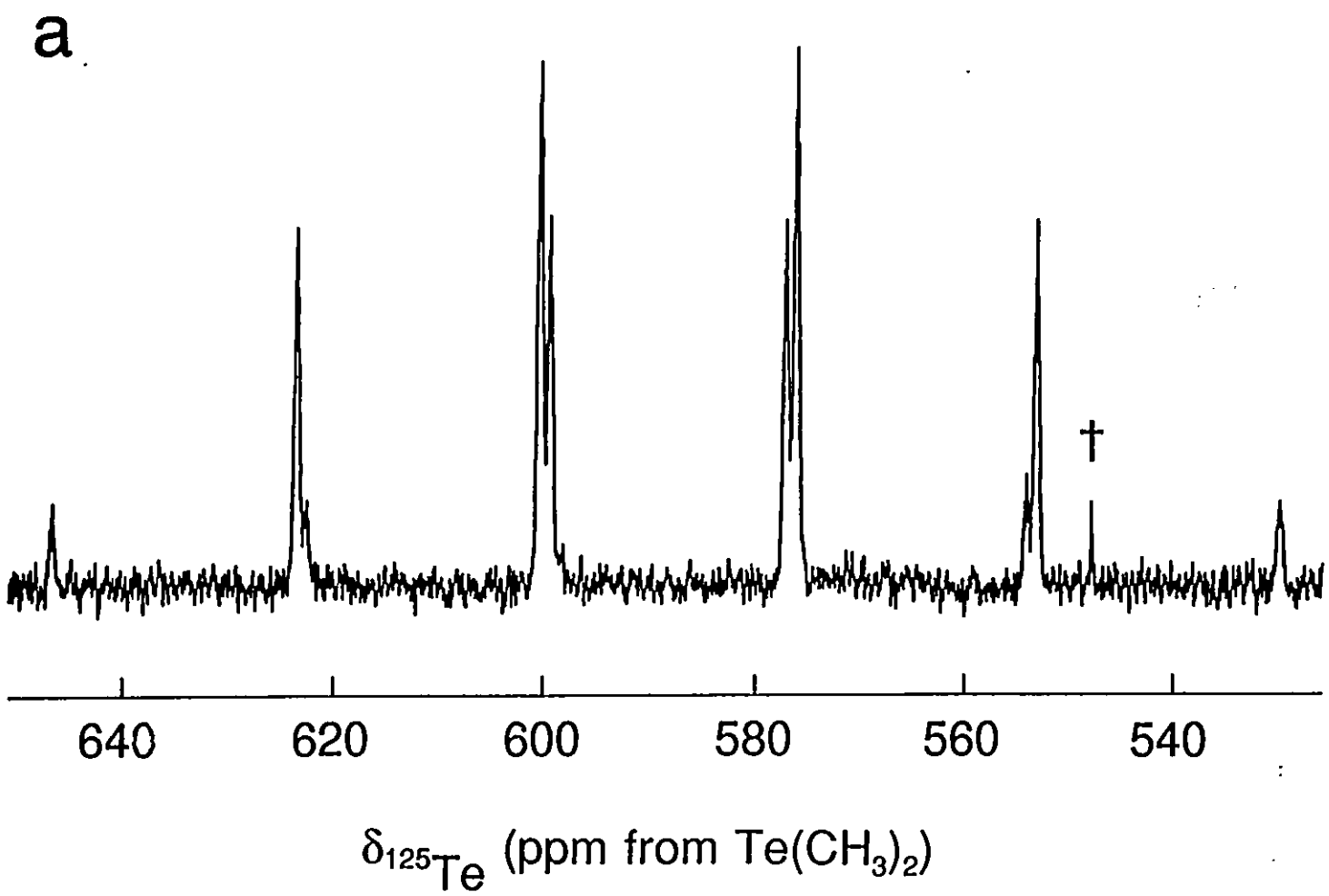
a
†
640
620
600
580
560
540
$\delta_{^{125}Te}$ (ppm from $Te(CH_3)_2$)

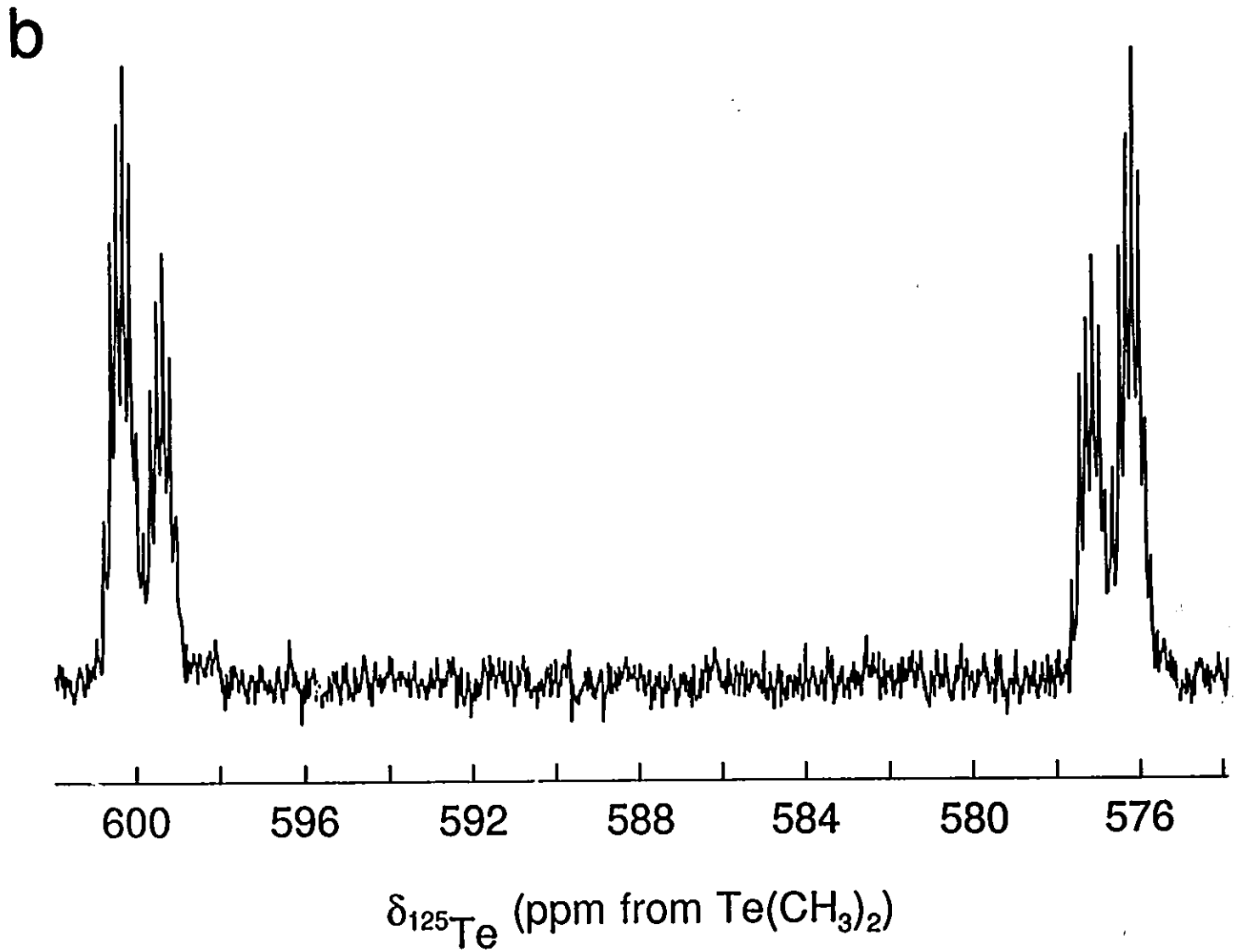
b
600
596
592
588
584
580
576
$\delta_{^{125}Te}$ (ppm from $Te(CH_3)_2$)

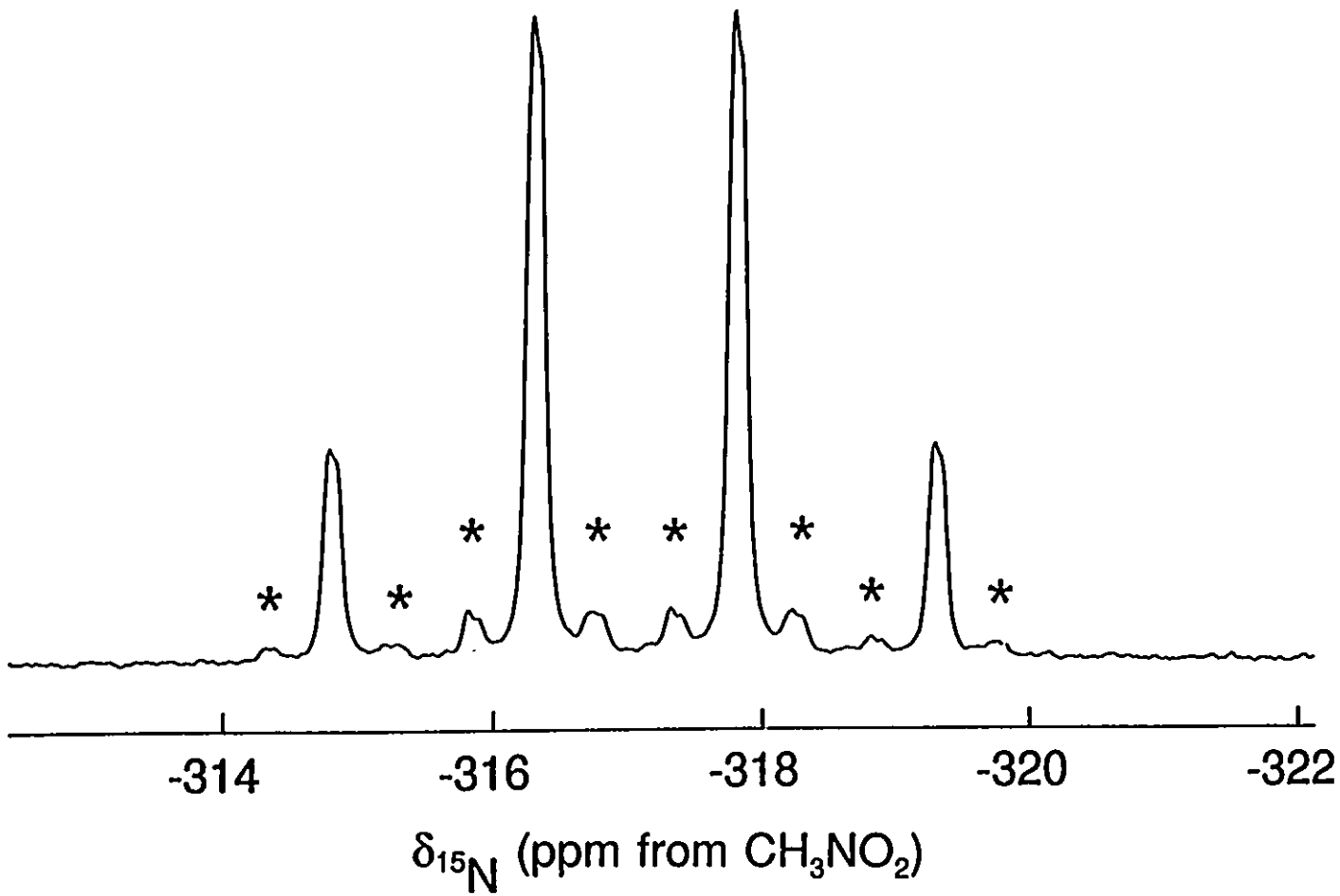

Figure 4.8 ^{15}N NMR spectrum (50.698 MHz) of 99.5 atom % $F_5TeNH_3^+AsF_6^-$ in HF solvent (-40 °C). Asterisks (*) denote ^{125}Te satellites.

Table 4.4. ^{19}F, ^{1}H, ^{125}Te and ^{15}N NMR Chemical Shifts and Coupling Constants for $F_5TeNH_3^+AsF_6^-$ and $[^{15}N]F_5TeNH_3^+AsF_6^-$.

Chemical Shifts (ppm)[a]		Coupling Constants, Hz	
$\delta(^{19}F)$[b]	-55.6 (δ_A)	$^{2}J(^{19}F_{ax.}-^{19}F_{eq.})$	162
	-30.2 (δ_B)	$^{1}J(^{19}F_{eq.}-^{123}Te)$	3024
$\delta(^{1}H)$[c]	7.45	$^{1}J(^{1}H-^{15}N)$	76
$\delta(^{125}Te)$[d]	588	$^{1}J(^{125}Te-^{19}F_{ax.})$	3801
$\delta(^{15}N)$[e]	-317.1	$^{1}J(^{125}Te-^{19}F_{eq.})$	3651
		$^{1}J(^{125}Te-^{15}N)$	48
		$^{2}J(^{125}Te-^{1}H)$	25

[a] The ^{19}F, ^{1}H, ^{125}Te, and ^{15}N NMR spectra were referenced to external neat $CFCl_3$, $(CH_3)_4Si$, $Te(CH_3)_2$ and CH_3NO_2 at 30 °C, respectively, with positive (negative) shifts denoting high (low) frequency resonances with respect to the standards. [b]Recorded at -44 °C in BrF_5 solvent. [c] Recorded at -53 °C in BrF_5 solvent. [d] Recorded at -45 °C in HF solvent. [e] Recorded at -40 °C in HF solvent.

consistent with that observed in the ^{125}Te NMR spectrum. The ^{15}N NMR chemical shift is intermediate between those observed for $NH_4^+AsF_6^-$ in HF (-369.6 ppm)[244] and $FNH_3^+O_3SCF_3^-$ in HF (-252.1 ppm).[244] The trend in the ^{15}N NMR chemical shifts is explained by an approximate formulation of the local paramagnetic term, restricted to electronic circulations on observed atom N bonded to other atoms [equation (4.21)]. In this equation, σ_p^{NN} is the local paramagnetic

$$\sigma_p^{NN} = [-\mu_o\mu_B\langle r^{-3}\rangle_{2p}/2\pi(\Delta E)][Q_{NN} + \Sigma_{N\neq X}Q_{NX}] \qquad (4.21)$$

contribution to the shielding of nitrogen, and an increase in the absolute magnitude of σ_p^{NN} deshields the nucleus; μ_o is the permeability of a vacuum, μ_B the Bohr magneton, and $\langle r^{-3}\rangle_{2p}$ the average radius of the valence p electrons on nitrogen. The ΣQ term expresses the imbalance of electronic charge that allows the paramagnetic circulation in the magnetic field. The Q_{NN} part depends on the 2p orbital populations on nitrogen, whereas ΣQ_{NX} is a multiple bond term. The fact that the ^{15}N NMR resonance of the FNH_3^+ cation is deshielded by 117 ppm relative to the NH_4^+ cation can be attributed to the σ fluoro effect (electron withdrawal by the electronegative fluorine atom) which contracts the nitrogen 2p orbitals, increasing $\langle r^{-3}\rangle_{2p}$. Also, the substitution of one hydrogen in NH_4^+ with fluorine to give FNH_3^+ increases the Q_{NN} term by reducing the valence orbital symmetry around nitrogen. Both of these effects increase the magnitude of the paramagnetic contribution to the nitrogen shielding (σ_p^{NN}) thus deshielding the nitrogen nucleus in FNH_3^+ relative to NH_4^+.[244] The less shielded ^{15}N NMR resonance of the $F_5TeNH_3^+$ cation relative to NH_4^+ is expected following the same arguments as for the FNH_3^+ cation since the F_5Te- group is undoubtedly more electronegative than H. Although a subject of debate,[52] the larger body of evidence indicates that the group electronegativity of F_5TeO- is less than that of

fluorine.[181] Although the group electronegativity of the F_5Te- group has not been estimated, by analogy with F_5TeO- the electronegativity of the F_5Te- group is probably less than that of fluorine. As a result, the σ withdrawing effect of the F_5Te- group in the $F_5TeNH_3^+$ cation is assumed to be less than that of fluorine in the FNH_3^+ cation, resulting in a smaller $\langle r^{-3}\rangle_{2p}$ term on nitrogen in the former and a smaller value of σ_p^{NN}.

(E) CHARACTERIZATION OF $F_5TeNH_3^+AsF_6^-$ AND $[^{15}N]F_5TeNH_3^+AsF_6^-$ IN THE SOLID STATE BY RAMAN SPECTROSCOPY

The ambient temperature Raman spectra of the white microcrystalline product isolated from the reaction of natural abundance F_5TeNH_2 with excess AsF_5 in HF solvent are shown in Figure 4.9. Figure 4.10 illustrates the regions of the Raman spectra of the natural abundance and 99.5 atom % ^{15}N enriched salts which exhibit $^{14/15}N$ isotopic shifts and frequencies obtained from both Raman spectra are listed in Table 4.5.

The Raman spectra are consistent with the formation of $F_5TeNH_3^+AsF_6^-$ in the solid state. The $F_5TeNH_3^+$ cation is expected to give rise to 3N - 6 = 24 normal modes. The lowest energy conformation, where the NH_3 protons are staggered with respect to the equatorial fluorines of the F_5Te- group, results in C_s point symmetry for the $F_5TeNH_3^+$ cation. The modes of this point symmetry belong to the irreducible representations 14 A' + 10 A", and all are Raman and infrared active. In Table 4.5, the modes for the $F_5TeNH_3^+$ cation have been assigned by considering the F_5TeN- (C_{4v}) and $TeNH_3$ (C_{3v}) groups separately. This has been done primarily to allow for direct comparison of modes of the F_5TeN- group with the large body of vibrational data available for F_5TeX- compounds [see Section (B) of this Chapter]. This is reasonable since the infrared and Raman selection rules are not altered by this approximation, and the large frequency difference

Figure 4.9 Raman spectrum of natural abundance $F_5TeNH_3^+AsF_6^-$ recorded at ambient temperature by use of 514.5-nm excitation.

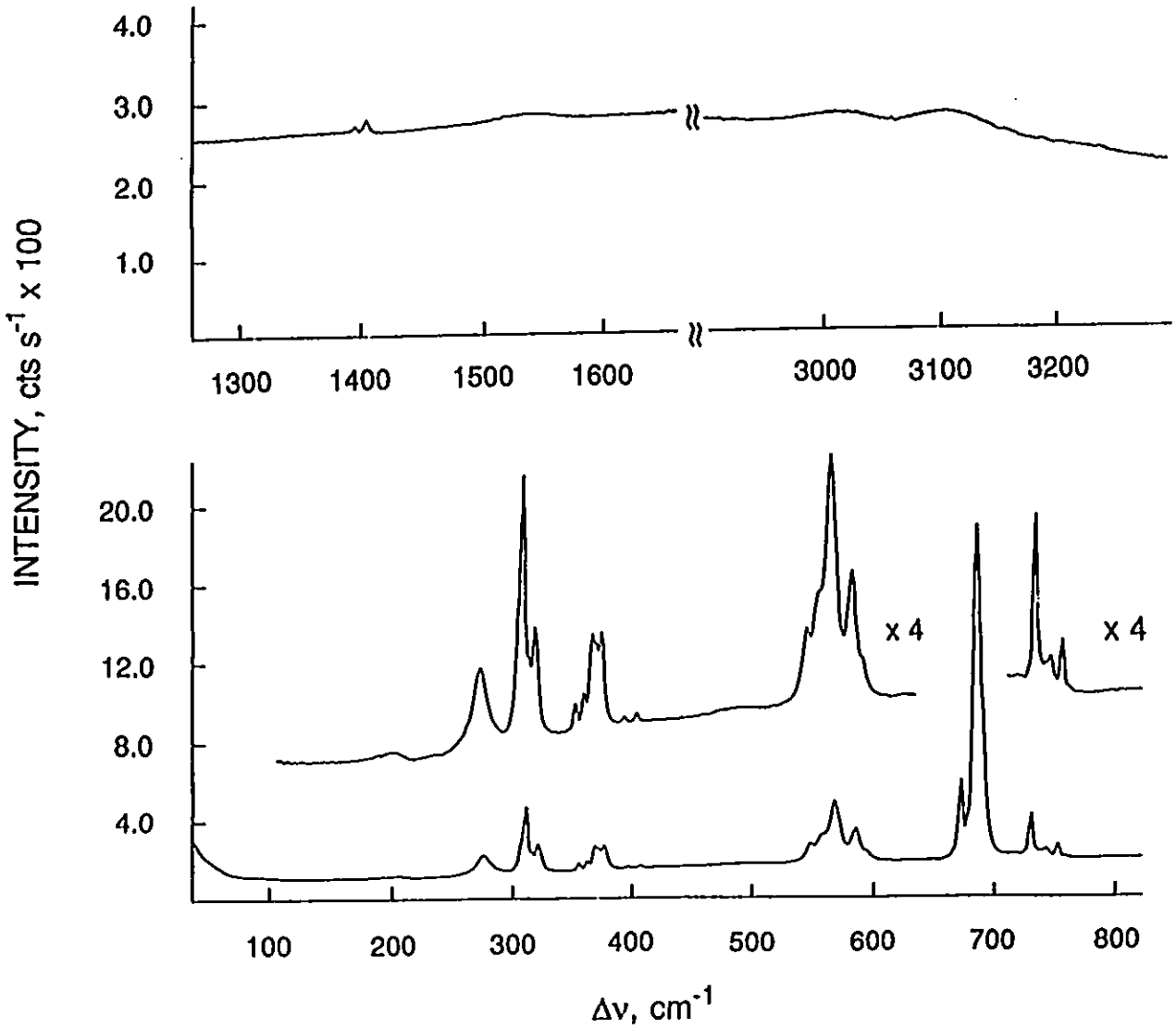
INTENSITY, cts s-1 x 100
4.0
3.0
2.0
1.0
1300
1400
1500
1600
3000
3100
3200
20.0
16.0
12.0
8.0
4.0
x 4
x 4
100
200
300
400
500
600
700
800
Δν, cm-1

Figure 4.10 Raman spectra of natural abundance (lower trace) and 99.5 atom % ^{15}N-enriched (upper trace) $F_5TeNH_3^+AsF_6^-$ recorded at ambient temperature by use of 514.5-nm excitation.

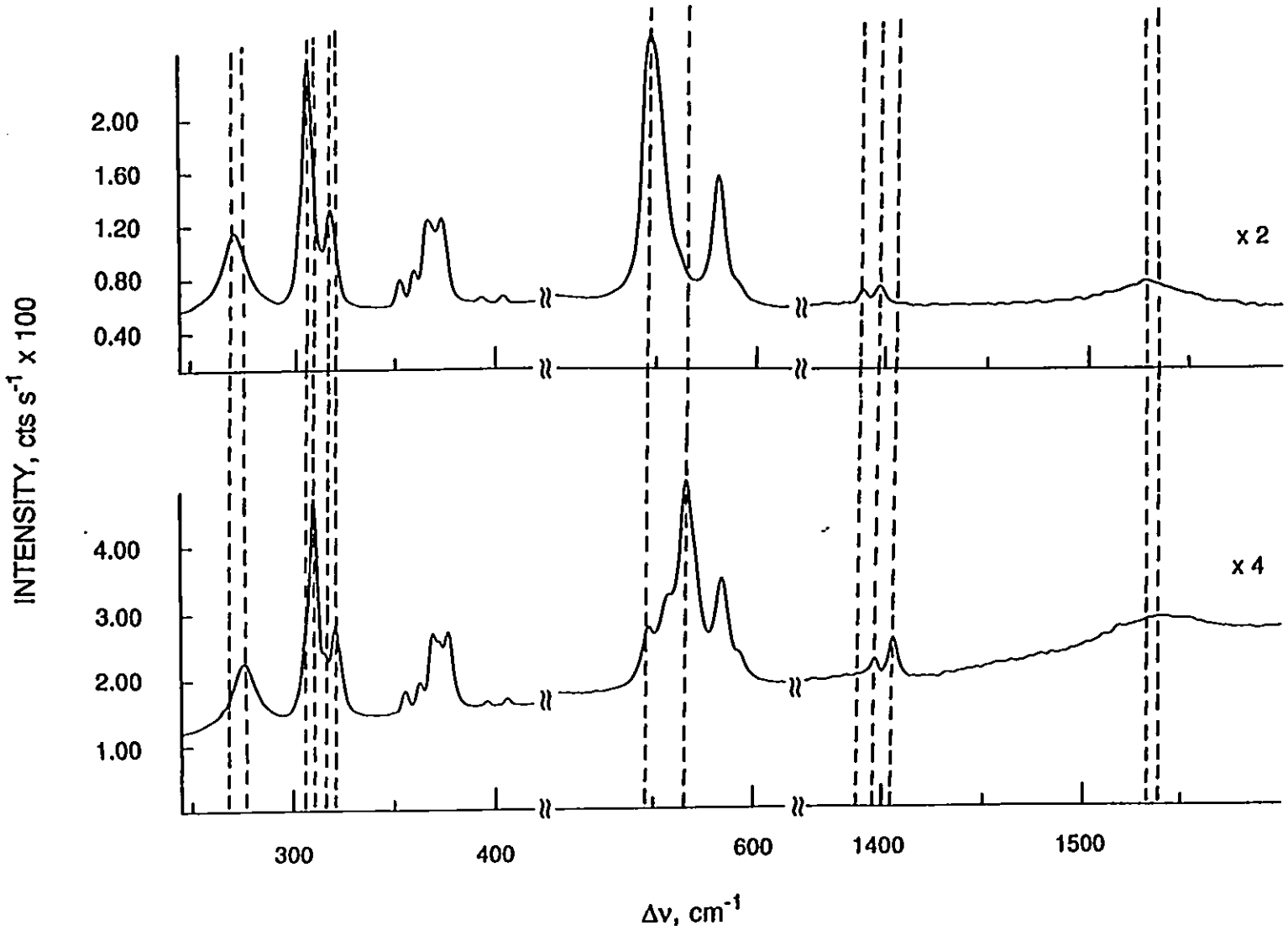
INTENSITY, cts s-1 x 100
2.00
1.60
1.20
0.80
0.40
x 2
4.00
3.00
2.00
1.00
x 4
300
400
600
1400
1500
Δν, cm-1

between modes of the F_5TeN- and -$TeNH_3$ groups minimizes vibrational coupling.

All 3N - 6 = 15 modes of the F_5TeN- group of the $F_5TeNH_3^+$ cation have been assigned under C_{4v} point symmetry. The large isotopic shift of the band at 566.5 cm^{-1} [$\Delta\nu(^{14/15}N)$ = -15.7 cm^{-1}] indicates that it may be assigned to ν(Te-N) (A_1). Similarly, the band at 276.3 cm^{-1} which also exhibits a large isotopic shift [$\Delta\nu(^{14/15}N)$ = -3.4 cm^{-1}], is assigned to $\delta(NTeF_4)$ (E). Comparisons with the band attributable to $\delta(OTeF_4)$ in the vibrational spectra F_5TeOF (309-325 cm^{-1}),[233] F_5TeOCl (316 cm^{-1}),[233] and F_5TeO^- (328 cm^{-1})[205,206] provide further evidence for the assignment.

The peaks at 730.2 and 682.2 cm^{-1} are assigned to the $\nu(Te\text{-}F_{ax.})$ and $\nu_{sym}(TeF_4)$ modes of A_1 symmetry by comparison with F_5TeOF,[233] F_5TeCl,[234] F_5TeOCl,[233] and F_5TeOH.[220] The intensity of the peak at 682.2 cm^{-1} also supports its assignment to $\nu_{sym}(TeF_4)$ since bands attributed to this mode are invariably the most intense in the Raman spectra of the related F_5TeX compounds (Table 4.5). As expected, $^{14/15}N$ isotopic shifts are observed for the bands attributed to $\nu(Te\text{-}F_{ax.})$ [$\Delta\nu(^{14/15}N)$ = -0.9 cm^{-1}] and $\nu_{sym}(TeF_4)$ [$\Delta\nu(^{14/15}N)$ = -0.7 cm^{-1}].
The assignment of all other modes associated with the F_5Te- group are made by analogy with related compounds (Table 4.5). An $^{14/15}N$ isotopic shift is observed for the band at 315.7 cm^{-1} assigned to ν_4, $\delta_{sym}(TeF_4)$, although the band overlaps with the peak assigned to ν_4, $\delta_{sym}(TeF_4)$ at 320.4 cm^{-1} in the Raman spectrum of $[^{15}N]F_5TeNH_3^+AsF_6^-$. Therefore the isotopic shift cannot be determined accurately. A mass dependence of the band attributed to ν_4, $\delta_{sym}(TeF_4)$ has been observed in the Raman and infrared spectra of F_5TeOF and F_5TeOCl,[233] which has been attributed to vibrational coupling of ν(Te-O), ν(O-X) [X = Cl, F], and $\nu_{sym}(TeF_4)$.

The small $^{14/15}N$ isotopic shift [$\Delta\nu(^{14/15}N)$ = -0.7 cm^{-1}] observed for the band attributed to ν_9, $\delta(FTeF_4)$ (E) may result from coupling of the ν_9 mode with ν_{10}, $\delta(NTeF_4)$, which also belongs

Table 4.5. Raman Frequencies and Assignments for $F_5TeNH_3^+AsF_6^-$ and $[^{15}N]F_5TeNH_3^+AsF_6^-$ and the Related F_5TeOF, F_5TeOH and F_5TeO^-

frequency, cm^{-1} [a]							
F_5TeOF [b]	F_5TeO^- [c]	F_5TeOH [e]	$F_5TeNH_3^+$ AsF_6^- [g]	$[^{15}N]F_5TeNH_3^+$ AsF_6^- [g]	$\Delta\nu(^{14/15}N)$ [h]		approx mode description
						C_{4v}	
721 (1.6)	584 (30	735	730.2 (13.66)	729.3 (13.07)	-0.9	A_1	ν_1, $\nu(Te\text{-}F_{ax.})$
669 (10)	652 (100)	685	682.9 (100)	682.2 (100)	-0.7		ν_2, $\nu_{sym}(TeF_4)$
613 (3.8)	868 (47)	735	566.5 (18.26)	550.8 (18.35)	-15.7		ν_3, $\nu(Te\text{-}N)$
301 (0.5)	319[d]	319	315.7 (6.03)	310 sh			ν_4, $\delta_{sym}(TeF_4)$
		310					
660 (0.3)	584 (30)	652	671.6 (23.94)	671.5 (21.88)		B_1	ν_5, $\nu_{sym}(TeF_4)$
n.o.	n.o.	n.o.	n.o.	n.o.			ν_6, $\delta(TeF_4)$
309 (1.0)	283 (6)		311.1 (19.60)	310.2 (16.84)	-0.9	B_2	ν_7, $\delta_{scis}(TeF_4)$
738 (sh)	636[d]	733.5 [f]	752.4 (4.30)	751.6 (2.81)	-0.8	E	ν_8, $\nu_{asym}(TeF_4)$
325 (sh)	346 (6)		321.1 (8.13)	320.4 (6.42)	-0.7		ν_9, $\delta(FTeF_4)$
309-325	328 (40)		276.3 (5.64)	272.9 (5.19)	-3.4		ν_{10}, $\delta(NTeF_4)$
279 (0.2)	196 (3)	168	203 (0.63)	203 (0.59)			ν_{11}, $\delta_{asym}(TeF_4)$
		145					
						C_{3v}	
			3018.0 (1.20)	3017.8 (1.05)		A_1	ν_{12}, $\nu_{sym}(NH_3)$
			1396.0 (0.40)	1391.2 (0.42)	-5.7		ν_{13}, $\delta_{sym}(NH_3)$
			1405.7 (0.86)	1399.8 (0.50)	-5.9		
			3110.1 (1.92)	3110.0 (1.75)		E	ν_{14}, $\nu_{asym}(NH_3)$
			1539.7 (0.59)	1531.6 (0.59)	-8.1		ν_{15}, $\delta_{asym}(NH_3)$

n.o.	n.o.		ν_{16}, δ_{sym}(TeNH)
		O_h	
743 (2.92)		T_{1u}	ν_3 (AsF_6^-)
739 (2.46)			
716 (1.69)			
689 sh		A_{1g}	ν_1 (AsF_6^-)
593 (3.15)		E_g	ν_2 (AsF_6^-)
585 (9.59)			
557 (8.29)			
548 (5.60)			
407 (0.76)		T_{1u}	ν_4 (AsF_6^-)
396 (0.61)			
377 (7.09)		T_{2g}	ν_5 (AsF_6^-)
373 (6.24)			
369 (6.89)			
363 (2.71)			
355 (1.95)			
n.o.		T_{1u}	ν_6 (AsF_6^-)

Table 4.5 (continued)

[a]Data obtained from Raman spectra unless otherwise specified. Assignments for the modes of the F_5TeX groups have made assuming C_{4v} symmetry using the mode species descriptions from ref (233). Assignments for the NH_3 group of the $F_5TeNH_3^+$ cation have been made under approximate C_{3v} symmetry. All frequencies are reported in cm^{-1}. [b]Ref (233); liquid at -55 °C. [c]Ref (205); solid $N(CH_3)_4^+OTeF_5^-$ at 25 °C. ν_1 and ν_2 have been described as antisymmetric and symmetric combinations of $\nu_{sym}(TeF_4)$ and $\nu(Te\text{-}F_{ax.})$, respectively. [d]Obtained from the infrared spectra at 25 °C. [e]Refs (220) and (203); Raman spectrum of the liquid, recorded at room temperature. [f]Obtained from the gas phase infrared spectrum, ref (220). [g]This work; Raman spectra recorded at 25 °C using 154.4-nm excitation. [h]Isotopic shifts $\Delta\nu(^{14/15}N) = \nu(^{15}N) - \nu(^{14}N)$, where the frequencies of the bands ν are given in cm^{-1}.

to the E symmetry species.

The band at 311.1 cm^{-1} assigned to ν_7, $\delta_{sciss}(TeF_4)$ has an observed isotopic shift [$\Delta\nu(^{14/15}N) = -0.9\ cm^{-1}$] that is forbidden under C_{4v} point symmetry since the symmetry species for ν_7 (B_2) is neither A_1 nor E, which are the symmetry species for ν_3, ν(Te-N) and ν_{10} $\delta(NTeF_4)$, respectively. However, vibrational coupling of ν_7 and ν_{10} is possible if one considers the point symmetry for the entire $F_5TeNH_3^+$ cation (C_s). The E representation of the point group C_{4v} correlates with A' + A" of the C_s point group. Likewise, the B_2 representation in C_{4v} correlates with A' or A" in C_s. Under the lower point symmetry, the modes belong to the same representations, and thus can couple. Similarly, the observed isotopic shift ($\Delta\nu^{14/15}N = -0.8\ cm^{-1}$) of the band assigned to ν_8, $\nu_{sym}(TeF_4)$ (E) can be explained by vibrational coupling with ν_3, ν(Te-N) (A_1) since the A_1 representation correlates with A' in C_s.

As for F_5TeNH_2, a band attributable to ν_6, $\delta(TeF_4)$ is not observed in the Raman spectrum of $F_5TeNH_3^+AsF_6^-$, presumably owing to an inherently low intensity [see Section (B) of this Chapter].

All of the bands attributable to the $TeNH_3$ group have been assigned to symmetry species of the C_{3v} point group. A total of 3N - 6 = 9 normal modes belonging to the irreducible representations 3 A_1 + 3 E are expected under C_{3v} symmetry. One A_1 mode [ν(Te-N)] is the same as ν_3 of the F_5TeN- group and is therefore not repeated. The remaining 2 A_1 + 3 E modes and the corresponding bands (ν_{12} to ν_{16}) observed in the Raman spectra of $F_5TeNH_3^+AsF_6^-$ are listed in Table 4.5.

The very broad bands at 3018 and 3110 cm^{-1} have been assigned to ν_{12} [$\nu_{sym}(NH_2)$] and ν_{14} [$\nu_{asym}(NH_2)$], from the expected NH stretching frequency range for compounds containing an NH_3^+ group (3030 - 3130 cm^{-1}).[249] It is noteworthy that the NH stretches for F_5TeNH_2 occur

at considerable higher frequency [3280.1, 3297.2, 3385.3 cm^{-1}; see Section (B) of this Chapter]. This is consistent with the higher frequency range expected for neutral primary amines (3300 - 3500 cm^{-1}).[250] No significant $^{14/15}N$ isotopic shifts are observed for the NH stretching vibrations. This has been attributed to the broadness of the bands, making the shifts undetectable.

The symmetric bend, $\delta_{sym}(NH_3)$, has been assigned to the bands at 1396.9 and 1405.7 cm^{-1}, which exhibit $^{14/15}N$ isotopic shifts of -5.7 and -5.9 cm^{-1}, respectively. The band assigned to ν_{15}, $\delta_{asym}(NH_3)$ is observed at 1539.7 cm^{-1} and exhibits an $^{14/15}N$ isotopic shift of -8.1 cm^{-1}. Assignment of $\nu_{sym}(NH_3)$ and $\delta_{asym}(NH_3)$ has been made by comparison with the vibrational spectra of salts of the FNH_3^+ cation[239] and FCH_3.[67]

By comparison with F_5TeOH,[220] ν_{16} [δ_{sym}(TeNH)] is expected to occur at approximately 1000 cm^{-1}. Since no bands are observed in this region, it is assumed that the band has a very weak Raman intensity. It is worth noting that δ(TeOH) is too weak to be observed in the Raman spectrum of F_5TeOH; the band was observed in the infrared gas phase spectrum.

A total of 15 bands are assigned to the AsF_6^- anion in the Raman spectrum of $F_5TeNH_3^+AsF_6^-$. For undistorted AsF_6^- of O_h point symmetry, only three Raman-active bands are expected. The bands have been assigned to the modes of O_h point symmetry in Table 4.5 although a reduction in symmetry is apparent. Possible sources of deviation from O_h point symmetry are solid state effects such as a low site-symmetry in the solid and intermolecular vibrational coupling, which gives rise to factor group splitting; the effects of both may be predicted from a knowledge of the crystallographic unit cell. Also, interactions between cation and anion may result in an authentic distortion of the anion symmetry, such as the reduction of AsF_6^- symmetry to C_{4v} upon fluorine bridge formation with the XeF^+ [67,68] and KrF^+ [69] cations.

An anion site symmetry of C_{2v} or lower, where all mode degeneracies are removed, would

result in the observation of all 3N - 6 = 15 bands in the Raman spectrum, since no selection rules forbid the vibrational activity of any of the modes. It is possible that a low site-symmetry for the AsF_6^- anion results from H---F hydrogen-bonding interactions with the $F_5TeNH_3^+$ cation. Christe *et al.*[171] have explained the observation of ν_1 through ν_5 and the splittings of the bands in the Raman spectrum of $OH_3^+AsF_6^-$ at -120 °C in terms of weak H---F cation-anion interactions that dominate at low temperature in a rigid lattice containing AsF_6^- anions in a non-octahedral field (i.e., a low site symmetry). The Raman spectrum at 25 °C resembles that for octahedral AsF_6^-; the weak cation-anion interactions are assumed to be overcome by thermal motion, thus resulting in an effective increase in the AsF_6^- site symmetry. It is possible that the lattice in $F_5TeNH_3^+AsF_6^-$ is rigid at room temperature, resulting in a sufficiently low AsF_6^- site-symmetry to account for the number of observed bands.

A reduction in AsF_6^- site symmetry from O_h to C_{2v} or lower by weak cation-anion interactions or simply by a the existence of a low site symmetry for AsF_6^- in the solid state would result in the removal of all O_h degeneracies. As seen in Table 4.5, the number of bands in the Raman spectrum of $F_5TeNH_3^+AsF_6^-$ which correlate with ν_2 (E_g) and ν_5 (T_{2g}) are greater than can be accounted for by simple removal of degeneracies through a reduction of AsF_6^- symmetry. Intermolecular coupling may account for the additional splitting, and could possibly be confirmed by factor-group analysis if X-ray structural data were available.

(F) ASSESSMENT OF THE BONDING IN F_5TeNH_2 AND THE $F_5TeNH_3^+$ CATION USING RAMAN AND ^{19}F NMR SPECTROSCOPY

In Table 4.6 the vibrational frequencies associated with the modes of the F_5TeX- groups in F_5TeNH_2 and the $F_5TeNH_3^+$ cation are compared with those of F_5TeOH and the F_5TeO^- anion.

As can be seen, the trends observed in a comparison of the vibrational spectra of F_5TeOH and F_5TeO^- are also present in F_5TeNH_2 and the $F_5TeNH_3^+$ cation. The deprotonation of F_5TeOH to give the F_5TeO^- anion results in a shift to high frequency of ν(TeO) by 133 cm^{-1} resulting from an increase in the Te-O bond order.[206] Accompanying the increase in ν(TeO) is a decrease of the Te-F stretching modes. The largest effect is observed for ν($TeF_{ax.}$), which is 151 cm^{-1} lower for the F_5TeO^- anion than for F_5TeOH. The weakening of the Te-F bonds and strengthening of the Te-O bond in the F_5TeO^- anion (and similarly for F_5SeO^- and F_5SO^-) relative to the parent acids has been attributed to donation of electron density from oxygen to the X-F bonds (X = S, Se, Te) as discussed in Section (A) of this Chapter. A close parallel is observed in a comparison of the Raman spectra of the acid/base pairs F_5TeOH/F5TeO^- and those of the $F_5TeNH_3^+$ cation and F_5TeNH_2. Deprotonation of the $F_5TeNH_3^+$ cation results in an increase in the Te-N bond order, which is reflected in the low value of ν_3 [ν(Te-N)] for $F_5TeNH_3^+$ compared to the band at 761.0 cm^{-1} in the Raman spectrum of F_5TeNH_2, which has a component from the Te-N stretching mode. This accompanied by an increase in the Te-F stretching force constants, particularly that for Te-$F_{ax.}$ This is reflected in the high frequency of ν_1 [ν(Te-$F_{ax.}$)], 730.2 cm^{-1}, for $F_5TeNH_3^+$. Although strong vibrational coupling of the ν(Te-N) and ν(Te-$F_{ax.}$) stretching modes prevents the assignment of ν(Te-$F_{ax.}$) to a particular band, it contributes strongly to the band at 582.7 cm^{-1}, which is significantly lower than the band assigned to ν(Te-$F_{ax.}$) in $F_5TeNH_3^+$. These observations are consistent with a close parallel in the bonding of the acid/base pairs F_5TeOH/F_5TeO^- and $F_5TeNH_3^+/F_5TeNH_2$.

The ^{19}F NMR spectra of F_5TeNH_2 and $F_5TeNH_3^+AsF_6^-$ are shown in Figure 4.11 and the ^{19}F NMR chemical shifts are listed in Table 4.7. As can be seen, protonation of F_5TeNH_2

Table 4.6. Vibrational Frequencies and Assignments for F_5TeO^-, F_5TeOH, F_5TeNH_2 and $F_5TeNH_3^+$ [a]

F_5TeO^- [d]	F_5TeOH [f]	Δν	F_5TeNH_2 [h]	$F_5TeNH_3^+$ [i]	Δν	Assgnt and Approx Mode Decription
584 (30)	735	151		730.2 (13.66)		A_1 ν_1, $\nu(Te\text{-}F_{ax.})$
			582.7 (10)			sym $[\nu_1 + \nu_3]$
652 (100)	685	33	619.6 (8.42)	682.9 (100)	63.6	ν_2, $\nu_{sym}(TeF_4)$
868 (47)	735	-133		566.5 (18.35)		ν_3, $\nu(Te\text{-}X)$
			761.0 (1.03)			asym $[\nu_1 + \nu_3]$
319[e]	319	0	300.7 (3.36)	315.7 (6.03)	15	ν_4, $\delta_{sym}(TeF_4)$ umbrella
	310					
584 (30)	652	68	628.6 (sh)	671.6 (23.94)	43	B_1 ν_5, $\nu_{sym}(TeF_4)$ out-of-phase
n.o.	n.o.		n.o.			ν_6, $\delta_{pucker}(TeF_4)$
283 (6)			326.8 (2.06)	311.1 (19.60)	-15.7	B_2 ν_7, $\Delta_{sciss}(TeF_4)$ in-plane
636[e]	733.5[g]	97.5	680.4 (4.38)	752.4 (4.30)	72	E ν_8, $\nu_{asym}(TeF_4)$
			689.1 (7.14)			
346 (6)			336.8 (2.29)	321.1 (8.13)	-15.7	ν_9, $\delta(FTeF_4)$
328 (40)			286.7 (2.41)	276.3 (5.64)	-10.4	ν_{10}, $\delta(XTeF_4)$
196 (3)	168	-28	194.6 (0.46)	203 (0.63)	8.4	ν_{11}, $\delta_{asym}(TeF_4)$
	145		210.1 (0.21)			

[a]Data obtained from Raman spectra unless otherwise specified. Assignments for the modes of the F_5TeX group have made assuming C_{4v} symmetry using the mode species descriptions from ref (233). [b]Ref (233); liquid at -55 °C. [c]Ref (234); liquid at ambient temperature. [d]Ref (29); $N(CH_3)_4^+OTeF_5^-$ at 25 °C. ν_1 and ν_2 have been described as asymmetric and symmetric combinations of $\nu_{sym}(TeF_4)$ and $\nu(Te\text{-}F_{ax.})$, respectively. [e]Obtained from the infrared spectra at 25 °C. [f]Ref (220) and (203); Raman spectrum of the liquid, recorded at room temperature. [g]Obtained from the gas phase infrared spectrum. [h]This work; recorded at -150 °C using 514.5-nm excitation. [i]This work; recorded at ambient temperature using 514.5-nm excitation.

Table 4.7. ^{19}F NMR Parameters for F_5TeNH_2 and $F_5TeNH_3^+AsF_6^-$.

Compound	^{19}F NMR Chemical Shifts [a]	
F_5TeNH_2 [b]	δ_A	-37.8
	δ_B	-42.8
$F_5TeNH_3^+$ AsF_6^- [c]	δ_A	-55.6
	δ_B	-30.2

[a] ^{19}F NMR spectra referenced with respect to neat external $CFCl_3$ at 30 °C. Negative chemical shifts indicate low frequency resonances with respect to $CFCl_3$. Recorded in BrF_5 solvent. [b] -44 °C. [c] -50 °C.

Figure 4.11 (a) ^{19}F NMR spectrum (470.599 MHz) of F_5TeNH_2 in BrF_5 solvent (-44 °C); (A) multiplet assigned to the axial fluorine atom bonded to tellurium, (B) resonance of equatorial fluorine atoms bonded to tellurium, (C) TeF_6. (b) ^{19}F NMR spectrum (470.599 MHz) of $F_5TeNH_3^+AsF_6^-$ in BrF_5 solvent (-50 °C); (A) resonance of equatorial fluorine atoms bonded to tellurium, (B) resonance of axial fluorine atom bonded to tellurium, (C) unidentified resonance, (D) TeF_6, (E) AsF_6^-. Asterisks (*) in both spectra denote ^{125}Te satellites.

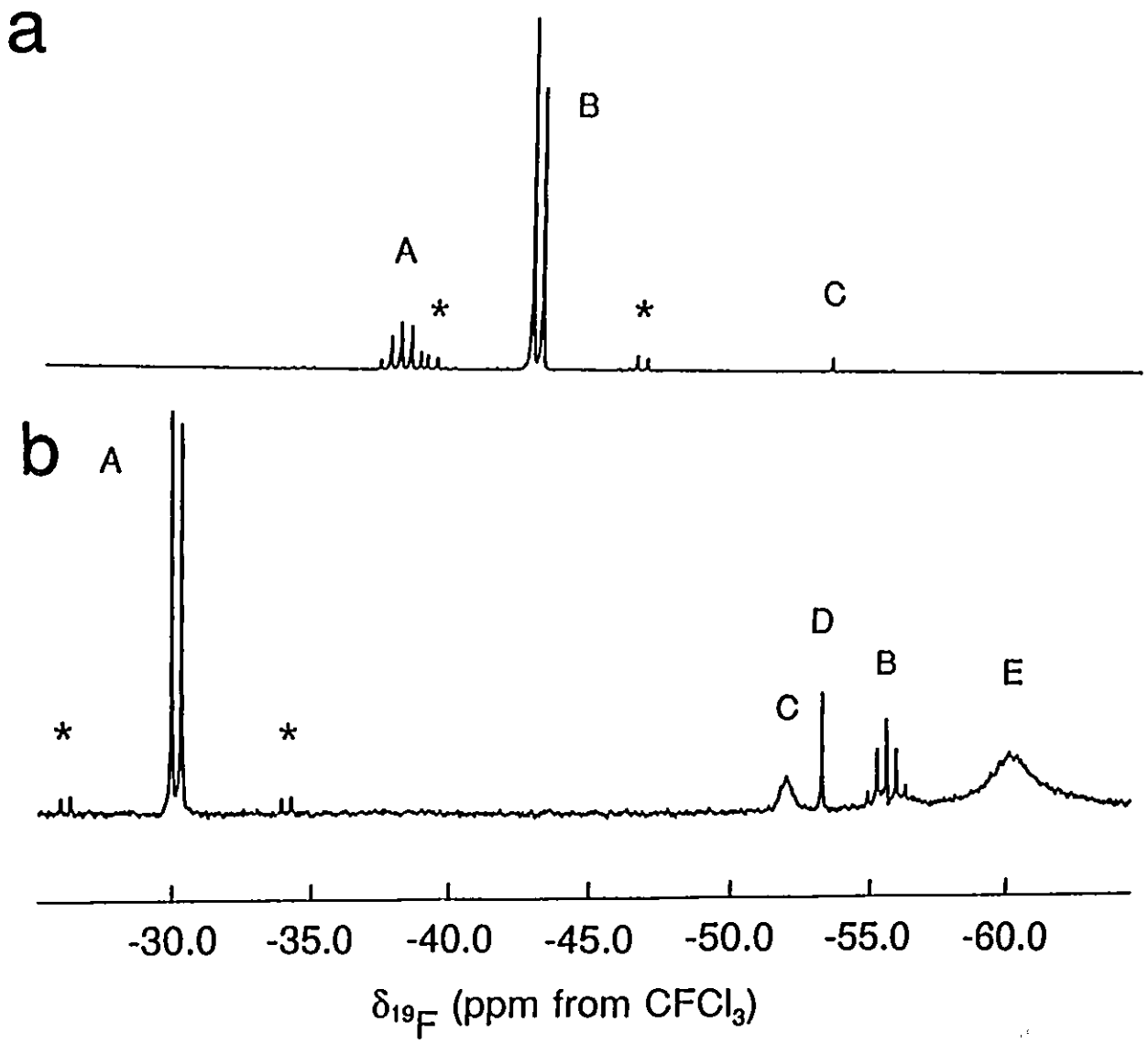
a
A
*
B
*
C
b
A
*
*
C
D
B
E
-30.0
-35.0
-40.0
-45.0
-50.0
-55.0
-60.0
δ19F (ppm from CFCl3)

significantly alters the ^{19}F NMR shieldings of the axial and equatorial fluorines of the F_5Te- group. The axial fluorine resonance (δ_A) is shielded by 18.5 ppm on protonation, whereas the equatorial resonance (δ_B) is deshielded by 5.2 ppm. The greater shift for the axial fluorine resonance is consistent with the trans effect observed in the ^{19}F NMR spectra of the acid/base pairs F_5XOH/F_5XO^- for X = S, Se, Te [see Section (A) of this Chapter].

(G) CONCLUSION

The differences in bonding reflected in the Raman and ^{19}F NMR spectral parameters for the acid/base pair $F_5TeNH_3^+/F_5TeNH_2$ are analogous to those observed for F_5TeOH and F_5TeO^- anion. The Te-N bond order in F_5TeNH_2 is greater than in the $F_5TeNH_3^+$ cation, indicating some degree of π-donation from the lone pair on nitrogen to acceptor orbitals of the F_5Te- group, possibly σ^*(Te-F). The presence of electron density in these antibonding orbitals reduces the strengths of the Te-F bonds. The greater weakening of the axial Te-F bond is attributed to the fact that $\pi_N \rightarrow \sigma^*(Te\text{-}F_{ax.}) > \pi_N \rightarrow \sigma^*(Te\text{-}F_{eq.})$. Protonation of the nitrogen in F_5TeNH_2 reduces the strength of the Te-N bond since the nitrogen lone pair is no longer available for Te-N π bonding. The depopulation of the σ^*(Te-F) orbitals results in an increase in the strength of the Te-F bonds.

CHAPTER 5

[PENTAFLUOROTELLURIUM(VI)AMIDO] XENONIUM(II) HEXAFLUOROARSENATE; $F_5TeN(H)\text{-}Xe^+AsF_6^-$

INTRODUCTION

While many examples of xenon bonded to oxygen or fluorine and of xenon bonded to other highly electronegative ligands through oxygen were synthesized immediately following the discovery of noble-gas reactivity,[25] over a decade had elapsed before an example with a ligating atom other than oxygen and fluorine, namely nitrogen, was synthesized,[56] and two decades before the Xe-N bond in $FXeN(SO_2F)_2$ was definitively characterized in the solid state by X-ray crystallography and in solution by multinuclear magnetic resonance spectroscopy.[57] Other imidodisulfurylfluoride derivatives containing Xe(II)-N bonds have since been characterized primarily by use of NMR spectroscopy, namely, $Xe[N(SO_2F)_2]_2$,[58,59] $F[XeN(SO_2F)_2]_2^+$,[58-60] $XeN(SO_2F)_2^+AsF_6^-$,[60] and $XeN(SO_2F)_2^+Sb_3F_{16}^-$.[60] The compound $Xe[N(SO_2CF_3)_2]_2$[61] has also been prepared and characterized and is the most thermally stable of the imido derivatives of xenon.

More recently, the significant Lewis acidity of the XeF^+ cation, as seen from the propensity of XeF^+ to form fluorine bridges in the solid state,[21] has been utilized to form species with Xe(II)-N bonds from the reaction of oxidatively resistant bases with the XeF^+ cation [equation (5.1)].[26]

$$D: + XeF^+ \longrightarrow D\text{-}XeF^+ \qquad (5.1)$$

Reactions of XeF^+ with hydrogen cyanide,[72,73] alkylnitriles,[72] pentafluorobenzenenitrile,[72] and perfluoroalkylnitriles[71,72] form the adduct cations $RC{\equiv}N\text{-}Xe\text{-}F^+$. Perfluoropyridines[75] and *s*-trifluorotriazine[71] likewise react with XeF^+, resulting in cations in which xenon is bonded to a formally sp^2 hybridized nitrogen atom incorporated in the aromatic ring. With the exception of the adduct with *s*-trifluorotriazine, $s\text{-}C_3F_3N_2N\text{-}XeF^+$,[71] all of the adduct cations are only kinetically stable below room temperature.

More recently the krypton(II) adduct cations, $HC{\equiv}N\text{-}KrF^+$ [78] and $R_FC{\equiv}N\text{-}KrF^+$ ($R_F = CF_3$, C_2F_5, $n\text{-}C_3F_7$)[71] have also been characterized in this laboratory as the AsF_6^- salts, all of which are unstable above *ca.* -40 °C.

In the present paper the HF elimination reaction of XeF_2 with the novel ammonium salt $F_5TeNH_3^+AsF_6^-$ has been shown to result in the formation of the $F_5TeN(H)\text{-}Xe^+$ cation, which represents the second example of xenon(II) bonded to a formally sp^3 hybridized nitrogen. The first example, $F_5SN(H)\text{-}Xe^+$, was formed by solvolysis of $F_3S{\equiv}N\text{-}XeF^+$ in HF solvent.[26] The salt, $F_5TeN(H)\text{-}Xe^+AsF_6^-$, has been characterized in the solid state by Raman spectroscopy and in solution by ^1H, ^{129}Xe, ^{125}Te, ^{15}N, and ^{19}F NMR spectroscopy. Assignment of vibrational bands in the Raman spectra and elucidation of scalar couplings to nitrogen in the NMR spectra have been aided by preparation of ^{15}N-enriched (99.5 atom %) $F_5TeN(H)\text{-}Xe^+AsF_6^-$.

RESULTS AND DISCUSSION

(A) PREPARATION AND ISOLATION OF $F_5TeN(H)\text{-}Xe^+AsF_6^-$

The $F_5TeN(H)\text{-}Xe^+$ cation was prepared in solution by the reaction of stoichiometric amounts $XeF^+AsF_6^-$ and F_5TeNH_2 in anhydrous HF solvent with warming to -45 to -35 °C to effect reaction and dissolution. The base, F_5TeNH_2, was protonated in HF acidified with the strong Lewis fluoroacid, $XeF^+AsF_6^-$, according to equations (5.2) and (5.3). The ammonium cation $F_5TeNH_3^+$ underwent an HF elimination reaction with XeF_2, and produced the $F_5TeN(H)\text{-}Xe^+$ cation [equation (5.4)]. The salt, $F_5TeNH_3^+AsF_6^-$, which was prepared by reaction of F_5TeNH_2

$$XeF^+AsF_6^- + HF \longrightarrow XeF_2 + H_2F^+AsF_6^- \tag{5.2}$$

$$F_5TeNH_2 + H_2F^+AsF_6^- \longrightarrow F_5TeNH_3^+AsF_6^- + HF \tag{5.3}$$

$$F_5TeNH_3^+AsF_6^- + XeF_2 \rightleftharpoons F_5TeN(H)\text{-}Xe^+AsF_6^- + 2\ HF \tag{5.4}$$

with excess AsF_5 in HF solvent (Chapter 4), underwent an HF elimination reaction with XeF_2 according to equation (5.4) in both HF (-45 to -35 °C) and BrF_5 (-62 to -45 °C) solvents to give $F_5TeN(H)\text{-}Xe^+AsF_6^-$. The $F_5TeNH_3^+$ and $F_5TeN(H)\text{-}Xe^+$ cations were both observed in HF and BrF_5 solvents by ^1H, ^{19}F, ^{15}N and ^{125}Te NMR spectroscopy, which indicated that the HF elimination depicted in equation (5.4) was an equilibrium. The $F_5TeN(H)\text{-}Xe^+$ cation was completely decomposed after several hours in HF solution at -20 °C. Decomposition was rapid (*ca.* 1 minute) in HF solution at -1 °C and is discussed in Chapter 6.

A pale orange microcrystalline solid, which crystallized from anhydrous HF at -40 °C, was isolated by decanting the supernatant from the solid followed by pumping under vacuum for 20 h at -50 °C. The Raman spectrum of the solid (-165 °C) is consistent with $F_5TeN(H)\text{-}Xe^+AsF_6^-$ contaminated with $F_5TeNH_3^+AsF_6^-$, which arises according to equation (5.4), and $Xe_2F_3^+AsF_6^-$. The salt, $Xe_2F_3^+AsF_6^-$, is believed to result primarily from the reaction of XeF_2 and AsF_5 produced in the decomposition of $F_5TeN(H)\text{-}Xe^+AsF_6^-$ in HF solvent (see Chapter 6). The pale orange color of the solid, which is attributed to $F_5TeN(H)\text{-}Xe^+AsF_6^-$, decomposed rapidly at -30 °C.

The $F_5TeN(H)\text{-}Xe^+$ cation was also generated in SO_2ClF solution from the reaction of stoichiometric amounts of $F_5TeNH_3^+As(OTeF_5)_6^-$ and $Xe(OTeF_5)_2$ at -61 °C in an $HOTeF_5$ elimination reaction according to equation (5.5), which is directly analogous to the HF elimination reaction depicted in equation (5.4). The reagents were soluble down to -115 °C, because of the large size of the anion, resulting in low lattice energies for $F_5TeN(H)\text{-}Xe^+As(OTeF_5)_6^-$ and $F_5TeNH_3^+As(OTeF_5)_6^-$.

$$F_5TeNH_3^+As(OTeF_5)_6^- + Xe(OTeF_5)_2 \rightleftharpoons F_5TeN(H)\text{-}Xe^+As(OTeF_5)_6^- + 2\ HOTeF_5 \qquad (5.5)$$

(B) CHARACTERIZATION OF NATURAL ABUNDANCE AND ^{15}N-ENRICHED $F_5TeN(H)\text{-}Xe^+AsF_6^-$ by ^{129}Xe, ^{125}Te, ^{19}F, ^{15}N, AND ^{1}H NMR SPECTROSCOPY

Every element in the $F_5TeN(H)\text{-}Xe^+$ cation possesses at least one nuclide which is suitable for observation by NMR spectroscopy, namely, the spin-½ nuclei ^{1}H, ^{15}N, ^{125}Te, ^{129}Xe and ^{19}F, and the spin-1 nuclide ^{14}N. The multinuclear magnetic resonance spectra in BrF_5 and HF solvents

for all five spin-½ nuclei are consistent with Structure 5.1 for the $F_5TeN(H)\text{-}Xe^+$ cation in solution (see Table 5.1).

The ^{129}Xe NMR spectra of natural abundance $F_5TeN(H)\text{-}Xe^+$ consist of a broad singlet at -2840 ppm in HF solvent (-45.0 °C; Figure 5.1a) and at -2903 ppm in BrF_5 solvent (-48.3 °C). The absence of xenon-fluorine scalar coupling indicates that the Xe-F bond is ionized in solution [cf., XeF_2 (BrF_5 solvent, -52 °C): $^1J(^{19}F\text{-}^{129}Xe)$ = 5621 Hz].[71] The failure to observe the xenon-nitrogen scalar coupling is attributed to quadrupolar collapse resulting from fast relaxation of the ^{14}N nucleus (I = 1). In prior studies of the imidodisulfurylfluoride derivatives of xenon(II), the low symmetry and resultant large electric field gradient (efg) at the ^{14}N nucleus (I = 1) in the trigonal planar $\text{-}N(SO_2F)_2$ group resulted in quadrupolar collapse of the xenon-nitrogen scalar couplings in $FXeN(SO_2F)_2$,[57] $XeN(SO_2F)_2^+$,[60] $Xe[N(SO_2F)_2]_2$,[59] and $F[XeN(SO_2F)_2]_2^+$ [60] in SbF_5, BrF_5, and SO_2ClF solvents. Nitrogen-15 enrichment (30%) facilitated the observation of the xenon-nitrogen scalar couplings. It was also necessary to prepare the ^{15}N-enriched $HC{\equiv}N\text{-}XeF^+$ cation to observe all possible scalar couplings.[73] Similarly, the lone pair of electrons and the unsymmetrical geometry at the formally sp^3-hybridized nitrogen center in $F_5TeN(H)\text{-}Xe^+$ results in a large efg at nitrogen, so that ^{14}N undergoes rapid relaxation, which prevents the observation of scalar couplings to nitrogen. The Xe(II)-N scalar coupling, $^1J(^{129}Xe\text{-}^{15}N)$, was observed on ^{15}N-enrichment, confirming the xenon-nitrogen linkage.

The ^{129}Xe NMR spectra of 99.5% ^{15}N-enriched $F_5TeN(H)\text{-}Xe^+AsF_6^-$ recorded at 11.7440 T consists of a doublet centered at -2840 ppm in HF solvent at -45.0 °C, $^1J(^{129}Xe\text{-}^{15}N)$ = 138 Hz (Figure 5.1b), and at -2902 ppm in BrF_5 solvent at -45 °C, $^1J(^{129}Xe\text{-}^{15}N)$ = 142 Hz. The magnitude of $^1J(^{129}Xe\text{-}^{15}N)$ is comparable to directly bonded $^{129}Xe\text{-}^{15}N$ scalar couplings of related xenon(II)-nitrogen bonded compounds such as $(FO_2S)_2N\text{-}Xe^+$ (91.7 Hz)[60] and

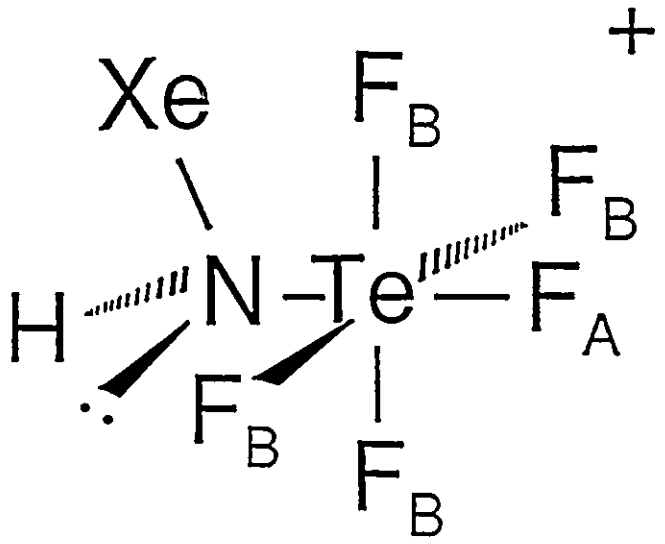

5.1

Figure 5.1 (a) ^{129}Xe NMR spectrum (139.051 MHz) of natural abundance $F_5TeN(H)$-$Xe^+AsF_6^-$ in HF solvent (-45.0 °C) with an external magnetic field strength of 11.7440 T. (b) ^{129}Xe NMR spectrum (139.051 MHz) of 99.5% ^{15}N-enriched $F_5TeN(H)$-$Xe^+AsF_6^-$ in HF solvent (-45.0 °C) with an external magnetic field strength of 11.7440 T. (c) ^{129}Xe NMR spectrum (83.445 MHz) of 99.5% ^{15}N-enriched $F_5TeN(H)$-$Xe^+AsF_6^-$ in HF solvent (-38.8 °C) with an external magnetic field strength of 7.0463 T.

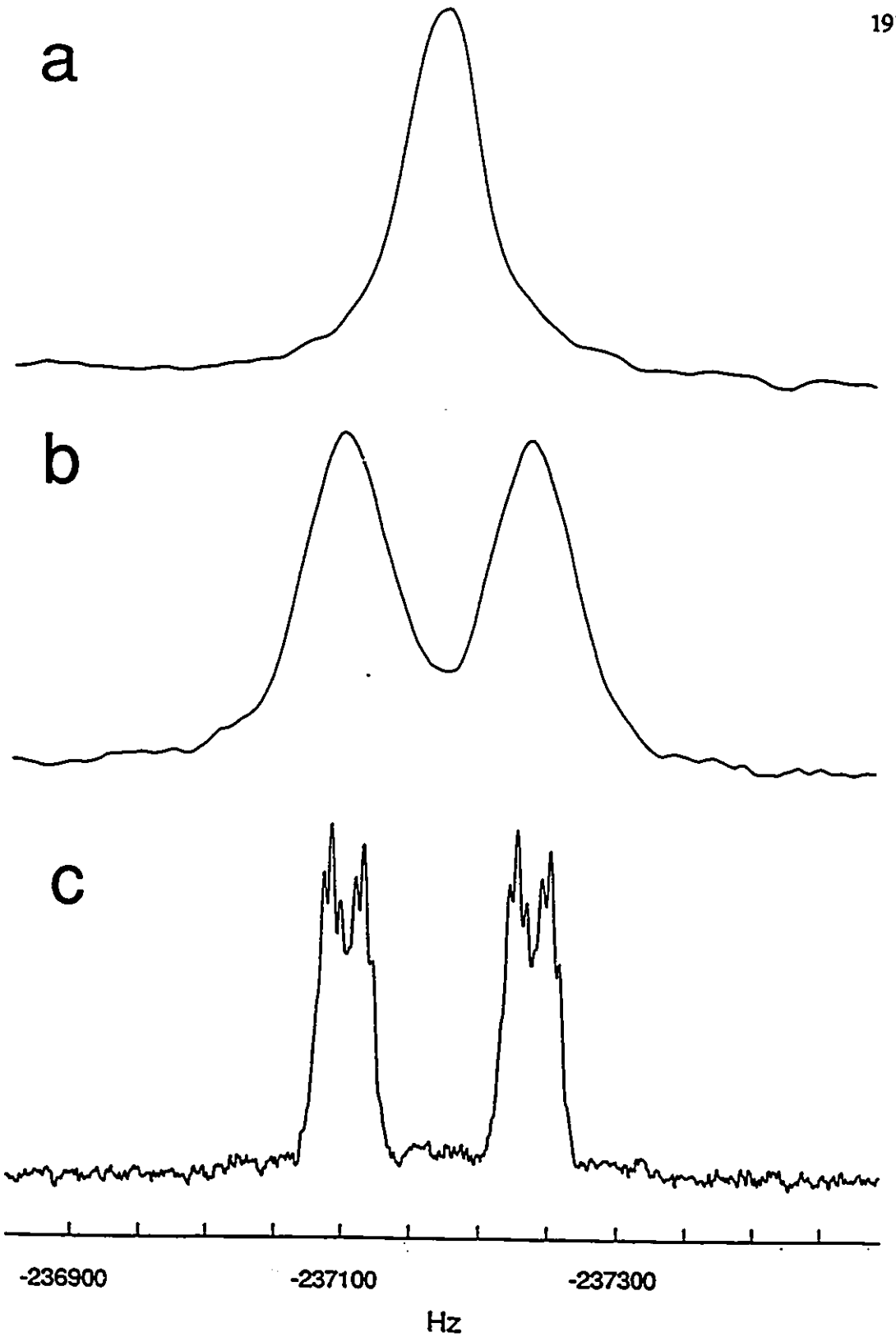
a
b
c
-236900
-237100
-237300
Hz

Table 5.1

NMR Chemical Shifts and Spin-Spin Coupling Constants for the $F_5TeN(H)\text{-}Xe^+$ Cation.

Chemical Shifts (ppm)[a]		T, °C
$\delta(^{129}Xe)$	-2841	-38.8
	(-2902)	-45.0
	-2832[b]	-61.2
$\delta(^{125}Te)$[c]	598	-34.1
$\delta(^{19}F)$[d]	-51.6 (-51.9), $F_{ax.}$ -43.4 (-43.2), $F_{eq.}$	-31.2 (-44.0)
$\delta(^{15}N)$[c]	-268.0 (-266.3)	-40.0 (-45.0)
$\delta(^{1}H)$[c]	(6.90)	(-44.2)

Coupling Constants, Hz[c]

$^{1}J(^{129}Xe\text{-}^{15}N)$	138 (142)	$^{1}J(^{123}Te\text{-}^{19}F_{eq.})$	(3113)
$^{2}J(^{129}Xe\text{-}^{1}H)$	24	$^{1}J(^{15}N\text{-}^{1}H)$	62
$^{3}J(^{129}Xe\text{-}^{19}F_{eq.})$	6	$^{2}J(^{19}F_{ax.}\text{-}^{19}F_{eq.})$[d]	166
$^{1}J(^{125}Te\text{-}^{19}F_{ax.})$	3578	$^{1}J(^{125}Te\text{-}^{19}F_{eq.})$	3766
$^{1}J(^{125}Te\text{-}^{15}N)$	333	$^{2}J(^{125}Te\text{-}^{1}H)$	46

Table 5.1 (continued)

a Samples were referenced externally at 30 °C with respect to the neat liquid references; $XeOF_4$ (^{129}Xe), $(CH_3)_2Te$ (^{125}Te), $CFCl_3$ (^{19}F), CH_3NO_2 (^{15}N) and $(CH_3)_4Si$ (^{1}H). A positive chemical shift denotes a resonance occurring to high frequency of the reference compound. The values in parentheses have been measured in BrF_5 solvent. All other values have been measured in HF solvent unless otherwise specified.

b Value obtained from the reaction of $F_5TeNH_3^+As(OTeF_5)_6^-$ and $Xe(OTeF_5)_2$ in SO_2ClF solvent.

c Obtained from a 99.5% ^{15}N-enriched sample of $F_5TeN(H)$-$Xe^+AsF_6^-$.

d All ^{19}F spectra in HF solvent displayed a broad saddle-shaped feature at *ca.* -68 ppm arising from the partially quadrupole collapsed $^1J(^{75}As$-$^{19}F)$ of the octahedral AsF_6^- anion. In BrF_5 solvent, the resonance at *ca.* -68 ppm was completely quadrupole collapsed, resulting in a broad singlet. Values obtained from natural abundance samples of $F_5TeN(H)$-$Xe^+AsF_6^-$ in HF and BrF_5 solvents.

$FO_2SN(H)$-Xe^+ (107 Hz; see Chapter 8). The magnitude of the Xe-N scalar coupling is also discussed in Section (E) of this Chapter. Because of the large linewidth ($\Delta\nu_{1/2}$ = 80 Hz) of each peak of the doublet, the long range couplings to xenon, namely, $^2J(^{129}Xe\text{-}^1H)$, $^2J(^{129}Xe\text{-}^{125}Te)$, $^3J(^{129}Xe\text{-}^{19}F_{ax})$ and $^3J(^{129}Xe\text{-}^{19}F_{eq})$, were not observed in the ^{129}Xe NMR spectra of $F_5Te^{15}N(H)$-Xe^+ at 11.7440 T. The large linewidth presumably results from line broadening caused by shielding anisotropy (SA) relaxation of the ^{129}Xe nucleus, which is field dependent and is significant for xenon. This is exemplified in the field dependence of the ^{129}Xe linewidth for the 30% ^{15}N-enriched $(FO_2S)_2N$-Xe^+ cation in SbF_5 solvent,[60] which is proportional to the inverse of the spin-lattice relaxation time constant, T_1. At an external field strength of 5.8719 T, the linewidth of the ^{129}Xe resonance for $(FO_2S)_2N$-Xe^+ was 139 Hz, and the $^{129}Xe\text{-}^{15}N$ scalar coupling was not resolved. However, at 2.3488 T, the linewidth was significantly reduced and the $^{129}Xe\text{-}^{15}N$ scalar coupling was resolved. The contribution to spin-lattice relaxation (T_1) arising from SA is inversely proportional to the square of the external magnetic field B_o and is given by equation (5.6), where ϖ is the resonance frequency, γ is the gyromagnetic ratio, τ_c is the molecular

$$T_1 = [15(1 + \varpi^2\tau_c^2)] / [\gamma^2 B_o^2 \Delta\sigma^2 2\tau_c] \qquad (5.6)$$

correlation time for isotropic tumbling in solution, and $\Delta\sigma$ refers to the anisotropy of the ^{129}Xe shielding tensor.[251] As B_o increases, one can see that T_1 decreases. The relaxation rate ($1/T_1$) is therefore increased and the resonance line is broadened. As expected, the SA broadening of the ^{129}Xe resonance for $F_5TeN(H)$-Xe^+ was significantly reduced at 7.0463 T in HF solvent at -38.8 °C, as shown in Figure 5.1c. The ^{129}Xe resonance is centered at $\delta(^{129}Xe)$ = -2841.5 ppm and consists of a doublet of doublet of quintets. Figure 5.2b illustrates a resolution enhancement of

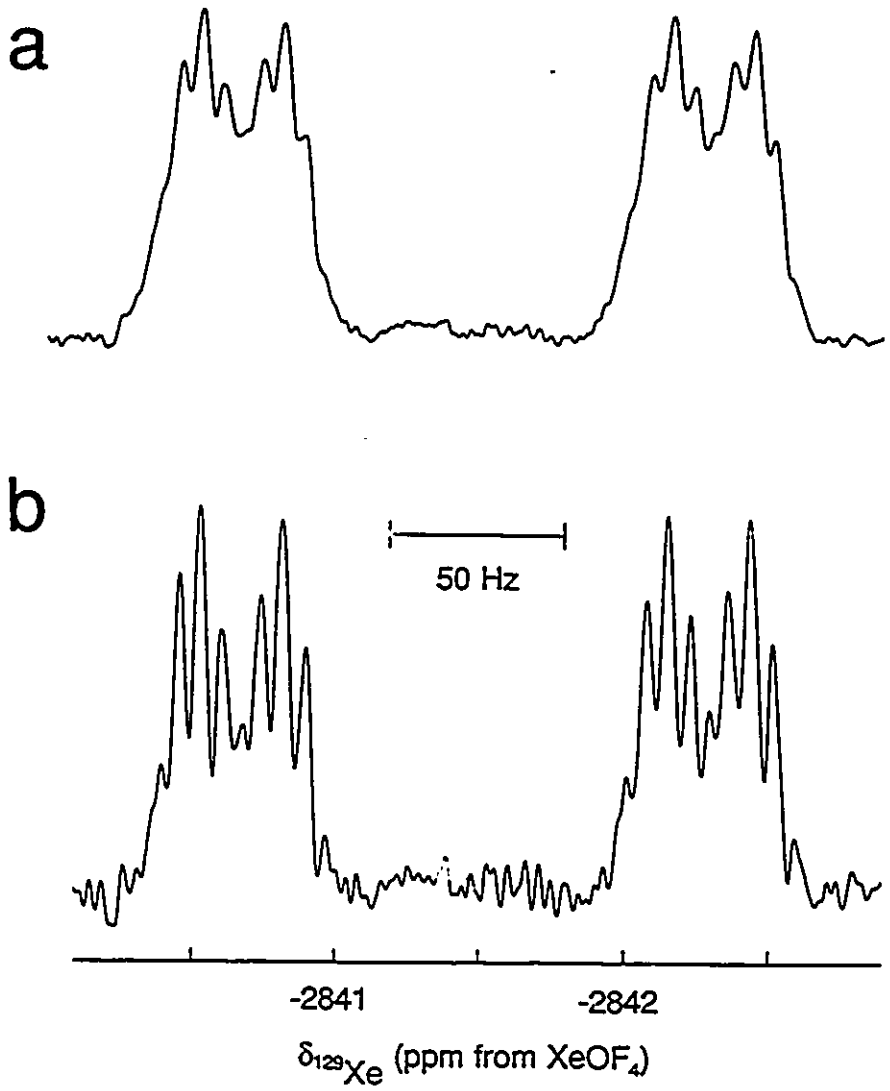

Figure 5.2 (a) ^{129}Xe NMR spectrum (83.445 MHz) of 99.5% ^{15}N-enriched $F_5TeN(H)$-$Xe^+AsF_6^-$ in HF solvent (-38.8 °C) with an external magnetic field strength of 7.0463 T. (b) Resolution of ^{129}Xe spectrum enhanced by application of a Gaussian function to the free induction decay before Fourier transformation.

the ^{129}Xe resonance obtained by the application of a Gaussian function to the free induction decay before Fourier transformation. The largest doublet splitting arises from $^{1}J(^{129}Xe\text{-}^{15}N)$ = 136 Hz, which was the only resolved coupling in the ^{129}Xe NMR spectrum at 11.7440 T (Figure 5.1b). At 7.0463 T (Figure 5.2b), each line of the doublet is further split into a doublet arising from $^{2}J(^{129}Xe\text{-}^{1}H)$ 24 Hz. The quintet splitting arises from the scalar coupling of xenon with the four chemically equivalent equatorial fluorine atoms bonded to tellurium [$^{3}J(^{129}Xe\text{-}^{19}F_{eq.})$ = 6 Hz]. The magnitude of $^{3}J(^{129}Xe\text{-}^{19}F_{eq.})$ is smaller than that observed for the related $F_5TeO\text{-}Xe^+$ cation (18.5 Hz),[54] $F_5TeOXeF$ (30 Hz)[141] and $Xe(OTeF_5)_2$ (31 Hz).[141] A coupling corresponding to $^{2}J(^{129}Xe\text{-}^{125}Te)$ is not observed in the ^{129}Xe or the ^{125}Te NMR spectrum of $F_5TeN(H)\text{-}Xe^+$ (see below). The scalar coupling of ^{129}Xe with the axial fluorine bonded to tellurium is not resolved. This coupling was also not resolved in the ^{129}Xe NMR spectra of $F_5TeO\text{-}Xe^+$,[54] $F_5TeO\text{-}XeF$[141] and $Xe(OTeF_5)_2$.[141] There is a potential ambiguity in the ^{129}Xe NMR spectrum of $F_5TeN(H)\text{-}Xe^+$ at 7.0463 T, since one could argue that the doublet splitting of 24 Hz assigned to $^{2}J(^{129}Xe\text{-}^{1}H)$ may arise from $^{3}J(^{129}Xe\text{-}^{19}F_{ax.})$ as opposed to $^{2}J(^{129}Xe\text{-}^{1}H)$. However, the assignment of this coupling to $^{2}J(^{129}Xe\text{-}^{1}H)$ was confirmed by an $^{129}Xe\text{-}^{1}H$ INEPT experiment,[252] with ^{129}Xe as the observed nucleus. In the ^{1}H pulse sequence, a fixed delay of $(4J)^{-1}$ was used in which J is the magnitude of the coupling assigned to $^{2}J(^{129}Xe\text{-}^{1}H)$. After completion of the INEPT experiment, the quintets of the ^{129}Xe resonance which are separated by J Hz are out of phase (see Figure 5.3b). This indicates polarization transfer from ^{1}H to ^{129}Xe and confirms that the coupling of 24 Hz results from $^{2}J(^{129}Xe\text{-}^{1}H)$ and not from $^{3}J(^{129}Xe\text{-}^{19}F_{ax.})$.

The ^{15}N NMR spectrum of the 99.5 atom % ^{15}N-enriched $F_5TeN(H)\text{-}Xe^+$ cation in HF solvent at -40 °C (Figure 5.4), consists of a doublet centered at -268.0 ppm, $^{1}J(^{15}N\text{-}^{1}H)$ = 62 Hz. Satellite doublets are also observed, corresponding to $^{1}J(^{15}N\text{-}^{129}Xe)$ = 138 Hz (natural abundance

Figure 5.3 (a) ^{129}Xe NMR spectrum (83.445 MHz) of 99.5% ^{15}N-enriched $F_5TeN(H)$-$Xe^+AsF_6^-$ in HF solvent (-38.8 °C) with an external magnetic field strength of 7.0463 T. Resolution enhanced by Gaussian multiplication before Fourier transformation of the free induction decay. (b) ^{129}Xe-^1H INEPT of 99.5% ^{15}N-enriched $F_5TeN(H)$-$Xe^+AsF_6^-$ in HF solvent at (-38.8 °C) with an external field strength of 7.0463 T. Resolution enhanced by applying a Gaussian function to the free induction decay before Fourier transformation.

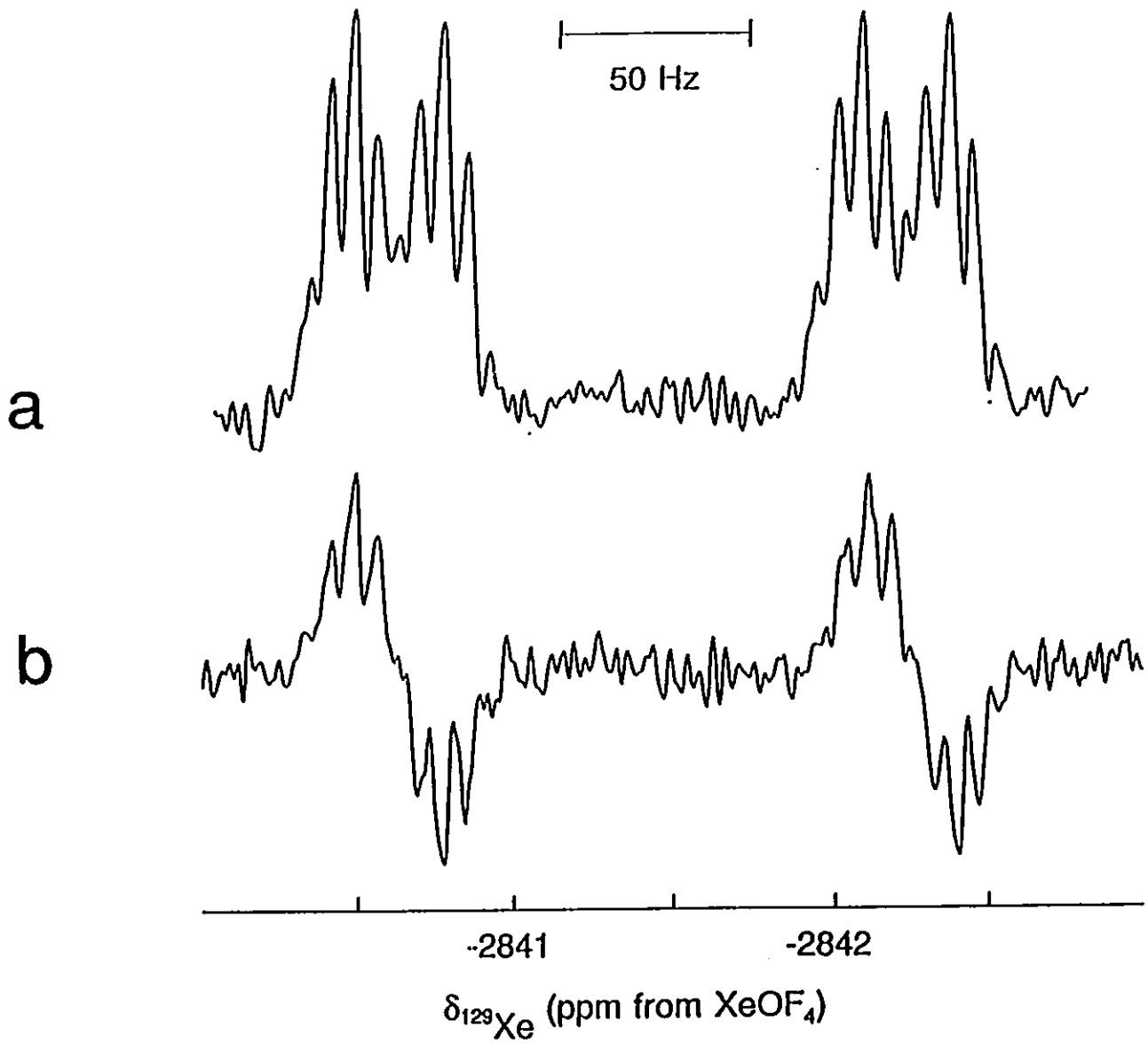
50 Hz
a
b
-2841
-2842
$\delta_{^{129}Xe}$ (ppm from $XeOF_4$)

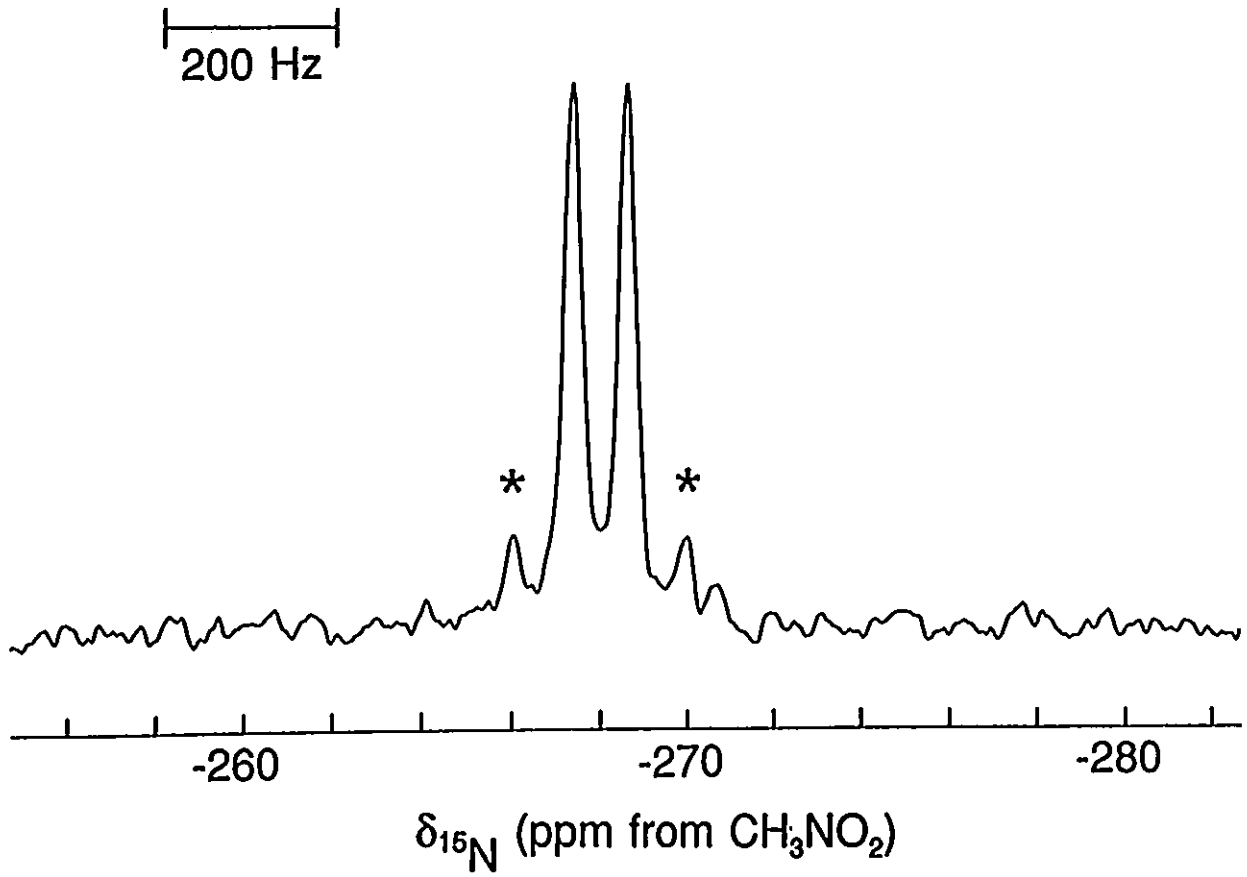

Figure 5.4 ^{15}N NMR spectrum (50.698 MHz) of 99.5% ^{15}N-enriched $F_5TeN(H)\text{-}Xe^+AsF_6^-$ in HF solvent (-40.0 °C). Asterisks (*) denote ^{129}Xe satellites arising from $^1J(^{15}N\text{-}^{129}Xe)$. The inner peak of each satellite doublet overlaps with a peak of the higher intensity doublet.

^{129}Xe, 26.44%; I = 1/2). The inner peaks of each satellite doublet are coincident with the central doublet peaks and therefore are not observed. The scalar coupling $^1J(^{15}N\text{-}^{129}Xe)$ = 138 Hz was calculated by subtracting the $^1J(^{15}N\text{-}^1H)$ = 62 Hz from the frequency separation of the visible satellite peaks. A similar ^{15}N NMR spectrum is observed in BrF_5 solvent at -45 °C centered at -266.3 ppm, $^1J(^{15}N\text{-}^1H)$ = 62 Hz, but because of insufficient signal-to-noise, the satellite peaks arising from $^1J(^{15}N\text{-}^{129}Xe)$ were not observed. The ^{15}N chemical shift is similar to those observed for the related ^{15}N enriched compounds, $FXeN(SO_2F)_2$ (-247.9),[57] $Xe[N(SO_2F)_2]_2$ (-232.5)[59] and $XeN(SO_2F)_2^+$ (-243.0 ppm).[60] The ^{15}N NMR resonance of the $F_5TeN(H)\text{-}Xe^+$ cation is significantly deshielded relative to the $F_5TeNH_3^+$ cation [$\delta(^{15}N)$ = -317.1 ppm], which is present in samples containing the $F_5TeN(H)\text{-}Xe^+$ cation according to equation (5.4). The more deshielded ^{15}N resonance observed for the $F_5TeN(H)\text{-}Xe^+$ cation is expected from examination of the factors contributing to the local paramagnetic shielding term for nitrogen, σ_P^N [equation (5.7)].[244] The greater inductive effect of the Xe^+ group is expected to increase the radial factor $\langle r^{-3}\rangle_{2p}$,

$$\sigma_P^N = -[\mu_o\mu_B^2\langle r^{-3}\rangle_{2p}\Sigma Q] / [2\pi(\Delta E)] \qquad (5.7)$$

lower the σ^* LUMO relative to the nonbonding orbital on nitrogen, thus reducing ΔE for paramagnetic $n_N \rightarrow \sigma^*$ circulations, and increase ΣQ, the charge-imbalance term for the valence electrons of the nitrogen atom. All of these terms reinforce each other, thus contributing to an increase in the magnitude of σ_P^N, that deshields the nitrogen nucleus. In a comparison of $HN(SO_2F)_2$ and $FXeN(SO_2F)_2$,[57] the ^{15}N chemical shifts were observed to be almost the same (-249.2 and -250.4 ppm, respectively). Since inductive effects through the σ framework predict a deshielding of $FXeN(SO_2F)_2$ relative to $HN(SO_2F)_2$, it was argued that since the nitrogen lone

pair of electrons is part of the π framework of the $-N(SO_2F)_2$ group, σ_p^N is dominated by the deshielding of the nitrogen atom by the $n_N \rightarrow \pi^*$ circulation of the nitrogen lone-pair electrons in π^* orbitals of the sulfur-nitrogen bonds. There is little influence from the inductive effects of XeF and H, which act primarily through the σ framework.[57] In the present case, σ inductive effects appear to dominate. This is reasonable, since the absence of a free lone pair dictates that Te-N π-bonding is not possible for the $F_5TeNH_3^+$ cation. It is possible that some degree of Te-N or Xe-N π-bonding contributes to the bonding in the $F_5TeN(H)$-Xe^+ cation, which would deshield the nitrogen atom through $n_N \rightarrow \pi^*$ circulations of the nitrogen atom lone-pair of electrons in π^* orbitals of the Te-N and Xe-N bonds. Evidence for Te-N π-bonding in F_5TeNH_2 has been given in Chapter 4. Xenon-nitrogen π-bonding in the $F_5TeN(H)$-Xe^+ cation is reasonable by analogy with the R-Xe^+ cations (R = C_6F_5,[95,99] 2,4,6-$F_3C_6H_2$,[98] 2,6-$F_2C_6H_3$,[253] 2-FC_6H_4[253] and 4-FC_6H_4[253]), where the deshielding of the aryl fluorine ^{19}F and aryl carbon ^{13}C NMR resonances in the 2, 4 and 6 positions on the aryl ring was consistent with Xe-C π-bonding.[253]

The ^1H NMR spectrum of natural abundance $F_5TeN(H)$-Xe^+ consists of a singlet at 6.90 ppm; no coupling to nitrogen is observed, as a result of the fast relaxation of the quadrupolar nitrogen nucleus (quadrupolar collapse), but a satellite doublet that arises from $^2J(^1H\text{-}^{125}Te)$ = 46 Hz is observed (Figure 5.5a). The failure to observe the scalar coupling $^2J(^1H\text{-}^{129}Xe)$ is attributed to SA broadening of the ^{129}Xe satellites at the high field strength (11.7440 T) used to obtain the ^1H NMR spectra. The one-bond proton-nitrogen coupling, $^1J(^{15}N\text{-}^1H)$ = 62 Hz, is observed in the ^1H NMR spectrum of the 99.5% ^{15}N-enriched $F_5TeN(H)$-Xe^+ cation in BrF_5 solvent at -44.2 °C (Figure 5.5b). Satellite peaks arising from $^2J(^1H\text{-}^{125}Te)$ are visible but not well resolved because of insufficient signal-to-noise.

The ^{125}Te NMR spectrum of an equimolar mixture of 99.5% ^{15}N-enriched F_5TeNH_2 and

Figure 5.5 ^{1}H NMR spectra (500.138 MHz) of (a) natural abundance (-55.5 °C) and (b) 99.5% ^{15}N-enriched $F_5TeN(H)\text{-}Xe^{+}AsF_6^{-}$ (-44.2 °C) in BrF_5 solvent. Asterisks (*) denote ^{125}Te satellites arising from $^{2}J(^{1}H\text{-}^{125}Te)$.

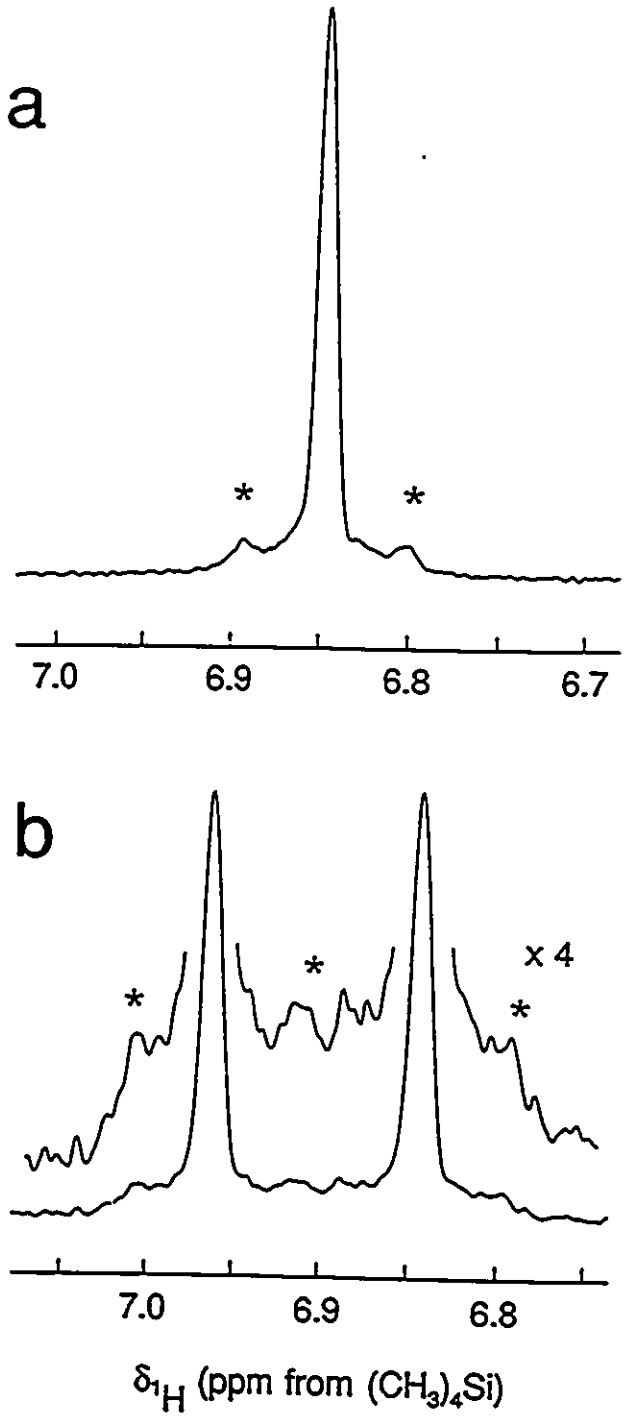
a
*
*
7.0
6.9
6.8
6.7
b
*
*
*
x 4
7.0
6.9
6.8
$\delta_{^1H}$ (ppm from $(CH_3)_4Si$)

Figure 5.6 (a) ^{125}Te NMR spectrum (157.795 MHz) of equilibrium mixture resulting from the reaction of 99.5% ^{15}N-enriched $F_5TeNH_3^+AsF_6^-$ and XeF_2 in HF solvent at -34.1 °C; (A) center of multiplet assigned to $F_5TeNH_3^+$, (B) center of multiplet assigned to $F_5TeN(H)\text{-}Xe^+$, (C) center of multiplet assigned to TeF_6. (b) ^{125}Te NMR spectrum (157.795 MHz) of 99.5% ^{15}N-enriched $F_5TeN(H)\text{-}Xe^+AsF_6^-$ in HF solvent at -34.1 °C; peaks labelled (A) are part of the multiplet assigned to $F_5TeN(H)\text{-}Xe^+$; an asterisk (*) denotes a peak of the TeF_6 multiplet; all other peaks arise from the $F_5TeNH_3^+$ multiplet. (c) Expansion of a portion of the $F_5TeN(H)\text{-}Xe^+$ multiplet; peaks labelled (A) and (B) arise from $F_5TeNH_3^+$ and TeF_6, respectively.

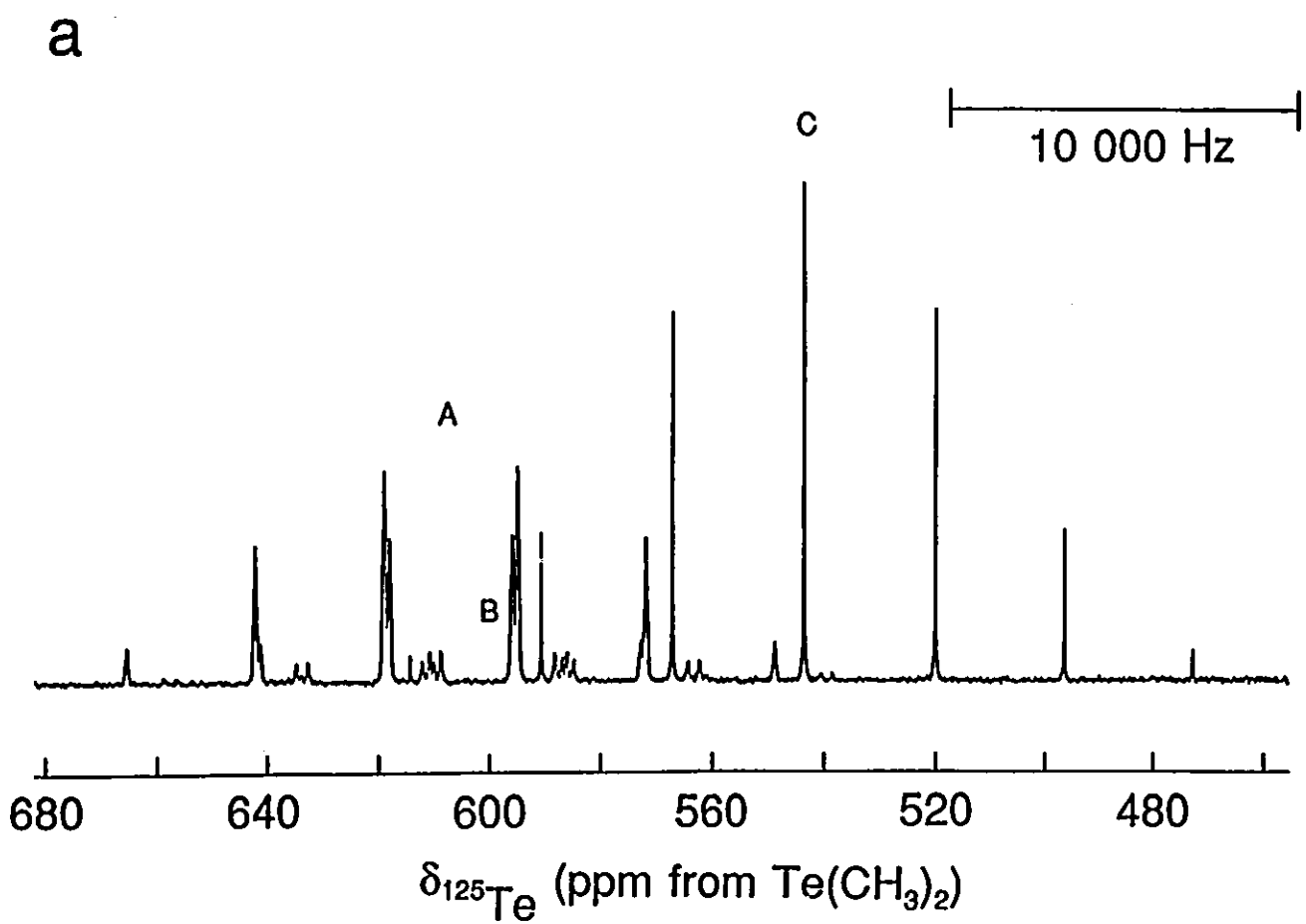
a
C
10 000 Hz
A
B
680
640
600
560
520
480
δ125Te (ppm from Te(CH3)2)

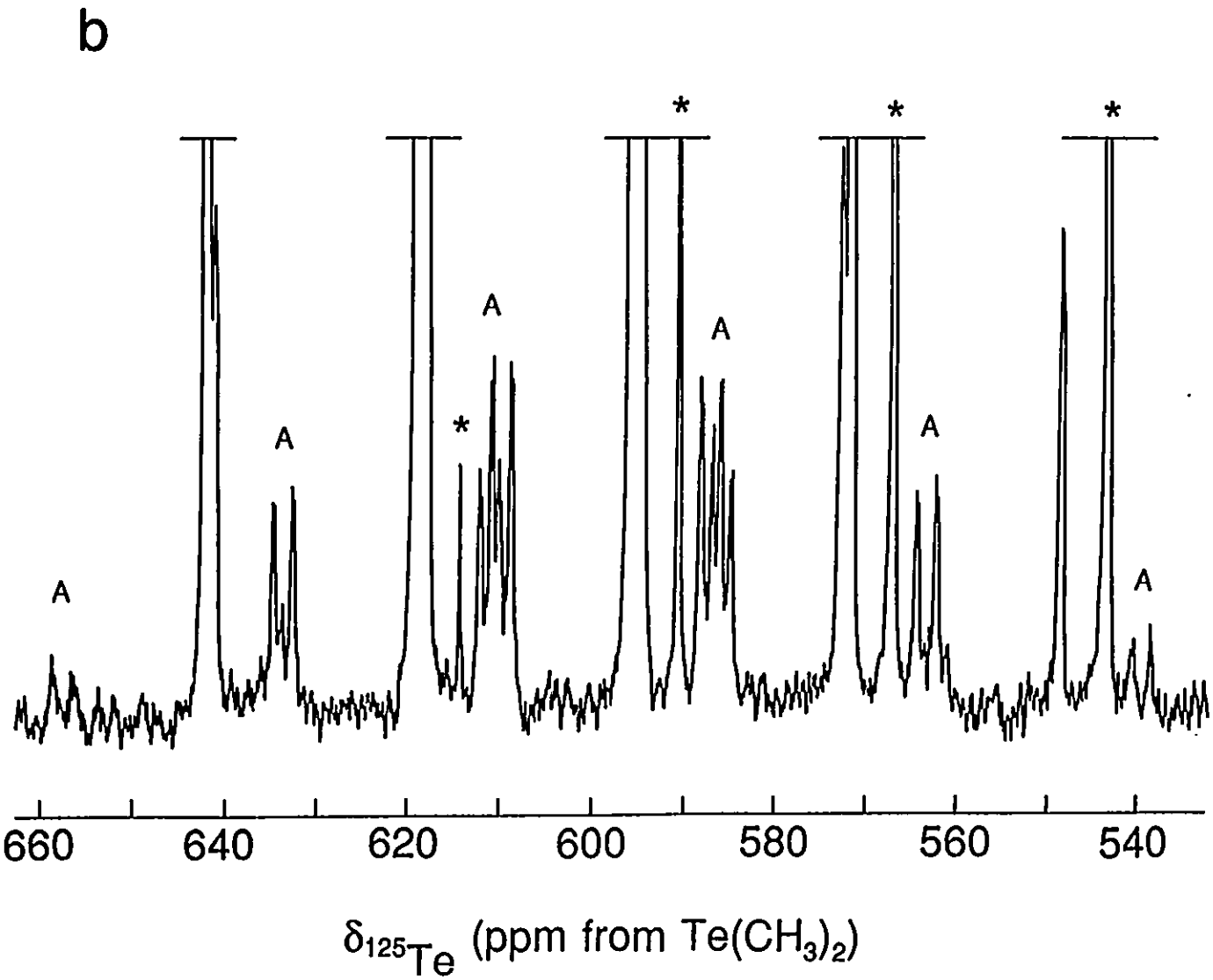
b
A
A
*
A
*
A
*
A
*
A
660
640
620
600
580
560
540
δ125Te (ppm from Te(CH3)2)

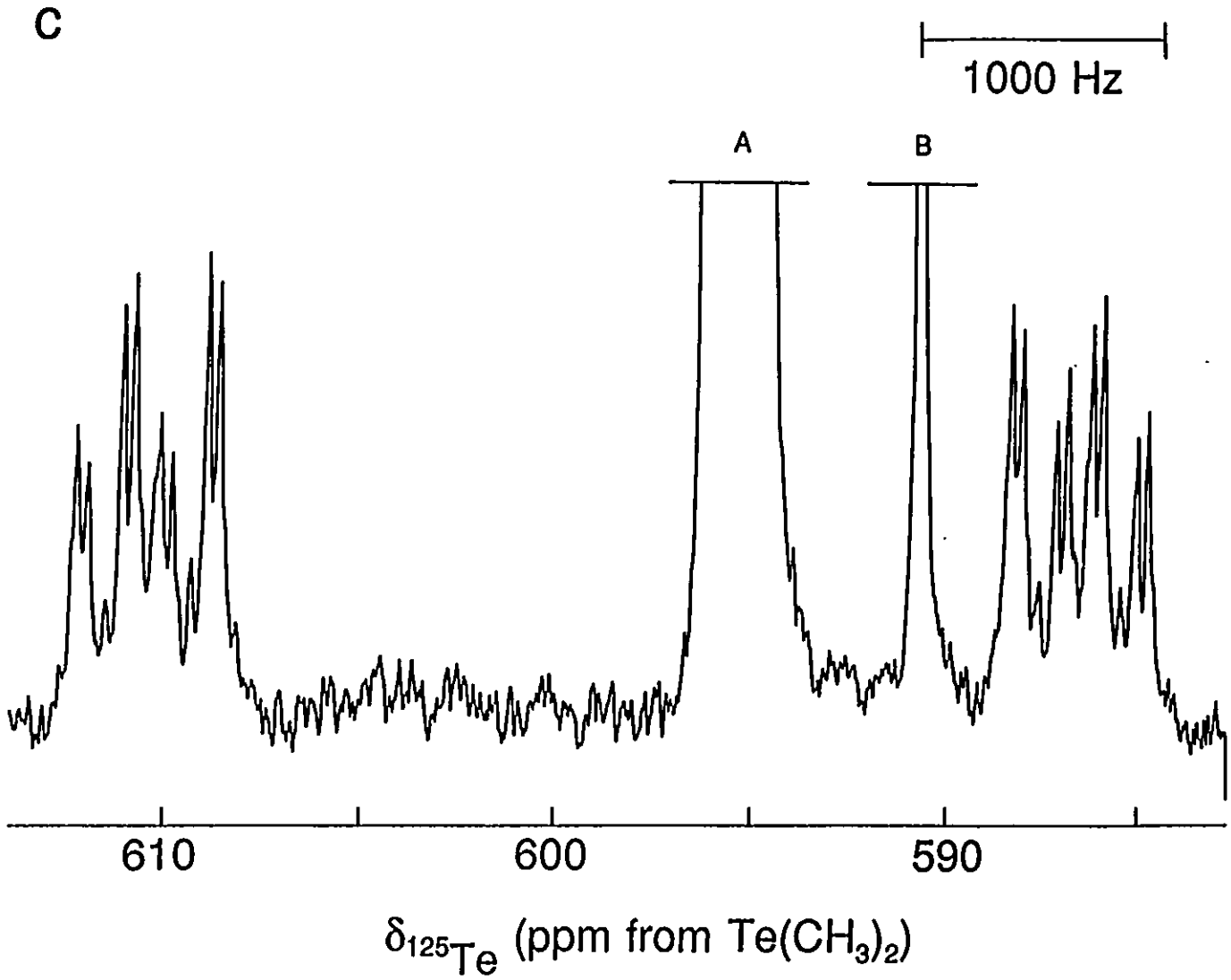
C
1000 Hz
A
B
610
600
590
$\delta_{^{125}Te}$ (ppm from $Te(CH_3)_2$)

$XeF^+AsF_6^-$ in HF solvent (-34.1 °C) is shown in Figure 5.6a. The ^{15}N-enriched $F_5TeN(H)$-Xe^+ cation is unambiguously assigned to the multiplet centered at 598 ppm, since the two other resonances, centered at 543 and 607 ppm, are attributable to TeF_6 and the ^{15}N-enriched $F_5TeNH_3^+$ cation (Chapter 4), respectively. The presence of the $F_5TeNH_3^+$ cation in the ^{125}Te spectrum is consistent with equation (5.4). A detailed analysis of the solution equilibria and decomposition of $F_5TeN(H)$-$Xe^+AsF_6^-$ in HF and BrF_5 solvents will be discussed in Chapter 6. The ^{125}Te NMR resonance of ^{15}N-enriched $F_5TeN(H)$-Xe^+ consists of a first order multiplet centered at 598 ppm (Figure 5.6b), and is consistent with Structure 5.1. The ^{125}Te chemical shift is comparable to that observed for the isoelectronic F_5TeO-Xe^+ cation (576 ppm).[54] The resonance is split into a quintet arising from $^1J(^{125}Te\text{-}^{19}F_{eq}) = 3766$ Hz. Referring to the expansion in Figure 5.6c, a doublet splitting arises from $^1J(^{125}Te\text{-}^{19}F_{ax}) = 3578$ Hz, and two further doublet splittings arise from $^1J(^{125}Te\text{-}^{15}N) = 333$ Hz and $^2J(^{125}Te\text{-}^1H) = 46$ Hz. As expected, $^2J(^{125}Te\text{-}^{129}Xe)$ is not observed, because of the relatively low receptivity of ^{125}Te (2.24×10^{-3})[254] and ^{129}Xe (5.69×10^{-3})[254] relative to ^1H, and the low concentration of ^{15}N-enriched $F_5TeN(H)$-Xe^+ in solution.

The ^{19}F NMR spectrum of the $F_5TeN(H)$-Xe^+ cation in HF solvent at -31.2 °C and in BrF_5 solvent at -44.0 °C each consist of a typical AX_4 pattern and the spectral parameters are listed in Table 5.1. The axial fluorine resonance is split into a quintet at -51.6 ppm in HF solvent (-51.9 ppm in BrF_5) arising from the two-bond scalar coupling to the four chemically equivalent equatorial fluorine atoms bonded to tellurium [$^2J(^{19}F_{ax.}\text{-}^{19}F_{eq.}) = 166$ Hz]. The equatorial fluorine resonance is likewise split into a doublet centered at -43.4 ppm in HF (-43.2 ppm in BrF_5). Of the four possible couplings to ^{125}Te, only $^1J(^{19}F_{eq.}\text{-}^{125}Te) = 3767$ Hz (HF or BrF_5 solvent) is observed because of the low concentration of the $F_5TeN(H)$-Xe^+ cation in solution. The observation of $^1J(^{19}F_{eq.}\text{-}^{125}Te)$ confirms that the AX_4 pattern arises from the $F_5TeN(H)$-Xe^+

cation, since the same coupling is observed in the ^{125}Te NMR spectrum of $F_5TeN(H)$-Xe^+ (see above). The scalar coupling, $^1J(^{19}F_{eq.}$-$^{123}Te)$ = 3113 Hz, is also resolved from satellite peaks which flank the $^{19}F_{eq.}$ resonance. Long range scalar couplings to ^{129}Xe, ^{1}H and ^{15}N were not observed in the ^{19}F spectra of natural abundance or 99.5% ^{15}N-enriched $F_5TeN(H)$-$Xe^+AsF_6^-$. A resonance attributable to the AsF_6^- anion is observed at *ca.* -68 ppm in the ^{19}F spectra in HF solvent (-40 °C). The resonance is saddle-shaped ($\Delta\nu_{1/2}$ = 2588 Hz) because of the partially quadrupole collapsed scalar coupling $^1J(^{75}As$-$^{19}F)$. In BrF_5 (-60 °C) solvent a similar ^{19}F resonance is observed for the AsF_6^- anion, without a saddle-shaped structure ($\Delta\nu_{1/2}$ = 617 Hz).

Resonances arising from the $F_5TeNH_3^+$ cation are also observed in the ^{19}F, ^{125}Te, and ^{1}H NMR spectra in HF and BrF_5 solvents and are consistent with equation (5.4). In a sample that had initial XeF_2 and $F_5TeNH_3^+AsF_6^-$ concentrations of 0.38 and 0.36 M, respectively, in BrF_5 solution, the relative concentrations [$F_5TeNH_3^+$] : [$F_5TeN(H)$-Xe^+] were determined to be 1.0 : 1.2 in the ^{19}F NMR spectrum recorded at -60 °C after warming to the sample -40 °C for 10 minutes. In HF solvent at -33.3 °C, the same ratio was determined to be 1.0 : 0.3 with initial $XeF^+AsF_6^-$ and F_5TeNH_2 concentrations of 0.71 M. The lower relative amount of $F_5TeN(H)$-Xe^+ in HF solvent is reasonable since the presence of excess HF is expected to drive the HF elimination reaction depicted in equation (5.4) towards the starting materials. The observation of XeF_2 in the ^{19}F and ^{129}Xe spectra is also consistent with equation (5.4). The XeF_2 resonance in the ^{19}F NMR spectrum in BrF_5 solvent (-58 °C) is observed at -184.1 ppm [$^1J(^{19}F$-$^{129}Xe)$ = 5621 Hz]. A doublet assignable to HF is observed at -192.8 ppm [$^1J(^{19}F$-$^1H)$ = 527 Hz]. The observation of scalar couplings in the ^{19}F NMR spectrum indicate that XeF_2 and HF are not undergoing fast intermolecular exchange in BrF_5 solution at this temperature. In HF solvent at -41 °C, the ^{19}F NMR resonance of XeF_2 is observed at -199.7 ppm, similar to the value of

-199.6 ppm for pure XeF_2 in HF at -68 °C,[111] and is significantly broadened ($\Delta\nu_{1/2}$ = 386 Hz). The presence of XeF_2 is consistent with solvolysis of $XeF^+AsF_6^-$ according to equation (5.2). The absence of peaks in the ^{19}F NMR spectra assignable to F_5TeNH_2 (see Chapter 4) or XeF^+ indicated that the reactions represented by equations (5.2) and (5.3) went essentially to completion in HF solvent. The absence of solid material in the sample was also consistent with solvolysis of $XeF^+AsF_6^-$ represented by equation (5.2), since it was reported to be insoluble in HF at low temperatures.[111]

(C) CHARACTERIZATION OF $F_5TeN(H)$-$Xe^+As(OTeF_5)_6^-$ IN SO_2ClF SOLVENT BY ^{129}Xe AND ^{19}F NMR SPECTROSCOPY

The reaction of equimolar amounts of the salt $F_5TeNH_3^+As(OTeF_5)_6^-$ and $Xe(OTeF_5)_2$ in SO_2ClF solvent at -61.2 °C resulted in a complex equilibrium mixture. The ^{129}Xe NMR spectrum consisted of two singlets assignable to $Xe(OTeF_5)_2$ [$\delta(^{129}Xe$ = -2271 ppm; $\Delta\nu_{1/2}$ = 126 Hz] and the $F_5TeN(H)$-Xe^+ cation [$\delta(^{129}Xe$ = -2832 ppm; $\Delta\nu_{1/2}$ = 61 Hz]. No long range couplings, such as $^3J(^{129}Xe\text{-}^{19}F_{ax.})$, $^3J(^{129}Xe\text{-}^{19}F_{eq.})$ and $^2J(^{129}Xe\text{-}^1H)$, were resolved for either compound. In a sample having initial $Xe(OTeF_5)_2$ and $F_5TeNH_3^+As(OTeF_5)_6^-$ concentrations of 0.23 and 0.24 M, respectively, integration of the ^{129}Xe NMR resonances indicates a ratio [$Xe(OTeF_5)_2$] : [$F_5TeN(H)$-Xe^+] of 1.7 : 1.0.

The ^{19}F NMR spectrum (470.599 MHz) indicated rapid exchange of F_5TeO- and F_5TeN- groups at -61.2 °C, that prevented analysis of the spectrum. Cooling to -115.4 °C resulted in substantial slowing of the exchange on the ^{19}F NMR time scale as shown in Figure 5.7. The doublet at $\delta(^{19}F)$ = -30.73 ppm (A) and the quintet at $\delta(^{19}F)$ = -52.57 ppm (K) are assigned to the equatorial and axial fluorine resonances of $F_5TeNH_3^+$, respectively [$^2J(^{19}F_{eq.}\text{-}^{19}F_{ax.})$ = 163

Figure 5.7 ^{19}F NMR spectrum (470.599 MHz) of the equilibrium mixture resulting from the reaction of $F_5TeNH_3^+As(OTeF_5)_6^-$ and $Xe(OTeF_5)_2$ recorded at -115.4 °C in SO_2ClF solvent; (A) equatorial fluorine atom peaks of $F_5TeNH_3^+$, (a) ^{125}Te satellites, (B) equatorial fluorine atom peaks of two unidentified F_5Te- groups, (b) ^{125}Te satellites, (C) unidentified species, (D) equatorial fluorine atom peaks of $F_5TeN(H)$-Xe^+, (E) equatorial fluorine atom peaks of $As(OTeF_5)_5$, (F) second order AB_4 spectrum of $As(OTeF_5)_6^-$, (f) ^{125}Te satellites, (G) equatorial fluorine atom peaks of $Xe(OTeF_5)_2$, (H) equatorial fluorine atom peaks of $HOTeF_5$, (h) ^{125}Te satellites, (I) axial fluorine atom peaks of $As(OTeF_5)_5$, (J) TeF_6, (j) ^{125}Te satellites, (K) axial fluorine atom peaks of $F_5TeNH_3^+$.

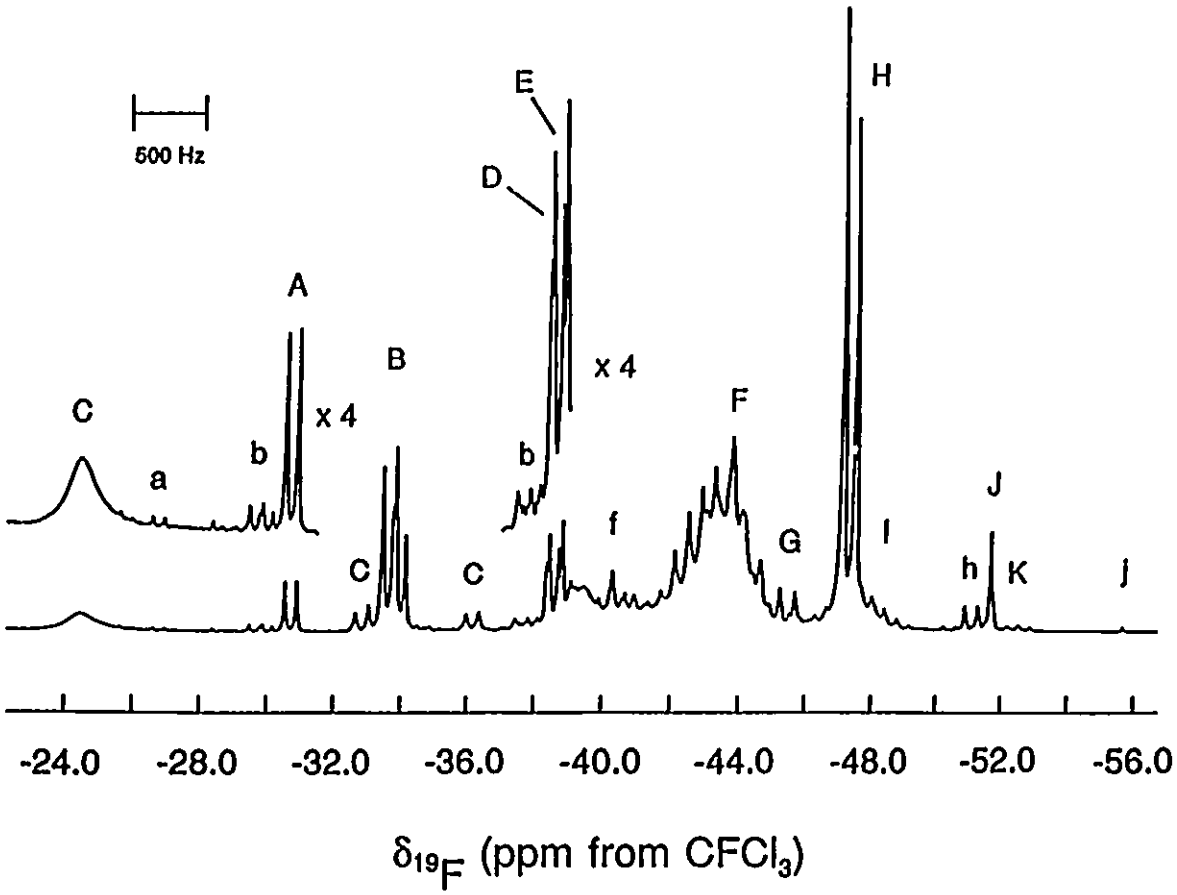
500 Hz
A
B
C
D
E
F
G
H
I
J
K
a
b
c
f
h
j
x 4
x 4
-24.0
-28.0
-32.0
-36.0
-40.0
-44.0
-48.0
-52.0
-56.0
δ19F (ppm from CFCl3)

Hz]. Doublets at -38.55 (D), -38.65 (E), -45.48 (G) and -47.28 (H) ppm are assignable to the equatorial fluorines of $F_5TeN(H)\text{-}Xe^+$, $As(OTeF_5)_5$,[255] $Xe(OTeF_5)_2$[255] and $HOTeF_5$,[255] respectively. The quintet at -48.02 ppm (I) is assigned to the axial fluorines of $As(OTeF_5)_5$.[255] The axial fluorine resonances of $HOTeF_5$ (*ca.* -44.5 ppm)[255] and $Xe(OTeF_5)_2$ (*ca.* -41.5 ppm)[255] are obscured by the AB_4 pattern of $As(OTeF_5)_6^-$ at *ca.* -44 ppm[110] (F) and several unidentified exchange-broadened species in the region from -39 to -44 ppm. The singlet at -51.6 ppm (J) exhibiting ^{125}Te satellites (j) is assigned to TeF_6 and is expected to overlap with the low intensity resonance of the axial fluorine atom of $F_5TeN(H)\text{-}Xe^+$ (*ca.* -52 ppm). The species present in solution are consistent with the $HOTeF_5$ elimination reaction represented by equation (5.5). The presence of $As(OTeF_5)_5$ is not attributed to dissociation of $As(OTeF_5)_6^-$ according to equation (5.8) since there is no evidence for $OTeF_5^-$ or the bridged species, $H(OTeF_5)_2^-$,[203] resulting from the reaction of $HOTeF_5$ and the $OTeF_5^-$ anion [equation (5.9)] in the ^{19}F NMR spectrum. Dissociation of $F_5TeNH_3^+As(OTeF_5)_6^-$ according to equation (5.10) also does not occur since the

$$As(OTeF_5)_6^- \rightleftharpoons OTeF_5^- + As(OTeF_5)_5 \tag{5.8}$$

$$HOTeF_5 + OTeF_5^- \rightleftharpoons [F_5TeO\cdots H\cdots OTeF_5]^- \tag{5.9}$$

$$F_5TeNH_3^+As(OTeF_5)_6^- \rightleftharpoons F_5TeNH_2 + HOTeF_5 + As(OTeF_5)_5 \tag{5.10}$$

free base, F_5TeNH_2, was not observed in the ^{19}F NMR spectrum (see Chapter 4 for ^{19}F NMR parameters). This is consistent with the stability of $N(CH_3)_4^+As(OTeF_5)_6^-$ with respect to

dissociation to give $N(CH_3)_4^+OTeF_5^-$ and $As(OTeF_5)_5$ in SO_2ClF solvent at 30 °C.[110] The presence of $As(OTeF_5)_5$ in the reaction mixture cannot be accounted for with the available data.

The two doublets at -33.67 [$^2J(^{19}F_{ax.}-^{19}F_{eq.})$ = 178 Hz] and -33.96 ppm [$^2J(^{19}F_{ax.}-^{19}F_{eq.})$ = 178 Hz] (B) exhibit ^{125}Te satellites (b) and result from unidentifiable F_5Te- groups. The broad resonance at -24.5 ppm and the doublets centered at -32.86 and -36.18 ppm (C) are not assigned. Broad resonances at -2.8, -11.1, -13.5 and -22.2 ppm are also unidentified.

(D) CHARACTERIZATION OF $F_5TeN(H)$-$Xe^+AsF_6^-$ BY LOW-TEMPERATURE RAMAN SPECTROSCOPY

The low-temperature Raman spectrum (-165 °C) of the pale orange microcrystalline solid isolated from the reaction of equimolar amounts of natural abundance $F_5TeNH_3^+AsF_6^-$ with XeF_2 in anhydrous HF solvent is shown in Figure 5.8. The observed frequencies along with their assignments are listed in Table 5.2. The 99.5 atom % ^{15}N-enriched salt was prepared in order to aid in the assignments of modes of vibration that involve the displacement of an X-N bond (X = Te, Xe). The Raman frequencies for 99.5% ^{15}N-enriched $F_5TeN(H)$-$Xe^+AsF_6^-$ are also listed in Table 5.2, and regions of the Raman spectra of natural abundance and 99.5% ^{15}N-enriched $F_5TeN(H)$-$Xe^+AsF_6^-$ that exhibit $^{14/15}N$ isotopic shifts are shown in Figure 5.9. The isotopic shifts, $\Delta\nu(^{14/15}N)$, are given as $[\nu(^{15}N) - \nu(^{14}N)]$ where ν is the observed Raman frequency.

The Raman spectra are consistent with the formation of $F_5TeN(H)$-$Xe^+AsF_6^-$ in the solid state. Impurities present in the solid have been identified from the known Raman spectra as $F_5TeNH_3^+AsF_6^-$ (see Chapter 4) and $Xe_2F_3^+AsF_6^-$,[176] which have been crystallized from the HF solution of $F_5TeN(H)$-$Xe^+AsF_6^-$. Attempts to remove the contaminants by washing with HF or recrystallization resulted in thermal decomposition of the $F_5TeN(H)$-Xe^+ cation. A peak of low

Figure 5.8 Raman Spectrum of natural abundance $F_5TeN(H)\text{-}Xe^+AsF_6^-$, recorded at -165 °C with use of 514.5-nm excitation. Asterisks (*) denote FEP sample tube lines, a dagger (†) denotes an artifact characteristic of the Raman instrument; (A), $Xe_2F_3^+AsF_6^-$, (B), $F_5TeNH_3^+AsF_6^-$, (C), unidentified impurities or decomposition products.

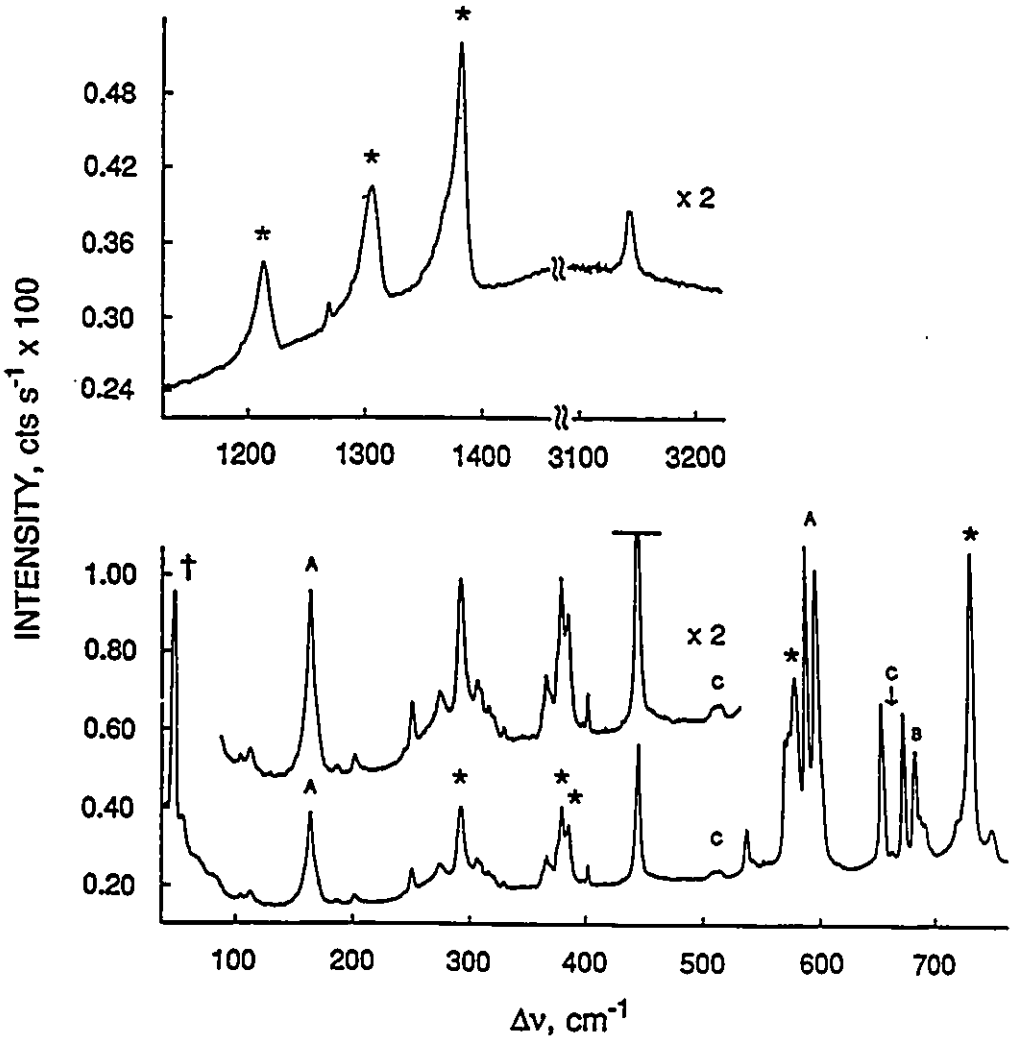
INTENSITY, cts s-1 x 100
0.48
0.42
0.36
0.30
0.24
1200
1300
1400
3100
3200
x 2
1.00
0.80
0.60
0.40
0.20
100
200
300
400
500
600
700
Δν, cm-1
A
B
C
x 2

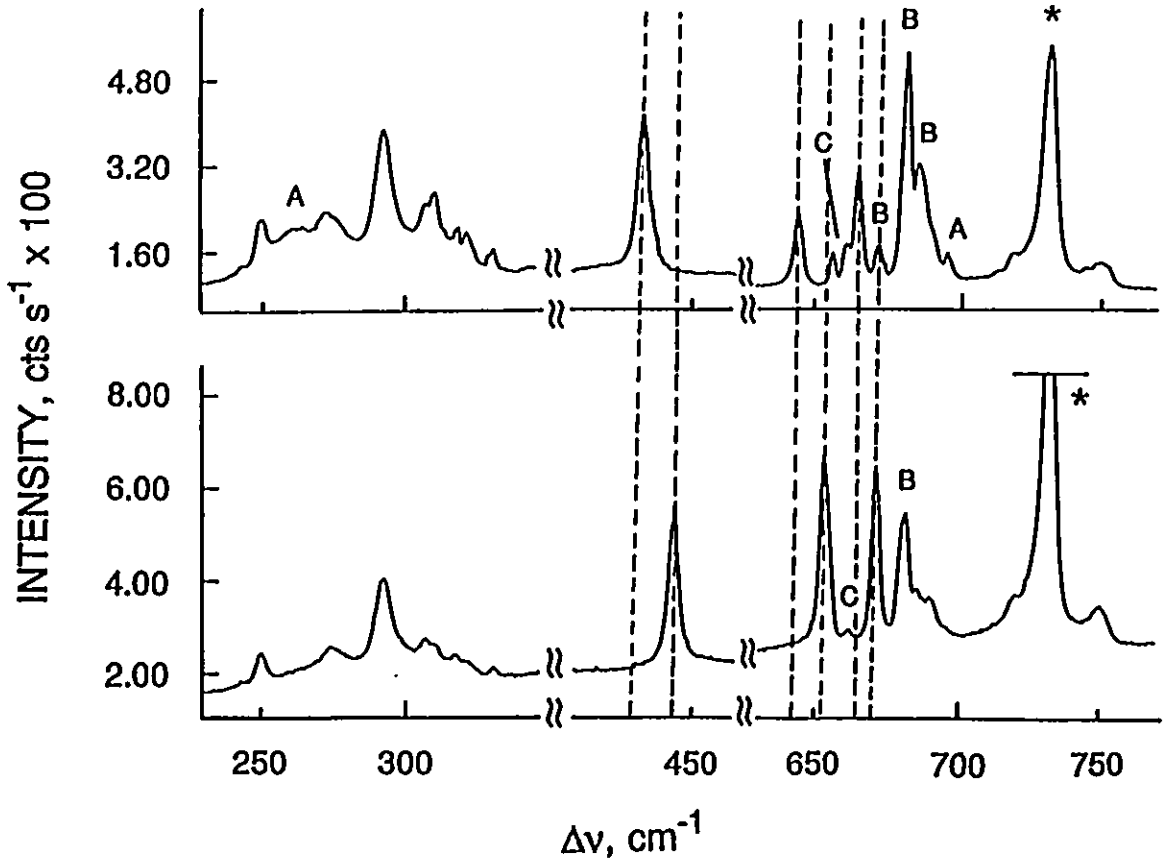

Figure 5.9a Raman spectra of natural abundance (lower trace) and 99.5% ^{15}N-enriched (upper trace) $F_5TeN(H)\text{-}Xe^+AsF_6^-$ recorded at -165 °C by use of 514.5-nm excitation (200 - 800 cm^{-1} region; asterisks (*) denote FEP sample tube lines; (A) $Xe_2F_3^+AsF_6^-$, (B) $F_5TeNH_3^+AsF_6^-$, (C) unidentified impurities or decomposition products.

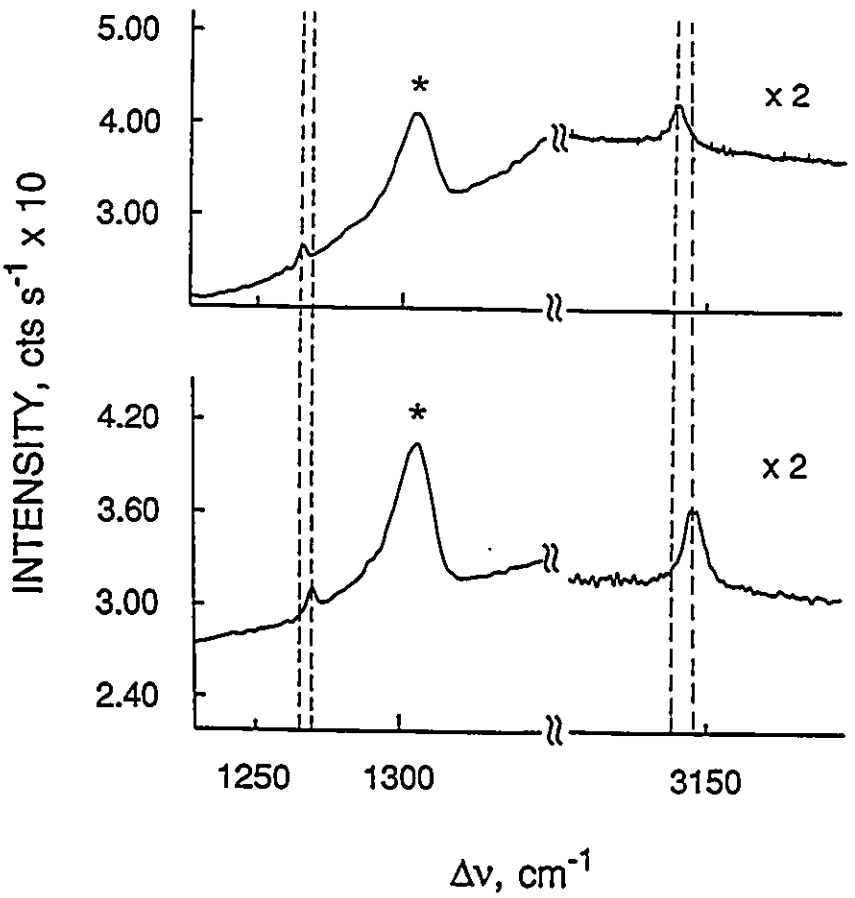

Figure 5.9b Raman spectra of natural abundance (lower trace) and 99.5% ^{15}N-enriched (upper trace) $F_5TeN(H)\text{-}Xe^+AsF_6^-$ recorded at -165 °C with use of 514.5-nm excitation (1200 - 1350 and 3100 - 3200 cm^{-1} regions); an asterisk (*) denotes an FEP sample tube lines.

intensity centered at 511 cm^{-1} and two peaks at 656.9 and 661.6 cm^{-1} (see Figures 5.8 and 5.9) have not been assigned and are attributed to minor impurities or decomposition products. The intensities of the peaks assigned to impurities, including $Xe_2F_3^+AsF_6^-$ and $F_5TeNH_3^+AsF_6^-$, varied from sample to sample relative to those of $F_5TeN(H)\text{-}Xe^+AsF_6^-$.

The Raman spectrum of the $F_5TeN(H)\text{-}Xe^+$ cation has been assigned by the assumption of sp^3 hybridization at the nitrogen atom, and a staggered conformation of the N-Xe group with respect to the equatorial fluorine atoms of the F_5Te- group, by analogy with the isoelectronic $F_5TeO\text{-}Xe^+$ cation.[54] The resulting C_1 point symmetry is expected to give rise to 3N - 6 = 21 normal modes belonging to irreducible representations of symmetry species A. All 21 modes are predicted to be infrared and Raman active, and since no modes are degenerate, 21 bands are expected in the Raman spectrum. However, 16 bands have been assigned to the $F_5TeN(H)\text{-}Xe^+$ cation. In Table 5.2 the modes of the $F_5TeN\text{-}Xe$ group of the $F_5TeN(H)\text{-}Xe^+$ cation have been assigned with the assumption of C_s point symmetry, so that a direct comparison could be made with the modes of the $F_5TeO\text{-}Xe^+$ cation,[54] which are also listed in Table 5.2. The vibrations of the NH group have been assigned by analogy with similar molecules, without consideration of point symmetry.

Assignments for the $F_5TeN(H)\text{-}Xe^+$ cation have been aided by comparison with the vibrational frequencies of F_5TeOCl,[233] F_5TeOF,[233] $F_5TeO\text{-}Xe^+AsF_6^-$,[54] $F_5TeNH_3^+AsF_6^-$ (see Chapter 4) F_2NH[256] and Cl_2NH.[257] Assignments for the AsF_6^- anion have been made by comparison with those of $XeF^+AsF_6^-$,[73] $HC{\equiv}NXeF^+AsF_6^-$,[73] and $O_2^+AsF_6^-$.[159]

The band assigned to ν(NH) is observed at 3145.9 cm^{-1} and exhibits an $^{14/15}N$ isotopic shift of -7.1 cm^{-1}. The presence of one band in the NH stretching region is consistent with the vibrational spectra of secondary amines, R_2NH.[250] The NH stretch is comparable to those

observed in the related compounds difluoramine, F_2NH (3193 cm^{-1})[256] and Cl_2NH (3279.0 cm^{-1})[257] although the anomolously high value for Cl_2NH likely arises from reduced intermolecular hydrogen bonding in the gas phase.[258]

Although two NH bending modes are expected, only one is observed at 1270.8 cm^{-1}, exhibiting an $^{14/15}N$ isotopic frequency dependence [$\Delta\nu(^{14/15}N) = -2.6$ cm^{-1}]. By comparison with F_2NH [$\delta(NH) = 1307$ (a'), 1424 cm^{-1} (a")][256] and Cl_2NH [$\delta(NH) = 1002$ (a'), 1295 cm^{-1} (a")],[257] it is possible that a band arising from the second NH bending vibration overlaps with one of the relatively intense FEP bands at 1217, 1310, or 1385 cm^{-1}. Because of the larger masses of the groups attached to the nitrogen atom in the $F_5TeN(H)\text{-}Xe^+$ cation, it is also possible that the second NH bend occurs at lower frequency than in F_2NH and Cl_2NH, but is too low in intensity to be observed.

The band observed at 444.1 cm^{-1} has been assigned to the asymmetric and symmetric (Te-N-Xe) stretching modes, because of the large isotopic shift [$\Delta\nu(^{14/15}N) = -10.9$ cm^{-1}] and similar frequency to that observed in the related $F_5TeO\text{-}Xe^+$ cation (see Table 5.2). Although a band assigned to ν(Te-N) is observed at 566.5 cm^{-1} in the Raman spectrum of $F_5TeNH_3^+AsF_6^-$ (see Chapter 4), a shift to lower frequency is expected in $F_5TeN(H)\text{-}Xe^+$ because of the mass effect of xenon. The only intense band at lower frequency than 566.5 cm^{-1} which has an $^{14/15}N$ isotopic dependence is at 444.1 cm^{-1}. The observation of only one band in this region indicates that ν(Te-N) and ν(Xe-N) are strongly coupled, as stated above. The bands in the Raman spectrum of $F_5TeO\text{-}Xe^+AsF_6^-$ assigned to ν_{sym}(Xe-O-Te) [492 (16), 483 (14) cm^{-1}] and ν_{asym}(Xe-O-Te) [476 sh, 470 (18) cm^{-1}] were close together in frequency, so it is possible by analogy that bands due to ν_{asym}(Te-N-Xe) and ν_{sym}(Xe-N-Te) are not resolved in the Raman spectrum of $F_5TeN(H)\text{-}Xe^+AsF_6^-$.

The known range of Xe-F stretching frequencies for compounds of xenon(II) containing the X-Xe-F linkage (X = F, N, O) is defined by XeF_2 [ν_{sym}(Xe-F) = 496 cm^{-1}],[175b] which exhibits the most ionic Xe(II)-F bond, and $XeF^+Sb_2F_{11}^-$ [ν(Xe-F) = 619 cm^{-1}],[68] where the terminal Xe-F bond is substantially more covalent, because of the weak basicity of $Sb_2F_{11}^-$. Since the Xe-F stretching vibration involves a large polarizability change, the bands are usually the most intense in the Raman spectra. The absence of an intense band between 494 and 619 cm^{-1} that could be assigned to ν(Xe-F) in the Raman spectrum of $F_5TeN(H)$-$Xe^+AsF_6^-$ is consistent with the absence of a covalent Xe-F bond.

By analogy with the AsF_6^- salts of F_5TeO-Xe^+,[54] XeF^+,[68] and KrF^+,[69] it is possible that a fluorine-bridge interaction between the cation and anion in $F_5TeN(H)$-$Xe^+AsF_6^-$ exists (e.g., $F_5TeN(H)$-Xe^+···F-AsF_5^-). However, the band attributable to ν(Xe···F) in the Raman spectra of F_5TeO-$Xe^+AsF_6^-$ (365 cm^{-1}),[54] $XeF^+AsF_6^-$ (339 cm^{-1}),[68] and α-$KrF^+AsF_6^-$ (328 cm^{-1}),[69] was usually more intense than the $\nu_4(AsF_6^-)$ and $\nu_5(AsF_6^-)$ modes which occurred in the same region. Such a band is not observed in the Raman spectrum of $F_5TeN(H)$-$Xe^+AsF_6^-$. Bands observed between 307 and 330 cm^{-1} in the Raman spectrum of $F_5TeN(H)Xe^+AsF_6^-$ have been tentatively assigned to bending modes of the F_5Te- group, although one of these bands might be assigned to ν(Xe···F). The band assigned to ν(Xe···F) in the Raman spectrum of F_5TeO-$Xe^+AsF_6^-$ [54] is twice as intense as the F_5Te- bending modes, allowing a distinction to be made between them. For $F_5TeN(H)$-$Xe^+AsF_6^-$, all modes in the F_5Te- bending region are similar in intensity, and given the established regularity of these bending mode frequencies,[233] none are assigned to ν(Xe···F). The absence of a band in the 300 - 370 cm^{-1} region which may be attributed to ν(Xe···F), or alternatively, the reduced intensity of this band relative to that observed in the Raman spectrum of F_5TeO-$Xe^+AsF_6^-$, may be explained by comparing the bonding in the F_5TeO-Xe^+ and

$F_5TeN(H)$-Xe^+ cations. The lower electronegativity of $F_5TeN(H)$- than the F_5TeO- group [see Section (E) of this Chapter] is expected to result in a lower Lewis acidity for $F_5TeN(H)$-Xe^+ than for F_5TeO-Xe^+. As a result, the Xe···F bridge bond in the former cation may be substantially more ionic than in the latter, if not completely ionic. The small polarizability change associated with the vibration of a predominantly ionic bond is expected to result in a low Raman intensity. Support for this statement was provided by George *et al.*,[259] who calculated the Raman intensity for the first vibrational transition for a purely electrostatic linkage in Tl^+OH^-. Comparison with the vibrations of covalent linkages indicated that the Raman intensities from vibrations of purely electrostatic linkages are 10^2 to 10^5 lower than those from covalent linkages.

Assignment of the band at 273.8 cm^{-1} to $\delta(NTeF_4)$ was made by comparison to $F_5TeNH_3^+$ (Chapter 4). This is confirmed by the $^{14/15}N$ isotopic shift (-0.8 cm^{-1}) of the band. The in-plane (δ) and out-of-plane (τ) Te-N-Xe bends have been assigned to the bands at 201.6 and 186.8 cm^{-1} by comparison with F_5TeO-$Xe^+AsF_6^-$ (see Table 5.2), but it was not possible to assign each of these bands to a particular mode.

The assignment of the modes of the F_5Te- group for $F_5TeN(H)$-Xe^+ have been made by comparison with the Raman spectrum of F_5TeO-$Xe^+AsF_6^-$,[54] with the assumption that the stretching and bending force constants of the F_5Te- moieties in F_5TeO-Xe^+ and $F_5TeN(H)$-Xe^+ are not significantly different. This assumption is true for compounds of the form F_5TeX, where X is an electronegative group such as Cl,[233] F,[233] OH,[220] OXe^+.[54] Comparison with F_5TeO^- [205] and F_5TeNH_2 (Chapter 4) is not possible since electron donation from the lone pairs on the oxygen and nitrogen atoms to the tellurium atom results in a significant decrease in the axial and equatorial Te-F bond force constants. All modes associated with the F_5Te- group have been assigned to bands in the Raman spectrum, except for the asymmetric out-of-plane bend,

$\delta_{asym}(TeF_4)$. This mode correlates with ν_6 (b_1) for compounds of the form F_5TeX (X = Cl,[234] OH,[220] OF,[233] OCl[233]) under C_{4v} point symmetry, and is not observed in the vibrational spectra of these compounds. A value of ν_6 for F_5TeCl (199.1 cm^{-1}) was calculated from the force constants obtained by use of the Wilson F and G matrix method.[234]

The bands assigned to the out-of-phase $\nu_{sym}(TeF_4)$ (672.3 cm^{-1}) and the $\nu_{sym}(TeF_4)$ breathing (653.8 cm^{-1}) modes exhibit large $^{14/15}N$ isotopic shifts. This provides evidence for vibrational coupling of these modes and ν(Te-N). This is likely since these vibrational modes all involve displacement of the tellurium atom, and under the true point symmetry of $F_5TeN(H)\text{-}Xe^+$ (C_1), all modes belong to the same irreducible representation, A, and all modes could in theory couple.

The octahedral AsF_6^- anion is expected to give rise to three Raman active bands under O_h symmetry, namely, $\nu_1(a_{1g})$, $\nu_2(e_g)$ and $\nu_5(t_{2g})$. The presence of $F_5TeNH_3^+AsF_6^-$ and $Xe_2F_3^+AsF_6^-$ in the solid prevents a rigorous assignment of the anion bands of $F_5TeN(H)\text{-}Xe^+AsF_6^-$. The amount of $F_5TeNH_3^+AsF_6^-$ in the natural abundance sample is small, and only the band at 682.1 cm^{-1} [$\nu_{sym}(TeF_4)$; labelled (B) in Figure 5.8], which is the most intense band in the Raman spectrum of $F_5TeNH_3^+AsF_6^-$ (see Chapter 4), is assigned to this impurity. This band is also coincident with ν_1 (a_{1g}) of the AsF_6^- anions of all three species. Overlap of the ν_2 (e_g) and ν_5 (t_{2g}) AsF_6^- bands for $F_5TeN(H)\text{-}Xe^+AsF_6^-$ and $Xe_2F_3^+AsF_6^-$ is also expected. Bands at 686.6 and 690.8 cm^{-1} and at 397.3 and 401.5 cm^{-1} are assigned to the split $\nu_3(t_{1u})$ and $\nu_4(t_{1u})$ AsF_6^- modes. Since these bands are not observed in the Raman spectrum of $Xe_2F_3^+AsF_6^-$,[176] they must arise from $F_5TeN(H)\text{-}Xe^+AsF_6^-$. The observation of ν_3 and ν_4 in the Raman spectrum indicates an AsF_6^- point symmetry which is lower than O_h. A point symmetry of C_{4v} or lower would account for the Raman activity of the ν_3 and ν_4 modes, and lowering of the AsF_6^- point symmetry may

Table 5.2. Raman Frequencies and Assignments for $[^{14}N]F_5TeN(H)\text{-}Xe^+AsF_6^-$ and $[^{15}N]F_5TeN(H)\text{-}Xe^+AsF_6^-$, Compared to Those of $F_5TeO\text{-}Xe^+AsF_6^-$.

frequency, cm^{-1} [a]			frequency, cm^{-1} [b]	
$F_5TeN(H)\text{-}Xe^+AsF_6^-$	$[^{15}N]F_5TeN(H)\text{-}Xe^+AsF_6^-$	$\Delta\nu(^{14/15}N)$ [c]	$F_5TeO\text{-}Xe^+AsF_6^-$	assignt and approx mode description
3145.9 (6.2)	3138.8 (8.5)	-7.1		ν(NH)
1270.8 (4.3)	1268.2 (5.1)	-2.6		δ(NH)
750.1 (18.6)	751.0 (22.0)		739 (6)	a", $\nu_{asym}(TeF_4)$, asym to Te-X-Xe plane
			775 (20)	a', $\nu_{asym}(TeF_4)$, sym to Te-X-Xe plane
719.6 (24.8)	719.3 (25.8)		713 (34)	a', $\nu(Te\text{-}F_{ax.})$
672.3 (90.1)	666.1 (100.0)	-6.2	663 (58)	a', $\nu_{sym}(TeF_4)$ out of phase
653.8 (100.0)	644.6 (67.2)	-9.2	668 (100)	a", $\nu_{sym}(TeF_4)$ breathing
			492 (16)	a', $\nu_{sym}(Xe\text{-}O\text{-}Te)$
			483 (14)	
444.1 (85.7)	433.2 (76.1)	-10.9		a', $\nu_{sym}(Xe\text{-}N\text{-}Te)$ + $\nu_{asym}(Xe\text{-}N\text{-}Te)$
			476 sh	a', $\nu_{asym}(Xe\text{-}O\text{-}Te)$
			470 (18)	
			365 (15)	ν(Xe···F)
320.6 (9.6)	321.2 (20.1)		333 (2)	a", $\delta(FTeF_4)$, out of Te-X-Xe plane
316.7 (13.0)	318.1 (22.2)		320 (7)	a', $\delta(FTeF_4)$,

				in Te-X-Xe plane
329.8 (4.6)	330.4 (8.6)		312 (8)	a', $\delta_{sym}(TeF_4)$, out of TeF_4 plane
310.1 (19.2)	310.2 (39.2)		295 (3)	a', $\delta_{sciss}(TeF_4)$, in Te-X-Xe plane
306.9 (22.1)	307.4 (34.4)			
250.3 (19.2)	250.9 (22.4)		252 (25)	a', $\delta_{asym}(TeF_4)$, sym to Te-X-Xe plane
				a", $\delta_{asym}(TeF_4)$, asym to Te-X-Xe plane
274.4 (20.9)	273.0 (32.0)	-1.4	205 (1)	a", $\delta(XTeF_4)$, out of Te-X-Xe plane
			191 (5)	a', $\delta(XTeF_4)$, in Te-X-Xe plane
201.6 (5.7)	202.4 (4.8)		174 (32)	a", τ(Te-X-Xe) or a', δ(Te-X-Xe)
186.8 (2.6)	186.5 (2.7)			

Table 5.2 (continued)

[a]The Raman data for $F_5TeN(H)\text{-}Xe^+AsF_6^-$ were obtained at -165 °C in an FEP sample tube by use of 514.5-nm excitation. The estimated precision of each value is ± 0.6 cm^{-1}. Although the point symmetry of the $F_5TeN(H)\text{-}Xe^+$ cation is C_1, assignments of modes have been made for the $F_5Te\text{-}N\text{-}Xe$ group under C_s symmetry to allow direct comparison with the modes of the $F_5TeO\text{-}Xe^+$ cation [see reference (54)]. The modes of the NH group are assigned by analogy with similar molecules, without consideration of molecular point symmetry. [b]Raman data for $F_5TeO\text{-}Xe^+AsF_6^-$ were recorded at -196 °C in a glass sample tube at -196 °C by use of 514.5-nm excitation [reference (54)]. Low frequency lattice or bending modes reported in reference (54) have been omitted from the present table. [c]Isotopic shifts $\Delta\nu(^{14/15}N) = \nu(^{15}N) - \nu(^{14}N)$, where the frequencies of the bands ν are given in cm^{-1}. Isotopic shifts less than the estimated error are not considered to be significant.

Table 5.3 Raman Frequencies and Assignments for AsF_6^-, Compared to Those of $XeF^+AsF_6^-$ and $HC{\equiv}NXeF^+AsF_6^-$

frequency, cm^{-1}			assignt and approx mode description	
$F_5TeN(H)\text{-}Xe^+AsF_6^-$ [a]	$XeF^+AsF_6^-$ [b]	$HC{\equiv}NXeF^+AsF_6^-$ [b]	O_h (AsF_6^-)	C_s
690.8 (20.3)	735 (20)		t_{1u}, ν_3	a"
686.6 (25.0)	730 (5)			
	723 (13)	707 (2)		a'
		693 (11)		a'
682.1 (68.0)	681 (56)	680 (49)	a_{1g}, ν_1	a'
573.7 sh	582 (12)		e_g, ν_2	a'
570.6 sh	577 (5)			a'
543.2 (6.6)				
	465 (3)		ν(As···F)	
401.5 (10.5)	421 (11)	419 (<1)	t_{1u}, ν_4	a'
		415 (1)		
397.3 (4.1)	406 (1)			a'
	401 (2)			a"
	386 (14)	397 (1)	t_{2g}, ν_5	a'
		392 (<1)		
363.2 sh	378 (5)	372 (15)		a"
		370 (10)		
366.5 (20.3)				

369.6 sh			
			a"
	244 (1)	t_{1u}, ν_6	a'
			a"
			a"
113.9 (6.7)		lattice modes and/or hydrogen bonding modes	
104.7 (2.8)			
83.4 (3.6)			
68.9 (3.6)			
56.0 (10.3)			
41.4 (5.1)			

[a]This work; Raman spectrum obtained at -165 °C in an FEP sample tube by use of 514.5-nm excitation. The estimated precision of each value is ± 0.6 cm^{-1}. The Raman intensities and multiplicities of ν_1, ν_2 and ν_5 are affected by the presence of $Xe_2F_3^+AsF_6^-$ [reference (176)] and $F_5TeNH_3^+AsF_6^-$ (Chapter 4) and do not reflect those of pure $F_5TeN(H)\text{-}Xe^+AsF_6^-$. [b]Raman spectra recorded at -196 °C by use of 514.5-nm excitation [see reference (73)].

arise from a low crystallographic site symmetry. Confirmation of this statement would require a crystal structure of the pure compound.

Although it is not possible to assess the site symmetry from the Raman data, the bands of the AsF_6^- anion have been assigned to modes under C_s point symmetry by correlating the representations of O_h with C_s (Table 5.10). The assignments for AsF_6^- must remain tentative since the bands assigned to ν_1 (a_{1g}), ν_2 (e_g) and ν_5 (t_{2g}) overlap with those of $Xe_2F_3^+AsF_6^-$. A similarity of modes is observed upon comparison of $F_5TeN(H)$-$Xe^+AsF_6^-$ with $XeF^+AsF_6^-$ [73] and $HC{\equiv}NXeF^+AsF_6^-$.[73] Although two bands are reported for $\nu_2(e_g)$ under O_h symmetry in the Raman spectrum of $F_5TeN(H)$-$Xe^+AsF_6^-$, further bands may be obscured by the FEP sample tube band at 579 cm^{-1}. A band assignable to a derivative of $\nu_6(t_{1u})$ under O_h symmetry is not observed.

(E) NATURE OF THE BONDING IN THE $F_5TeN(H)$-Xe^+ CATION

Previous NMR studies of xenon(II) derivatives containing Xe-F groups bonded to oxygen or fluorine atoms have shown that the NMR parameters measured in ^{19}F and ^{129}Xe spectra could be used to assess the relative covalent characters of the Xe-O, Xe···F bridge, and Xe-F terminal bonds.[103,104,108] Schrobilgen[26] recently extended this work to include derivatives with xenon(II)-nitrogen bonds. In general, as the covalent character of the Xe-L (L = ligand atom) bond increases, the terminal Xe-F bond becomes more ionic, decreasing the formal charge on xenon. These trends are paralleled by increased shielding of the ^{129}Xe resonance, a decrease in the magnitude of $^1J(^{129}Xe\text{-}^{19}F)$, and increased ^{19}F chemical shifts for the terminal Xe-F group. The ^{129}Xe chemical shift is therefore a powerful tool for estimating the relative covalent characters of the Xe-L bond for a series of xenon(II) compounds, and is used to assess qualitatively the bonding in $F_5TeN(H)$-Xe^+ in the following discussion. Table 5.3 lists the ^{129}Xe chemical shifts and

reduced scalar couplings ^1K(Xe-N) for a number of compounds containing xenon(II)-nitrogen bonds. NMR data for the XeF^+ cation in SbF_5 solvent are included for comparison since the ^{129}Xe chemical shift and $^1J(^{129}Xe\text{-}^{19}F)$ are representive of uncoordinated XeF^+, because of the very weak basicity of SbF_5 solvent and the polymeric $Sb_nF_{5n+1}^-$ anion in solution. The compounds are listed approximately in order of increasing Xe-N bond covalent character. The $HC{\equiv}N\text{-}XeF^+$ and $F_3S{\equiv}N\text{-}XeF^+$ cations have the most ionic Xe-N bonds in Table 5.3. This is apparent from the ^{129}Xe NMR resonances, which are deshielded relative to the other compounds containing Xe(II)-N bonds. As also shown in Table 5.3, the ^{129}Xe resonances become increasingly shielded as the *s*-character of the nitrogen valence hybrid orbitals decreases. This is consistent with decreasing electronegativity of the ligand group,[105] resulting in a more covalent Xe-N bond. Thus the highly shielded ^{129}Xe NMR resonance indicates that the $F_5TeN(H)\text{-}Xe^+$ cation, with formal sp^3 hybridization at the nitrogen atom, has one of the most covalent Xe-N bonds known and that the Xe-N bond covalent characters of the $F_5TeN(H)\text{-}Xe^+$ and $F_5SN(H)\text{-}Xe^+$ cations are similar. Examination of Table 5.3 reveals that the magnitude of ^1K(Xe-N) decreases as the % *s*-character of the nitrogen valence orbitals decreases. This is predicted by the Fermi contact mechanism which is usually the dominant mechanism for scalar couplings that involve heavy nuclei.[260] In a formalism developed by Pople and Santry,[242] the Fermi contact mechanism is proportional to the product of the valence *s*-electron densities at the coupled nuclei, so that decreased *s*-character in the nitrogen valence hybrid orbitals on moving down Table 5.3 predicts a decrease in the magnitude of ^1K(Xe-N). A scalar coupling model which assumes dominance of the Fermi contact term for Xe(II)-N bonds has been used to assess the hybridization at nitrogen in the $HC{\equiv}N\text{-}XeF^+$ cation. This was achieved by comparing the magnitude of the Xe-N scalar coupling with that in $(FO_2S)_2N\text{-}XeF$, which was shown to contain a formally sp^2-hybridized nitrogen center from the

short S-N bond lengths [1.628(3) and 1.623(3) Å] and trigonal planar geometry at nitrogen by X-ray crystallography.[57] The use of the xenon-nitrogen scalar coupling to determine the hybridization at the nitrogen atom assumes that the *s*-electron density at the xenon atom is approximately the same in $HC{\equiv}N\text{-}XeF^+$ and $(FO_2S)_2N\text{-}XeF$. The successful prediction of *sp* hybridization at the nitrogen atom in $HC{\equiv}N\text{-}XeF^+$ indicated that this assumption was valid. In attempting to evaluate the hybridization at the nitrogen atom in the $F_5TeN(H)\text{-}Xe^+$ cation, a species which could be assumed to have a similar *s*-electron density at xenon is the $(FO_2S)_2N\text{-}Xe^+$ cation. The crystallographically determined trigonal planar geometry and short S-N bond lengths [1.68(1) and 1.70(1) Å] for the $(FO_2S)_2N\text{-}Xe^+$ cation indicated formal sp^2 hybridization at the nitrogen atom.[60] Thus, with the assumption that the Xe-N scalar coupling is dominated by the Fermi contact term, it should be possible to estimate the hybridization at the nitrogen atom in $F_5TeN(H)\text{-}Xe^+$ with use of the values of ^1K(Xe-N), but problems arise in this treatment. If the hybridization of the nitrogen atom is sp^3 in $F_5TeN(H)\text{-}Xe^+$, one would expect a lower value of ^1K(Xe-N) than in $(FO_2S)_2N\text{-}Xe^+$, which is opposite to the observed values. Resonance Structures 5.4 and 5.5 indicate the potential for N $\rightarrow$ Te π-donation in $F_5TeN(H)\text{-}Xe^+$, which was established for F_5TeNH_2 in Chapter 4, and may increase the nitrogen valence *s*-character in the Xe-N bond. However, it is unlikely that the nitrogen atom is formally sp^2-hybridized, since a normal coordinate analysis of the related $OTeF_5^-$ anion[206] indicated that the Te-O bond is intermediate between a single and a double bond. Therefore a formal nitrogen atom hybridization which is intermediate between sp^2 and sp^3 may be closer to reality. It is likely that S-N π-bonding in $(FO_2S)_2N\text{-}Xe^+$ surpasses the degree of Te-N π-bonding in $F_5TeN(H)\text{-}Xe^+$, given the planarity of the nitrogen center in the former cation, and the short S-N bond lengths (see above). Thus it is not possible to use X-N π-bonding (X = S, Te) to rationalize the magnitudes of ^1K(Xe-N). An alternative approach, which

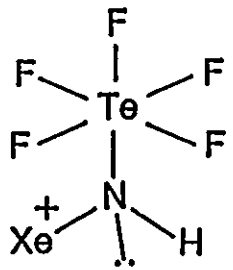

5.2

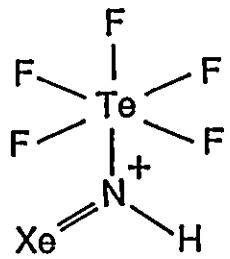

5.3

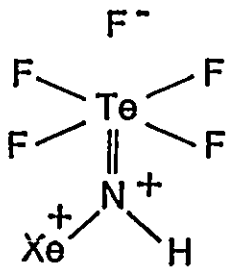

5.4

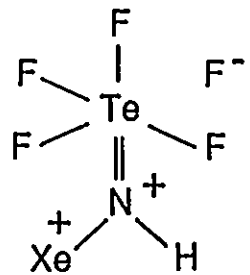

5.5

etc.

also assumes dominance of the Fermi contact term, is derived from a study of $^1J(^{15}N\text{-}^1H)$ in nitrogen-15 enriched main group compounds of the form XNH_2 and X_2NH, by Cowley and Schweiger,[124] which relied on the so-called isovalent hybridization hypothesis.[261] This hypothesis, applied to nitrogen, states that the nitrogen atom valence *s*-character concentrates in the bonds directed toward electropositive substituents. It was observed that in most cases $^1J(^{15}N\text{-}^1H)$ increases as the electronegativity of X increases for XNH_2 and X_2NH compounds.[124] Since it is clear from the ^{129}Xe chemical shifts of $(FO_2S)_2N\text{-}Xe^+$ and $F_5TeN(H)\text{-}Xe^+$ that the $(FO_2S)_2N$- group is more electronegative than the $F_5TeN(H)$- group, the isovalent hypothesis predicts greater valence *s*-character in the Xe-N bond of $(FO_2S)_2N\text{-}Xe^+$. It follows that this model also incorrectly predicts a greater value of $^1K(Xe\text{-}N)$ in $(FO_2S)_2N\text{-}Xe^+$. The failure to predict the relative magnitudes of $^1K(Xe\text{-}N)$, by solely considering the contribution of the Fermi contact term to the scalar coupling, indicates that the dipolar or orbital contributions to the xenon-nitrogen scalar coupling may be important. Although the Fermi contact term is expected to be the largest contributor to the Xe-N scalar coupling,[260] it may be similar for the $F_5TeN(H)\text{-}Xe^+$ and $(FO_2S)_2N\text{-}Xe^+$ cations. The presence of Xe-N π bonding in the $F_5TeN(H)\text{-}Xe^+$ and $(FO_2S)_2N\text{-}Xe^+$ cations, which is represented by resonance Structures (5.3) and (8.11), respectively, may give rise to a significant orbital contribution, K^2_{AB}. Factors contributing to the magnitude of K^2_{AB} are described in equation (5.11), which uses an average energy approximation in an LCAO

$$K^2_{AB} = \mu_o(\mu_B)^2\langle r_A^{-3}\rangle_p\langle r_B^{-3}\rangle_p(^3\Delta E)^{-1}$$

$$\times\ [2(P_\sigma^2 + P_\pi^2 + P_{\pi'}^2) + 3(P_\sigma P_\pi + P_\sigma P_{\pi'} + P_\pi P_{\pi'})] \qquad (5.11)$$

framework.[251] The terms μ_o and μ_B are the permittivity of a vacuum and the Bohr magneton, respectively, $<r_A^{-3}>_p$ and $<r_B^{-3}>_p$ are the inverse cube radial distributions of the valence *p* orbitals for the coupled nuclei, $^3\Delta E$ is the average excitation energy, and P_σ, P_π and $P_{\pi'}$ are the σ and π bond orders for the bonding between nuclei A and B. In comparing $F_5TeN(H)$-Xe^+ and $(FO_2S)_2N$-Xe^+, an argument for a greater Xe-N π-bonding contribution in the former could be made, which in turn rationalizes the relative magnitudes of ^1K(Xe-N). The greater electronegativity of $(FO_2S)_2N$- than $F_5TeN(H)$- is expected to result in a greater Xe-N π-bonding contribution in the $F_5TeN(H)$-Xe^+ cation. A larger Xe-N π-bonding contribution in $F_5TeN(H)$-Xe^+ is expected to result in larger values of P_π and $P_{\pi'}$ in equation (5.11), thus increasing ^1K(Xe-N) relative to $(FO_2S)_2N$-Xe^+. The possibility of Xe(II)-N π-bonding is proposed by analogy with the xenon(II)-carbon bonded cations R-Xe^+ (R = fluorophenyl).[253]

The absence of detectable amounts of the neutral compound $F_5TeN(H)$-XeF in BrF_5, SO_2ClF and HF solvents is consistent with the NMR parameters for the series of compounds, shown in Table 5.3. As mentioned at the beginning of this Section, increasing covalent character of the Xe-L bond (L = N, F, O ligand atom) results in increasing Xe-F bond ionic character. This is seen in the magnitude of $^1J(^{129}Xe\text{-}^{19}F)$, which decreases as the Xe-F bond ionic character increases on moving down Table 5.3, towards increasing Xe-L bond covalent character. The cations $F_5TeN(H)$-Xe^+, $F_5SN(H)$-Xe^+, $FO_2SN(H)$-Xe^+ and $F_4S{=}N$-Xe^+ form a series whose ^{129}Xe resonances are significantly shielded relative to all other known compounds containing Xe(II)-N bonds. This shielding indicates that these Xe(II)-N bonds are highly covalent. In agreement with the ^{129}Xe and ^{19}F NMR trends discussed at the beginning of this section, the Xe-F bonds are completely ionized in solution as a result of the covalent character of the Xe-N bonds.

The relationship of Xe-F bond ionization in compounds of the form L-Xe-F and

electronegativity of the ligand L is made explicit by a comparison of F_5TeO-Xe-F and the $F_5TeN(H)$-Xe^+ cation, since F_5TeO- and $F_5TeN(H)$- are isoelectronic. Structures 5.6 and 5.7 are the canonical forms that describe the relative ionic characters of the Xe-O and Xe-F bonds in the known compound, F_5TeO-XeF, and the analogous canonical forms of the hypothetical neutral compound, $F_5TeN(H)$-Xe-F, are shown in Structures 5.8 and 5.9. The significant Xe-F bond

$$F_5TeO\text{-}Xe^+\ \ F^- \longleftrightarrow F_5TeO^-\ \ Xe\text{-}F^+$$

5.6 5.7

$$F_5TeN(H)\text{-}Xe^+\ \ F^- \longleftrightarrow F_5TeN(H)^-\ \ Xe\text{-}F^+$$

5.8 5.9

covalent character in F_5TeO-Xe-F is reflected in the ^{129}Xe NMR chemical shift, -2051 ppm, which is similar to that for XeF_2, -1913 ppm in the same solvent and at the same temperature (SO_2ClF, 26 °C).[181] The scalar coupling $^1J(^{129}Xe\text{-}^{19}F)$ for F_5TeO-XeF is 5743 Hz, which is 122 Hz larger than the corresponding value for XeF_2 (5621 Hz).[181] The NMR data are consistent with a greater weighting of Structure of 5.7 over 5.6, and reflects the greater electronegativity of F than F_5TeO-.[181] However, the F_5TeO- group is sufficiently electronegative that the F_5TeO-Xe^+ cation has significant Lewis acid character. This is reflected in the fact that ionization of the Xe-F bond of F_5TeO-XeF required the use of the strong Lewis acids AsF_5 or SbF_5 to form F_5TeO-$Xe^+AsF_6^-$ [54] and F_5TeO-$Xe^+Sb_2F_{11}^-$.[54] The significant Lewis acid strength of the F_5TeO-Xe^+ cation was also evident from the presence of a band that was attributed to a covalent fluorine bridge interaction

between the cation and anion in the Raman spectrum of solid $F_5TeO\text{-}Xe^+AsF_6^-$.[54] The Lewis acid strength of the $F_5TeO\text{-}Xe^+$ cation is also reflected in the formation of the Lewis acid-base adducts $B\text{-}Xe\text{-}OTeF_5^+$ ($B = C_5F_5N$, $s\text{-}C_3F_3N_2N$, $CH_3C{\equiv}N$) upon reaction of $F_5TeO\text{-}Xe^+As(OTeF_5)_6^-$ with the appropriate nitrogen base in SO_2ClF solvent.[26]

The ionization of the Xe-F bond of the hypothetical neutral compound $F_5TeN(H)\text{-}XeF$ in HF, BrF_5 and SO_2ClF solution indicates that resonance Structure 5.8 contributes essentially 100% to the bonding. The Lewis acidity of $F_5TeN(H)\text{-}Xe^+$ is expected to be low relative to $F_5TeO\text{-}Xe^+$, resulting from the lower electronegativity of $F_5TeN(H)$- than F_5TeO-. The relative electronegativities of these ligands is reflected in the acid characters of F_5TeNH_2 and F_5TeOH. The former is basic, being quantitatively protonated in HF (see Chapter 4). The latter, F_5TeOH, is a strong acid, having an acidity lying between those of HNO_3 and HCl,[200] and there is no evidence of protonation of F_5TeOH in HF acidified with AsF_5.[180] Further evidence for the low Lewis acid strength of $F_5TeN(H)\text{-}Xe^+$ is indicated by the absence of a band that could be attributed to the Xe···F bridge stretch in the Raman spectrum of solid $F_5TeN(H)\text{-}Xe^+\ AsF_6^-$.

The instability of $F_5TeN(H)\text{-}XeF$ relative to $F_5TeN(H)\text{-}Xe^+$ is evident from unsuccessful attempts to isolate the neutral compound $F_5TeN(H)\text{-}XeF$ from the reaction of F_5TeNH_2 or $F_5TeN(H)\text{-}Si(CH_3)_3$ with XeF_2 in SO_2ClF solvent according to equation (5.12). No reaction was

$$F_5TeN(H)\text{-}R + XeF_2 \longrightarrow F_5TeN(H)\text{-}XeF + RF \qquad (5.12)$$

$$[R = H, (CH_3)_3Si]$$

observed on warming the samples to 0 °C (R = H) and -12 °C ($R = Si(CH_3)_3$), well above the temperature at which $F_5TeNH_3^+AsF_6^-$ and XeF_2 reacted to give the $F_5TeN(H)\text{-}Xe^+$ cation.

Table 5.4 Comparison of ^{129}Xe NMR Chemical Shifts, $^{1}K(Xe\text{-}N)$ and $^{1}J(^{129}Xe\text{-}^{19}F)$ for Some Xenon(II) Compounds.[a]

Species	$\delta(^{129}Xe)$, (ppm)	Hybridization at Nitrogen	$^{1}J(^{129}Xe\text{-}^{19}F)$, Hz	$^{1}K(Xe\text{-}N)$ (10^{22} $NA^{-2}m^{-3}$)	T (°C)	Ref.
$XeF^{+}\cdots FSb_2F_{10}^{-}$	-574		7594		25	108
$HC{\equiv}N\text{-}XeF^{+}AsF_6^{-}$	-1555 (-1570)	*sp*	6181	1.381[b]	-10 (-58)	73
$F_3S{\equiv}N\text{-}XeF^{+}AsF_6^{-}$	-1661	*sp*	6248	1.435	-60	26
$s\text{-}C_3F_3N_2N\text{-}XeF^{+}AsF_6^{-}$	-1808 (-1863)	sp^2	5932	1.013	-5 (-50)	71
$C_5F_5N\text{-}XeF^{+}AsF_6^{-}$	-1872 (-1922)	sp^2	5926	0.983	-30 (-30)	75
$(FO_2S)_2N\text{-}XeF$[c]	-2009	sp^2	5586	0.913[b]	-40	59
XeF_2	-1685		5621		-52	71
$(FO_2S)_2N\text{-}Xe^{+}Sb_nF_{5n+1}^{-}$	-1943	sp^2		0.272[b]	25	60
$FO_2SN(H)\text{-}Xe^{+}AsF_6^{-}$	-2616 (-2660)	sp^2 or sp^3		0.322[b]	-61	c
$F_4S{=}N\text{-}Xe^{+}AsF_6^{-}$	-2672	sp^2			-20	26
$F_5TeN(H)\text{-}Xe^{+}AsF_6^{-}$	-2840 (-2902)	sp^3		0.401[b]	-45	This work
$F_5SN(H)\text{-}Xe^{+}AsF_6^{-}$	-2886	sp^3			-20	26

[a] ^{129}Xe NMR parameters, unless otherwise indicated, were determined in HF and in BrF_5 (in parentheses) solvent. [b] Recorded for the ^{15}N enriched cation. [c] Measured in SO_2ClF solvent. [d] Measured in SbF_5 solvent. [e] Chapter 8 of this work.

CHAPTER 6

STUDY OF THE DECOMPOSITION OF $F_5TeN(H)\text{-}Xe^+AsF_6^-$

AND

CHARACTERIZATION AND DECOMPOSITION OF F_5TeNF_2 IN SOLUTION

INTRODUCTION

As discussed in Chapter 5, the $F_5TeN(H)\text{-}Xe^+$ cation was generated as the AsF_6^- salt from the reaction of $XeF^+AsF_6^-$ and F_5TeNH_2 in HF solvent or from the reaction of XeF_2 and $F_5TeNH_3^+AsF_6^-$ in HF or BrF_5 solvents. The salt, $F_5TeN(H)\text{-}Xe^+AsF_6^-$, was isolated from HF solvent at -40 °C, and the Raman spectrum at -165 °C indicated the presence of $F_5TeNH_3^+AsF_6^-$ and $Xe_2F_3^+AsF_6^-$. It was not possible to isolate $F_5TeN(H)\text{-}Xe^+AsF_6^-$ as a pure material for two reasons: (1) $F_5TeN(H)\text{-}Xe^+$ is in equilibrium with XeF_2 and $F_5TeNH_3^+$ in HF solvent [see equation (5.4)], and small amounts of $F_5TeNH_3^+AsF_6^-$ crystallized with $F_5TeN(H)\text{-}Xe^+AsF_6^-$; (2) $F_5TeN(H)\text{-}Xe^+$ decomposes slowly at the temperatures which also maximized the yield of $F_5TeN(H)\text{-}Xe^+$ in solution. The presence of $Xe_2F_3^+AsF_6^-$ can be traced to the decomposition of $F_5TeN(H)\text{-}Xe^+AsF_6^-$ in HF solvent. In the present Chapter, the composition of the HF solution from which $F_5TeN(H)\text{-}Xe^+AsF_6^-$ was isolated and the decomposition of $F_5TeN(H)\text{-}Xe^+$ in HF solvent were primarily investigated by ^{19}F NMR spectroscopy.

RESULTS AND DISCUSSION

(A) ^{19}F NMR SPECTROSCOPIC STUDY OF THE DECOMPOSITION OF $F_5TeN(H)$-$Xe^+AsF_6^-$ IN HF SOLVENT

The formation and decomposition of $F_5TeN(H)$-$Xe^+AsF_6^-$ in HF solvent which resulted from the reaction of equimolar amounts of $XeF^+AsF_6^-$ and F_5TeNH_2 was followed by ^{19}F NMR spectroscopy in the range of -40.9 to -1.2 °C.

Figure 6.1 shows the ^{19}F NMR spectrum at -40.9 °C of an equimolar mixture of $XeF^+AsF_6^-$ and F_5TeNH_2 in HF solvent, which was previously warmed to -35 °C for five minutes, which resulted a pale yellow solution, before it was placed in the NMR probe. Integration of the NMR resonances indicated that the ratio $F_5TeNH_3^+$: $F_5TeN(H)$-Xe^+ : TeF_6 was 1.00 : 0.03 : 0.06. A trace of the primary decomposition product, F_5TeNF_2, prepared for the first time, was also observed. A singlet assigned to HF solvent was observed at $\delta(^{19}F)$ = -195.0 ppm ($\Delta\nu_{1/2}$ = 47 Hz). A singlet at $\delta(^{19}F)$ = -199.8 ppm assigned to XeF_2 was also observed ($\Delta\nu_{1/2}$ = 386 Hz) on the low frequency shoulder of the solvent resonance; the high-frequency ^{129}Xe satellite was not observed because of overlap with the HF resonance. Although the initial reactants were $XeF^+AsF_6^-$ and F_5TeNH_2, the absence of a pale yellow precipitate indicative of $XeF^+AsF_6^-$ or $Xe_2F_3^+AsF_6^-$, which are both sparingly soluble in HF at low temperature,[111] and the presence of a resonance assigned to XeF_2 indicated that solvolysis of $XeF^+AsF_6^-$ occurred according to equation (5.2). This was also confirmed by the absence of a ^{19}F NMR resonance attributable to F_5TeNH_2 (see Figure 4.11).

The sample was then warmed to -33.3 °C, and after ca. one hour, an intense yellow solution and a pale yellow precipitate resulted. As shown in Figure 6.2, the amount of $F_5TeN(H)$-Xe^+ increased relative to $F_5TeNH_3^+$. The formation of $F_5TeN(H)$-Xe^+ was accompanied by

Figure 6.1 ^{19}F NMR spectrum (499.599 MHz) of the fluorine-on-tellurium(VI) region of an equimolar mixture of natural abundance F_5TeNH_2 and $XeF^+AsF_6^-$ in HF solvent, warmed to -35 °C for 5 minutes before accumulating at -40.9 °C; (A) equatorial fluorine resonance of $F_5TeNH_3^+$, (a) and (a') ^{125}Te and ^{123}Te satellites, respectively, (B) overlapping resonances of TeF_6 and axial fluorine of $F_5TeNH_3^+$, (b) ^{125}Te satellites, (C) equatorial fluorine resonance of $F_5TeN(H)\text{-}Xe^+$, (D) axial fluorine resonance of $F_5TeN(H)\text{-}Xe^+$, (E) equatorial fluorine-on-tellurium resonance of F_5TeNF_2. The broad saddle-shaped resonance at *ca.* -68 ppm results from AsF_6^-.

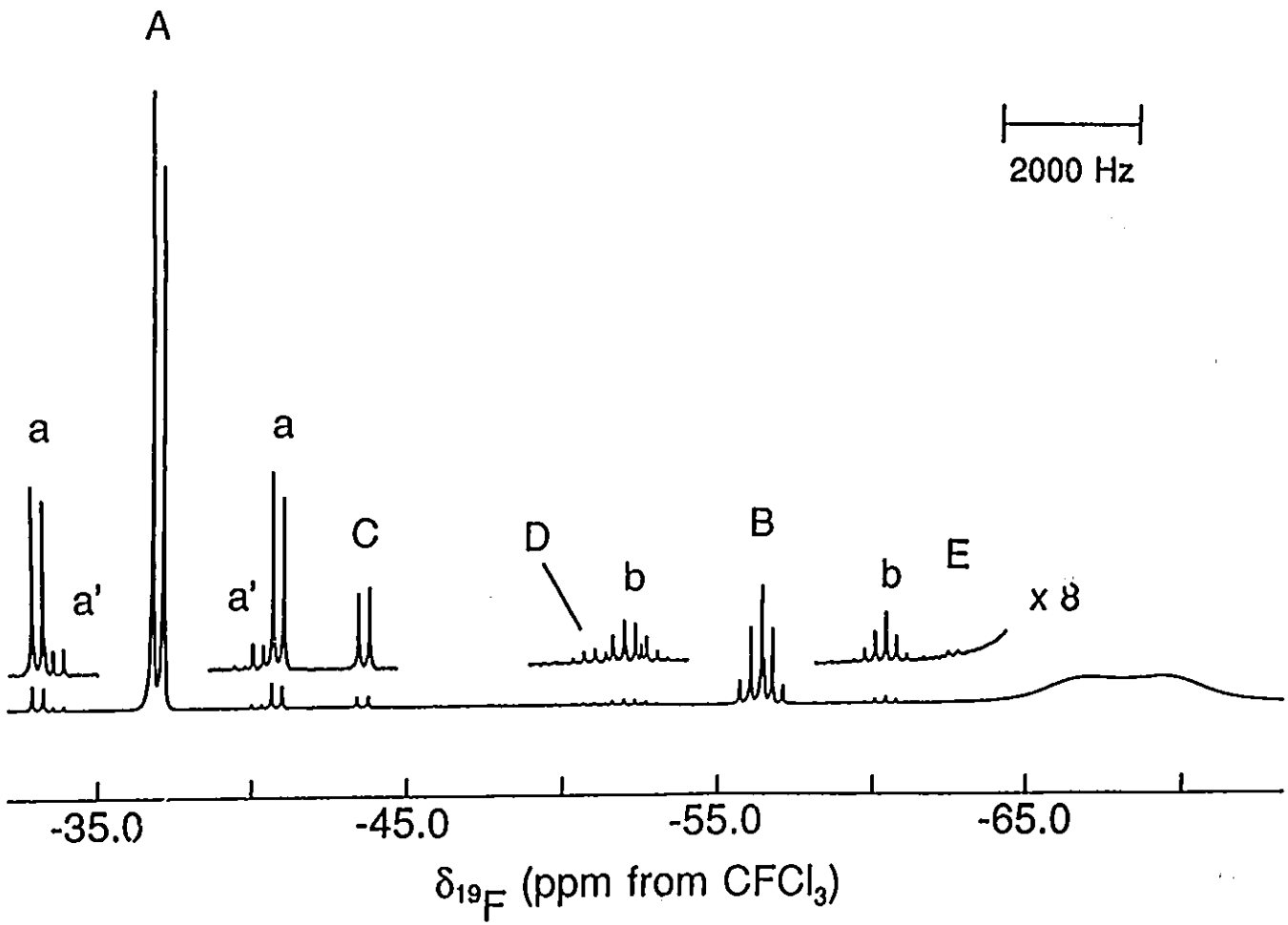
A
2000 Hz
a
a'
a
a'
C
D
b
B
b
E
x 8
-35.0
-45.0
-55.0
-65.0
δ19F (ppm from CFCl3)

Figure 6.2 ^{19}F NMR spectrum (499.599 MHz) of the fluorine-on-tellurium region of an equimolar mixture of natural abundance F_5TeNH_2 and $XeF^+AsF_6^-$ in HF solvent, after 1 hour at -33.3 °C before accumulating the spectrum at the same temperature; (A) equatorial fluorine resonance of $F_5TeNH_3^+$, (a) and (a') ^{125}Te and ^{123}Te satellites, respectively, (B) axial fluorine resonance of $F_5TeNH_3^+$, (C) equatorial fluorine resonance of $F_5TeN(H)\text{-}Xe^+$, (c) and (c') ^{125}Te and ^{123}Te satellites, respectively, (D) axial fluorine resonance of $F_5TeN(H)\text{-}Xe^+$, (E) equatorial fluorine-on-tellurium resonance of F_5TeNF_2, (F) TeF_6, (f) ^{125}Te satellites. The broad saddle-shaped resonance at *ca.* -68 ppm arises from AsF_6^-.

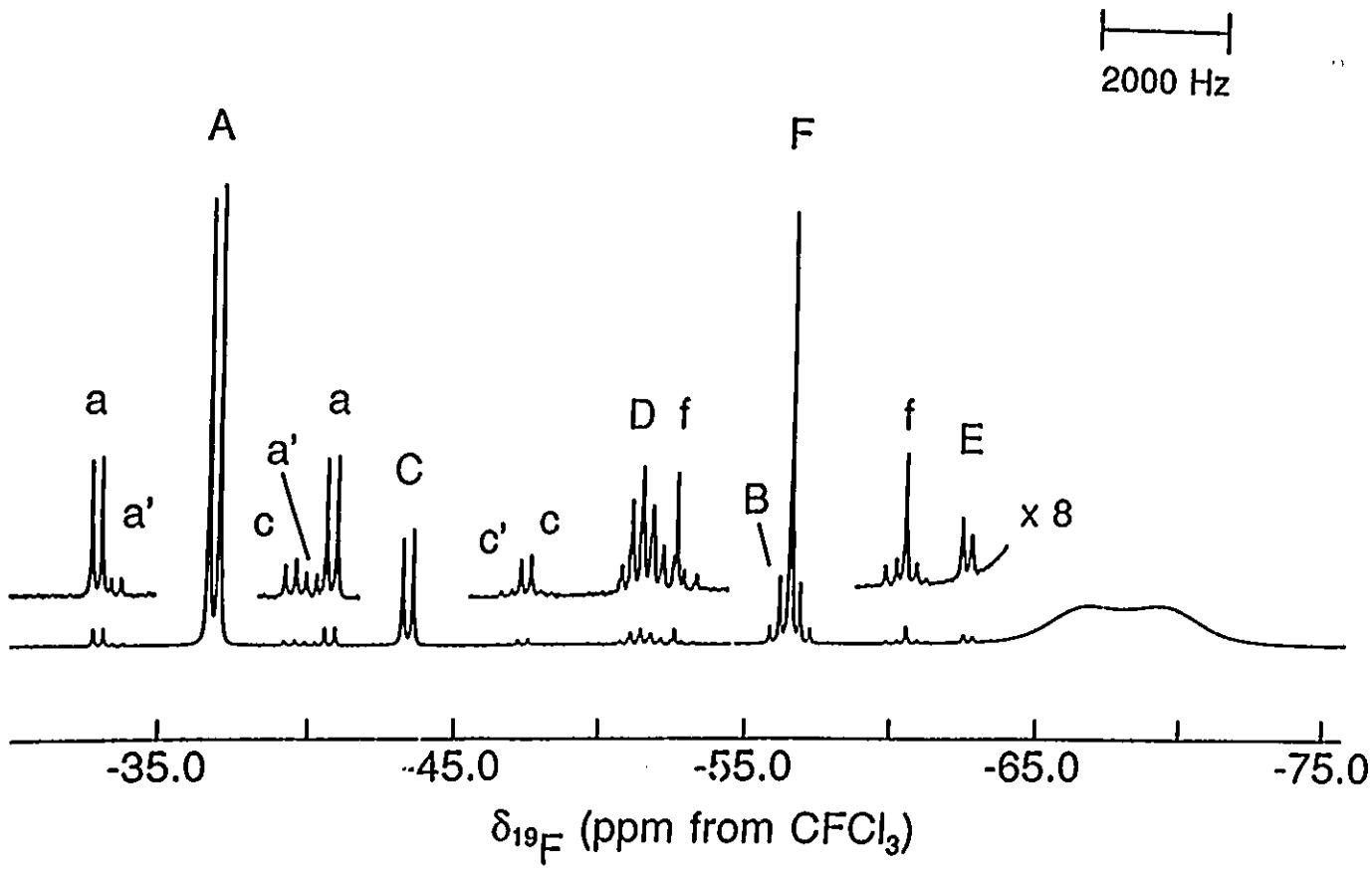
2000 Hz
A
F
a
a'
a'
a
c
C
c'
c
D
f
B
f
E
x 8
-35.0
-45.0
-55.0
-65.0
-75.0
$\delta_{^{19}F}$ (ppm from $CFCl_3$)

decomposition, as evidenced by the increased amounts of F_5TeNF_2 and TeF_6. From integration of the ^{19}F NMR resonances, the ratio $F_5TeNH_3^+$: $F_5TeN(H)\text{-}Xe^+$: F_5TeNF_2 : TeF_6 was found to be 1.00 : 0.26 : 0.02 : 0.28.

The decomposition of $F_5TeN(H)\text{-}Xe^+AsF_6^-$ to give F_5TeNF_2 is consistent with nucleophilic fluorination of $F_5TeN(H)\text{-}Xe^+$ with liberation of xenon gas, which was observed in the ^{129}Xe NMR spectrum at $\delta(^{129}Xe)$ = -5306 ppm (HF solvent; -37.0 °C). Atomic xenon can be envisaged as a very good leaving group, producing a transient divalent nitrenium ion [equation (6.1)]. Nucleophilic attack of the nitrenium ion by a fluoride ion donor, $M\text{-}F^-$, is expected to result in the monofluoramine, $F_5TeN(H)\text{-}F$ [equation (6.2)]. Likely fluoride ion donors are HF solvent

$$F_5TeN(H)\text{-}Xe^+M\text{-}F^- \longrightarrow F_5TeN(H)^+M\text{-}F^- + Xe \qquad (6.1)$$

$$(M = H^+, AsF_5)$$

$$F_5TeN(H)^+M\text{-}F^- \longrightarrow F_5TeN(H)\text{-}F + M \qquad (6.2)$$

$$(M = H^+, AsF_5)$$

or AsF_6^-. The mode of decomposition of $F_5TeN(H)\text{-}Xe^+AsF_6^-$ is similar to that observed for salts of the phenylxenon(II) cations, $R\text{-}Xe^+$ (R = C_6F_5,[96,99,262] *m*-$CF_3C_6H_{96}$ and *p*-FC_6H_{96}) which contain xenon(II) bonded to a carbon of the aromatic ring. The reaction of $[C_6F_5\text{-}Xe]^+[(C_6F_5)_2BF_2]^-$ with the nucleophiles X^- (X = Br, I) lead to the formation of halogenopentafluorobenzenes, C_6F_5X,[95] and interaction of $[C_6F_5\text{-}Xe]^+[C_6F_5BF_3]^-$ with C_6F_5X and $(p\text{-}CF_3C_6H_4)_3P$ resulted in the formation of $[(C_6F_5)_2X]^+[C_6F_5BF_3]^-$ [95] and $C_6F_5(p\text{-}CF_3C_6H_4)_3P^+[C_6F_5BF_3]^-$,[95] respectively. Reaction of $[C_6F_5\text{-}Xe]^+[(C_6F_5)_2BF_2]^-$ with species

containing acidic C-H protons, such as $(C_6H_5)CH_2CN$, $(C_6H_5)_3CH$ and $C_6H_5CF_3$ resulted in replacement of an acid proton by the C_6F_5 group.[96,263,264] Naumann and Tyrra[99] also prepared $[(C_6F_5)_3Te]^+[B(C_6F_5)_3F)]^-$ and $[(C_6F_5)_2I]^+[B(C_6F_5)_3F)]^-$ from the reaction of $Te(C_6F_5)_2$ and C_6F_5I with $[C_6F_5Xe]^+[B(C_6F_5)_3F)]^-$. All of these reactions are consistent with the generation of electrophilic "$C_6F_5^+$" and atomic xenon, and nucleophiles present in the system react with the aryl cation.

Although $F_5TeN(H)$-F is expected to be the primary product resulting from the nucleophilic fluorination of $F_5TeN(H)$-Xe^+, the observed product is F_5TeNF_2. This may be explained by considering the effect of the decomposition of $F_5TeN(H)$-Xe^+ on the fluoroacidity of the medium. It is clearly seen that fluoride donation from AsF_6^- will increase the fluoroacidity of the solution by generating AsF_5. If the HF solvent is the primary fluoride donor towards $F_5TeN(H)$-Xe^+, H_2F^+ is formally generated, which will also increase the fluoroacidity of the medium through equilibrium (6.3). Increased fluoroacidity of the medium generates cationic xenon(II) species [equations (6.4) and (6.5)], which are substantially stronger oxidative fluorinators

$$H_2F^+ + AsF_6^- \rightleftharpoons 2\,HF + AsF_5 \qquad (6.3)$$

$$AsF_5 + XeF_2 \rightleftharpoons XeF^+AsF_6^- \qquad (6.4)$$

$$XeF^+AsF_6^- + XeF_2 \rightleftharpoons Xe_2F_3^+AsF_6^- \qquad (6.5)$$

than XeF_2,[79] which is present in the system according to equilibrium (5.1). The generation of cationic xenon(II) species was indicated by the precipitation of pale yellow crystals, which were

shown to be $Xe_2F_3^+AsF_6^-$ by comparing the crystallographically determined unit cell parameters of a single crystal with the previously published data.[265] The salt $Xe_2F_3^+AsF_6^-$ was also observed as an impurity in the Raman spectrum of solid $F_5TeN(H)\text{-}Xe^+AsF_6^-$ (Chapter 5). The cationic xenon(II) species present in solution are assumed to rapidly oxidize $F_5TeN(H)\text{-}F$ to $F_5TeN(H)F_2^+$ [equation (6.6)], and the electron withdrawing effect of the three highly electronegative ligands is expected to result in deprotonation of $F_5TeN(H)F_2^+$ [equation (6.7)], by analogy with NF_3,[173]

$$F_5TeN(H)\text{-}F + XeF^+AsF_6^- \longrightarrow F_5TeN(H)F_2^+AsF_6^- + Xe \qquad (6.6)$$

$$F_5TeN(H)F_2^+AsF_6^- + HF \longrightarrow F_5TeNF_2 + H_2F^+AsF_6^- \qquad (6.7)$$

which is too weakly basic to be protonated in HF / SbF_5 solution. In Equation (6.4), the XeF^+ cation is formally behaving as an "F^+" donor. Similar behavior has been observed in the reaction of $XeF^+MF_6^-$ (M = As, Sb) with the sulfur (IV) species $CF_3S(O)F$, which results in the formation of $CF_3S(O)F_2^+MF_6^-$.[85] Sulfur (II) species such as the disulfane CF_3SSCF_3[80] are also oxidized by $XeF^+MF_6^-$ to give $CF_3SS(F)CF_3^+MF_6^-$.

The possibility that F_5TeNF_2 might arise from the reaction of HF with F_5TeNH_2 was investigated by observing the ^{19}F and ^1H NMR spectra of F_5TeNH_2 in HF solvent at -33.3 °C. The ^{19}F NMR spectrum indicated the presence of $F_5TeNH_3^+$ and TeF_6; integration of the ^{19}F NMR resonances indicated that the ratio $F_5TeNH_3^+$: TeF_6 was 1.00 : 0.08. In the ^1H NMR spectrum, a 1 : 1 : 1 triplet at $\delta(^1H)$ = 5.67 ppm[173] [$^1J(^1H\text{-}^{14}N)$ = 54 Hz][244] indicated the presence of NH_4^+. These observations are consistent with the slow displacement of NH_4^+ from $F_5TeNH_3^+$ by HF solvent at -33.3 °C [equation (6.8)], and that F_5TeNF_2 arises solely from the

oxidative fluorination of $F_5TeN(H)\text{-}Xe^+AsF_6^-$.

$$F_5TeNH_3^+AsF_6^- + HF \longrightarrow TeF_6 + NH_4^+AsF_6^- \quad (6.8)$$

(B) RELATIONSHIP OF THE BONDING AND THE MODE OF DECOMPOSITION OF $F_5TeN(H)\text{-}Xe^+$ IN SOLUTION

The similar decomposition modes of $F_5TeN(H)\text{-}Xe^+$ and the phenylxenon(II) cations, R-Xe^+ (R = fluorinated phenyl group), are unique for compounds of xenon(II). Previous studies on compounds containing Xe(II)-N and Xe(II)-O bonds have indicated radical decomposition mechanisms as shown in equations (6.9) and (6.10).[20] The radicals L· may dimerize or undergo further reactions. Detailed studies have indicated radical mechanisms for the decompositions of

$$XeL_2 \longrightarrow Xe + 2\,L\cdot \quad (6.9)$$

$$F\text{-}Xe\text{-}L \longrightarrow XeF_2 + Xe + 2\,L\cdot \quad (6.10)$$

$Xe[N(SO_2CF_3)_2]_2$,[61] $Xe[N(SO_2F)_2]_2$,[58] $FXe(NSO_2F)_2$,[58] $Xe[OP(O)F_2]_2$,[43] $FXeOP(O)F_2$,[43] $Xe[OSO_2F]_2$,[28] $FXeOSO_2F$,[28] $Xe[OTeF_5]_2$,[142] $Xe[OSeF_5]_2$,[142] $FXeOTeF_5$,[41] $FXeOC(O)CF_3$[39,41] and $Xe[OC(O)CF_3]_2$.[28,39,41] The radical decomposition of the neutral xenon(II) derivatives XeL_2 and FXe-L mentioned above are analogous to the radical decomposition of XeF_2, to give fluorine radicals and xenon at temperatures above 500 °C[20] [equation (6.11)]. The similarity of the

$$XeF_2 \longrightarrow Xe + 2\,F\cdot \quad (6.11)$$

decomposition of XeF_2, FXeL and XeL_2 is related to the fact that the electronegativities of the ligands L approach that of fluorine, so that the ionic characters of the Xe-F and Xe-L bonds are similar, resulting in homolytic cleavage of the Xe-F and Xe-L bonds upon decomposition. For $F_5TeN(H)$-Xe^+ and the phenylxenon(II) cations such as C_6F_5-Xe^+, the Xe-N and Xe-C bonds are much more covalent than in the class of compounds FXeL and XeL_2 mentioned above, which results from the lower electronegativities of the $F_5TeN(H)$- and C_6F_5- ligands. The lower electronegativities of these ligands are reflected in the ^{129}Xe NMR resonances for $F_5TeN(H)$-Xe^+ (-2902 ppm; Chapter 5) and C_6F_5-Xe^+ (-3763 ppm),[95,96] which are significantly more shielded relative to the values observed for the neutral Xe(II) derivatives. The relationship of ligand electronegativity and ^{129}Xe chemical shift is discussed in Chapter 5. Representative ^{129}Xe NMR chemical shifts for the class of neutral xenon(II) derivatives are XeF_2,[108] -1708 ppm (BrF_5 solvent; -40 °C), $FXeOSO_2F$,[108] -1613 ppm (BrF_5 solvent; -40 °C), $FXeN(SO_2F)_2$,[59] -2009 ppm (SO_2ClF solvent; -40 °C), and $Xe[N(SO_2F)_2]_2$,[59] -2257 ppm, (SO_2ClF solvent; -40 °C).

Owing to the covalent character of the Xe-N and Xe-C bonds in the $F_5TeN(H)$-Xe^+ and R-Xe^+ cations (R = fluorophenyl group), the most favorable decomposition pathway involves complete transfer of the Xe-N or Xe-C bond electron pair to xenon, giving xenon gas and a transient, highly electrophilic cation, such as $F_5TeN(H)^+$ or $C_6F_5^+$, which is immediately attacked by a nucleophile in solution.

(C) CHARACTERIZATION OF F_5TeNF_2 BY ^{15}N AND ^{19}F NMR SPECTROSCOPY

Difluoraminotellurium(VI) pentafluoride, F_5TeNF_2, is the primary decomposition product resulting from the nucleophilic fluorination of $F_5TeN(H)$-Xe^+ in HF and BrF_5 solvents [see Section (A) of this Chapter]. The structure of F_5TeNF_2 in solution was determined from the ^{19}F

and ^{15}N NMR spectra of the natural abundance and 99.5% ^{15}N-enriched compounds in HF and BrF_5 solvents and were consistent with Structure 6.1. The best NMR spectra of F_5TeNF_2 were obtained in BrF_5 solvent, and these spectra are discussed below.

The fluorine-on-nitrogen resonance in the ^{19}F NMR spectrum of natural abundance F_5TeNF_2 in BrF_5 solvent (-60.1 °C) consists of a singlet at 64.2 ppm ($\Delta\nu_{1/2}$ = 209 Hz) which results from quadrupole collapse of the one-bond scalar coupling to ^{14}N (I = 1). The chemical shift is comparable to that observed for other difluoramino compounds such as F_5SNF_2[266] (68.2 ppm) and F_2N-NF_2[267] (60.4 ppm). The fluorine-on-nitrogen region of the ^{19}F NMR spectrum of 99.5% ^{15}N-enriched F_5TeNF_2 consisted of a broad doublet centered at 64.2 ppm (Figure 6.3; BrF_5 solvent, -44.4 °C). The doublet arises from the one-bond scalar coupling $^1J(^{19}F_N\text{-}^{15}N)$ = 165 Hz, and is flanked by satellite doublets attributed to the two-bond scalar coupling $^2J(^{19}F_N\text{-}^{125}Te)$ = 1025 Hz. Gaussian multiplication of the free induction decay before Fourier transformation resulted in the resolution of quintet structure arising from the scalar coupling of the fluorine-on-nitrogen environment with the four chemically equivalent fluorines directly bonded to tellurium [$^3J(^{19}F_N\text{-}^{19}F_{eq.})$ = 15 Hz]. The scalar coupling of the fluorine-on-nitrogen environment with the axial fluorine is not resolved. In general, three-bond couplings with the axial fluorine-on-tellurium in F_5TeO- and F_5TeN- derivatives are not resolved. Examples include the inability to resolve the three-bond scalar couplings $^3J(^{129}Xe\text{-}^{19}F_{ax.})$ in $XeOTeF_5^+$,[54] $Xe(OTeF_5)_2$,[141] $FXeOTeF_5$[141] and $F_5TeN(H)$-Xe^+ (see Chapter 5).

The fluorine-on-tellurium(VI) region of the ^{19}F NMR spectrum (470.599 MHz) of 99.5% ^{15}N-enriched F_5TeNF_2 (BrF_5 solvent; -44.4 °C) consists of a typical AB_4 pattern (Figure 6.4).

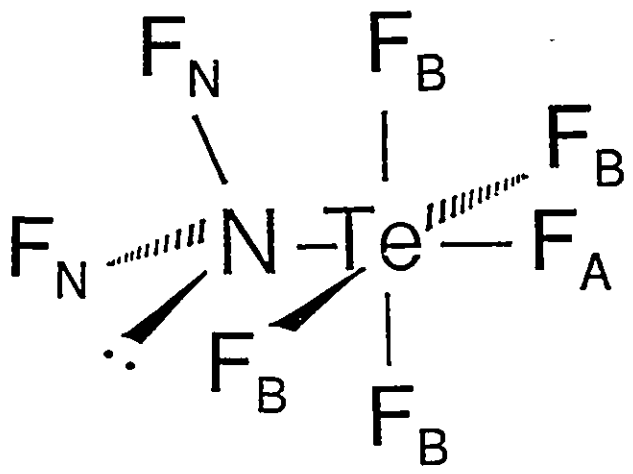

6.1

Figure 6.3 ^{19}F NMR spectrum (470.599 MHz) of the fluorine-on-nitrogen environment (F_N) of 99.5% ^{15}N-enriched F_5TeNF_2 in BrF_5 solvent at -44.4 °C: Asterisks (*) denote ^{125}Te satellites arising from the scalar coupling $^2J(^{19}F_N\text{-}^{125}Te)$ = 1025 Hz; (A) resolution of central doublet enhanced by Gaussian multiplication of the free induction decay before Fourier transformation.

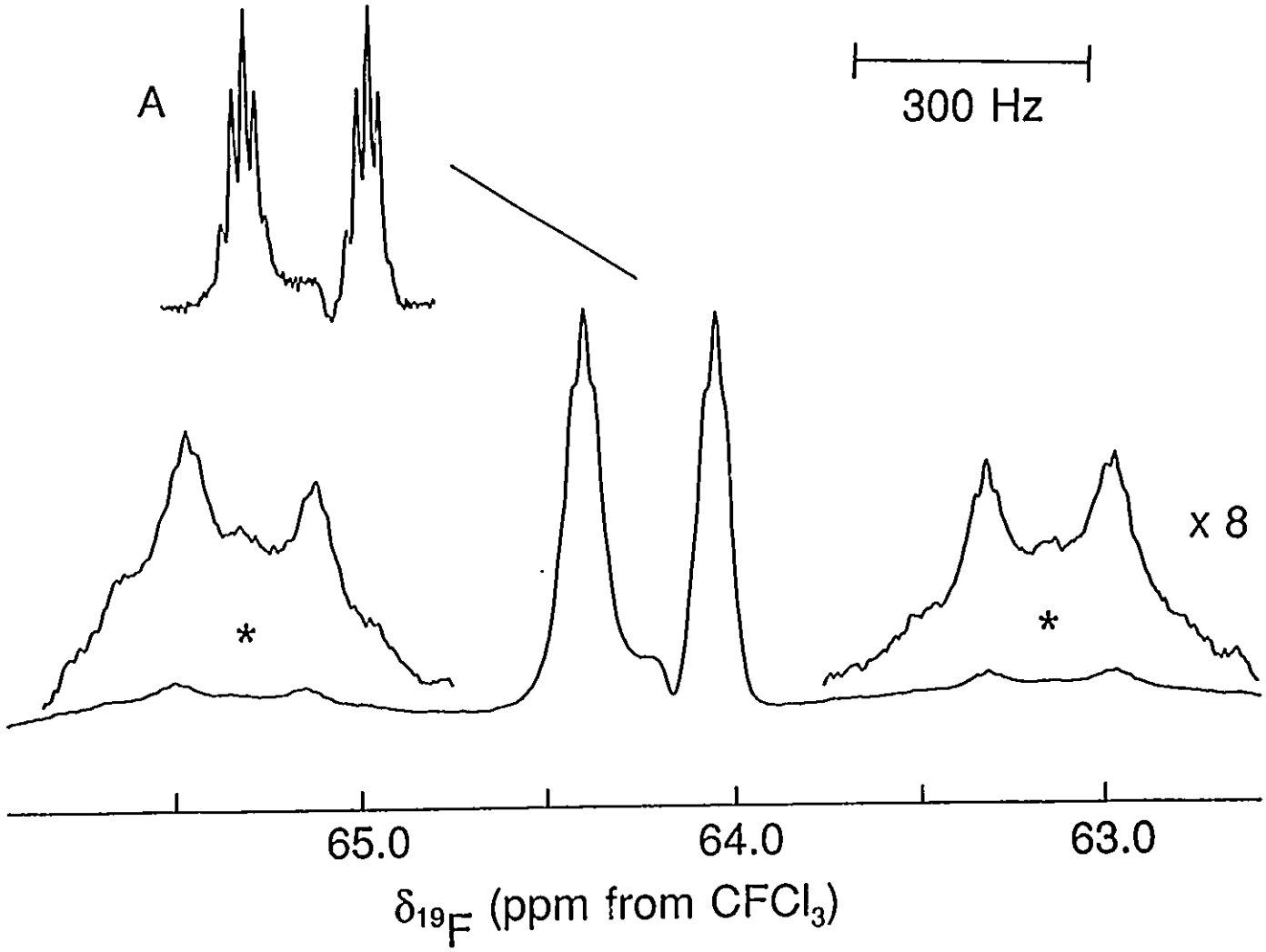
A
300 Hz
x 8
*
*
65.0
64.0
63.0
$\delta_{^{19}F}$ (ppm from $CFCl_3$)

Figure 6.4 ^{19}F NMR spectrum (470.599 MHz) of the fluorine-on-tellurium environment of 99.5% ^{15}N-enriched F_5TeNF_2 in BrF_5 solvent at -44.4 °C, the asterisk (*) and dagger (†) denote a ^{125}Te and a ^{123}Te satellite, respectively, that arise from the scalar couplings $^1J(^{19}F\text{-}^{125}Te)$ and $^1J(^{19}F\text{-}^{123}Te)$ of TeF_6 present in the sample.

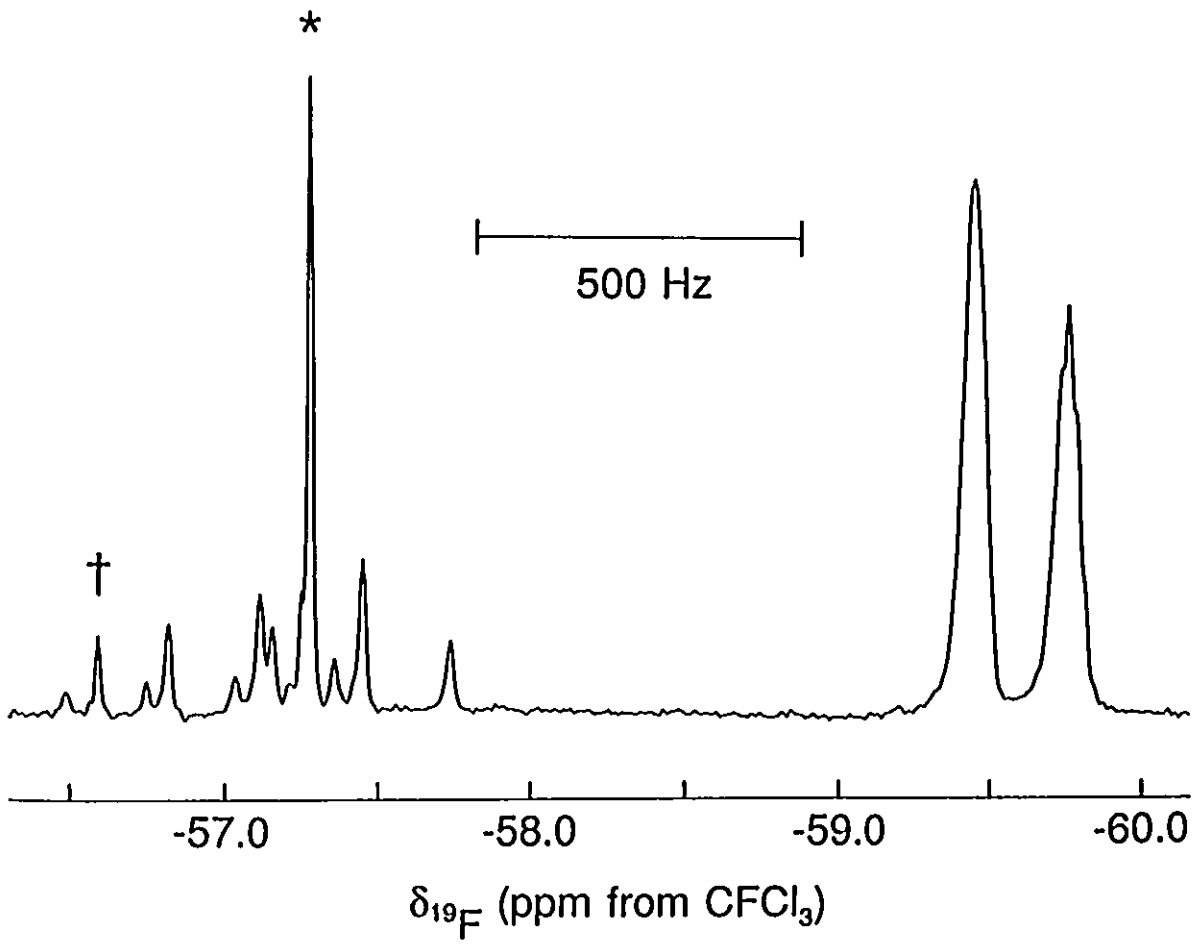
*
†
500 Hz
-57.0
-58.0
-59.0
-60.0
δ19F (ppm from CFCl3)

From the ratio $^2J(^{19}F_{ax.}\text{-}^{19}F_{eq.})/\nu_o\delta(^{19}F_{ax.}\text{-}^{19}F_{eq.}) = 0.125$, resolution of the individual transitions in the B_4 portion of the spectrum of the F_5Te- should be possible. This was shown in the ^{19}F NMR spectrum of $XeOTeF_5^+$,[54] where $^2J(^{19}F_{ax.}\text{-}^{19}F_{eq.})/\nu_o\delta(^{19}F_{ax.}\text{-}^{19}F_{eq.}) = 0.1497$, and the individual transitions of the AB_4 pattern were well resolved. This comparison is based on the fact that the appearance of the AB_4 spin system depends solely on this ratio.[268] However, in the AB_4 spectrum of F_5TeNF_2, the individual transitions of the B_4 portion (centered at *ca.* -59.5 ppm) were not resolved because of the scalar couplings $^2J(^{19}F_{eq.}\text{-}^{15}N) = 11$ Hz (obtained from the ^{15}N NMR spectrum, see below) and $^3J(^{19}F_N\text{-}^{19}F_{eq.}) = 15$ Hz, which further split each transition of the B_4 subspectrum into a triplet of doublets, resulting in two broad envelopes. The NMR parameters of the AB_4 spin system of natural abundance F_5TeNF_2 were obtained using the method of Harris and Packer[268] and the LAOCOON simulation program. The ^{19}F chemical shifts for the axial and equatorial fluorine resonances were determined to be -57.0 and -59.5 ppm, respectively, and the two-bond scalar coupling, $^2J(^{19}F_{ax.}\text{-}^{19}F_{eq.})$, was determined to be 148 Hz.

The ^{15}N NMR spectrum of 99.5% ^{15}N-enriched F_5TeNF_2 in BrF_5 solvent at -57.3 °C (Figure 6.5) consists of a triplet of quintets centered at $\delta(^{15}N) = -11.1$ ppm. The quintet structure arises from the scalar coupling of ^{15}N with the four chemically equivalent fluorine atoms bonded to tellurium(VI), $^2J(^{15}N\text{-}^{19}F_{eq.}) = 11$ Hz. The unresolved scalar coupling, $^2J(^{15}N\text{-}^{19}F_{ax.})$, of ^{15}N and the axial fluorine on tellurium is consistent with the inability to resolve two- and three-bond couplings with the axial fluorine in NMR studies of compounds containing F_5TeN- or F_5TeO-groups[54,141] (see also Chapters 4 and 5). The triplet splitting arises from the one-bond scalar coupling of ^{15}N with the fluorines on nitrogen, $^1J(^{15}N\text{-}^{19}F_N) = 165$ Hz, confirming the coupling observed in the ^{19}F NMR spectrum (Figure 6.3). The ^{15}N NMR chemical shift of F_5TeNF_2 is deshielded relative to 99.5% ^{15}N-enriched $F_5TeNH_3^+$ (-317.9 ppm) and $F_5TeN(H)\text{-}Xe^+AsF_6^-$

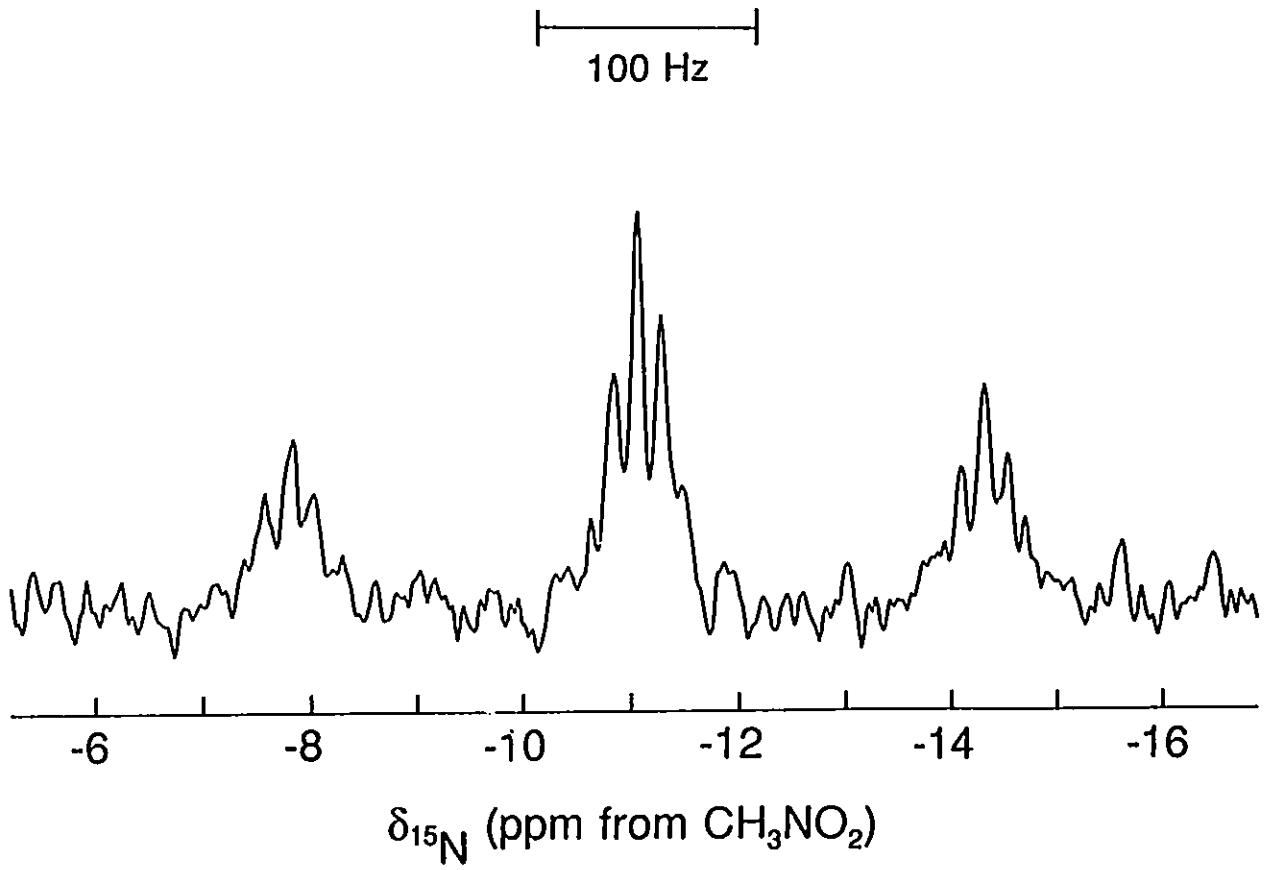

Figure 6.5 ^{15}N NMR spectrum (50.698 MHz) of 99.5% ^{15}N-enriched F_5TeNF_2 in BrF_5 solvent (-57.3 °C).

(-266.1 ppm), which were present in the solution. The deshielding can be rationalized from a consideration of the factors contributing to an approximate version[244] of the local paramagnetic shielding term[269,270] for nitrogen, σ_P^N [equation (6.12)]. A negative value for the local

$$\sigma_P^N = - [\mu_o \mu_B^2 \langle r^{-3} \rangle_{2p}] / 2\pi(\Delta E)][Q_{NN} + \Sigma_{N \neq X} Q_{NX}] \qquad (6.12)$$

paramagnetic contribution to the shielding of nitrogen, σ_P^N, deshields the nitrogen nucleus; μ_o and μ_B are the permittivity of a vacuum and the Bohr magneton, respectively, and $\langle r^{-3} \rangle_{2p}$ is the inverse cube of the average radius of the valence *p* electrons on nitrogen. The ΣQ term expresses the imbalance of electronic charge that allows the paramagnetic circulation in the magnetic field. The Q_{NN} part of this term depends on the 2*p* orbital populations on nitrogen, whereas ΣQ_{NX} is a multiple bond term. The term ΔE refers to the average energy for promotion of electrons to excited states that result in paramagnetic circulations. For molecules where the lone-pairs are strongly linked to the σ framework, such as the molecules discussed in the present Chapter, the electronic circulations deshielding nitrogen are all of $\sigma \rightarrow \sigma^*$ and $n_N \rightarrow \sigma^*$ type, where n_N represents a nitrogen lone-pair.[244] The greater deshielding of ^{15}N in F_5TeNF_2 relative to $F_5TeN(H)\text{-}Xe^+$ and $F_5TeNH_3^+$ results mainly from σ fluoro effects.[244] The replacement of hydrogen by fluorine is expected to remove electron density from nitrogen, increasing the radial term $\langle r^{-3} \rangle_{2p}$ and thus deshielding ^{15}N by increasing σ_P^N. This argument qualitatively explains the deshielding of nitrogen in NF_3 relative to NH_3 [$\Delta\delta(^{15}N) \approx 370$ ppm] and NF_4^+ relative to NH_4^+ [$\Delta\delta(^{15}N) \approx 280$ ppm], since for these two pairs $\langle r^{-3} \rangle_{2p}$ decreases by 17 and 20%, respectively.[244] It is noteworthy that the ^{15}N chemical shifts of NF_3 [$\delta(^{15}N) = -14$ ppm][271] and F_5TeNF_2 are similar, which relects, in part, the high electronegativity of the F_5Te- group.

A resonance assignable to F_5TeNF_2 was not observed in the ^{125}Te NMR spectrum of the mixture resulting from the reaction of F_5TeNH_2 and $XeF^+AsF_6^-$ in HF solvent. This was attributed to the low concentration of F_5TeNF_2 in the decomposition of $F_5TeN(H)\text{-}Xe^+$ in HF solvent, as shown in the ^{19}F NMR spectrum at -33.3 °C (Figure 6.2).

(D) ^{19}F NMR SPECTROSCOPIC STUDY OF THE DECOMPOSITION OF F_5TeNF_2 IN HF SOLVENT ACIDIFIED WITH AsF_5

The sample of an equimolar mixture of F_5TeNH_2 and $XeF^+AsF_6^-$ in HF solvent studied in Section (A) of this Chapter was warmed to -20 °C for 5 minutes, and the resulting ^{19}F NMR spectrum of the fluorine-on-tellurium(VI) region is shown in Figure 6.6 (-36.4 °C). Resonances assignable to $F_5TeNH_3^+$, $F_5TeN(H)\text{-}Xe^+$ and TeF_6 were observed. A 1 : 1 : 1 triplet centered at 96.8 ppm [$^1J(^{19}F\text{-}^{14}N)$ = 335 Hz] is assigned to $FN{\equiv}N^+$ by comparison with the published ^{19}F NMR data for $FN{\equiv}N^+AsF_6^-$ in HF solvent at room temperature [$\delta(^{19}F)$ = 103 ppm; $^1J(^{19}F\text{-}^{14}N)$ = 328 Hz].[272a] Resonances assignable to AsF_6^- and F_5TeNF_2 were not observed (see below).

It should be noted that careful sample warming was required in order to observe $FN{\equiv}N^+$ by ^{19}F NMR spectroscopy. This is expected since $FN{\equiv}N^+$ is a powerful oxidative fluorinator,[272b] capable of fluorinating xenon gas in HF solvent at 25 °C according to equation (6.13).[273] It is likely that $FN{\equiv}N^+$ is capable of oxidatively fluorinating several species present in the system,

$$FN{\equiv}N^+AsF_6^- + Xe \longrightarrow Xe\text{-}F^+AsF_6^- + N{\equiv}N \qquad (6.13)$$

including xenon gas formed in the decomposition of $F_5TeN(H)\text{-}Xe^+$. Taking care not to warm samples above the temperatures at which the ^{19}F NMR spectra were recorded sufficiently slowed

Figure 6.6 ^{19}F NMR spectrum (499.599 MHz) of the fluorine-on-tellurium(VI) region of an equimolar mixture of natural abundance F_5TeNH_2 and $XeF^+AsF_6^-$ in HF solvent, warmed for 5 minutes at -20 °C before accumulating the spectrum at -36.4 °C; (A) equatorial fluorine resonance of $F_5TeNH_3^+$, (a) and (a') ^{125}Te and ^{123}Te satellites, respectively, (B) axial fluorine resonance of $F_5TeNH_3^+$, (C) equatorial fluorine resonance of $F_5TeN(H)\text{-}Xe^+$, (c) ^{125}Te satellites; (D) unassigned resonance, (E) axial fluorine resonance of $F_5TeN(H)\text{-}Xe^+$, (F) TeF_6, (f) ^{125}Te satellites.

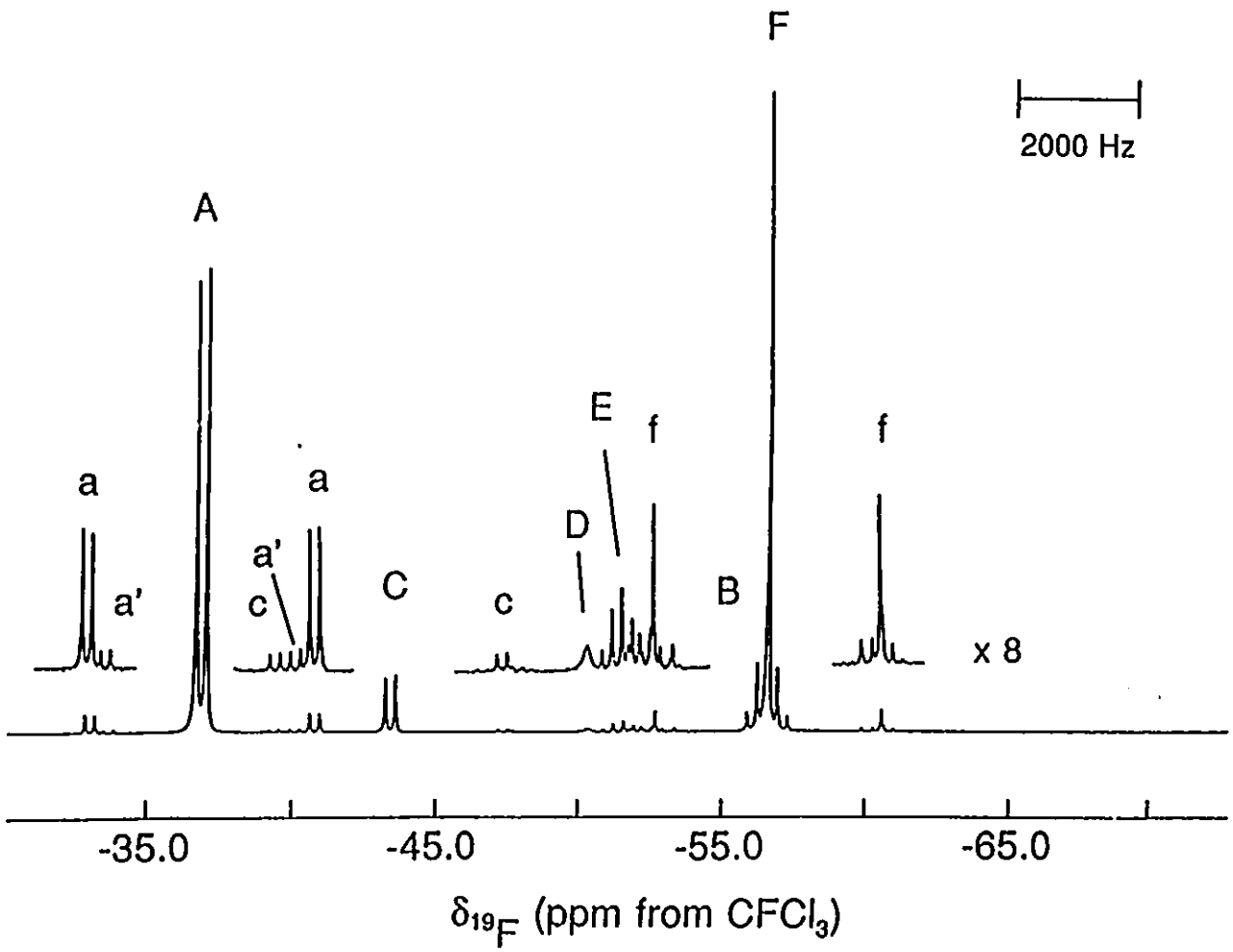
F
2000 Hz
A
E
f
f
a
a
a'
a'
c
C
c
D
B
x 8
-35.0
-45.0
-55.0
-65.0
δ19F (ppm from CFCl3)

the oxidative fluorination reactions so that $FN{\equiv}N^+$ could be observed in the ^{19}F NMR spectra. Evidence for the reaction of $FN{\equiv}N^+$ was provided by the observation of a peak [$\delta(^{15}N)$ = -73.0 ppm] in the ^{15}N NMR spectra of the 99.5% ^{15}N-enriched system which is assignable to nitrogen gas[274] dissolved in HF solvent.

From the integrations of the ^{19}F NMR resonances (Figure 6.6), the ratio $F_5TeNH_3^+$: $F_5TeN(H)\text{-}Xe^+$: TeF_6 : $FN{\equiv}N^+$ was found to be 1.00 : 0.03 : 0.44 : 0.03, and resonances due to AsF_6^- and F_5TeNF_2 were not observed (see below). The presence of $FN{\equiv}N^+$ and the increased amount of TeF_6 relative to $F_5TeNH_3^+$ when compared to the observed ratio prior to warming to -20 °C [see Section (A) of this Chapter] is consistent with the decomposition of F_5TeNF_2 to TeF_6 and $FN{\equiv}N^+$. The HF resonance [$\delta(^{19}F)$ = -191.4 ppm] is shifted to high frequency by 3.7 ppm relative to that observed before warming of the sample to -20 °C. The HF resonance was also significantly broadened [$\Delta\nu_{1/2}$ = 3450 Hz] and the XeF_2 resonance was no longer observed. The absence of a resonance assignable to AsF_6^- and the high frequency shift of the HF resonance is consistent with AsF_5 formation and the resulting exchange equilibrium (6.3) with HF. Since a large amount of $F_5TeNH_3^+$ is still present in solution, the XeF_2 has not completely reacted and is believed to undergo exchange with AsF_5 generated in the decomposition of $F_5TeN(H)\text{-}Xe^+$ according to equilibria (6.4) and (6.5).

The decomposition of F_5TeNF_2 in AsF_5-acidified HF solution to give TeF_6 and $FN{\equiv}N^+$ appeared to indicate that a Lewis acid induced intramolecular redox decomposition of F_5TeNF_2 had occurred. A detailed study of this process was published by Christe *et al.* for the difluoramino compounds R-NF_2 (R = Cl, F_3C, F_5S, F_3CO, F_5SO).[275] Difluoramino compounds are in general thermodynamically unstable, and their stability results from a kinetic barrier to decomposition. Suitable catalysts such as the strong Lewis acids, SbF_5 and AsF_5, lower the energy barrier to

decomposition, resulting in multiply bonded nitrogen species such as F-N=N-F and N≡N, and more highly fluorinated byproducts. Christe *et al.*[275] showed by Raman spectroscopy that $ClNF_2$ forms an adduct with AsF_5 at -78 °C which is best interpreted as a fluorine-bridged adduct, ClN(F)···F-AsF_5, which decomposed on warming via the Lewis acid induced intramolecular redox decomposition process mentioned above. This indicated that the initial step in the decomposition of difluoramine compounds, RNF_2, involved fluoride abstraction from nitrogen by the Lewis acid, MF_5 (M = As, Sb). It has been proposed that the fluorine-bridged adduct decomposes according to equation (6.14), producing fluoronitrene, F-N, which dimerizes to give

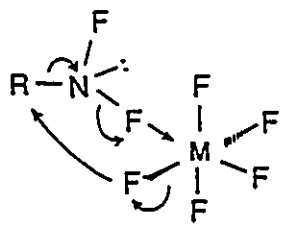

$$\longrightarrow \text{R-F} + \text{[F-N]} + MF_5 \qquad (6.14)$$

cis- and *trans*- isomers of F-N=N-F. The *cis*-isomer of N_2F_2 behaves as a fluoride ion donor towards the strong Lewis acid, MF_5 (M = As, Sb), forming $FN{\equiv}N^+MF_6^-$, but the *trans*-isomer of N_2F_2 is not a fluoride ion donor.[276] The decomposition of F_5TeNF_2 in the present system may, in fact, be catalyzed by AsF_5, which is produced in the nucleophilic fluorination of $F_5TeN(H)\text{-}Xe^+$ [see Section (A)]. It is, however, unlikely that the source of $FN{\equiv}N^+$ results from the dimerization of fluoronitrene radicals as in the study of Christe *et al.*[275] since no *trans*-N_2F_2 was observed in the reaction mixture after complete decomposition of F_5TeNF_2; dimerization of fluoronitrene is expected to give a mixture of *cis*- and *trans*-isomers.[275,277] It was postulated that the absence of *trans*-N_2F_2 in the present system might result from the isomerization of the *cis*- and *trans*-isomers,

with *cis*-N_2F_2 acting as a sink for $FN{\equiv}N^+$ formation in the presence of AsF_5 [equation (6.15)]. However, isomerization of *trans*-N_2F_2 is very slow, and attempts to increase the rate at elevated temperatures result in low yields due to decomposition of N_2F_2 to N_2 and F_2.[278] Christe *et al.*[273] were able to obtain an 80% yield of $FN{\equiv}N^+AsF_6^-$ by combining *trans*-N_2F_2 with an excess of AsF_5 at 70 °C, however, the process was slow, requiring three days. The possibility of HF

$$\textit{trans}\text{-}N_2F_2 \rightleftharpoons \textit{cis}\text{-}N_2F_2 + AsF_5 \longrightarrow FN{\equiv}N^+AsF_6^- \qquad (6.15)$$

solvent acting as a catalyst for trans/cis isomerization at -20 °C was investigated in the present study by combining equimolar amounts of *trans*-N_2F_2 and AsF_5 in HF at -196 °C. The sample was warmed to -20 °C for five minutes, similar to the conditions under which $FN{\equiv}N^+$ was formed in the reaction of F_5TeNH_2 and $XeF^+AsF_6^-$ in HF solvent, and the ^{19}F NMR spectrum was observed at -37 °C. Only *trans*-N_2F_2 was observed [$\delta(^{19}F)$ = 89.01 ppm],[121] which indicated that isomerization of *trans*-N_2F_2 did not occur. The second reason to discount fluoronitrene dimerization as the major source of $FN{\equiv}N^+$ is apparent when one considers the low concentration of F_5TeNF_2 relative to the $F_5TeNH_3^+$ cation in HF solvent before warming the sample to -20 °C [see Section (A) and Figure 6.2], and there is precedent in the literature for the reaction of fluoronitrene with primary amines.[279,280] It is very unlikely that fluoronitrene is sufficiently unreactive towards F_5TeNH_2 to react solely by dimerization, given the slow fluoronitrene dimerization kinetics expected from the low concentration of fluoronitrene in solution. In considering this, it is important to realize that nitrenes are highly reactive species, usually requiring trapping agents to infer their existence.[281] Primary amines undergo deamination reactions with difluoramine, HNF_2, or isopropyl N,N,-difluorocarbamate, which behaves as a source of

HNF_2,[121] as shown in equation (6.16).[279,280] It was postulated that the initial step involved

$$3\ RNH_2 + HNF_2 \longrightarrow 2\ RNH_3^+F^- + N_2 + R\text{-}H \qquad (6.16)$$

the reaction of the primary amine with fluoronitrene to give $RNH_2^+NF^-$ [equation (6.17)], followed by rearrangement to give a substituted hydrazine, from which elimination of HF resulted in the

$$RNH_2 + NF \longrightarrow RNH_2^+NF^- \longrightarrow$$

$$RN(H)N(H)F \xrightarrow[-\ HF]{} RN{=}NH \xrightarrow[-\ N_2]{} R\text{-}H \qquad (6.17)$$

unstable diazene, RN=NH, which eliminated N_2 to give R-H. Bumgardner and Liebman[282] have proposed an alternative mechanism for the reaction of primary amines with HNF_2, in which the first step is the bimolecular displacement of fluoride from HNF_2 by RNH_2, without inference of fluoronitrene formation [equation (6.18)]

$$RNH_2 + HNF_2 \longrightarrow R\text{-}NH_2\text{-}N(H)F^+ + F^- \qquad (6.18)$$

A mechanism for the formation of TeF_6 and $FN{\equiv}N^+$ from the Lewis acid-catalyzed reaction F_5TeNF_2 and $F_5TeNH_3^+$ in HF solvent is proposed and supported by literature analogies in the following discussion. The generation of fluoronitrene as an intermediate in the reaction of F_5TeNH_2 and F_5TeNF_2 in the present study cannot be addressed; however, by analogy with the

AsF_5-catalyzed decomposition of $ClNF_2$,[275] it is likely that the interaction of AsF_5 with a fluorine atom on nitrogen in F_5TeNF_2 facilitates the reaction [equation (6.19)]. This process is analogous to the bimolecular addition depicted in equation (6.18).[281] Equilibria (6.3) and (6.20) are expected

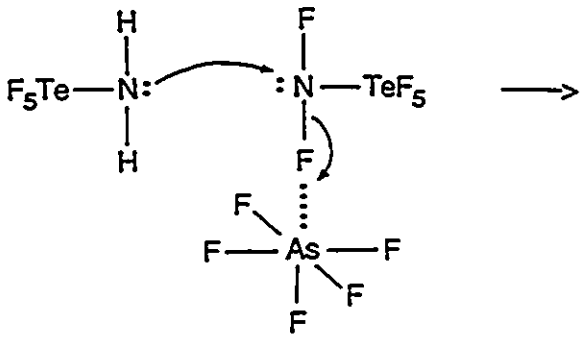

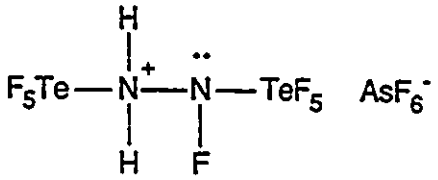

(6.19)

1

$$F_5TeNH_3^+AsF_6^- \rightleftharpoons F_5TeNH_2 + HF + AsF_5 \qquad (6.20)$$

to facilitate the reaction of F_5TeNH_2 and F_5TeNF_2 to give the protonated hydrazine, 1. The presence of AsF_5 also results from the nucleophilic fluorination of $F_5TeN(H)\text{-}Xe^+$ in the same system [see equation (6.2)]. The cationic xenon(II) species, XeF^+ and $Xe_2F_3^+$, are present from the increased fluoroacidity of the solution as discussed in Section (A) of this Chapter. The deprotonation equilibrium (6.21) to give 2 is expected to precede oxidative fluorination by XeF^+,

resulting in 3 [equation (6.22)]. Evidence for the oxidative fluorinating ability of the

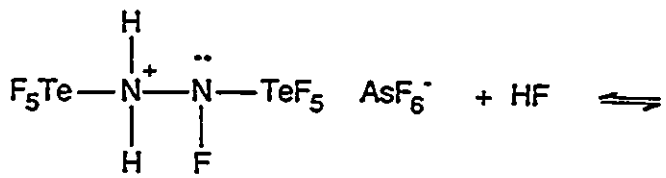

1

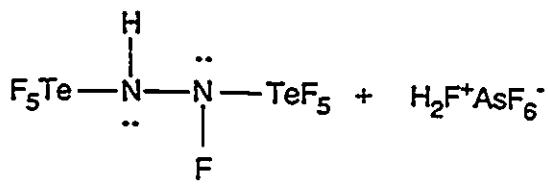

2 (6.21)

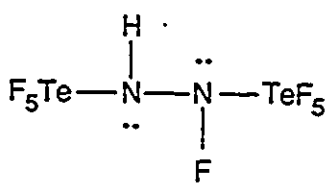

2

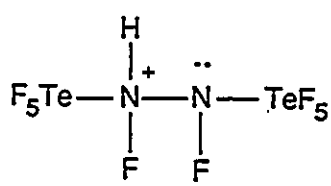

3 (6.22)

solution is provided by the fact that the monofluoramine, $F_5TeN(H)$-F, was not observed as the

initial product of the nucleophilic fluorination of $F_5TeN(H)\text{-}Xe^+$ [Section (A) of this Chapter]. This has been attributed to the immediate oxidative fluorination of the monofluoramine to the difluoramine, F_5TeNF_2, by XeF^+. By analogy with the weak basicity of $N(CF_3)_3$[283] and the inability to protonate NF_3[173] in superacid (HF / SbF_5) solution, species 3 is expected to be deprotonated, giving 4 in the AsF_5-acidified HF solution [equation (6.23)]. In the presence of AsF_5, 4 may undergo Lewis acid induced intramolecular redox decomposition by analogy with difluoramino compounds[275] [equation (6.24)]. The short-lived nitrene, 5, is expected to have some 1,1-diazene character (6) due to π-donation from the tricoordinate nitrogen.[281] Resonance contributor 6 is electronically similar to $F_2N{=}N$, which has been proposed by Christe *et al.*[273] as the intermediate in the formation of *cis*-N_2F_2 from the reaction of $FN{\equiv}N^+$ and the fluoride ion donor, FNO [equation (6.25)]. Although $F_2N{=}N$ rearranges by α-migration of fluorine to give *cis*-

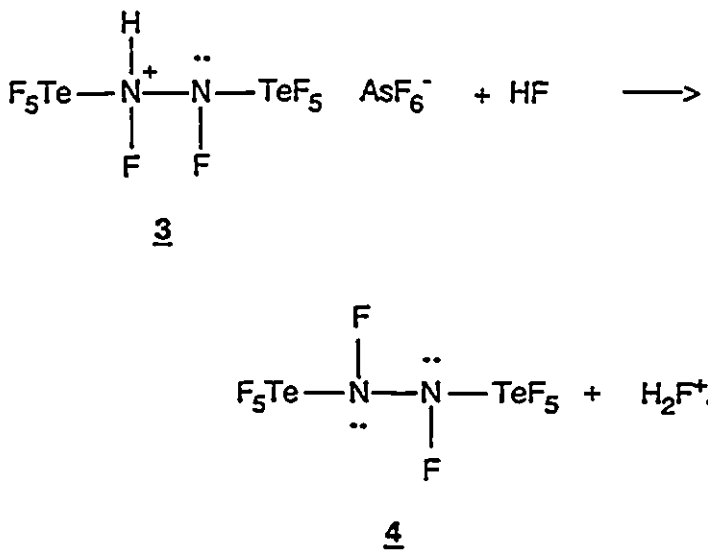

(6.23)

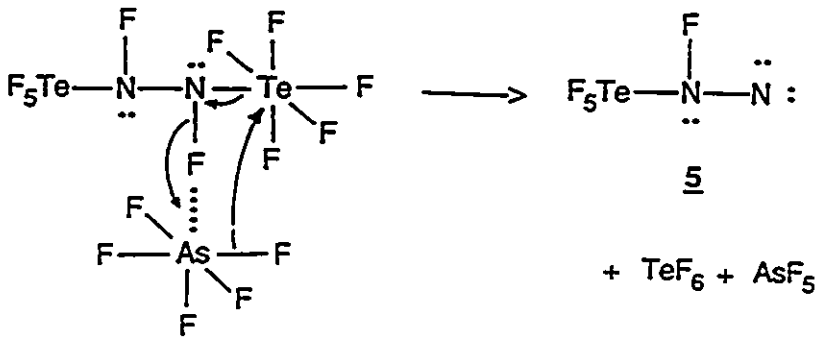

5

+ TeF_6 + AsF_5 (6.24)

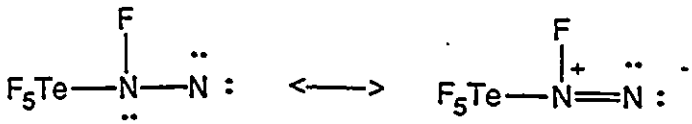

5 6

$$F\text{-}NO + F\text{-}N{\equiv}N^+ \longrightarrow NO^+ + [F_2N{=}N] \longrightarrow cis\text{-}N_2F_2 \qquad (6.25)$$

N_2F_2, the more favorable process in the case of the transient species 6 may involve elimination of "TeF_5^{-}" in the presence of XeF^+ to give the stable species TeF_6, xenon, and $FN{\equiv}N^+$ according to equation (6.26). It is also possible that a second decomposition process occurs. By analogy with $F_2N{=}N$, 6 may rearrange by α-migration of fluorine to give the diazene, $F_5Te\text{-}N{=}N\text{-}F$, which then

eliminates the stable species N_2 and TeF_6 [equation (6.27)]. This is analogous to the formation

$$F_5Te(F)N{=}N + XeF^+AsF_6^- \longrightarrow TeF_6 + FN{\equiv}N^+AsF_6^- + Xe \qquad (6.26)$$

$$F_5Te(F)N{=}N \longrightarrow F_5Te\text{-}N{=}N\text{-}F \longrightarrow TeF_6 + N{\equiv}N \qquad (6.27)$$

of RH, N_2 and HF in the reductive deamination of primary amines by HNF_2, which is believed to involve a similar short-lived diazene, R-N=N-H[279] [equation (6.17)]. Evidence for N_2 formation is provided by the observation of a resonance attributable to molecular nitrogen dissolved in HF [$\delta(^{15}N)$ = -73.0 ppm; -45 °C][274] in the ^{15}N NMR spectrum of the analogous 99.5% ^{15}N enriched materials.

It is noteworthy that, although the F_5TeNF_2 is completely reacted after warming to -20 °C for five minutes, a small amount of $F_5TeN(H)\text{-}Xe^+$ is still present in solution. This may result from the increased fluoroacidity of the HF solution, which decreases the nucleophilicity of the solvent medium, thus decreasing the rate of nucleophilic fluorination of $F_5TeN(H)\text{-}Xe^+$ according to equation (6.1). On warming the sample to -1.2 °C, ^{19}F NMR indicated that all but a trace of $F_5TeN(H)\text{-}Xe^+$ was decomposed. Also, a resonance assignable to $FN{\equiv}N^+$ was not observed. The only F-on-Te(VI) environments observed were those of $F_5TeNH_3^+$ and TeF_6 (relative integrated ratio = 1.00 : 0.50). The broad saddle-shaped resonance for AsF_6^- (*ca.* -68 ppm) was also not observed. Separate resonances for AsF_6^-, HF and XeF_2 were coalesced to a broad peak ($\Delta\nu_{1/2}$ = 386 Hz) at -188.9 ppm, which indicated exchange of these three species according to equilibria (6.3) to (6.5) in the AsF_5-acidified HF solution.

CHAPTER 7

CHARACTERIZATION OF FO_2SNH_2 AND $FO_2SNH_3^+AsF_6^-$ USING ^{19}F AND ^1H NMR AND RAMAN SPECTROSCOPY AND COMPARISON OF THE BONDING IN FO_2SNH_2 AND THE $FO_2SNH_3^+$ CATION

INTRODUCTION

The synthesis of fluorosulfuryl amide, FO_2SNH_2, was first reported in 1958 by two different routes, namely, fluorination of ClO_2SNH_2 with KF in boiling acetonitrile[133] [equation (7.1)] and fluorination of chlorosulfuryl isocyanate with NaF followed by careful hydrolysis[134]

$$ClO_2SNH_2 + KF \longrightarrow KCl + FO_2SNH_2 \qquad (7.1)$$

[equations (7.2) and (7.3)]. The preparation of FO_2SNH_2 from the reaction of disulfuryl fluoride,

$$ClO_2SNCO + NaF \longrightarrow NaCl + FO_2SNCO \qquad (7.2)$$

$$FO_2SNCO + H_2O \longrightarrow FO_2SNH_2 + CO_2 \qquad (7.3)$$

$S_2O_5F_2$, and NH_3 at low temperature was reported in 1961[129] [equation (7.4)] Fluorosulfuryl amide is a colorless liquid at room temperature (m.p. 8 °C) and is soluble in organic solvents such

$$S_2O_5F_2 + 2\,NH_3 \longrightarrow FO_2SNH_2 + NH_4^+OSO_2F^- \qquad (7.4)$$

as acetonitrile, ether and chloroform. Unlike ClO_2SNH_2, which reacts explosively with water to give sulfamic acid and HCl,[284] FO_2SNH_2 is soluble in water and hydrolyzes slowly, producing sulfamic acid and HF [equation (7.5)]. The compound, FO_2SNH_2, is isoelectronic with $O_3SNH_2^-$

$$FO_2SNH_2 + H_2O \longrightarrow O_3SNH_3 + HF \qquad (7.5)$$

and has similar bonding properties. For instance, the similar SN bond lengths in $K^+O_3SNH_2^-$ [1.60(1) Å][285] and FO_2SNH_2 [1.61(3) Å],[286] that were determined by X-ray crystallography and electron diffraction, respectively, are significantly shorter than a typical S-N single bond, such as that in O_3SNH_3 [1.7714(3) Å],[287] indicating the presence of S-N π bonding in FO_2SNH_2 and $O_3SNH_2^-$.[130,288] Sulfur-nitrogen π-bonding in O_3SNH_3 is not possible since the lone pair on nitrogen is not available for π-donation to the acceptor orbitals on sulfur. Recent *ab initio* SCF calculations utilizing natural population analysis[217] for the related molecules SO_2Cl_2, $SO_2(CH_3)Cl$ and $SO_2(CH_3)_2$ indicate that the hybrid acceptor orbitals on sulfur, that are predominantly 3*p* in character, arise from $\pi(O) \rightarrow \sigma^*(SX)$ negative hyperconjugation with a minor contribution (19 - 27%) from sulfur 3*d* orbitals. It seemed reasonable therefore to stress the importance of $\pi(N) \rightarrow \sigma^*(SX)$ negative hyperconjugation (X = F, O) over pure $[N(2p) \rightarrow S(3d)]\pi$ donation as a mechanism for S-N π bonding in FO_2SNH_2 and $O_3SNH_2^-$.

Semmoud and Vast[130] have used infrared spectroscopy to investigate the effect of deprotonation on the S-O, S-N and S-F symmetric stretching frequencies (and hence the bond orders) for the acid/base pairs FO_2SNH_2/FO_2SNHg and AgO_3SNH_2/Ag_3O_3SN. They have shown that the S-N bonds are strengthened through increased S-N π-bonding at the expense of the S-O and S-F bonds when lone pairs on nitrogen become available for S-N π-bonding upon deprotonation of FO_2SNH_2 and $O_3SNH_2^-$.

The present work involved a more detailed vibrational study of FO_2SNH_2 with use of $^{14/15}N$ isotopic shift information obtained from the Raman spectra of the natural abundance and 99.5% ^{15}N-enriched compounds. As well, the $FO_2SNH_3^+$ cation was prepared for the first time as the AsF_6^- salt. Assignments of the Raman spectra of natural abundance and 99.5% ^{15}N-enriched $FO_2SNH_3^+AsF_6^-$ completed the study of Semmoud and Vast,[130] by allowing a comparison of the S-O, S-F, and S-N symmetric stretching frequencies for the series FO_2SNHg, FO_2SNH_2 and $FO_2SNH_3^+$ with the isoelectronic sulfuramide series O_3SNAg_3, O_3SNH_2Ag, and O_3SNH_3.

RESULTS AND DISCUSSION

(A) PREPARATION AND ISOLATION OF NATURAL ABUNDANCE FO_2SNH_2 AND $FO_2SNH_3^+AsF_6^-$ AND THE 99.5% ^{15}N-ENRICHED ANALOGUES

Natural abundance FO_2SNH_2 was prepared by the fluorination of ClO_2SNCO with NaF [equation (7.6)] followed by reaction with a stoichiometric amount of H_2O in acetonitrile solution [equation (7.7)] by modifying the literature procedure.[134] The unstable carbamic acid,

$$ClO_2SNCO + NaF \longrightarrow NaCl + FO_2SNCO \qquad (7.6)$$

$$FO_2SNCO + H_2O \longrightarrow [FO_2SN(H)C(O)OH] \longrightarrow FO_2SNH_2 + CO_2 \quad (7.7)$$

$FO_2SN(H)C(O)OH$, is believed to be an intermediate in the hydrolysis of FO_2SNCO. The 99.5% ^{15}N-enriched compound FO_2SNH_2 was prepared from the stoichiometric reaction of $S_2O_5F_2$ and 99.5% ^{15}N-enriched NH_3 in diethyl ether solution at -45 °C by following the literature method[129] [equation (7.8)]

$$S_2O_5F_2 + [^{15}N]NH_3 \longrightarrow [^{15}N]FO_2SNH_2 + [^{15}N]NH_4SO_3F \quad (7.8)$$

The natural abundance and ^{15}N-enriched salts $FO_2SNH_3^+AsF_6^-$ are finely divided white powders that were prepared from the reaction of AsF_5 with FO_2SNH_2 or $[^{15}N]FO_2SNH_2$ in HF solvent at -40 °C according to equation (7.9) followed by vacuum removal of the HF solvent at

$$FO_2SNH_2 + HF + AsF_5 \longrightarrow FO_2SNH_3^+AsF_6^- \quad (7.9)$$

the same temperature. The white powder is indefinitely stable at room temperature under anhydrous conditions, but hydrolyses rapidly with fuming and liquefaction in the presence of moist air.

(B) CHARACTERIZATION OF NATURAL ABUNDANCE AND 99.5% ^{15}N ENRICHED FO_2SNH_2 AND $FO_2SNH_3^+AsF_6^-$ BY ^1H AND ^{19}F NMR SPECTROSCOPY

The ^{19}F and ^1H NMR spectra of neat liquid FO_2SNH_2 at ambient temperature consist of broad singlets at $\delta(^{19}F) = 56.51$ and $\delta(^1H) = 5.41$ ppm. The ^{19}F NMR resonance was consistent with the FO_2SN- group.[289] The scalar couplings are not resolved because of quadrupolar broadening from the presence of natural abundance nitrogen (I = 1). The ^1H and ^{19}F NMR spectra in BrF_5 solvent at -61.4 °C do not indicate any reaction of FO_2SNH_2 with the solvent and consisted of a broad doublet [$\delta(^1H) = 4.68$ ppm; Figure 7.1a] and a triplet [$\delta(^{19}F) = 56.91$ ppm; Figure 7.1b]. The multiplet structures arise from $^3J(^1H\text{-}^{19}F) = 6.3$ Hz. The collapse of the scalar coupling, $^1J(^1H\text{-}^{14}N)$, which is estimated to be 61.8 Hz from equation (7.10) (see below), results from scalar relaxation of the second kind,[290] when the tranverse relaxation rate of the quadrupolar

$$^1J(^1H\text{-}^{14}N) = [\gamma(^{14}N)/\gamma(^{15}N)] \times {}^1J(^1H\text{-}^{15}N) \qquad (7.10)$$

^{14}N, $1/T_2(^{14}N)$, is much greater than the magnitude of the scalar coupling to the proton. The coupling $^1J(^1H\text{-}^{14}N)$ is completely quadrupole collapsed, but is sufficiently narrow to allow resolution of $^3J(^1H\text{-}^{19}F)$.

All possible scalar couplings between spin-½ nuclei are observed in the ^1H and ^{19}F NMR spectra of 99.5% ^{15}N-enriched FO_2SNH_2 in acetonitrile solution (30 °C). The ^1H NMR spectrum consists of a doublet of doublets [$\delta(^1H) = 6.79$ ppm; Figure 7.2a] arising from $^3J(^1H\text{-}^{19}F) = 6.1$ and $^1J(^1H\text{-}^{15}N) = 86.7$ Hz, and the ^{19}F NMR spectrum consists of a triplet of doublets [$\delta(^{19}F) = 56.78$ ppm; Figure 7.2b] arising from $^2J(^{19}F\text{-}^{15}N) = 2.7$ and $^3J(^{19}F\text{-}^1H) = 6.3$ Hz.

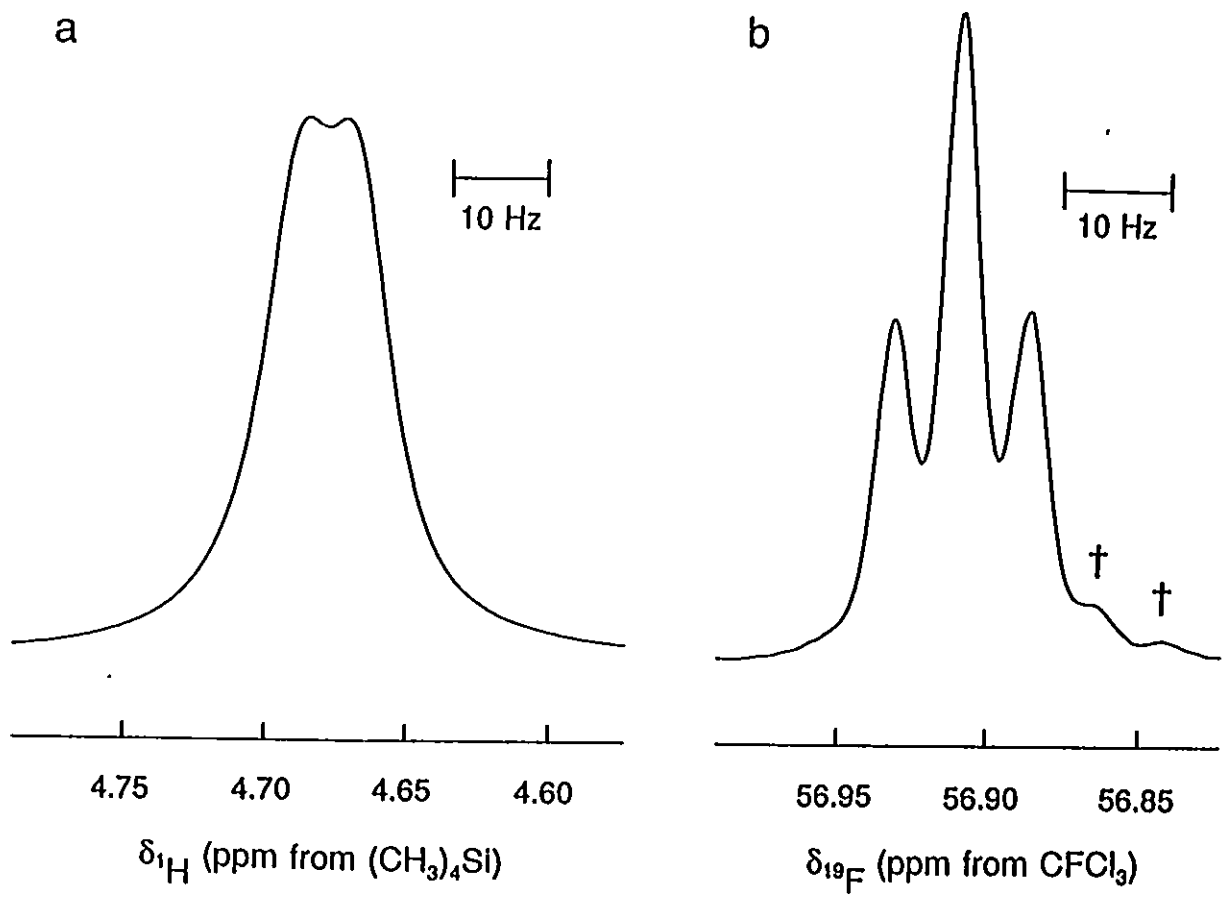

Figure 7.1 (a) ^{1}H NMR (500.138 MHz) and (b) ^{19}F (470.599 MHz) NMR spectra of natural abundance FO_2SNH_2 in BrF_5 solvent recorded at -61.4 °C. Daggers (†) denote F-on-^{34}S(VI) environment.

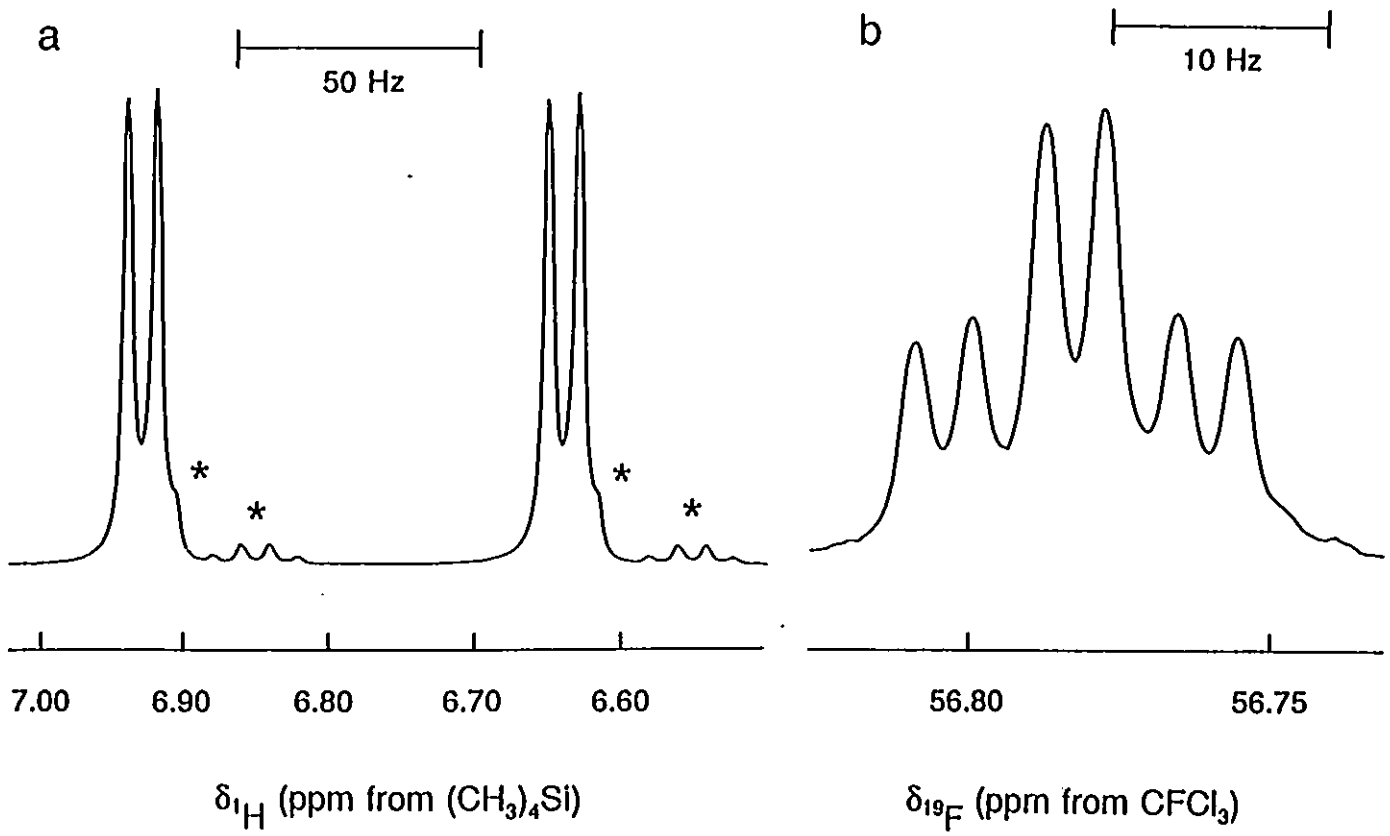

Figure 7.2 (a) ^1H NMR (500.138 MHz) and (b) ^{19}F (470.599 MHz) NMR spectra of 99.5% ^{15}N-enriched FO_2SNH_2 in acetonitrile recorded at 30 °C. Asterisks (*) denote impurities.

The ^1H NMR resonance of natural abundance $FO_2SNH_3^+AsF_6^-$ in BrF_5 solvent at -57.0 °C is a broad quadrupole collapsed singlet at $\delta(^1H)$ = 7.26 ppm. The ^1H chemical shift is deshielded by 2.58 ppm relative to FO_2SNH_2, as expected upon protonation [cf., F_2NH:[291] $\delta(^1H)$ = 7.2 ppm; $F_2NH_2^+$:[173] $\delta(^1H)$ = 14.2 ppm]. The ^1H NMR spectrum of 99.5% ^{15}N-enriched $FO_2SNH_3^+AsF_6^-$ in BrF_5 at -57.0 °C [$\delta(^1H)$ = 7.30 ppm] consists of a doublet arising from the scalar coupling $^1J(^1H\text{-}^{15}N)$ = 72 Hz. The magnitude of $^1J(^1H\text{-}^{15}N)$ is comparable to that observed in other inorganic amine derivatives,[124] and indicates protonation of FO_2SNH_2 at nitrogen but not at oxygen, since the magnitude of the resulting three-bond $^{15}N\text{-}^1H$ coupling would be significantly smaller. The long-range coupling, $^3J(^1H\text{-}^{19}F)$, was not resolved. The ^{19}F NMR resonances in BrF_5 solvent (-57.0 °C) of natural abundance and 99.5% ^{15}N enriched $FO_2SNH_3^+AsF_6^-$ are singlets at $\delta(^{19}F)$ = 56.47 and 56.25 ppm, respectively, with no resolution of the scalar couplings $^2J(^{19}F\text{-}^{15}N)$ and $^3J(^{19}F\text{-}^1H)$.

Significant decomposition of the salt $FO_2SNH_3^+AsF_6^-$ was observed in BrF_5 solvent at -57.0 °C. Singlets observed in the ^{19}F NMR spectra at $\delta(^{19}F)$ = 32.08 and 70.47 ppm are attributed to decomposition products containing FO_2S- groups. The former singlet is assignable to SO_2F_2, and the latter has not been identified. Integration of the ^{19}F NMR resonances at -57.0 °C indicates that the ratio $FO_2SNH_3^+$:SO_2F_2:X (X = unidentified product) is 1.00:0.63:0.73. The decomposition is believed to involve radical formation since a purple color was initially formed, which faded on mixing to give a clear colorless solution. The NMR resonances were not observed until the unidentified purple material was quenched. The AX_4 pattern of BrF_5 solvent is not exchange broadened. The ^1H NMR spectrum at -57.0 °C in BrF_5 solvent indicates the presence of several additional exchange broadened lines at $\delta(^1H)$ = 5.6, 5.2, 3.4, 2.9 and 2.3 ppm. The broad resonance at 5.6 ppm is attributed to HF, and the peak at 5.2 ppm is assigned to FO_2SNH_2,

indicating deprotonation of $FO_2SNH_3^+$. The resonances at 3.4, 2.9 and 2.3 ppm are assigned to H-on-N environments of oxidation products of the $FO_2SNH_3^+$ cation, where BrF_5 is the oxidizing agent. It is not possible to identify the nitrogen-containing oxidation products from the ^1H NMR resonances since no couplings are observed and exchange may affect the ^1H chemical shifts. By analogy with the decomposition of $F_5TeNH_3^+$ in BrF_5 (Chapter 6), likely nitrogen-containing decomposition products include NH_4^+, N_2, HN_3, N_2H_4, and N_2H_2. Deprotonation of the $FO_2SNH_3^+$ cation may involve proton exchange equilibria with the nitrogen-containing decomposition products [equation (7.11)]

$$FO_2SNH_3^+ + N_xH_y \rightleftharpoons FO_2SNH_2 + N_xH_{y+1}^+ \qquad (7.11)$$

(C) RAMAN SPECTROSCOPIC STUDY OF NATURAL ABUNDANCE AND 99.5% ^{15}N-ENRICHED FO_2SNH_2

The Raman spectra of liquid natural abundance and 99.5% ^{15}N-enriched FO_2SNH_2 were obtained at room temperature. Figure 7.3 depicts the Raman spectrum of FO_2SNH_2, and the frequencies are listed in Table 7.1. A total of 3N - 6 = 15 modes are expected for FO_2SNH_2. Without making assumptions about the orbitals involved in the S-N bond, the mutual orientation of the FO_2S- and -NH_2 groups could not be predicted. Therefore, in Table 7.1 the bands were assigned by treating the FO_2SN- and -SNH_2 groups as separate entities of C_s point symmetry, each having 9 and 6 vibrational modes, respectively, and by analogy with a previous infrared study of FO_2SNH_2 by Semmoud and Vast.[130] Since the highest symmetry for FO_2SNH_2 is C_s, all modes are infrared and Raman active.

The nine vibrational modes of the FO_2SN- group belong to the irreducible representations

Figure 7.3 Raman spectrum of neat liquid natural abundance FO_2SNH_2 recorded at 25 °C by use of 514.5-nm excitation.

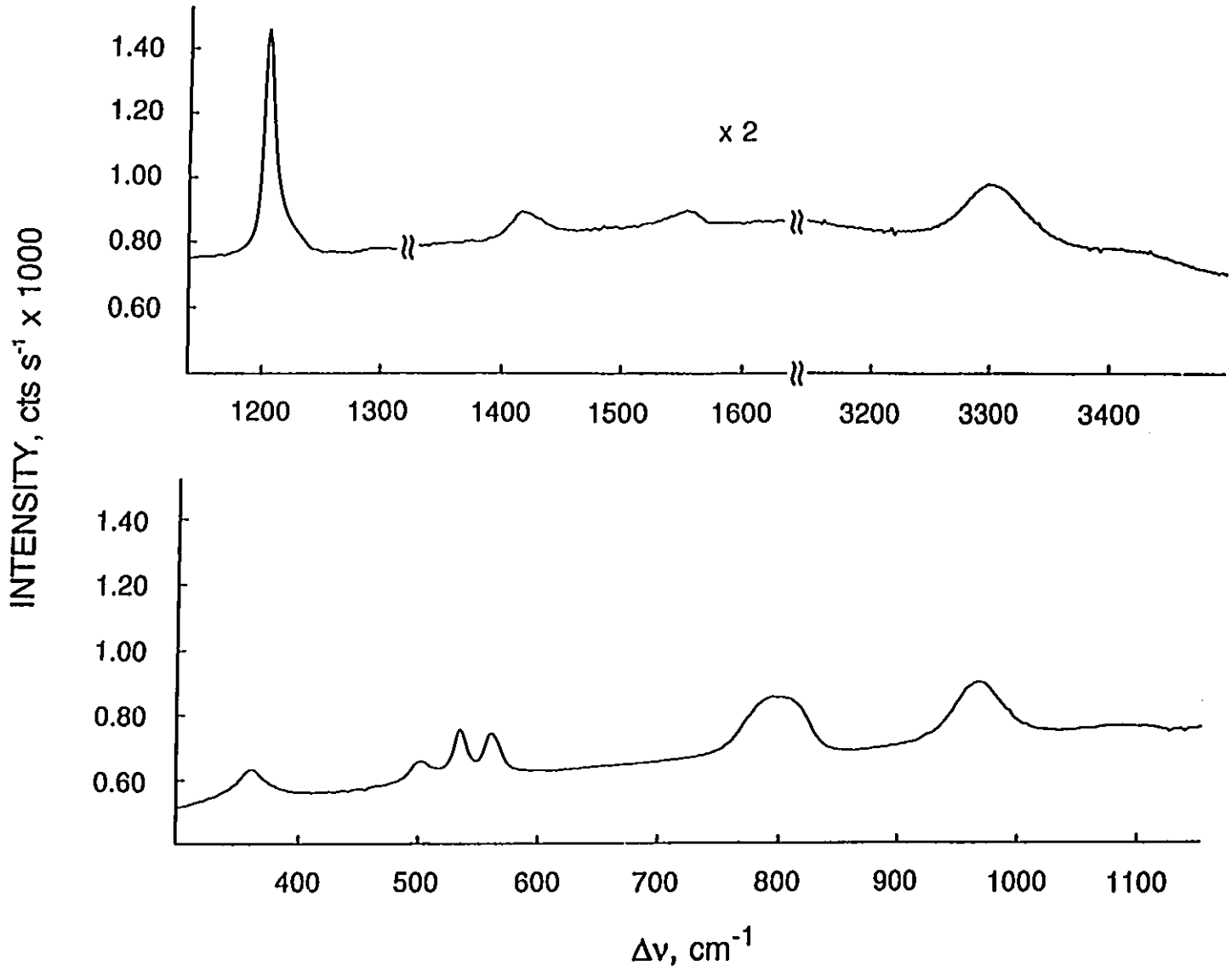
INTENSITY, cts s-1 x 1000
1.40
1.20
1.00
0.80
0.60
x 2
1200
1300
1400
1500
1600
3200
3300
3400
1.40
1.20
1.00
0.80
0.60
400
500
600
700
800
900
1000
1100
Δν, cm-1

Figure 7.4 Raman spectrum (300 - 1000 cm^{-1} region) of neat liquid 99.5% ^{15}N-enriched (upper trace) and natural abundance (lower trace) FO_2SNH_2 recorded at 25 °C by use of 514.5-nm excitation.

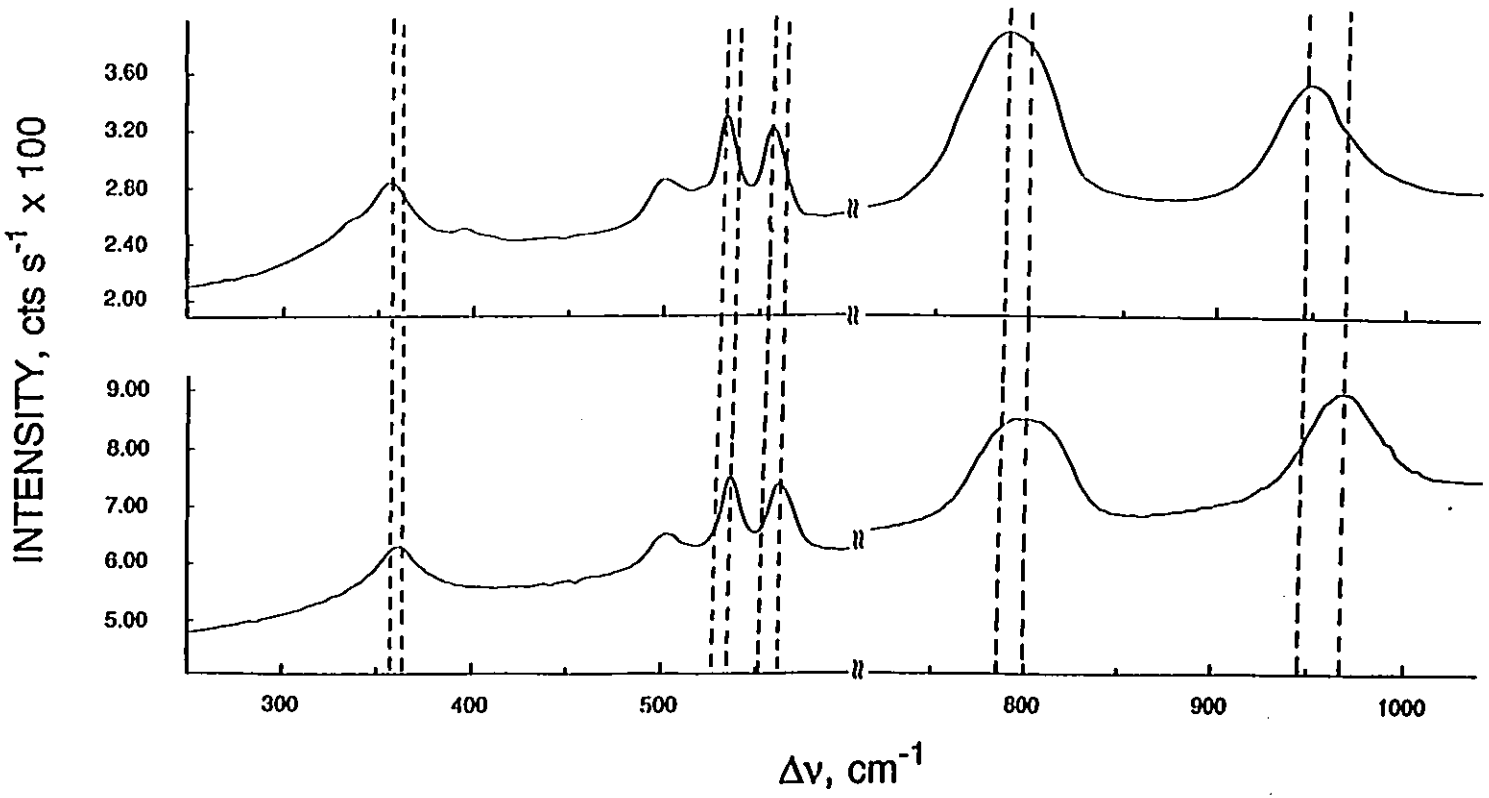
INTENSITY, cts s-1 x 100
3.60
3.20
2.80
2.40
2.00
9.00
8.00
7.00
6.00
5.00
300
400
500
800
900
1000
Δν, cm-1

6 A' + 3 A" and were assigned to bands observed in the Raman spectrum of FO_2SNH_2 (Table 7.1); however, all of the bands in the Raman spectrum of $[^{15}N]FO_2SNH_2$, except those assigned to the symmetric S-O (ν_1) and asymmetric S-O (ν_7) stretching modes (1205.5 and 1417.1 cm^{-1}, respectively) are shifted to lower frequency relative to those in the Raman spectrum of natural abundance FO_2SNH_2 (see Figure 7.4 and Table 7.1). The $^{14/15}N$ isotopic shifts of these bands indicate vibrational coupling of modes that was not implied in the assignments of Semmoud and Vast.[130] This justified a revision of their assignments. Firstly, the bands at 964.5 and 797.2 cm^{-1} were assigned to symmetric S-N and S-F stretching modes in the infrared spectrum of FO_2SNH_2,[130] but because both Raman bands exhibit large $^{14/15}N$ isotopic shifts, it is clear that both bands have contributions from the S-N stretching mode. Thus, the bands at 964.5 and 797.2 cm^{-1} were assigned to asymmetric and symmetric combinations of the S-N and S-F stretching modes. Crow and Lagemann[292] reported a similar coupling of ν(S-Br) and ν(S-F) in the infrared spectrum of FO_2SBrF, referring to asymmetric and symmetric Br-S-F stretches. Gillespie and Robinson[128] chose to treat the S-F and S-Br bonds separately in their assignment of the vibrational spectrum of SO_2BrF.

The low frequency bands (360 - 560 cm^{-1}) have also been reassigned in light of the observed $^{14/15}N$ isotopic shifts. The Raman band at 361.0 cm^{-1} [$\Delta\nu(^{14/15}N)$ = -4.3 cm^{-1}] is attributed to the A" torsional mode, which involves torsional motion of the entire FSO_2N- group and is therefore expected to have an $^{14/15}N$ isotopic dependence. Similar frequencies have been assigned for SO_2F_2[128] (360 cm^{-1}) and SO_2Cl_2 (388 cm^{-1}).[128] The Raman band at 560.0 cm^{-1} [$\Delta\nu(^{14/15}N)$ = -3.1 cm^{-1}] was assigned to the in-plane F-S-N bend by analogy with SO_2F_2[128] ($\delta(SF_2)$ = 545 cm^{-1}). The bands at 501.4 [$\Delta\nu(^{14/15}N)$ = -1.2] and 534.5 [$\Delta\nu(^{14/15}N)$ = -1.7] cm^{-1} are attributed to bending and rocking modes of the FSO_2N- group by analogy with SO_2F_2 (545

cm^{-1})[128] and SO_2BrF (497 - 608 cm^{-1}).[128,292] Of these two bands, the band at 534.5 cm^{-1} has the greater $^{14/15}N$ isotopic shift and is, therefore, tentatively assigned to the A' rocking mode [$\rho_r(FO_2SN\text{-})$] since this mode involves motion of the entire FO_2SN- group. The ν_2 [$\delta_{sym}(SO_2)$] and ν_8 [ρ_r (SO_2)] modes are tentatively assigned to the band at 501.4 cm^{-1}.

The six modes of the -SNH_2 group of FO_2SNH_2 belong to the irreducible representations 4 A' + 2 A" and all but one are assignable to bands in the Raman spectrum (Figure 7.3 and Table 7.1), by analogy with the vibrational assignments for FNH_2[239], $ClNH_2$[257] and aniline $C_6H_5NH_2$.[232] The S-N stretch is identical with ν_3 of the FO_2SN- group and is not repeated. The symmetric (ν_{10}) and asymmetric (ν_{13}) stretches of the NH_2 group are assigned to the broad bands at 3422 and 3298 cm^{-1}, which are characteristic for primary amines.[250] The symmetric NH_2 bend (ν_{12}) and the symmetric S-N-H bend (ν_{11}) are observed at 1553.6 and 1088.1 cm^{-1}, respectively. An $^{14/15}N$ isotopic shift is not observed for ν_{11} because of the presence of bands from organic impurities in this region of the Raman spectrum of 99.5% ^{15}N-enriched FO_2SNH_2 (see Chapter 2). A band attributable to the NH_2 wag, ν_{14} [δ_{asym}(SNH)] was not observed although it is expected at *ca.* 1200 cm^{-1} by analogy with FNH_2 (1233 cm^{-1}).[239] A band attributable to this mode is not observed in the infrared spectrum of $ClNH_2$.[257]

Table 7.1. Raman Spectra and Assignments for $[^{14}N]FO_2SNH_2$ and $[^{15}N]FO_2SNH_2$.[a]

frequency, cm^{-1}						
$[^{14}N]FO_2SNH_2$ [b]	$[^{15}N]FO_2SNH_2$ [b]	$\Delta\nu(^{14/15}N)$	Molecular Group	Point Group	Assgnt and Approx Mode Description	
			FO_2S-	C_s		
1417.1 (5.7)	1419.4 (6.3)	2.3			A"	ν_7, $\nu_{asym}(SO_2)$
1205.5 (100.0)	1206.1 (100.0)	0.6			A'	ν_1, $\nu_{sym}(SO_2)$
964.5 (26.9)	947.6 (24.0)	-16.9			A'	ν_{asym} [ν_3, ν(SN) + ν_4, ν(SF)]
797.2 (25.6)	786.9 (36.2)	-10.3			A'	ν_{sym} [ν_3, ν(SN) + ν_4, ν(SF)]
560.0 (19.3)	556.9 (22.8)	-3.1			A'	ν_6, δ(FSN)
534.5 (22.1)	532.8 (26.1)	-1.7			A'	ν_5, $\rho_r(FO_2SN\text{-})$
501.4 (10.1)	500.2 (13.9)	-1.2			A'	ν_2, $\delta_{sym}(SO_2)$
					A"	ν_8, $\rho_r(SO_2)$
361.0 (14.9)	356.7 (18.8)	-4.3			A"	ν_9, FO_2SN- torsion
			$-SNH_2$	C_s		
3422 (5.8)[c]	3404 (2.4)[c]	-18			A'	ν_{10}, $\nu_{sym}(NH_2)$
3298 (26.6)[c]	3295 (10.3)[c]	-3			A"	ν_{13}, $\nu_{asym}(NH_2)$
1553.3 (3.9)	1551.5 (4.0)	-1.8			A'	ν_{12}, $\delta(NH_2)$
1088.1 (4.7)	n.o.[d]				A'	ν_{11}, δ_{sym}(SNH)
n.o.	n.o.				A"	ν_{14}, δ_{asym}(SNH)

Table 7.1 (continued)

[a] Assignments for the modes of the FO_2SN- group have been made assuming C_s symmetry with use of the mode descriptions from reference (292). The assignments for the modes of the -SNH_2 group have been made by assuming C_s symmetry and with use of the mode descriptions from reference (293). Only five of the six normal modes have been tabulated for the SNH_2 group since the sixth, ν(SN) is the same as ν_3 for the FO_2SN- group. [b] Raman spectra obtained at room temperature with use of 514.5-nm excitation. [c]Because of the broadness of the bands attributed to asymmetric and symmetric NH_2 stretching modes, the accuracy of the reported frequencies is estimated to be ± 1 cm^{-1}. [d]Peaks caused by organic impurities are observed in this region.

(D) CHARACTERIZATION OF NATURAL ABUNDANCE AND 99.5 % ^{15}N-ENRICHED $FO_2SNH_3^+AsF_6^-$ BY RAMAN SPECTROSCOPY

The Raman spectra of natural abundance and 99.5 % ^{15}N enriched $FO_2SNH_3^+AsF_6^-$ were obtained at room temperature. Figure 7.5 depicts the Raman spectrum of $FO_2SNH_3^+AsF_6^-$, and the frequencies are listed in Table 7.2. A total of 3N - 6 = 18 modes are expected for the $FO_2SNH_3^+$ cation; the highest possible point symmetry is C_s, so that all modes are both infrared and Raman active. Assignments for the $FO_2SNH_3^+$ cation have been aided by observing the $^{14/15}N$ isotopic shifts in the Raman spectrum of 99.5% ^{15}N-enriched $FO_2SNH_3^+AsF_6^-$ (Table 7.2 and Figure 7.6). Following the procedure for FO_2SNH_2, assignments for the $FO_2SNH_3^+$ cation have been made by treating the FO_2SN- (C_s) and the -SNH_3^+ (C_{3v}) groups separately.

The nine modes of the FO_2SN- group have been assigned following the method used for FO_2SNH_2 (see above). The band at 1503.4 cm^{-1} has been assigned to ν_7, $\nu_{asym}(SO_2)$ by analogy with SO_2F_2 (1502 cm^{-1})[128] and SO_2BrF (1460 cm^{-1}).[128,292] Similarly, comparison with these compounds allows the assignments of the bands at 1270.3, 1259.1 and 1254.8 cm^{-1} to $\nu_{sym}(SO_2)$ (cf., SO_2F_2: 1269 cm^{-1};[128] SO_2BrF: 1228 cm^{-1} [128,292]). The presence of three bands assigned to $\nu_{sym}(SO_2)$ may arise from factor group splitting. The only band assigned to the SO_2 stretching modes which exhibits a measurable $^{14/15}N$ isotopic shift is the most intense band attributed to $\nu_{sym}(SO_2)$ at 1259.1 cm^{-1}. The value of the shift (-0.6 cm^{-1}) is at the detection limit for the $^{14/15}N$ frequency shifts. Therefore these bands do not contain significant contributions from modes that involve the motion of the nitrogen center.

The S-F stretch has been assigned to the band at 862.3 cm^{-1} [cf., SO_2F_2:[128] 885 cm^{-1}], which does not have an $^{14/15}N$ isotopic shift. The bands at 709.9 and 677.2 cm^{-1} exhibit large $^{14/15}N$ isotopic shifts (-5.1 and -2.1 cm^{-1}, respectively) and are similar to ν(SN) for FO_2SNH_2 and

Figure 7.5 Raman spectrum of solid natural abundance $FO_2SNH_3^+AsF_6^-$ recorded at 25 °C by use of 514.5-nm excitation.

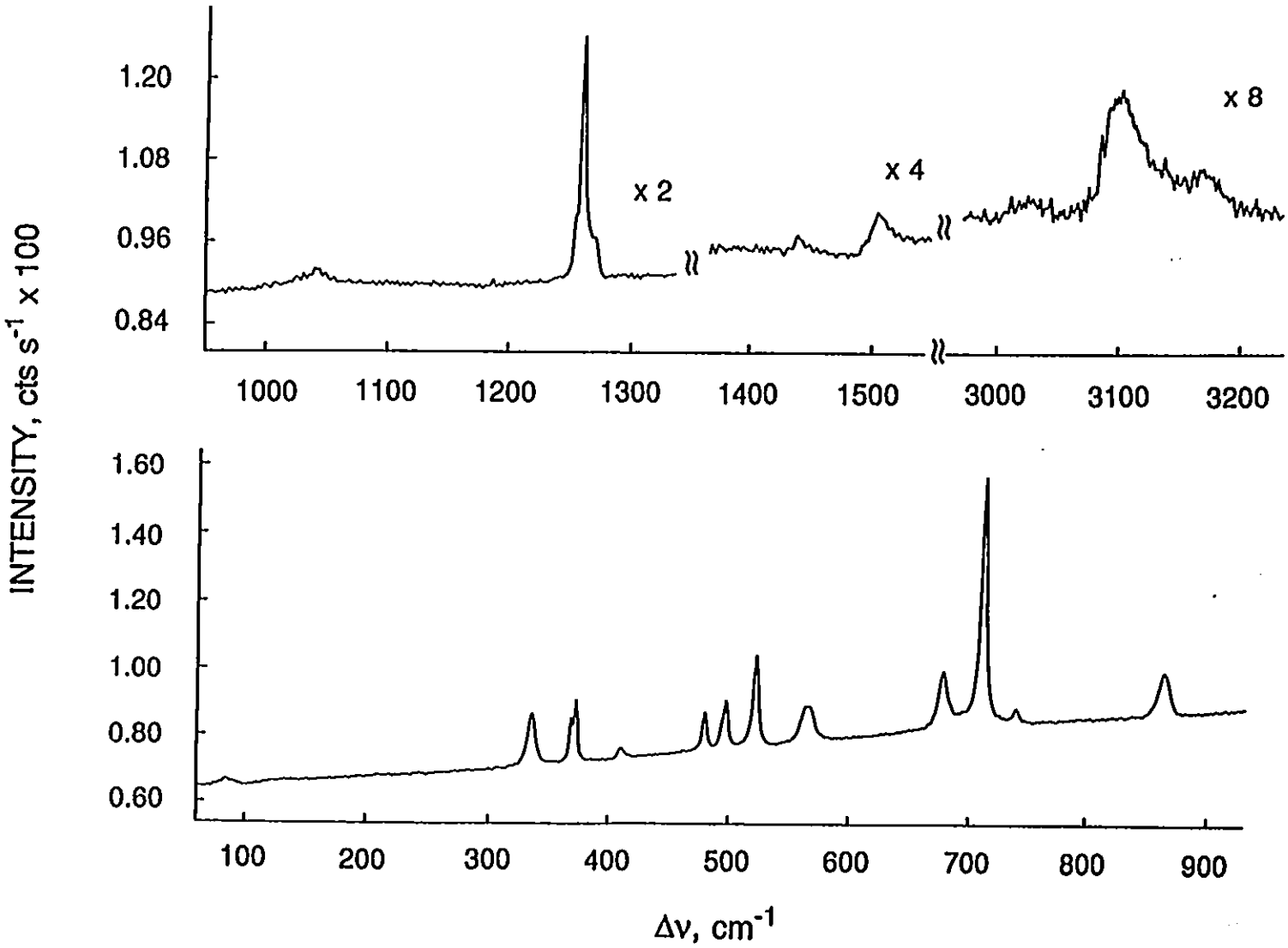
INTENSITY, cts s-1 x 100
1.20
1.08
0.96
0.84
x 2
x 4
x 8
1000
1100
1200
1300
1400
1500
3000
3100
3200
1.60
1.40
1.20
1.00
0.80
0.60
100
200
300
400
500
600
700
800
900
Δν, cm-1

Figure 7.6 Raman spectrum (300 - 750 cm^{-1} region) of solid 99.5% ^{15}N-enriched (upper trace) and natural abundance (lower trace) $FO_2SNH_3^+AsF_6^-$ recorded at 25 °C by use of 514.5-nm excitation.

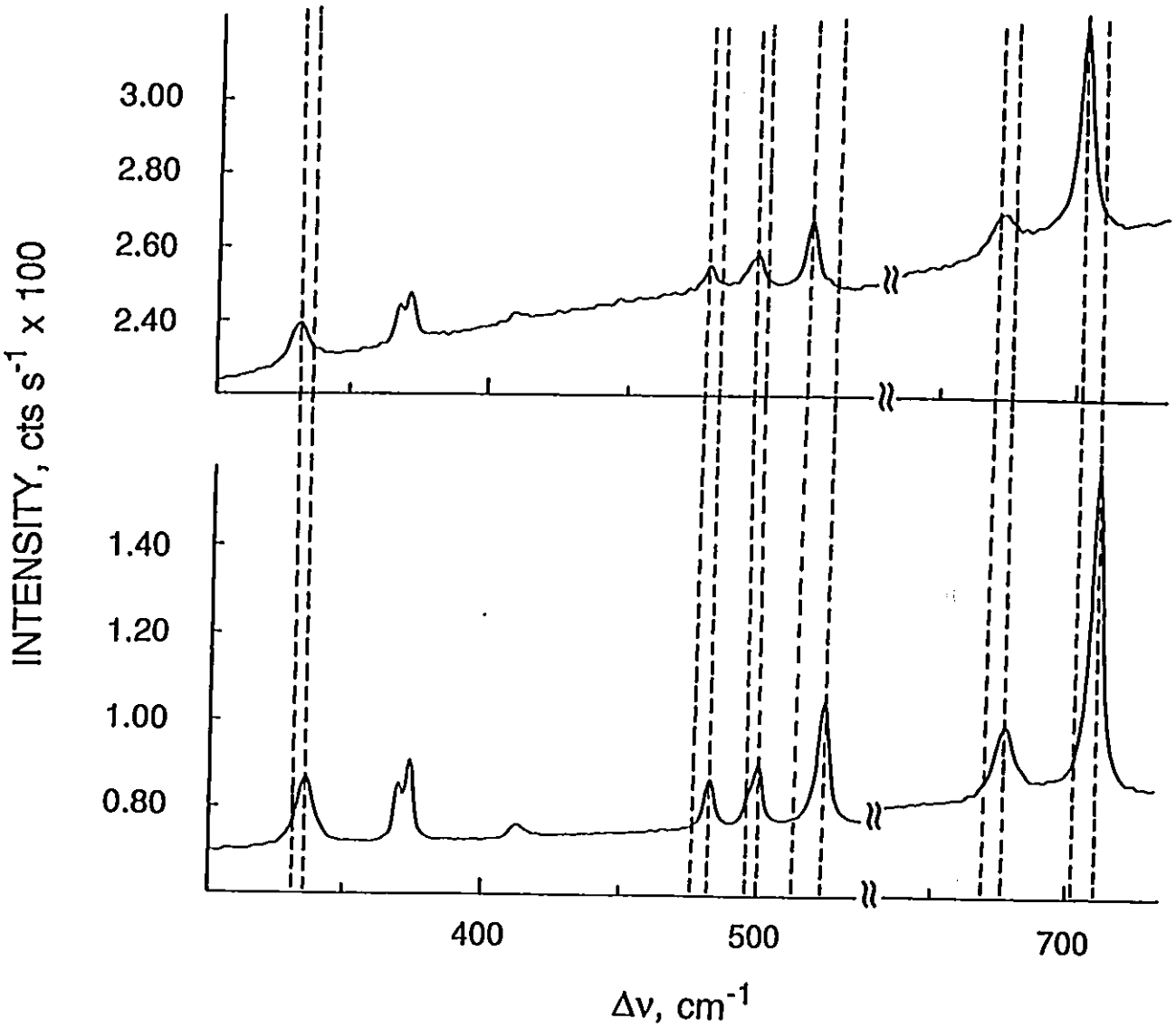
INTENSITY, cts s-1 x 100
3.00
2.80
2.60
2.40
1.40
1.20
1.00
0.80
400
500
700
Δν, cm-1

thus are both assigned to ν_3 [ν(S-N)]. The presence of two bands is attributed to solid state effects.

The band at 521.4 cm^{-1} has the largest $^{14/15}N$ isotopic shift (-5.69 cm^{-1}) of the bands attributable to the bending modes; by analogy with FO_2SNH_2 it is assigned to ν_6, the in-plane F-S-N bend.

The bands at 479.7 and 496.9 cm^{-1} are assigned to the bending modes of the FSO_2N-group, namely ν_2 [$\delta_{sym}(SO_2)$], ν_5 [$\rho_r(FO_2SN\text{-})$; in-plane FSN rock] and ν_8 [SO_2 asymmetric rock]. The rocking motion of the FO_2SN- group is assigned to the band at 496.9 cm^{-1} which has the larger $^{14/15}N$ isotopic shift [-1.1 cm^{-1}] since this mode involves motion of the nitrogen atom. The SO_2 rocking modes, ν_8 [$\delta_{asym}(SO_2)$] and ν_2 [$\delta_{sym}(SO_2)$] are assigned to the band at 479.7 cm^{-1} although these modes may also contribute to the band at 496.9 cm^{-1}. The $^{14/15}N$ isotopic shifts of the bands at 479.7 and 496.9 cm^{-1} imply some vibrational coupling of the SO_2 asymmetric rock and symmetric bending modes with the FO_2SN- rocking and F-S-N bending modes. An exact description of the vibrational coupling would require a normal coordinate analysis, which is not necessary for the assignment of the Raman spectra in the present study.

The band at 334.6 cm^{-1} is assigned to the torsional mode of the FO_2SN- group, which is similar to that observed in FO_2SNH_2 (361.0 cm^{-1}) and SO_2F_2 (388 cm^{-1}).[128]

The nine modes of the $-SNH_3$ group belong to the irreducible representations 3 A_1 + 3 E (C_{3v} point symmetry), all of which are infrared and Raman active. All nine modes have been assigned to bands in the Raman spectrum of $FO_2SNH_3^+AsF_6^-$ (Figure 7.5) and are listed in Table 7.2. The S-N stretching mode is identical to ν_3 of the FO_2SN- group and is not repeated. Fluorescence prevented the observation of the low-intensity bands associated with the $-SNH_3$ group in the Raman spectrum of 99.5% ^{15}N-enriched $FO_2SNH_3^+AsF_6^-$, so that $^{14/15}N$ isotopic

shift data are not available to confirm the bands in the Raman spectrum of the natural abundance $FO_2SNH_3^+AsF_6^-$. However, assignments other than those given are unlikely.

The asymmetric stretching modes are assigned to the peaks at 3168, 3100 and 3024 cm^{-1}, by analogy with $FNH_3^+SO_3F^-$ [294,295] [$\nu_{asym}(NH_2)$ = 3000 cm^{-1}, $\nu_{sym}(NH_2)$ = 2735 cm^{-1}]. Since three peaks are observed, it is not possible to assign the peaks rigorously to the asymmetric and symmetric stretching modes, although $\nu_{asym}(NH_2)$ is usually greater than $\nu_{sym}(NH_2)$.

The bending modes $\delta_{sym}(NH_3)$ [ν_{11}] and $\delta_{asym}(NH_3)$ [ν_{13}] are assigned to the bands at 1438.6 and 1503.4 cm^{-1}, respectively, by analogy with FCH_3[296] [$\delta_{sym}(CH_3)$ = 1460 cm^{-1}; $\delta_{asym}(CH_3)$ = 1468 cm^{-1}] and the FNH_3^+ cation in $FNH_3^+CF_3SO_3^-$[295] [$\delta_{sym}(NH_3)$ = 1523 cm^{-1}; $\delta_{asym}(NH_3)$ = 1585 cm^{-1}]. The rocking mode ν_{14} [ρ_r(SNH)] is assigned to the band at 1040.5 cm^{-1} by analogy with FCH_3 (1183 cm^{-1})[296] and the FNH_3^+ cation (1262 cm^{-1}).[295] The somewhat lower value of $\rho_r(NH_3)$ in the $FO_2SNH_3^+$ cation is expected since the mass of the FO_2S- group is much greater than F in FCH_3 and FNH_3^+.

A total of six bands can be attributed to the AsF_6^- anion (Figure 7.5 and Table 7.2). These bands are best assigned modes which belong to the irreducible representations $A_{1g} + E_g + T_{2g} + 3\ T_{1u}$ under O_h point symmetry by comparison with $M^+AsF_6^-$ salts. (M = O_2,[159] Cs,[297] and OH_3.[171] Bands in the Raman spectrum of $FO_2SNH_3^+AsF_6^-$ are attributable to all modes of AsF_6^- except ν_6 (T_{1u}), which is often not observed[159,171] although it is expected at *ca.* 252 cm^{-1}. The totally symmetric ν_1 (A_{1g}) mode, which usually gives rise to the most intense AsF_6^- band in the Raman spectra of AsF_6^- salts, is believed to overlap with ν(S-N) of the $FO_2SNH_3^+$ cation at 709.9 cm^{-1}. From the number of bands observed, it is clear that the symmetry of the AsF_6^- anion in $FO_2SNH_3^+AsF_6^-$ is lower than O_h, since under O_h symmetry only ν_1, ν_2 and ν_5 are Raman active. However, lowering of the AsF_6^- site symmetry to C_{2v} or lower would result in the observation of

bands attributable to all modes. The lowering of the AsF_6^- symmetry in the solid may result from interactions with the cation through fluorine bridging or from a low site symmetry for AsF_6^- within the unit cell. Of the doubly or triply degenerate modes, ν_5 (T_{2g}) is split with unequal intensities and ν_2 (E_g) is broad, indicating that the degeneracy has been removed but the peak separation has not been resolved. Qureshi and Aubke[298] reported a similar splitting of ν_5 in the hexafluoroarsenate salts of several nitrogen cations (ONF_2^+, $N_2F_3^+$, NO^+, NO_2^+) and noted that this mode appeared to be particularly sensitive to site symmetry lowering effects.

The low intensity peak at 83.8 cm^{-1} is attributed to a lattice mode vibration.

Table 7.2. Raman Spectra and Assignments for $[^{14}N]FO_2SNH_3^+AsF_6^-$ and $[^{15}N]FO_2SNH_3^+AsF_6^-$.[a]

frequency, cm^{-1}					
$[^{14}N]FO_2SNH_3^+$ AsF_6^- [b]	$[^{15}N]FO_2SNH_3^+$ AsF_6^- [b]	$\Delta\nu(^{14/15}N)$	Molecular Group	Point Group	Assgnt and approx mode description
			FO_2S-	C_s	
1503.4 (3.8)					A" ν_7, $\nu_{asym}(SO_2)$
1270.3 (sh)	n.o.				A' ν_1, $\nu_{sym}(SO_2)$
1259.1 (48.1)	1258.5 (40.0)	-0.6			A' ν_1, $\nu_{sym}(SO_2)$
1254.8 (sh)	n.o.				A' ν_1, $\nu_{sym}(SO_2)$
862.3 (16.5)	862.1 (17.5)				A' ν_4, ν(SF)
709.9 (100.0)	704.8 (100.0)	-5.1			A' ν_3, ν(SN)
677.2 (23.1)	675.1 (19.5)	-2.1			A' ν_3, ν(SN)
521.4 (35.5)	515.7 (29.9)	-5.7			A' ν_6, δ(FSN)
496.9 (17.9)	495.8 (15.6)	-1.1			A' ν_2, $\delta_{sym}(SO_2)$
479.7 (14.4)	479.1 (12.6)	-0.6			A' ν_5, $\rho_r(FO_2SN\text{-})$
					A" ν_8, $\rho_r(SO_2)$
334.6 (21.0)	332.2 (19.1)	-2.4			A' ν_9, FO_2SN- tortion
					A" ν_8, δ(NSF)
			-SNH_3	C_{3v}	
3167.9 (2.3)					E ν_{12}, $\nu_{asym}(NH_3)$
3100.4 (6.0)					E ν_{12}, $\nu_{asym}(NH_3)$
3024.4 (0.9)					A_1 ν_{10}, $\nu_{sym}(NH_3)$
1503.4 (3.8)					E ν_{13}, $\delta_{asym}(NH_3)$
1438.6 (1.8)					A_1 ν_{11}, $\delta_{sym}(NH_3)$
1040.5 (3.0)					E ν_{14}, $\rho_r(NH_3)$
			AsF_6^-	O_h	
738.6 (5.6)					T_{1u} ν_3
709.9 (100.0)[c]					A_{1g} ν_1
565.6 (13.7)					E_g ν_2
410.3 (4.2)					T_{1u} ν_4

371.9 (25.0)	T_{2g}	ν_5
368.1 (18.0)		
n.o.	T_{1u}	ν_6

[a] Assignments for the modes of the FO_2SN- group have been made by assuming C_s symmetry and with use of the mode descriptions from references (130), (292), and (299). Assignments for the -SNH_3 group have been made by assuming C_{3v} symmetry, and with use of the mode description of reference (300). Only five of the six normal modes of the -SNH_3 group have been tabulated; the sixth is identical to ν_3 for the FO_2SN- group [ν(SN)]. [b] Raman spectra obtained at room temperature by use of 514.5-nm excitation. [c]The totally symmetric ν_1 (A_{1g}) mode is presumed to overlap with the intense band at 709.9 cm^{-1} assigned to ν_3 [ν(SN)] of the $FO_2SNH_3^+$ cation. [d]Because of broadness, the errors associated with the bands assigned to ν_{10} [$\nu_{asym}(NH_3)$] and ν_{12} [$\nu_{sym}(NH_3)$] are estimated to be ± 1 cm^{-1}.

(E) COMPARISON OF THE BONDING IN FO_2SNH_2 AND THE $FO_2SNH_3^+$ CATION BY RAMAN SPECTROSCOPY

The bonding in FO_2SNH_2 and the mercury salt $HgNSO_2F$ was investigated using infrared spectroscopy by Semmoud and Vast.[130] Differences in the S-O, S-F, and S-N bond orders of FO_2SNH_2 and FO_2SNHg, as reflected in the corresponding symmetric infrared stretching frequencies, was investigated and compared with several sulfur(VI) oxyacid derivatives. The present Raman spectroscopic study of FO_2SNH_2 and the $FO_2SNH_3^+$ cation provides information that allows the bonding changes resulting from protonation of FO_2SNH_2 to be assessed and related to the work of Semmoud and Vast.[130]

Semmoud and Vast[130] have shown that deprotonation of FO_2SNH_2 to give FO_2SNHg results in decreases in ν_{sym}(S-O) and ν(S-F) by 46 and 37 cm^{-1}, respectively and an increase in ν(S-N) by 70 cm^{-1}, as shown in Table 7.3. This has been explained by invoking $(p\text{-}d)\pi$ bonding involving vacant 3*d* orbitals on sulfur and filled 2*p* orbitals on oxygen and nitrogen.[130] The S-N bond length in FO_2SNH_2, as determined by electron diffraction[286], was 1.60(1) Å, which is significantly shorter than the single bond in H_3NSO_3 [1.7714(3) Å].[287] and has been interpreted as evidence for S-N π bonding.[286] Deprotonation of FO_2SNH_2 increases the availability of 2*p* orbitals on the nitrogen atom for π-bonding to the sulfur atom, resulting in an increase in the S-N bond order, which is reflected in the increase in ν(S-N). The S-O bonds are weakened since the same 3*d* orbitals on sulfur ($d_{x^2-y^2}$ and d_{z^2}) are used to form S-O π-bonds.[288] The decrease in ν(S-F) may result from an increase in the S-F bond ionic character or a decrease in the S-F π-bonding. As noted by Semmoud and Vast,[130] similar effects are observed for the isoelectronic compounds AgO_3SNH_2 and Ag_3O_3SN. The existence of S-N π-bonding in $O_3SNH_2^-$ is evidenced by the S-N bond length [1.60(1) Å],[285] which is substantially shorter than the S-N single bond in H_3NSO_3[287]

(see above). As shown in Table 7.3, deprotonation of the $H_2NSO_3^-$ anion to give NSO_3^{3-} results in a decrease in ν_{sym}(S-O) by 38 cm^{-1} and an increase in ν_{sym}(S-N) by 134 cm^{-1}, again a result of increased S-N π-bonding.

The higher ν_{sym}(S-O) frequencies for the H_xNSO_2F derivatives relative to the analogous H_xNSO_3 (x = 0, 2, 3) species in Table 7.3 may be explained by use of the resonance structures proposed by Gillespie and Robinson[301] to describe the covalent and ionic contributions to the bonding of sulfuryl compounds (resonance Structures 7.1 and 7.2). The covalent resonance

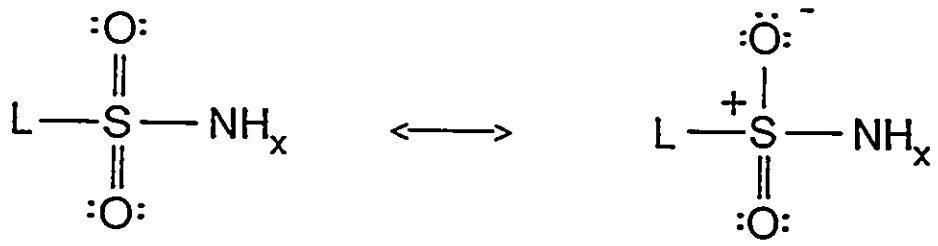

7.1 7.2

Structure 7.1 predominates in the presence of a highly electronegative ligand (L) which increases the electronegativity of sulfur. The greater electronegativity of F compared to O^- therefore results in increased S-O bond orders and correspondingly higher ν_{sym}(S-O) frequencies. In accordance with this, the values of ν_{sym}(S-O) for SO_2F_2 (1269 cm^{-1})[128] and F_2NSO_2F (1250 cm^{-1})[130] are among the highest values known.[301]

The Raman data for $FO_2SNH_3^+AsF_6^-$ extends the comparison of the sulfuryl amides H_xNSO_3 and the fluorosulfuryl amides H_xNSO_2F (x = 0, 2, 3) of Semmoud and Vast.[130] The

similarity of ν_{sym}(S-N) for H_3NSO_3 (680 cm^{-1}) and the $FO_2SNH_3^+$ (709.9 cm^{-1}) indicate similar S-N bond orders (i.e., SN single bonds). The larger value of ν_{sym}(SO) for $FO_2SNH_3^+$ than for H_3NSO_3 is predicted by the dominance of resonance Structure 7.1 over 7.2 (see above).[301] As shown in Table 7.3, protonation of FO_2SNH_2 to give the $FO_2SNH_3^+$ cation lowers ν(S-N) by 254.6 cm^{-1}, while ν(S-F) and ν_{sym}(S-O) are increased by 65.1 and 53.6 cm^{-1}, respectively. The changes in the stretching frequencies are consistent with weakening of the S-N bond and strengthening of the S-O and S-F bonds and are expected since the nitrogen atom lone pair is no longer available for S-N π-bonding upon protonation. Reduction of the S-N π bond order is accompanied by an increase in the S-O π bond order. Fluorine is not expected to be a good π donor to sulfur, thus S-F π bonding is not an appropriate explanation for the increase in ν(S-F). However, protonation of nitrogen is expected to increase the electronegativity of the sulfur center, thus reducing the ionic character and strengthening the S-F bond. The trends observed in ν_{sym}(S-O) and ν_{sym}(S-N) for the FO_2SNH_2 / $FO_2SNH_3^+$ pair parallel those observed for $H_2NSO_3^-$ / H_3NSO_3, indicating that similar bonding changes occur upon protonation of FO_2SNH_2 and $H_2NSO_3^-$.

Table 7.3. Selected Vibrational Frequencies and Bond Lengths of Some Sulfur(VI) Oxyacid Derivatives.

	Vibrational Frequencies, cm^{-1} [a]			Bond Lengths, Å [b]			
	$\nu_{sym}(SO)$	$\nu_{sym}(SN)$	$\nu_{sym}(SF)$	r(SO)	r(SN)	r(SF)	refs
H_3NSO_3	1065	680		1.4389(3)-	1.7714(3) 1.4440(3)		130,287
$H_2NSO_3^-$ [c]	1038	796		1.43(1)	1.60(1)		130,285
Ag_3NSO_3	1000	930					303
$H_3NSO_2F^+$ [d]	1259.1	709.9	862.3				
H_2NSO_2F [d,e]	1205.5	964.5	797.2	1.412(3)	1.61(3)	1.56(2)	286
$HgNSO_2F$	1160	1035	760				130
SO_2F_2 [f]	1269		848	1.405(3)		1.530(3)	128,302
F_2NSO_2F	1250	715	850				130

Table 7.3 (continued)

[a] Vibrational data obtained from infrared spectra unless otherwise specified. [b] Bond lengths obtained from single crystal X-ray diffraction unless otherwise specified. [c] Vibrational data obtained from infrared spectra of AgH_2NSO_3, ref (130). Bond lengths obtained from single crystal X-ray analysis of KH_2NSO_3, ref (285). [d] Vibrational frequencies obtained from Raman spectra; this work. [e] Bond lengths obtained from electron diffraction [ref (286)]. [f] Bond lengths obtained from microwave data [ref (302)].

CHAPTER 8

[FLUOROSULFURYLAMIDO]XENONIUM(II) HEXAFLUOROARSENATE

$FO_2SN(H)\text{-}Xe^+AsF_6^-$

INTRODUCTION

While many examples of compounds containing xenon bonded to oxygen or fluorine and of xenon bonded to other highly electronegative inorganic ligands through oxygen were synthesized immediately following the discovery of noble-gas reactivity,[25] over a decade had elapsed before an example with a ligating atom other than oxygen or fluorine, namely nitrogen, was synthesized[56] and two decades before the Xe-N bond in $FXeN(SO_2F)_2$ was definitively characterized in the solid state by X-ray crystallography and in solution by multinuclear magnetic resonance spectroscopy.[57] Other imidosulfurylfluoride xenon-nitrogen bonded species have since been synthesized and characterized primarily by use of NMR spectroscopy, namely $Xe[N(SO_2F)_2]_2$,[58,59] $F[XeN(SO_2F)_2]_2^+$,[58-60] $XeN(SO_2F)_2^+AsF_6^-$,[60] and $XeN(SO_2F)_2^+Sb_3F_{16}^-$;[60] the last salt has also been characterized by single-crystal X-ray diffraction. The compound, $Xe[N(SO_2CF_3)_2]_2$,[61] has also been prepared and characterized and is the most stable imido derivative of xenon presently known. Recently the scope of xenon-nitrogen chemistry has been dramatically expanded by taking advantage of the Lewis acid properties of noble-gas cations.[26] A significant number of oxidatively resistant nitrogen bases (D) have been shown to form xenon-nitrogen bonded Lewis acid-base adduct cations with XeF^+ of the form $D\text{-}XeF^+$, such as $HC{\equiv}N$,[72,73] alkylnitriles[72] and perfluoroalkylnitriles,[71,72] *s*-trifluorotriazine,[71] pentafluorobenzenenitrile,[72] and perfluoropyridines.[75] The krypton(II) adduct cations, $HC{\equiv}N$-

KrF^+ [78] and $R_FC{\equiv}N\text{-}KrF^+$ (R_F = CF_3, C_2F_5, $n\text{-}C_3F_7$)[71] have also been synthesized and characterized in this laboratory and provide the first examples of krypton bonded to an element other than fluorine.

The present Chapter describes the synthesis and characterization of the [fluorosulfurylamido] xenonium(II) cation, $FO_2SN(H)\text{-}Xe^+$, at low temperature in BrF_5 and HF solvents. The natural abundance and 99.5% ^{15}N-enriched salts, $FO_2SN(H)\text{-}Xe^+AsF_6^-$, have been synthesized in BrF_5 and HF solvents and characterized by ^{19}F, ^1H, and ^{129}Xe NMR spectroscopy.

RESULTS AND DISCUSSION

(A) PREPARATION OF $FO_2SN(H)\text{-}Xe^+AsF_6^-$ IN HF AND BrF_5 SOLVENTS

The reaction of $FO_2SNH_3^+AsF_6^-$ with XeF_2 was carried out according to equation (8.1) by combining stoichiometric amounts of the reactants in BrF_5 solvent and warming to -62 to -58 °C to effect reaction and dissolution, and gave a pale yellow solution. The $FO_2SN(H)\text{-}Xe^+$

$$FO_2SNH_3^+AsF_6^- + XeF_2 \rightleftharpoons FO_2SN(H)\text{-}Xe^+AsF_6^- + 2\ HF \qquad (8.1)$$

cation was significantly decomposed at this temperature. Alternately, $FO_2SN(H)\text{-}Xe^+AsF_6^-$ was generated according to equation (8.2) by combining stoichiometric amounts of FO_2SNH_2 and

$$FO_2SNH_2 + XeF^+AsF_6^- \rightleftharpoons FO_2SN(H)\text{-}Xe^+AsF_6^- + HF \qquad (8.2)$$

$XeF^+AsF_6^-$ in HF solvent and warming to -50 °C to effect reaction. A pale yellow solution above

white and yellow solids was present at this temperature; complete decomposition of the $FO_2SN(H)\text{-}Xe^+$ cation occurred after *ca.* 1 hour. Warming of reaction mixtures to -35 °C resulted in complete decomposition within *ca.* 30 seconds. Decomposed samples invariably consisted of a colorless supernatant and a white precipitate. As a result of the instability and relatively low concentration of $FO_2SN(H)\text{-}Xe^+AsF_6^-$ in BrF_5 and HF solvents, no attempt was made to isolate the salt.

(B) CHARACTERIZATION OF $FO_2SN(H)\text{-}Xe^+AsF_6^-$ BY ^{129}Xe, ^1H AND ^{19}F NMR SPECTROSCOPY

The ^{129}Xe, ^1H and ^{19}F NMR spectra of the natural abundance and 99.5% ^{15}N-enriched $FO_2SN(H)\text{-}Xe^+$ cation in solution are consistent with the xenon-nitrogen bonded structure illustrated in Structure 8.1.

The ^{129}Xe NMR spectrum of the $FO_2SN(H)\text{-}Xe^+$ cation in BrF_5 solvent (-57.7 °C) consists of a singlet at -2663 ppm ($\Delta\nu_{1/2}$ = 222 Hz) as shown in Figure 8.1a. The ^{129}Xe resonance was observed at $\delta(^{129}Xe)$ = -2616 ppm ($\Delta\nu_{1/2}$ = 183 Hz) in HF solvent at -48.9 °C, but the presence of undissolved material in the HF sample resulted in an irregular line shape. Attempts to dissolve the solid material by warming the HF sample to -35 °C resulted in rapid (*ca.* 30 seconds) decomposition of the $FO_2SN(H)\text{-}Xe^+$ cation, as shown by the disappearance of the ^{129}Xe resonance. As a result, all further work was performed in BrF_5 solvent, in which the reagents were soluble at lower temperatures. The absence of any resolved couplings in the ^{129}Xe NMR spectra is consistent with the absence of an Xe-F bond, since the range of the one-bond scalar couplings, $^1J(^{129}Xe\text{-}^{19}F)$, for xenon(II) is 7594 (XeF^+ in SbF_5 solvent, 25 °C)[108] to 5621 Hz (XeF_2 in BrF_5 solvent, -52 °C),[71] which is much greater than the line widths of the ^{129}Xe resonances for the

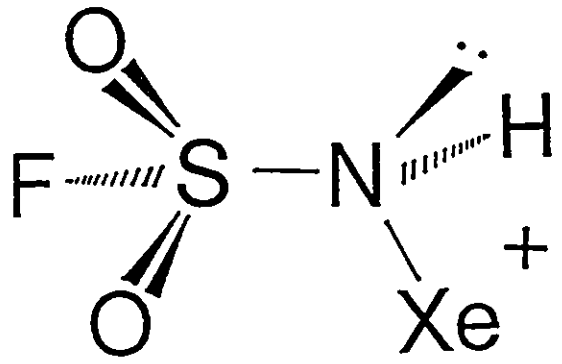

8.1

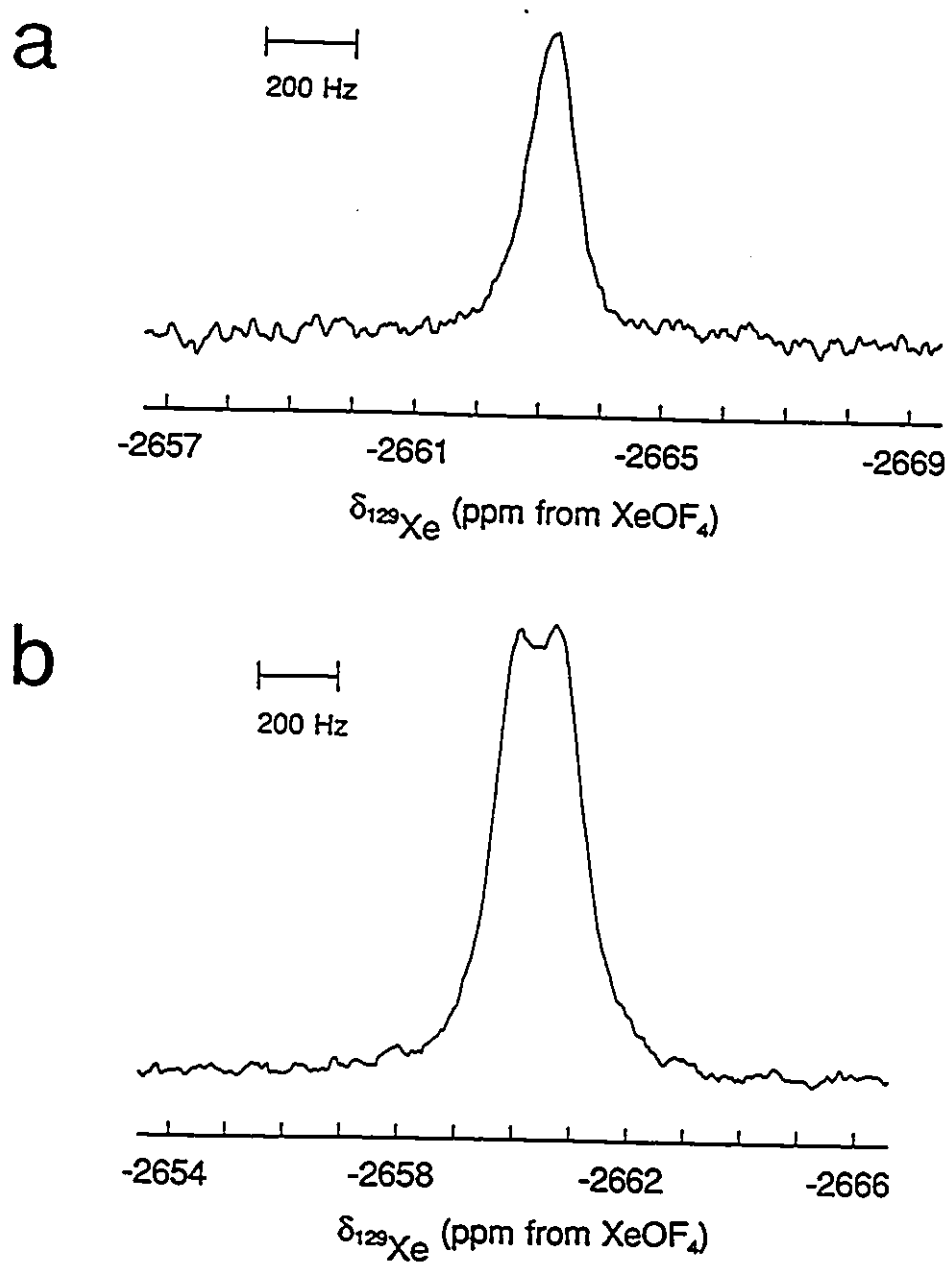

Figure 8.1 ^{129}Xe NMR spectra (139.051 MHz) of (a) natural abundance $FO_2SN(H)\text{-}Xe^+AsF_6^-$ recorded at -57.7 °C and (b) 99.5% ^{15}N-enriched $FO_2SN(H)\text{-}Xe^+AsF_6^-$ recorded at -61.0 °C in BrF_5 solvent.

$FO_2SN(H)$-Xe^+ cation. The ^{129}Xe NMR chemical shift is similar to that observed for xenon(II)-nitrogen bonded cations in which the group electronegativity of the ligand is relatively low [see Section (C) of this Chapter]. Examples include $F_5TeN(H)$-Xe^+ [$\delta(^{129}Xe)$ = -2902 ppm; see Chapter 5], $F_5SN(H)$-Xe^+ [$\delta(^{129}Xe)$ = -2886 ppm],[26,180] and $F_4S{=}N$-Xe^+ [$\delta(^{129}(Xe)$ = -2672 ppm].[26,180] The Xe-F bonds for all of these species are ionized in solution.

The one-bond Xe-N scalar coupling is not observed in the ^{129}Xe NMR spectra of natural abundance $FO_2SN(H)$-$Xe^+AsF_6^-$ in HF and BrF_5 solvents because of quadrupolar collapse of the Xe-N scalar coupling caused by the rapid relaxation of the directly bonded ^{14}N nucleus (I = 1) in an asymmetric electric field. The geometry at nitrogen in $FO_2SN(H)$-Xe^+ may be pyramidal or planar depending on the relative contributions of resonance Structures 8.2 - 8.4. Resonance Structure 8.2 represents a pure σ contribution to Xe-N and S-N bonding. Dominance of this resonance structure implies formal sp^3-hybridization with a pyramidal nitrogen geometry. The presence of a lone pair of electrons is expected to result in a significant efg at the nitrogen nucleus. Resonance Structures 8.3 and 8.4 represent Xe-N and S-N π bonding contributions, which imply a trigonal planar, formally sp^2-hybridized nitrogen center. Evidence in favor of xenon(II)-ligand π-bonding is provided in the ^{19}F and ^{13}C NMR spectra of the xenon-carbon bonded cations R-Xe^+ (R = C_6F_5-Xe^+,[95,99] 2,4,6-$F_3C_6H_2$-Xe^+,[98] 2,6-$F_2C_6H_3Xe^+$,[253] 2-FC_6H_4-Xe^+ [253] and 4-FC_6H_4-Xe^+ [253]), where the deshieldings of the aryl fluorine ^{19}F and aryl carbon ^{13}C NMR resonances in the 2, 4 and 6 positions on the aryl ring are consistent with xenon-carbon π-bonding.[98,253] Resonance Structure 8.4 represents the contribution of sulfur-nitrogen π-bonding, which may be significant by analogy with the $(FO_2S)_2NXe^+Sb_3F_{16}^-$ cation,[60] in which the trigonal planar nitrogen geometry and the S-N bond lengths [1.68(1) - 1.70(1) Å] that are significantly less than S-N single bonds [cf., O_3SNH_3: S-N = 1.7714(3) Å][287] indicate substantial S-N π-bonding

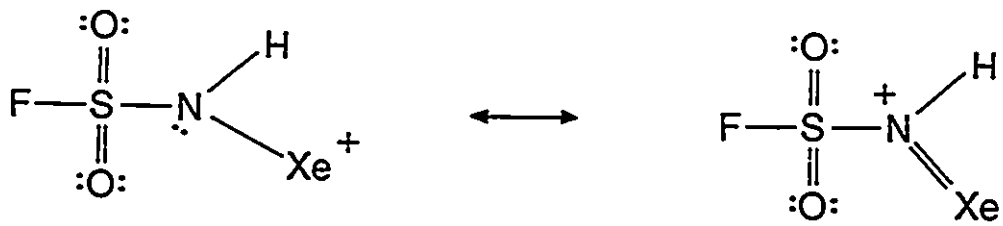

8.2 8.3

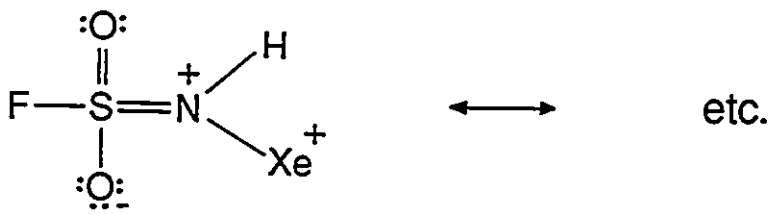

etc.

8.4

and formal sp^2-hybridization at the nitrogen atom. The trigonal planar nitrogen geometries in the related imidofluorosulfuryl xenon(II) compounds $FXeN(SO_2F)_2$,[57] $XeN(SO_2F)_2^+$ [60] and $Xe[N(SO_2F)_2]$[59] all have significant electric field gradients at nitrogen, resulting in rapid relaxation of the ^{14}N nuclei so that the ^{14}N NMR chemical shifts and the xenon-nitrogen scalar couplings were not observed. Nitrogen-15 enrichment was necessary to observe the xenon-nitrogen scalar couplings in these compounds. In the present study ^{15}N-enrichment of the $FO_2SN(H)$-Xe^+ cation was also required to observe the xenon-nitrogen scalar coupling. The ^{129}Xe NMR spectrum of 99.5% ^{15}N-enriched $FO_2SN(H)$-$Xe^+AsF_6^-$ in BrF_5 solvent at -61.0 °C (Figure 8.1b) consists of a doublet arising from $^1J(^{129}Xe\text{-}^{15}N)$ = 109 Hz [^1K(Xe-N) = 0.322 x 10^{22} $NA^{-2}m^{-3}$] centered at $\delta(^{129}Xe)$ = -2660 ppm [$\Delta\nu_{1/2}$ ≈ 63 Hz]. As shown in Table 8.1, the value of the reduced coupling constant, ^1K(Xe-N), for $FO_2SN(H)$-Xe^+ is similar in magnitude to those observed in related cations containing xenon-nitrogen bonds [cf., $F_5TeN(H)$-Xe^+ (see Chapter 5): 0.401 x 10^{22} $NA^{-2}m^{-3}$; $(FO_2S)_2N$-Xe^+:[60] 0.272 x 10^{22} $NA^{-2}m^{-3}$). The alternative xenon-oxygen bonded structure for the cation, namely FO(NH)SO-Xe^+, is shown in Structure 8.5, and may be discarded because the magnitude of the xenon-nitrogen scalar coupling is similar to known values of ^1K(Xe-N). The magnitude of ^2K(Xe-N) in the hypothetical xenon-oxygen bonded cation is expected to be less than that observed. Although no two bond xenon-nitrogen coupling constants are known for comparison, the one- and two-bond xenon-carbon coupling constants observed for $(CH_3)_3CC{\equiv}C$-Xe^+ [101] are 120 and 79 Hz, respectively, illustrating the expected decrease in magnitude. The hypothetical xenon-oxygen bonded cation is also unlikely since all xenon(II) derivatives of $HN(SO_2F)_2$ contain exclusively xenon-nitrogen bonds in solution [cf., $FXeN(SO_2F)_2$,[57,58] $Xe[N(SO_2F)_2]_2$[58,59] and $XeN(SO_2F)_2^+$ [60]]. The line width of the ^{129}Xe

Table 8.1. Comparison of ^{129}Xe NMR Chemical Shifts and One-Bond Xenon-Nitrogen Reduced Coupling Constants of Some Compounds Containing Xenon(II)-Nitrogen Bonds.[a]

Species	$\delta(^{129}Xe)$, (ppm)	Hybridization at Nitrogen	$^{1}K(Xe\text{-}N)$ (10^{22} $NA^{-2}m^{-3}$)	T (°C)	Ref.
$HC{\equiv}N\text{-}XeF^{+}$	-1555 (-1570)	*sp*	1.381[b]	-10 (-58)	72,73
$s\text{-}C_3F_3N_2N\text{-}XeF^{+}$	-1808 (-1863)	sp^2	1.013	-5 (-50)	71
$C_5F_5N\text{-}XeF^{+}$	-1872 (-1922)	sp^2	0.983	-30 (-30)	75
$(FO_2S)_2N\text{-}XeF$[c]	-2009	sp^2	0.913[b]	-40	59
$(FO_2S)_2N\text{-}Xe^{+}$ [d]	-1943	sp^2	0.272[b]	25	60
$FO_2SN(H)\text{-}Xe^{+}$	-2616 (-2660)	sp^2 or sp^3	0.322[b]	-61	This work
$F_4S{=}N\text{-}Xe^{+}$	-2672	sp^2		-20	26,180
$F_5TeN(H)\text{-}Xe^{+}$	-2840 (-2902)	sp^3	0.401[b]	-45	e
$F_5SN(H)\text{-}Xe^{+}$	-2886	sp^3		-20	26,180

[a] ^{129}Xe NMR parameters, unless otherwise indicated, were determined in HF and in BrF_5 (in parentheses) solvent. [b] Recorded for the ^{15}N enriched cation. [c] Measured in SO_2ClF solvent. [d] Measured in SbF_5 solvent. [e] Chapter 5 of this work.

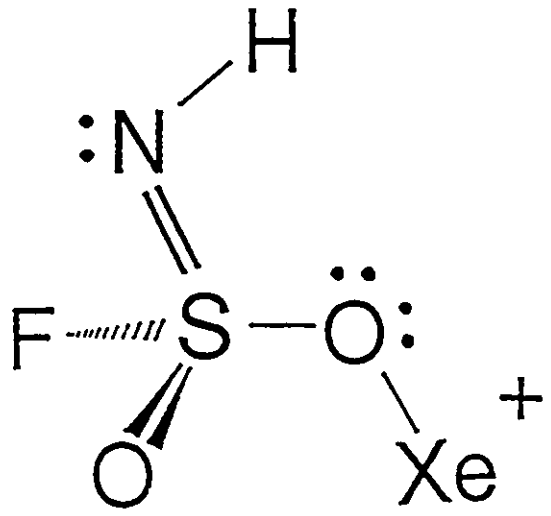

8.5

resonance is larger than previously known examples of the long range couplings $^2J(^{129}Xe\text{-}^1H)$ [cf., $F_5TeN(H)\text{-}Xe^+$ (Chapter 5), 24 Hz] and $^3J(^{129}Xe\text{-}^{19}F)$ [cf., $FXeN(SO_2F)_2$,[58] 18 Hz], so that they are not resolved.

The large line width of the ^{129}Xe NMR resonance for the $FO_2SN(H)\text{-}Xe^+$ cation results primarily from SA induced relaxation of ^{129}Xe, and is analogous to the $(FO_2S)_2N\text{-}Xe^+$ cation in SbF_5 solvent.[60] The SA broadening is proportional to B_o^2, where B_o is the strength of the external magnetic field used in the NMR experiment. Since the present ^{129}Xe NMR experiments were conducted with use of an 11.7440 T magnet, the SA broadening is significant. This is exemplified by the magnetic field dependence of the ^{129}Xe NMR line width for 30% ^{15}N-enriched $(FO_2S)_2NXe^+$ in SbF_5 solvent.[6] At an external field strength of 5.8719 T, the linewidth of the ^{129}Xe resonance was 139 Hz, and the $^{129}Xe\text{-}^{15}N$ scalar coupling was not resolved. At 2.3488 T, the linewidth was significantly reduced and the $^{129}Xe\text{-}^{15}N$ scalar coupling was resolved. Resolution of $^2J(^{129}Xe\text{-}^1H)$ and $^3J(^{129}Xe\text{-}^{19}F)$ in the ^{129}Xe NMR spectrum of 99.5% ^{15}N-enriched $FO_2SN(H)\text{-}Xe^+$ may be attained by use of a lower field strength. The field dependence of the ^{129}Xe NMR line width for the related $F_5TeN(H)\text{-}Xe^+$ cation is discussed in Chapter 5.

The ^1H NMR spectrum of the equilibrium mixture resulting from the reaction of equimolar amounts of natural abundance $FO_2SNH_3^+AsF_6^-$ and XeF_2 in BrF_5 solvent at -57.8 °C is shown in Figure 8.2. The initial concentrations of XeF_2 and $FO_2SNH_3^+$ were 1.12 and 0.974 M, respectively. The $FO_2SN(H)\text{-}Xe^+$ cation is assigned to the quadrupole collapsed singlet at $\delta(^1H) = 7.95$ ppm. It is deshielded by 0.58 ppm relative to the $FO_2SNH_3^+$ cation, which is also a quadrupole collapsed singlet, observed at $\delta(^1H) = 7.37$ ppm. The presence of both $FO_2SNH_3^+$ and $FO_2SN(H)\text{-}Xe^+$ is consistent with equilibrium (8.1). Integration of the ^1H NMR resonances indicates that the ratio $[FO_2SNH_3^+] : [FO_2SN(H)Xe^+]$ is 8 : 1. The singlets observed at 9.35 and

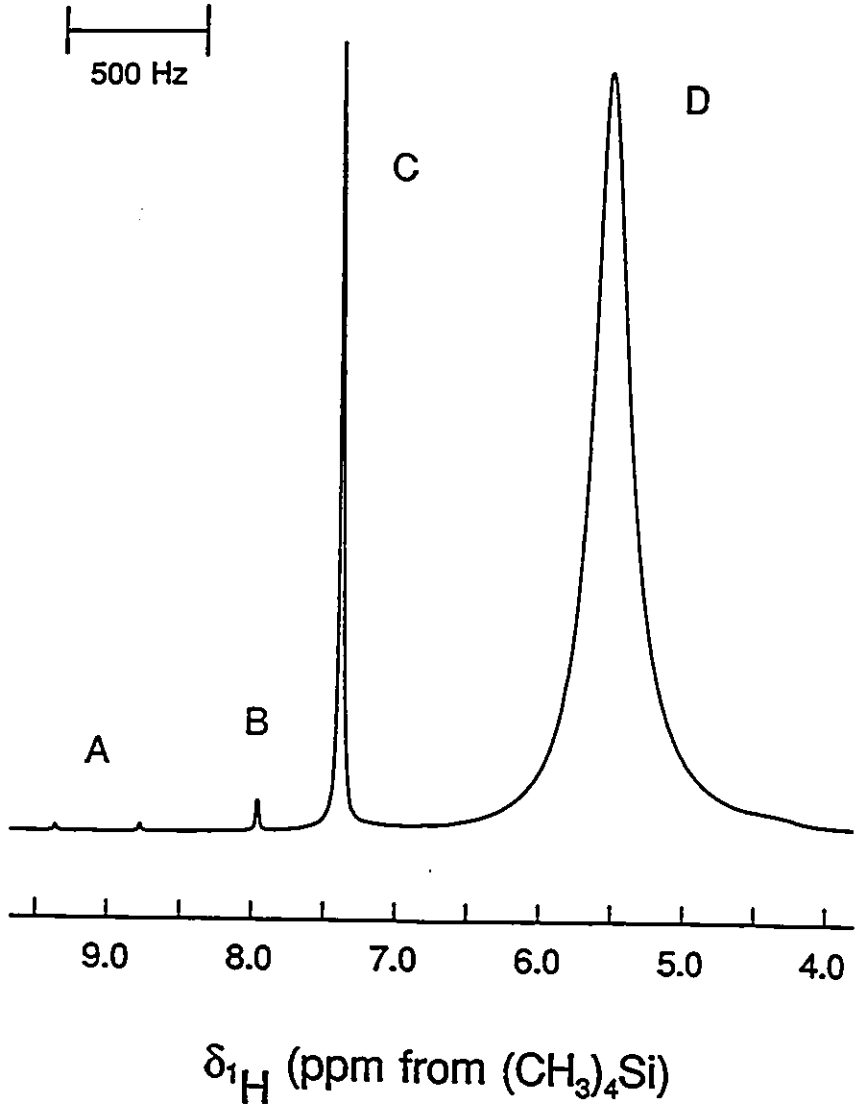

Figure 8.2 ^1H NMR spectrum (500.138 MHz) of the equilibrium mixture arising from the reaction of natural abundance $FO_2SNH_3^+AsF_6^-$ and XeF_2 in BrF_5 solvent recorded at -57.8 °C; (A) unidentified singlets, possibly divalent nitrenium ions, $RR'N:^+$, (B) $FO_2SN(H)\text{-}Xe^+$, (C) $FO_2SNH_3^+$, (D) HF.

8.77 ppm cannot be definitely assigned but may arise from small amounts of divalent nitrenium ions[304] such as $FO_2SN(H):^+$, which are likely decomposition products in the elimination of xenon gas from the $FO_2SN(H)$-Xe^+ cation (see decomposition of $F_5TeN(H)$-Xe^+ in Chapter 6). No NMR data has been obtained for nitrenium ions in solution, but one would expect that the ^1H NMR resonance for $FO_2SN(H):^+$ would be highly deshielded. Other resonances observed in the ^1H NMR spectrum include a broad singlet attributed to exchanging HF at 6.03 ppm [$\Delta\nu_{1/2}$ = 146 Hz], and broad resonances without fine structure at 4.94, 3.31 and 2.58 ppm, which are attributed to rapidly exchanging H-on-N environments resulting from oxidative attack on the $FO_2SNH_3^+$ cation by BrF_5 solvent (see Chapter 7).

The ^1H NMR spectrum of 99.5% ^{15}N-enriched $FO_2SN(H)$-$Xe^+AsF_6^-$ in BrF_5 at -59.9 °C consists of a doublet arising from $^1J(^1H\text{-}^{15}N)$ = 72 Hz centered at $\delta(^1H)$ = 7.48 ppm (Figure 8.3). The magnitude of $^1J(^1H\text{-}^{15}N)$ for the ^{15}N-enriched $FO_2SN(H)$-Xe^+ cation is comparable to other ^{15}N-enriched inorganic amines, such as $[(CH_3)_3Si]_2{}^{15}NH$ (66.5 Hz)[124] and $[CF_3S]_2{}^{15}NH$ (99.1 Hz).[124] A value of $^1J(^1H\text{-}^{15}N)$ = 62 Hz is also observed in the related $F_5Te^{15}N(H)$-Xe^+ cation (Chapter 5). Satellite peaks arising from $^2J(^1H\text{-}^{129}Xe)$ = 16 Hz were also observed in the ^1H NMR spectrum of the $FO_2S^{15}N(H)$-Xe^+ cation, as seen in Figure 8.3 [cf., $F_5Te^{15}N(H)$-Xe^+ (Chapter 5): $^2J(^{129}Xe\text{-}^1H)$ = 24 Hz].

The ^{19}F NMR spectrum of the identical sample used to obtain the ^1H NMR spectrum of natural abundance $FO_2SN(H)$-Xe^+ in BrF_5 solvent at -57.8 °C is shown in Figure 8.4. The singlets at 57.45 and 56.25 ppm are attributed to the fluorine-on-sulfur(VI) resonances of $FO_2SN(H)$-Xe^+ and $FO_2SNH_3^+$, respectively. Integration of these resonances indicates a ratio $[FO_2SNH_3^+]$: $[FO_2SN(H)\text{-}Xe^+]$ of 8 : 1. The ^{19}F integrations are in agreement with those from the ^1H NMR spectrum (see above), so that the number of hydrogens and fluorines is consistent with the

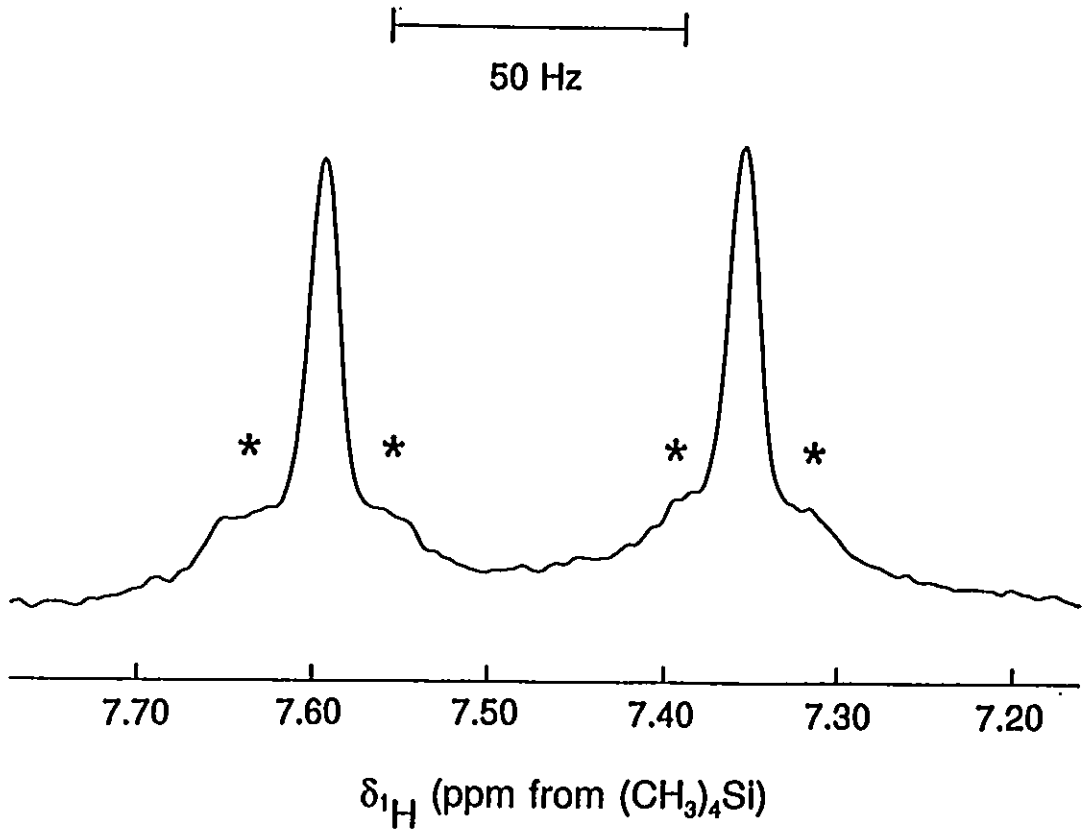

Figure 8.3 ^{1}H NMR spectrum (300.144 MHz) of 99.5% ^{15}N-enriched $FO_2SN(H)\text{-}Xe^+$ recorded at -59.9 °C in BrF_5 solvent. Asterisks (*) denote ^{129}Xe satellites.

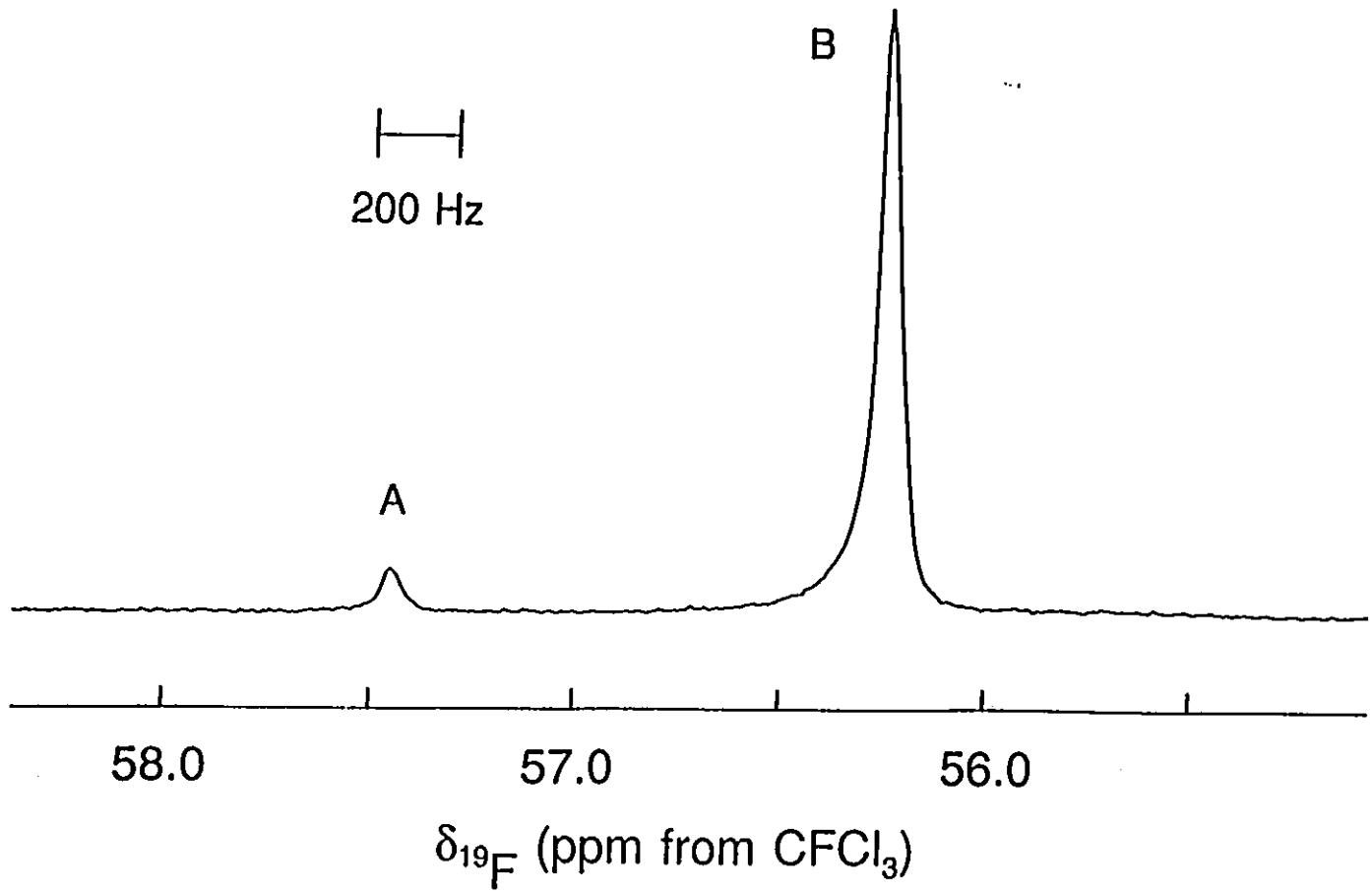

Figure 8.4 ^{19}F NMR spectrum (470.599 MHz) of the equilibrium mixture arising from the reaction of $FO_2SNH_3^+AsF_6^-$ and XeF_2 in BrF_5 solvent recorded at -57.8 °C; (A) $FO_2SN(H)\text{-}Xe^+$, (B) $FO_2SNH_3^+$.

assignment of the resonances to the $FO_2SN(H)\text{-}Xe^+$ and $FO_2SNH_3^+$ cations. The ^{19}F NMR spectra of the 99.5% ^{15}N-enriched $FO_2SNH_3^+$ and $FO_2SN(H)\text{-}Xe^+$ cations consists of singlets without resolution of the long range couplings $^2J(^{19}F\text{-}^{15}N)$ and $^3J(^{19}F\text{-}^1H)$. A broad singlet at $\delta(^{19}F)$ = -61.5 ppm [$\Delta\nu_{1/2}$ = 858 Hz] is attributed to the partially quadrupole collapsed AsF_6^- anion. Peaks from XeF_2 are observed in the ^{19}F and ^{129}Xe NMR spectra in BrF_5 solvent, consistent with equilibrium (8.1). The XeF_2 triplet in the ^{129}Xe NMR spectrum is observed at $\delta(^{129}Xe)$ = -1623 ppm, and is exchange broadened ($\Delta\nu_{1/2}$ = 1604 Hz). The ^{19}F NMR resonance of XeF_2 is centered at $\delta(^{19}F)$ = -186.5 ppm, $^1J(^{19}F\text{-}^{129}Xe)$ = 5670 Hz, and is also exchange broadened ($\Delta\nu_{1/2}$ = 392 Hz). The ^{19}F NMR resonance for XeF_2 is shielded by *ca.* 2 ppm relative to pure XeF_2 in BrF_5 at -52 °C[71] [$\delta(^{19}F)$ = -184.3 ppm], indicating exchange with HF at $\delta(^{19}F)$ = -192.5 ppm. The HF resonance is a singlet, $\Delta\nu_{1/2}$ = 301 Hz, and the absence of doublet structure arising from $^1J(^{19}F\text{-}^1H)$ confirms intermolecular exchange. The broadening of the XeF_2 resonances in the ^{129}Xe and ^{19}F NMR spectra may also be attributable to exchange of XeF_2 with H_2F^+ and AsF_5, producing trace amounts of XeF^+ and $Xe_2F_3^+$ according to equations (8.3) to (8.6). The presence of AsF_5

$$2\ HF + AsF_5 \rightleftharpoons H_2F^+ + AsF_6^- \tag{8.3}$$

$$XeF_2 + AsF_5 \rightleftharpoons XeF^+ + AsF_6^- \tag{8.4}$$

$$XeF_2 + H_2F^+ \rightleftharpoons XeF^+ + 2\ HF \tag{8.5}$$

$$XeF_2 + XeF^+ \rightleftharpoons Xe_2F_3^+ \tag{8.6}$$

is expected from the decomposition of $FO_2SN(H)\text{-}Xe^+AsF_6^-$ by analogy with the decomposition of $F_5TeN(H)\text{-}Xe^+AsF_6^-$ (Chapter 6), with HF arising from equilibrium (8.1) and from the oxidation of $FO_2SNH_3^+$ by BrF_5 solvent (see Chapter 7).

(C) NATURE OF THE BONDING IN THE $FO_2SN(H)\text{-}Xe^+$ CATION

Previous NMR studies of xenon(II) derivatives containing XeF groups bonded to oxygen or fluorine have shown that the NMR parameters measured in the ^{19}F and ^{129}Xe NMR spectra can generally be used to assess the relative covalent characters of the Xe-O, Xe---F bridge and Xe-F terminal bonds.[103,104,108] In general, as the covalent character of the Xe-L (L = ligand atom) bond increases, the terminal Xe-F bond becomes more ionic, decreasing the formal charge on xenon. These trends are paralleled by increased shielding of the ^{129}Xe resonance and decreases in both $^1J(^{129}Xe\text{-}^{19}F)$ and $\delta(^{19}F)$ for the terminal Xe-F group. Recently, Schrobilgen[26] extended the trend to include neutral and cationic species containing xenon(II)-nitrogen bonds. Table 8.1 lists the ^{129}Xe NMR chemical shifts and reduced coupling constants $^1K(Xe\text{-}N)$ for a number of representative xenon(II)-nitrogen bonded compounds for comparison with $FO_2SN(H)\text{-}Xe^+$. The $FO_2SN(H)\text{-}Xe^+$ cation has one of the most shielded ^{129}Xe NMR resonances for a compound containing a xenon-nitrogen bond. Compounds whose ^{129}Xe resonances are similar to that of the $FO_2SN(H)\text{-}Xe^+$ cation are $F_4S{=}N\text{-}Xe^+$ (-2672 ppm),[26,180] $F_5TeN(H)\text{-}Xe^+$ (-2841 ppm; Chapter 5) and $F_5SN(H)\text{-}Xe^+$ (-2886 ppm).[26,180] Assuming the validity of the NMR spectroscopic trends mentioned above, the highly shielded ^{129}Xe NMR resonance of $FO_2SN(H)\text{-}Xe^+$ indicates a very covalent Xe-N bond, which arises from the relatively low electronegativity of the $FO_2SN(H)$-ligand. From the highly shielded ^{129}Xe NMR resonance for the $FO_2SN(H)\text{-}Xe^+$ cation, a high degree of Xe-F bond ionic character is expected, and this is manifested in the absence of a xenon-

fluorine scalar coupling in the ^{129}Xe NMR spectra, indicating complete Xe-F bond ionization in solution. The same argument can be applied to $F_4S{=}N\text{-}Xe^+$, $F_5TeN(H)\text{-}Xe^+$ and $F_5SN(H)\text{-}Xe^+$, since the Xe-F bonds are also ionized in solution. The remaining xenon-nitrogen bonded compounds in Table 8.1 involve ligands of higher electronegativity, resulting in Xe-F bonds with considerable covalent character. In agreement with the above trends, the ^{129}Xe resonances of these compounds are between 600 and 1100 ppm more deshielded than those observed for $FO_2SN(H)\text{-}Xe^+$, $F_5XeN(H)\text{-}Xe^+$ (X = S, Te), and $F_4S{=}N\text{-}Xe^+$. An apparent anomaly in Table 8.1 is the $(FO_2S)_2N\text{-}Xe^+$ cation, for which $\delta(^{129}Xe) = -1943$ ppm, since according to the above trends, the ^{129}Xe resonance is expected to be much more shielded as a result of the ionized Xe-F bond. However, the high electronegativity of the $(FO_2S)_2N$- ligand results in substantial Xe-F bond covalent character in $(FO_2S)_2NXeF$. The crystallographically determined Xe-F and Xe-N bond lengths are similar [1.967(3) and 2.200(3) Å, respectively],[57] and a determination of the Xe-F and Xe-N bond orders using the bond order-bond length relationship of Pauling[305] indicates that the valence bond formulation $(FO_2S)_2N^-\ Xe\text{-}F^+$ dominates over the formulation $(FO_2S)_2N\text{-}Xe^+\ F^-$ by 59:41.[57] As expected, the Xe-F bond is not ionized in BrF_5 solvent.[56-58] Ionization of the Xe-F bond in solution to give $(FO_2S)_2N\text{-}Xe^+$ requires the use of the strong fluoride acceptor SbF_5 as solvent.[60]

The effect of ligand electronegativity on the ^{129}Xe chemical shift and Xe-F bond ionization is further illustrated by comparing resonance structures for the hypothetical compound, $FO_2SN(H)\text{-}Xe\text{-}F$, with those for the neutral fluorosulfate derivative, $FO_2SO\text{-}Xe\text{-}F$, since FO_2SO- and $FO_2SN(H)$- are isoelectronic. The electronegativity of FO_2SO- is undoubtedly greater than that of $FO_2SN(H)$-, since FO_2SOH is a strong acid ($H_o = -15.1$)[306] and FO_2SNH_2 is a nitrogen base

$FO_2SN(H)\text{-}Xe^+\ F^-$ <———> $FO_2SN(H)^-\ Xe\text{-}F^+$

8.6 8.7

$FO_2SO^-\ XeF^+$ <———> $FO_2SO\text{-}Xe^+\ F^-$

8.8 8.9

which can be protonated in HF solvent acidified with AsF_5 (see Chapter 7). The ionization of the Xe-F bond for $FO_2SN(H)$-Xe-F in solution is represented by dominance of resonance Structure 8.6 to the exclusion of Structure 8.7. The Xe-F bond in FO_2SO-Xe-F is not ionized in solution, since $^1J(^{129}Xe\text{-}^{19}F) = 5830$ Hz is observed in the ^{129}Xe NMR spectrum in BrF_5 solvent.[108] This indicates substantial Xe-F bond covalent character in FO_2SOXeF. The crystallographically determined Xe-F [1.940(8) Å] and Xe-O [2.155(8) Å] bond lengths for FO_2SOXeF have been used to assess relative covalent characters of the Xe-F and Xe-O bonds using the bond order-bond length relationship of Pauling.[38] This relationship indicates that the canonic form $FO_2SO^-\ Xe\text{-}F^+$ (Structure 8.8) has a 63:37 dominance over the canonical form $FO_2SO\text{-}Xe^+\ F^-$ (Structure 8.9). As expected from the substantial Xe-F bond covalent character, the ^{129}Xe NMR resonance of FO_2SOXeF [$\delta(^{129}Xe) = -1666$ ppm][108] is much more deshielded than the $FO_2SN(H)\text{-}Xe^+$ cation.

The magnitude of the reduced coupling constant ^1K(Xe-N) for the $FO_2SN(H)\text{-}Xe^+$ cation ($0.322 \times 10^{22}\ NA^{-2}m^{-3}$) may be used to gain insight into the bonding by comparison with other xenon(II)-nitrogen bonded compounds (see Table 8.1). In a previous study,[73] the hybridization at

nitrogen in the HC≡N-XeF$^+$ cation was determined to be *sp* by comparing the magnitude of ^1K(Xe-N) (1.389 x 10^{22} $NA^{-2}m^{-3}$) for the HC≡N-XeF$^+$ cation with that of $(FO_2S)_2N$-XeF (0.949 x 10^{22} $NA^{-2}m^{-3}$).[57] The use of ^1K(Xe-N) to assess the hybridization at nitrogen assumes that the Fermi contact term is the dominant mechanism for the xenon-nitrogen nuclear spin-spin coupling, which is generally true for spin-spin coupling involving heavy nuclides.[260] Assessment of the hybridization at nitrogen in Xe-N bonded compounds uses a formalism developed by Pople and Santry[242] for Fermi contact-dominated scalar couplings, which states that the magnitude of the scalar coupling between two nuclei is proportional to the product of the valence *s*-electron densities at the coupled nuclei. The use of the magnitude of ^1K(Xe-N) to assess the hybridization at nitrogen in HC≡N-XeF$^+$ depended on the assumption that the *s*-electron density at xenon in HC≡N-XeF$^+$ was essentially the same as in $(FO_2S)_2NXeF$, and the difference in the nitrogen hybridization in the two compounds accounted for the different magnitudes of ^1K(Xe-N).[73] Thus the hybridization at nitrogen in the HC≡N-XeF$^+$ cation could be determined, since the formal hybridization at nitrogen in $(FO_2S)_2NXeF$ is considered to be sp^2, as evidenced by the short S-N bond lengths [1.628(3) and 1.623(3) Å], indicating S-N π-bonding, and the trigonal planar nitrogen geometry.[57] The same treatment cannot be used to assess the nitrogen hybridization in the $FO_2SN(H)$-Xe$^+$ cation since the Xe-F bond is ionized in solution, and therefore the *s*-electron density at xenon cannot be assumed to be the same as in HC≡N-XeF$^+$ or $(FO_2S)_2N$-XeF. A comparison of the reduced coupling constants of $FO_2SN(H)$-Xe$^+$ and $(FO_2S)_2N$-Xe$^+$ would seem reasonable for assessing the nitrogen atom hybridization of the $FO_2SN(H)$-Xe$^+$ cation, but the magnitudes of ^1K(Xe-N) are opposite to what is expected. The single crystal X-ray structure of $(FO_2S)_2N$-Xe$^+Sb_3F_{16}^-$ [60] shows that the nitrogen center is trigonal planar in the $(FO_2S)_2N$-Xe$^+$ cation, and the S-N bond lengths [1.68(1) to 1.70(1) Å] are significantly shorter than S-N single

bonds [cf., O_3SNH_3: S-N = 1.7714(3) Å],[287] indicating substantial S-N π bonding and formal sp^2-hybridization at nitrogen. The $FO_2SN(H)$-Xe^+ cation is related to $(FO_2S)_2N$-Xe^+ by replacement of one FO_2S- group with a hydrogen atom, so that the degree of S-N π bonding in the former can be assumed to be reduced relative to the latter since only half the number of resonance structures involving S-N π bonding can be drawn [compare resonance Structures 8.10 - 8.13 with Structures 8.2 - 8.4]. As a result, the *s*-character of the nitrogen valence orbitals is expected to be lower (i.e., greater *p* character) in the $FO_2SN(H)$-Xe^+ cation. Assuming dominance of the Fermi contact mechanism for the Xe-N bond, a greater magnitude of ^1K(Xe-N) is expected, opposite to the measured values of ^1K(Xe-N). An alternative analysis of ^1K(Xe-N) in the $FO_2SN(H)$-Xe^+ and $(FO_2S)_2N$-Xe^+ cations, which also assumes dominance of the Fermi contact term, is derived from a study of the magnitudes of $^1J(^{15}N\text{-}^1H)$ in main group compounds of the form $X^{15}NH_2$ and $X_2{}^{15}NH$ by Cowley and Schweiger,[124] which relied on the so-called isovalent hybridization hypothesis.[261] This hypothesis states that *s*-character concentrates in the bonds which are directed toward electropositive substituents. It was observed that increasing electronegativity of X resulted in increasing magnitudes of $^1J(^{15}N\text{-}^1H)$, which implied that nitrogen 2*s* character was progressively diverted into the NH bonds with increased electronegativity of X. As expected from the Fermi contact term, in most cases the value of $^1J(^{15}N\text{-}^1H)$ increased in proceeding from the XNH_2 to the X_2NH compound. Once again, the opposite trend is observed in the $FO_2SN(H)$-Xe^+ and $(FO_2S)_2N$-Xe^+ cations since the $(FO_2S)_2N$- group is expected to be more electronegative than the $FO_2SN(H)$- group. The failure to qualitatively predict the relative magnitudes of ^1K(Xe-N) by only considering the Fermi contact term may indicate that the dipolar and orbital contributions[251] to the xenon-nitrogen scalar coupling may be important. Although the Fermi contact term is expected to be the largest contributor to the Xe-N scalar coupling,[260] it may be similar for the

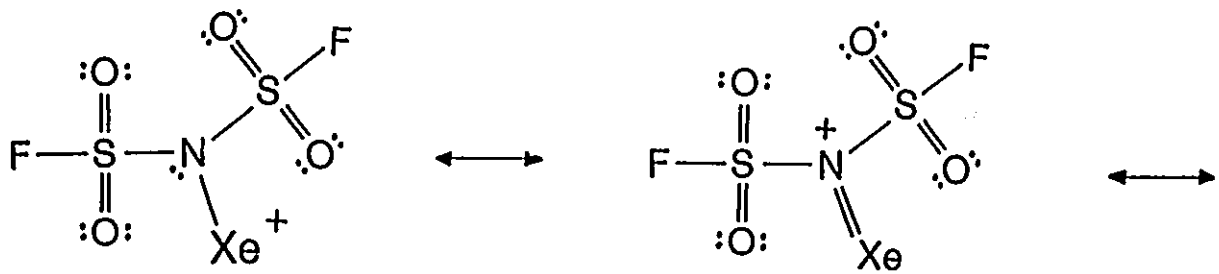

8.10 8.11

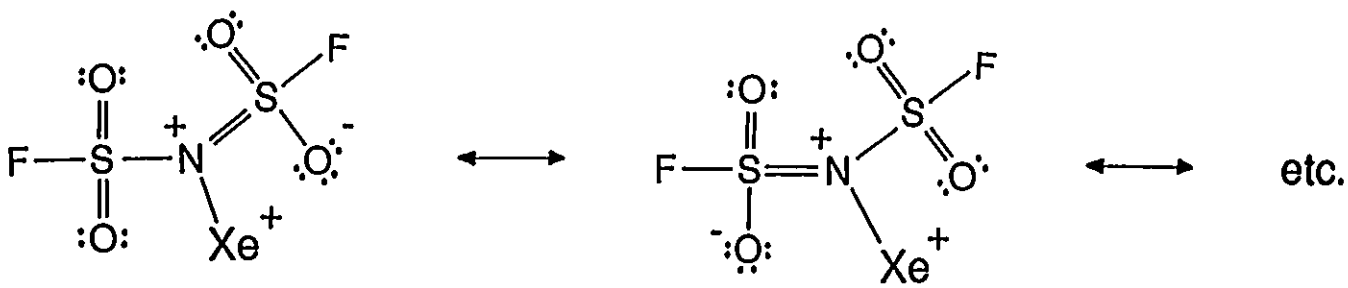

8.12 8.13

etc.

$FO_2SN(H)$-Xe^+ and $(FO_2S)_2NXe^+$ cations. The presence of Xe-N π-bonding in the $FO_2SN(H)$-Xe^+ and $(FO_2S)_2N$-Xe^+ cations, which is represented by resonance Structures 8.3 and 8.11, respectively, may give rise to a significant orbital contribution, K^2_{AB} to the scalar Xe-N coupling. Factors contributing to the magnitude of K^2_{AB} are described in equation (8.7) using an average

$$K^2_{AB} = \mu_o(\mu_B)^2\langle r_A^{-3}\rangle_p\langle r_B^{-3}\rangle_p(^3\Delta E)^{-1}$$

$$\times\ [2(P_\sigma^2 + P_\pi^2 + P_{\pi'}^2) + 3(P_\sigma P_\pi + P_\sigma P_{\pi'} + P_\pi P_{\pi'})] \qquad (8.7)$$

energy approximation in a LCAO framework.[251] The terms μ_o and μ_B are the permittivity of a vacuum and the Bohr magneton, respectively, $\langle r_A^{-3}\rangle_p$ and $\langle r_B^{-3}\rangle_p$ are the inverse cube radial distributions of the valence *p* orbitals for the coupled nuclei, $(^3\Delta E)$ is the average excitation energy and P_σ, P_π and $P_{\pi'}$ are the σ and π bond orders for the bonding between the coupled nuclei, A and B. In comparing $FO_2SN(H)$-Xe^+ and $(FO_2S)_2NXe^+$, an argument for a greater Xe-N π-bonding contribution in the former can be made by examining resonance Structures 8.2 to 8.4 and 8.10 to 8.13, which in turn rationalizes the relative magnitudes of ^1K(Xe-N). The greater electronegativity of $(FO_2S)_2N$- than $FO_2SN(H)$- and the greater proportion of resonance contributors involving S-N π-bonding in the $(FO_2S)_2N$-Xe^+ cation both contribute to a smaller degree of Xe-N π-bonding in the $(FO_2S)_2N$-Xe^+ cation than in the $FO_2SN(H)$-Xe^+ cation. A larger Xe-N π-bonding contribution in $FO_2SN(H)$-Xe^+ is expected to result in larger values of P_π and $P_{\pi'}$ in the orbital contribution to the Xe-N scalar coupling, thus increasing ^1K(Xe-N) relative to $(FO_2S)_2N$-Xe^+.

CHAPTER 9

SUMMARY, CONCLUSIONS AND DIRECTIONS FOR FURTHER RESEARCH

(A) SUMMARY

The present work represents a significant extension of noble-gas chemistry, in particular, the synthesis of several compounds containing xenon-nitrogen and xenon-oxygen bonds. This has been achieved by HF elimination reactions of the salts, $CF_3C(OH)NH_2^+AsF_6^-$, $F_5TeNH_3^+AsF_6^-$ and $FO_2SNH_3^+AsF_6^-$ with XeF_2 in HF and BrF_5 solvents, resulting in the preparation of AsF_6^- salts of the novel cations, $CF_3C(OXeF)NH_2^+$, $F_5TeN(H)\text{-}Xe^+$ and $FO_2SN(H)\text{-}Xe^+$. The HF elimination reactions are analogous to the reaction of the strong oxoacids $CF_3C(O)OH$, F_5TeOH and FO_2SOH with XeF_2, which result in the neutral xenon(II) derivatives, $CF_3C(O)O\text{-}XeF$, $F_5TeO\text{-}XeF$ and $FO_2SO\text{-}XeF$ which were prepared in the decade which followed the discovery of noble-gas reactivity (see Chapter 1). The ligands used in the present studies are among the least electronegative ligands known to form isolable xenon(II) derivatives. Since high ligand electronegativity is central to the stabilization of xenon(II) derivatives (see Chapter 1), the low stability of these compounds is to be expected. The salts $CF_3C(OXeF)NH_2^+AsF_6^-$ and $F_5TeN(H)\text{-}Xe^+AsF_6^-$ isolated from solution decompose rapidly at 0 and -30 °C, respectively, whereas $FO_2SN(H)\text{-}Xe^+AsF_6^-$ could not be isolated from solution owing to decomposition above *ca.* -40 °C. Prior to this work, only one example of xenon(II) bonded to an sp^3-hybridized nitrogen center was known, namely $F_5SN(H)\text{-}Xe^+AsF_6^-$.[26] In the $F_5TeN(H)\text{-}Xe^+$ and $FO_2SN(H)\text{-}Xe^+$ cations,

xenon(II) is bonded to nitrogen centers which are formally sp^3-hybridized, providing two new examples of a rare class of compounds.

The salts, $CF_3C(OH)NH_2^+AsF_6^-$, $F_5TeNH_3^+AsF_6^-$ and $FO_2SNH_3^+AsF_6^-$, which are starting materials for the preparation of the xenon cations, represent the first reported examples of the protonated forms of $CF_3C(O)NH_2$, F_5TeNH_2 and FO_2SNH_2. The natural abundance salts and 99.5% ^{15}N-enriched $F_5TeNH_3^+AsF_6^-$ and $FO_2SNH_3^+AsF_6^-$ have been fully characterized by ^{19}F, ^{13}C, ^{1}H, ^{15}N and ^{125}Te NMR spectroscopy in HF and/or BrF_5 solvents. They have also been characterized in the solid state by Raman spectroscopy, and the assignments for the Raman spectra of $F_5TeNH_3^+AsF_6^-$ and $FO_2SNH_3^+AsF_6^-$ were aided by obtaining the Raman spectra of the 99.5% ^{15}N-enriched salts and observing the $^{14/15}N$ isotopic shifts of bands associated with the vibrational motions of the nitrogen atom. The NMR and Raman spectral data for the unprotonated compounds, $CF_3C(O)NH_2$, F_5TeNH_2, and FO_2SNH_2 were compared with the data for the salts of the protonated compounds, and the effect of protonation on the bonding in these ligands was assessed.

(i) Preparation and Characterization of $CF_3C(OH)NH_2^+AsF_6^-$.

The $CF_3C(OXeF)NH_2^+$ cation was best prepared in BrF_5 solvent from the HF elimination reaction of the conjugate acid, $CF_3C(OH)NH_2^+$, with XeF_2 [equation (3.2)]. As well as facilitating the HF elimination reaction, protonation of $CF_3C(O)NH_2$ made the ligand more resistent to electrophilic attack by BrF_5 solvent. Xenon difluoride is also a weaker oxidative fluorinator than XeF^+, which reduced the rate of ligand oxidation. Attempting the reaction of $XeF^+AsF_6^-$ and $CF_3C(O)NH_2$ in BrF_5 solvent resulted in extensive oxidative decomposition of $CF_3C(O)NH_2$.

The salt, $CF_3C(OH)NH_2^+AsF_6^-$, was prepared by reacting $CF_3C(O)NH_2$ with an excess

of AsF_5 in anhydrous HF solvent at -50 °C. The resulting white powder decomposed slowly (*ca.* one month) with liquefaction at room temperature under anhydrous conditions, but was indefinitely stable at -78 °C. The solution structure of $CF_3C(OH)NH_2^+$ was determined by obtaining the ^{19}F, ^1H and ^{13}C NMR spectra of $CF_3C(OH)NH_2^+AsF_6^-$ in BrF_5 solvent. The ^1H NMR spectrum indicated chemical inequivalence of the amido protons resulting from hindered rotation of the C-N bond which possesses considerable double bond character; a proton resonance attributable to the protonated carbonyl group was also observed. The NMR data were consistent with resonance Structures 3.1 and 3.2. The assignment of the chemically inequivalent amido protons in the ^1H NMR spectrum was facilitated by use of a two-dimensional heteronuclear (^1H-^{19}F) NOESY experiment.

The Raman spectrum (-165 °C) of $CF_3C(OH)NH_2^+AsF_6^-$ was consistent with resonance Structures 3.1 and 3.2. O-protonation was evident from the increase and decrease, respectively, of the bands assigned to ν(C-N) and ν(C-O), relative to those for $CF_3C(O)NH_2$, since O-protonation is expected to increase and decrease, respectively, the C-N and C-O double bond characters. A band attributable to δ(OH) was observed but bands attributable to γ(OH) and ν(OH) were not observed. The characteristic low intensity of the vibrations of small atoms was assumed to be responsible for the unobserved γ(OH) and ν(OH) bands. Bands attributable to AsF_6^- were also observed.

(ii) <u>Preparation and Characterization of $CF_3C(OXeF)NH_2^+AsF_6^-$ and $CF_3C(OH)NH_2^+AsF_6^-\cdot XeF_2\cdot xHF$</u>

The first adiabatic ionization potential (IP_1) of $CF_3C(O)NH_2$ (10.77 eV)[106] is similar to the observed electron affinity of XeF^+ (10.77 eV),[26] suggesting that it may be resistent to oxidation by XeF^+ at low temperature. The reaction of equimolar amounts of $CF_3C(O)NH_2$ and

$XeF^+AsF_6^-$ in HF solvent did not result in measurable amounts of $CF_3C(OXeF)NH_2^+AsF_6^-$ (monitored by ^{19}F and ^{129}Xe NMR spectroscopy), owing to protonation of $CF_3C(O)NH_2$ to give $CF_3C(OH)NH_2^+$ in the XeF^+-acidified HF solvent [equation (3.3)]. However, slow removal of HF solvent under vacuum at -50 °C resulted in a white powder. The Raman spectrum (-165 °C) was consistent with the formulation, $CF_3C(OXeF)NH_2^+$ AsF_6^-. The solid decomposed with gas evolution and liquefaction at temperatures approaching 0 °C. The ^{129}Xe and ^{19}F NMR spectra of the undecomposed white powder dissolved in BrF_5 solvent at -60 °C confirmed that the material was $CF_3C(OXeF)NH_2^+AsF_6^-$. The solution structure of $CF_3C(OXeF)NH_2^+AsF_6^-$ was determined by dissolving equimolar amounts of $CF_3C(OH)NH_2^+AsF_6^-$ and XeF_2 in BrF_5 solvent at -60 °C and obtaining the ^{129}Xe, ^{19}F, ^1H and ^{13}C NMR spectra. The NMR spectra indicated an HF elimination equilibrium, resulting in the formation of $CF_3C(OXeF)NH_2^+AsF_6^-$ [equation (3.2)]; the ratio $[CF_3C(OH)NH_2^+]$: $[CF_3C(OXeF)NH_2^+]$ was determined to be 3 : 1 from integration of the NMR resonances. The $CF_3C(OXeF)NH_2^+$ cation can be thought of as an adduct cation, where $CF_3C(O)NH_2$ behaves as an oxygen-donor towards the Lewis acid cation, XeF^+; the synthesis of $CF_3C(OXeF)NH_2^+$ represents the second reported example of an adduct of XeF^+ with an oxygen donor ligand; the first to be reported was the thermally unstable SbF_6^-salt of the sulfurane adduct, $(CF_3)_2S{=}O\text{-}XeF^+SbF_6^-$.[85] The ^1H NMR spectrum of $CF_3C(OXeF)NH_2^+$ in BrF_5 solvent indicated chemical inequivalence of the amido protons, resulting from hindered rotation about the C-N bond. The hindered rotation results from substantial C-N double bond character, as depicted in resonance Structures 3.3 and 3.4. Assignment of the chemically inequivalent amido protons in the ^1H NMR spectrum was facilitated by use of a two-dimensional heteronuclear (^{19}F-^1H) NOESY experiment. The NOESY technique is well established as a very important tool for determining the spatial orientation of organic molecules in solution. This work represented the first use of a NOESY experiment to facilitate the NMR assignments of a thermally unstable noble-gas compound in

solution.

Combining stoichiometric amounts of $CF_3C(OH)NH_2^+AsF_6^-$ and XeF_2 in HF solvent at -50 °C resulted in pale yellow solutions. As described above, slow removal of HF under vacuum over four hours resulted in completion of the HF elimination reaction depicted in equation (3.2), resulting in the isolation of essentially pure $CF_3C(OXeF)NH_2^+AsF_6^-$. If the HF solvent was removed rapidly under vacuum at -50 °C, a white solid precipitated after removal of approximately half of the solvent. After complete removal of the solvent, the Raman spectrum (-165 °C) of the resulting white powder was consistent with a hydrogen-bonded solvate, which was formulated as $CF_3C(OH)NH_2^+AsF_6^-\cdot XeF_2\cdot xHF$. This indicated that the faster rate of HF removal resulted in the precipitation of a hydrogen-bonded solvate [see equation (3.4)] The Raman spectrum (Figure 3.9) exhibits two intense peaks at 515 and 511 cm^{-1}, which are best described as the factor group split symmetric F-Xe-F stretch of hydrogen-bonded XeF_2. The absence of a band assignable to the asymmetric F-Xe-F stretch indicates that the local $D_{\infty h}$ symmetry of XeF_2 in the solvate is preserved, since the asymmetric F-Xe-F stretch (Σ^+_u symmetry) is Raman forbidden for $D_{\infty h}$ symmetry. Bands were observed which were consistent with the presence of $CF_3C(OH)NH_2^+$ and AsF_6^-. It is likely that XeF_2 is hydrogen-bonded to the protons of $CF_3C(OH)NH_2^+$ in a fashion that conserves the local $D_{\infty h}$ symmetry of XeF_2. Possible arrangements of XeF_2 in the solid are shown in Structures 3.5 - 3.7.

The variation in products which resulted from the reaction of $CF_3C(OH)NH_2^+AsF_6^-$ and XeF_2 in HF solvent depended on the rate of HF removal. This illustrates the need to closely monitor the reaction conditions used for the preparations of xenon compounds. This is a reiteration of the same statement made by Bartlett *et al.*,[28] concerning the carefully controlled conditions required to properly conduct HF elimination reactions of strong oxoacids such as HSO_3F, $CF_3C(O)OH$ and $HClO_4$ with XeF_2.

(iii) Preparation and Characterization of F_5TeNH_2 and $F_5TeNH_3^+AsF_6^-$

The importance of $F_5TeNH_3^+AsF_6^-$ in this work lies primarily in its use as a precursor for the preparation of $F_5TeN(H)$-$Xe^+AsF_6^-$ in BrF_5 and HF solvents. This Thesis also reports the first isolation of the protonated form of F_5TeNH_2. The salt, $F_5TeNH_3^+AsF_6^-$, was prepared by reaction of F_5TeNH_2 and excess AsF_5 in HF solvent at -55 °C, which resulted in a white powder that was indefinitely stable at room temperature in the absence of moisture. The solution structures of natural abundance and 99.5% ^{15}N-enriched $F_5TeNH_3^+AsF_6^-$ were determined by ^{19}F, ^{1}H, ^{15}N and ^{125}Te NMR spectroscopy in HF and/or BrF_5 solvents. The Raman spectra at ambient temperature of natural abundance and 99.5% ^{15}N-enriched samples were obtained, and with the aid of $^{14/15}N$ isotopic shifts of bands associated with the vibrations of the nitrogen center, detailed assignments of all vibrational modes were made.

The vibrational assignments for F_5TeNH_2, although previously published,[230] were reassigned using additional information provided from the $^{14/15}N$ isotopic shifts in the Raman spectra of the natural abundance and 99.5% ^{15}N-enriched samples. A comparison of the Raman and ^{19}F NMR spectra of natural abundance and 99.5% ^{15}N-enriched $F_5TeNH_3^+AsF_6^-$ with those of natural abundance and 99.5% ^{15}N-enriched F_5TeNH_2 indicated that the Te-N bond order decreases on protonation of F_5TeNH_2. This implied some degree of Te-N π-bonding in F_5TeNH_2, which decreased upon incorporation of the nitrogen lone pair in an electron-pair bond with H^+ in $F_5TeNH_3^+$. The Raman spectra and ^{19}F NMR spectra also indicated that protonation increases the Te-F bond orders, particularly the axial Te-F bond.

The trends observed on protonation of F_5TeNH_2 to give $F_5TeNH_3^+$ are consistent with a reduction in Te-N π-bonding, and are directly analogous to the changes in the bonding of F_5XO^- upon protonation to give F_5XOH (X = S, Se, Te).[52]

(iv) [Pentafluorotellurium(VI)amido]xenonium(II) Hexafluoroarsenate; $F_5TeN(H)\text{-}Xe^+AsF_6^-$

The amine, F_5TeNH_2, is valence isoelectronic with F_5TeOH, which is known to undergo HF elimination reactions with XeF_2 to give $FXeOTeF_5$ and $Xe(OTeF_5)_2$. Although the resistence of F_5TeNH_2 to oxidation by XeF^+ could not be estimated in the absence of photoionization studies for this compound, it is reasonable to assume that the inductive effect of five fluorines on tellurium, by analogy with F_5TeOH, might result in considerable oxidative resistence. The basicity of F_5TeNH_2[230] was confirmed by the stability of the $F_5TeNH_2 \cdot AsF_5$ adduct at room temperature. Prior to this study, a considerable number of cations with Xe-N bonds were prepared from the reaction of the Lewis acid XeF^+ with oxidatively resistent nitrogen bases, D, such as the nitriles, RC≡N (R = alkyl, C_6F_5, fluoroalkyl, H) the pyridines C_5F_5N and $4\text{-}CF_3C_5F_4N$ and $s\text{-}C_3F_3N_3$ [equation (9.1)].[26] All of the ligands mentioned above contain *sp*- or sp^2-hybridized nitrogen

$$D + XeF^+AsF_6^- \longrightarrow D\text{-}XeF^+AsF_6^- \qquad (9.1)$$

centers, and prior to this work, no attempt was made to react an oxidatively resistent amine (sp^3-hybridized nitrogen center) with XeF^+ with the aim of preparing a cation of the form $R\text{-}NH_2\text{-}XeF^+$. It was shown in Chapter 5 that the reaction of F_5TeNH_2 and $XeF^+AsF_6^-$ in HF solvent or the reaction of $F_5TeNH_3^+AsF_6^-$ and XeF_2 in BrF_5 solvent resulted in the formation of $F_5TeN(H)\text{-}Xe^+AsF_6^-$. The $F_5TeN(H)\text{-}Xe^+$ cation was not the expected product from the simple adduct formation of the base F_5TeNH_2 and the Lewis acid, XeF^+. The anticipated cation, $F_5TeNH_2\text{-}XeF^+$, was not observed and it was postulated that $F_5TeNH_2\text{-}XeF^+$ eliminated HF according to equation (9.2). The $F_5TeN(H)\text{-}Xe^+$ cation was characterized in solution by ^{19}F, ^1H, ^{129}Xe and ^{125}Te NMR

$$F_5TeNH_2\text{-}XeF^+ \longrightarrow F_5TeN(H)\text{-}Xe^+ + HF \qquad (9.2)$$

spectroscopy in BrF_5 and HF solvents. Quadrupolar collapse of the ^{129}Xe-^{14}N scalar coupling prevented the use of NMR to definitively characterize the Xe-N bond in solution. It was possible to observe the ^{129}Xe-^{15}N scalar coupling, however, by preparing the 99.5% ^{15}N-enriched $F_5TeN(H)\text{-}Xe^+$ cation. This also facilitated the observation of the ^{15}N NMR spectrum of $F_5TeN(H)\text{-}Xe^+$.

A dominant relaxation mechanism for ^{129}Xe is shielding anisotropy, which results in significant line broadening at high field strengths. This was demonstrated in the ^{129}Xe NMR spectrum of 99.5% ^{15}N-enriched $F_5TeN(H)\text{-}Xe^+$ with an external magnetic field strength of 11.7440 T; only the one-bond scalar coupling $^1J(^{129}Xe\text{-}^{15}N)$ was resolved. However, all possible spin-spin couplings were observed in the ^{129}Xe NMR spectrum at 7.4630 T, except the three-bond scalar coupling of ^{129}Xe with the axial fluorine-on-tellurium(VI). This posed the possibility of a misassignment in the ^{129}Xe NMR spectrum, since $^2J(^{129}Xe\text{-}^1H)$ might have been the unresolved coupling, as opposed to $^3J(^{129}Xe\text{-}^{19}F_{ax.})$. The unresolved coupling was confirmed to be $^3J(^{129}Xe\text{-}^{19}F_{ax.})$ by performing a (^1H-^{129}Xe) INEPT experiment; this was the first example of the use of the well-established INEPT pulse sequence for the characterization of a noble-gas compound.

The salt $F_5TeN(H)\text{-}Xe^+AsF_6^-$ was isolated as an orange microcrystalline powder by precipitation from HF solvent at -40 °C. The salt decomposed rapidly in the solid state at -30 °C. Natural abundance and 99.5% ^{15}N-enriched samples of $F_5TeN(H)\text{-}Xe^+AsF_6^-$ were characterized by Raman spectroscopy at -165 °C. The $^{14/15}N$ isotopic shifts associated with the vibrations of the nitrogen atom allowed for the assignments of bands attributable to the asymmetric and symmetric stretches of the Xe-N-Te linkage, the NH stretches and bends, and vibrations of the F_5TeN- group. Minor amounts of the salts, $Xe_2F_3^+AsF_6^-$ and $F_5TeNH_3^+AsF_6^-$, were also detected

in the Raman spectra, and arise from decomposition reactions (Chapter 6) and equilibrium (5.4), respectively.

(v) Decomposition of $F_5TeN(H)\text{-}Xe^+$ in Solution and Characterization and Decomposition of F_5TeNF_2

Chapter 6 describes the decomposition of $F_5TeN(H)\text{-}Xe^+$ in HF and BrF_5 solvents, using primarily ^{19}F NMR spectroscopy. Slow decomposition of $F_5TeN(H)\text{-}Xe^+AsF_6^-$ in BrF_5 (-40 °C) and HF (-33 °C) solvents resulted in the formation of the difluoamino compound, F_5TeNF_2. This species was unknown prior to this study. Natural abundance and 99.5% ^{15}N-enriched F_5TeNF_2 have been characterized in HF and BrF_5 solvents by ^{19}F and ^{15}N NMR spectrocopy. The decomposition of $F_5TeN(H)\text{-}Xe^+AsF_6^-$ was postulated to involve nucleophilic fluorination of nitrogen with elimination of xenon gas and AsF_5 [equations (6.1) and (6.2)]. This mode of decomposition is similar to that observed for the phenylxenonium(II) cations, $R\text{-}Xe^+$ (R = C_6F_5, m-$CF_3C_6H_4$, p-FC_6H_4), as dicussed in Chapter 6. The nucleophilic fluorination of $F_5TeN(H)\text{-}Xe^+$ represents the first complete study of a non-radical decomposition mechanism for a compound containing a xenon(II)-nitrogen bond.

The complete decomposition of F_5TeNF_2 to $FN{\equiv}N^+$ and TeF_6 in HF solvent at -20 °C was observed by ^{19}F NMR spectroscopy; some $F_5TeN(H)\text{-}Xe^+$ was still observed. The decomposition of difluoramino compounds, RNF_2 (R = F_5S, Cl, F_3C, F_3CO, F_5SO)[275] in the presence of Lewis acids such as SbF_5 and AsF_5 indicates that transient fluoronitrenes, NF, may be produced. In the present system, an alternative mechanism for the formation of the decomposition products was proposed [see equations (6.16) to (6.27)]. It was postulated that $F_5TeNH_3^+$, which was present in HF solution according to equilibrium (5.4), reacted with F_5TeNF_2. The strong Lewis fluoroacid, AsF_5, which was generated from the decomposition of

$F_5TeN(H)\text{-}Xe^+AsF_6^-$ (see above), likely catalyzed the reaction by abstraction of fluoride from F_5TeNF_2 [equation (6.19)]. The reaction of $F_5TeNH_3^+$ and F_5TeNF_2 is directly analogous to the well-established reactions of primary amines with difluoramine, HNF_2.[282] One result of the decomposition of F_5TeNF_2 was the increased fluoroacidity of the HF solution. Evidence for this was provided by the coalescence of the AsF_6^-, HF and XeF_2 ^{19}F NMR resonances, which resulted from exchange of these species with AsF_5 according to equations (6.3) to (6.5).

(vi) Preparation and Characterization of FO_2SNH_2 and $FO_2SNH_3^+AsF_6^-$

The amides, FO_2SNH_2 and $FO_2SNH_3^+AsF_6^-$, were prepared primarily for their use as ligands for the preparation of $FO_2SN(H)\text{-}Xe^+AsF_6^-$. The salt, $FO_2SNH_3^+AsF_6^-$, was prepared by reaction of FO_2SNH_2 and excess AsF_5 in anhydrous HF solvent at -40 °C. Although preparations of FO_2SNH_2 were previously reported (see Chapter 7) no attempts to protonate FO_2SNH_2 have been published. Therefore a detailed Raman and NMR (^1H and ^{19}F) spectrocopic study of natural abundance and 99.5% ^{15}N-enriched FO_2SNH_2 and $FO_2SNH_3^+AsF_6^-$ was performed. The vibrational spectrum of FO_2SNH_2 was reported by Semmoud and Vast;[130] however, the assignments were improved in the present Raman spectrocopic study with the aid of $^{14/15}N$ isotopic shifts of bands associated with vibrations of the nitrogen center. In general, the assignments of Semmoud and Vast underestimate the degree of vibrational coupling of modes in FO_2SNH_2. This was evidenced by the fact that all bands in the Raman spectrum of FO_2SNH_2, except for those assigned to the symmetric and asymmetric S-O stretching modes, had an $^{14/15}N$ isotopic dependence. Assignments for the bands observed in the Raman spectra of $FO_2SNH_3^+AsF_6^-$ were also aided by the measurement of $^{14/15}N$ isotopic shifts. Comparing the Raman spectra of FO_2SNH_2 and $FO_2SNH_3^+AsF_6^-$ indicated changes in the bonding of the FO_2SN-group on protonation of FO_2SNH_2 to give $FO_2SNH_3^+$. Protonation of FO_2SNH_2 resulted in

increased values for the S-F and S-O stretches, and a decrease in the S-N stretch. This was consistent with S-N π-bonding in FO_2SNH_2, which is reduced upon protonation of the nitrogen center by making the nitrogen lone pair of electrons unavailable for S-N π-donation. In a previous vibrational study,[130] a similar reduction in S-N π-bonding was noted on protonation of NSO_2F^{2-} to give H_2NSO_2F. A similar reduction in S-N π-bonding was also reflected in the vibrational spectra and crystallographically determined bond lengths for the series, NSO_3^{3-}, $H_2NSO_3^-$ and H_3SO_3, and the analogous behavior in NSO_2F^{2-} and H_2NSO_2F was noted. The present work completes the comparison of the sulfurylamides and the fluorosulfurylamides[130] by providing detailed vibrational assignments for FO_2SNH_2 and $FO_2SNH_3^+$, which are isoelectronic with $H_2NSO_3^-$ and H_3NSO_3.

(vii) Preparation of [Fluorosulfurylamido]xenonium(II) Hexafluoroarsenate; $FO_2SN(H)\text{-}Xe^+AsF_6^-$

Fluorosulfuryl amide, FO_2SNH_2, is isoelectronic with fluorosulfuric acid, FO_2SOH. Since the latter is known to undergo HF elimination reactions with XeF_2 to give $FXeOSO_2F$ and $Xe(OSO_2F)_2$, it was postulated that FO_2SNH_2 might be sufficiently electronegative to form a compound containing a xenon(II)-nitrogen bond. Although no ionization potential data allowing an estimate of the oxidative resistence of FO_2SNH_2 was available, the success in the use of F_5TeNH_2 as a ligand for xenon(II) by analogy with F_5TeOH provided the incentive to attempt the analogous reactions with FO_2SNH_2. It was found that the reaction of equimolar amounts of FO_2SNH_2 and $XeF^+AsF_6^-$ in HF at -50 °C resulted in a yellow solution above white and yellow precipitates. The ^{129}Xe NMR spectrum was consistent with the preparation of $FO_2SN(H)\text{-}Xe^+$, however, the resonance was broadened, and had an irregular shape (non-Lorentzian) due to the large amount of solid present in the sample. Complete decomposition of $FO_2SN(H)\text{-}Xe^+$ had

occurred within one hour. Warming of a similar sample to -35 °C in an attempt to dissolve the solids resulted in complete decomposition of $FO_2SN(H)\text{-}Xe^+$ within 30 seconds.

Protonation of FO_2SNH_2 in HF solvent in the presence of an excess amount of AsF_5 resulted in the N-protonated salt, $FO_2SNH_3^+AsF_6^-$. Reaction of $FO_2SNH_3^+AsF_6^-$ with XeF_2 at -58 °C in BrF_5 solvent resulted in an HF elimination reaction to give $FO_2SN(H)\text{-}Xe^+$ [equation (8.1)]. The ^{129}Xe NMR resonance (-2663 ppm) was a singlet; the failure to observe the one-bond $^{129}Xe\text{-}^{14}N$ coupling was attributed to quadrupolar collapse resulting from the rapid relaxation of the quadrupolar ^{14}N (I = 1) nucleus. This was confirmed by preparing 99.5% ^{15}N-enriched $FO_2SN(H)\text{-}Xe^+$; the ^{129}Xe NMR spectrum consisted of a doublet arising from the one-bond scalar coupling, $^1J(^{129}Xe\text{-}^{15}N)$ = 109 Hz. The scalar couplings $^2J(^{129}Xe\text{-}^1H)$ and $^3J(^{129}Xe\text{-}^{19}F)$ were not resolved. This was assumed to result from SA broadening of the ^{129}Xe NMR resonance, since broadening of this nature is proportional to the square of the external magnetic field strength, and the ^{129}Xe NMR spectrum was recorded using a very strong magnetic field (11.7440 T). A broad ^{129}Xe NMR resonance was also observed for ^{15}N-enriched $F_5TeN(H)\text{-}Xe^+$ at 11.7440 T; a significant reduction in the ^{129}Xe linewidth was observed at lower field. Natural abundance and 99.5% ^{15}N-enriched samples of $FO_2SN(H)\text{-}Xe^+$ cation were also characterized by ^{19}F and ^1H NMR spectroscopy. The ^1H NMR spectrum of 99.5% ^{15}N-enriched $FO_2SN(H)\text{-}Xe^+$ consisted of a doublet arising from the one-bond scalar coupling, $^1J(^1H\text{-}^{15}N)$. The ^{19}F NMR spectrum consisted of a singlet, and the scalar couplings $^2J(^{19}F\text{-}^{15}N)$ and $^3J(^{19}F\text{-}^1H)$ were not resolved. Xenon-129 satellite peaks arising from $^3J(^{19}F\text{-}^{129}Xe)$ and $^2J(^1H\text{-}^{129}Xe)$ were not observed in the ^{19}F and ^1H NMR spectra, respectively. This was rationalized by considering the low concentration of $FO_2SN(H)\text{-}Xe^+$ in BrF_5 solvent; integration of the ^{19}F and ^1H NMR

resonances indicated that the ratio $[FO_2SNH_3^+]$: $[FO_2SN(H)\text{-}Xe^+]$ was 8 : 1. The low equilibrium concentration of $FO_2SN(H)\text{-}Xe^+AsF_6^-$ in BrF_5 solvent and its thermal instability indicated that it was not feasible to attempt to isolate $FO_2SN(H)\text{-}Xe^+AsF_6^-$ in the solid state. The $FO_2SN(H)\text{-}Xe^+$ cation is certainly the most unstable xenon(II)-nitrogen bonded species to have been characterized in solution.

(viii) Nature of the Bonding in $CF_3C(OXeF)NH_2^+$, $F_5TeN(H)\text{-}Xe^+$ and $FO_2SN(H)\text{-}Xe^+$, and the Relative Electronegativities of the $F_5TeN(H)$- and $FO_2SN(H)$-Ligand Groups

Previous NMR studies of xenon(II) derivatives containing Xe-F groups bonded to oxygen or fluorine have shown that the ^{19}F and ^{129}Xe NMR parameters can be used to assess the relative covalent characters of the Xe-O, Xe···F bridge and terminal Xe-F bonds. In general, as the ionic character of the Xe-F bond increases, the ^{129}Xe NMR resonance becomes more shielded. This accompanied by decreasing magnitudes of $^1J(^{129}Xe\text{-}^{19}F)$ and deshielded ^{19}F NMR resonances. In compounds of the form R-Xe-F, increased Xe-F bond ionic character results from decreased electronegativity of the ligand, R. Therefore it is possible to qualitatively rank compounds of the form R-Xe-F according to the relative ionic characters of the Xe-R and Xe-F bonds based on the ^{19}F and ^{129}Xe NMR parameters. The Raman data for compounds of the form R-Xe-F complements the bonding information obtained from the NMR parameters. In general, increased ionic character of the terminal Xe-F bond results in a decrease in the Xe-F stretching frequency.

Table 3.2 was used to assess the relative ionic characters of the Xe-O and Xe-F

bonds in $CF_3C(OXeF)NH_2^+$ by comparing the ^{19}F and ^{129}Xe NMR chemical shifts, $^1J(^{129}Xe\text{-}^{19}F)$ and ν(Xe-F) for a series of compounds of the form R-Xe-F. The compounds have been ranked in order of increasing Xe-F bond ionic character; the magnitude of $^1J(^{129}Xe\text{-}^{19}F)$ has been used to rank the species since the ^{19}F and ^{129}Xe chemical shifts for xenon(II) compounds often vary depending on the temperature and solvent, and ν(Xe-F) is often determined from the average of several peaks. The magnitude of $^1J(^{129}Xe\text{-}^{19}F)$ indicates that the Xe-F bond in $CF_3C(OXeF)NH_2^+$ is more ionic than those in the recently characterized xenon-nitrogen bonded adduct cations, $F_3S{\equiv}N\text{-}XeF^+$ and $HC{\equiv}N\text{-}XeF^+$. It follows that the Xe-O bond is more covalent than the xenon-nitrogen bonds of those cations. It is interesting to compare the spectroscopic parameters of $CF_3C(OXeF)NH_2^+$ and $(CF_3)_2S{=}O\text{-}XeF^+$, since these are the only known examples of adduct cations containing xenon-oxygen bonds. Using similar arguments, it is clear that the Xe-O bond in $CF_3C(OXeF)NH_2^+$ is more covalent. This is reasonable when one considers that π-donation from nitrogen to carbon in $CF_3C(OXeF)NH_2^+$ (see resonance Structures 3.3 and 3.4) may result in a formal oxygen hybridization that is intermediate between sp^2 and sp^3. No such resonance contributors can be drawn for $(CF_3)_2S{=}O\text{-}XeF^+$, and the formal oxygen hybridization is sp^2, which is expected to contribute to a higher ligand electronegativity due to the higher valence *s*-character of the oxygen hybrid orbitals.

The ^{129}Xe NMR chemical shifts of $F_5TeN(H)\text{-}Xe^+$ and $FO_2SN(H)\text{-}Xe^+$ are among the most shielded ^{129}Xe NMR resonances for xenon(II) compounds containing xenon-nitrogen bonds (see Table 5.3). Only two other cations containing xenon(II)-

nitrogen bonds have similar ^{129}Xe NMR chemical shifts, namely, $F_4S{=}N\text{-}Xe^+$ and $F_5SN(H)\text{-}Xe^+$. The ^{129}Xe NMR chemical shifts of all other compounds containing xenon(II)-nitrogen bonds are deshielded by 600 to 1000 ppm relative to the xenon(II)-nitrogen bonded cations mentioned above. The absence of Xe-F bonds in these cations is consistent with the highly shielded ^{129}Xe NMR resonances. As mentioned above, increasing Xe-F bond ionic character in R-Xe-F compounds is accompanied by increased shielding of the ^{129}Xe NMR resonances. The cations $F_5TeN(H)\text{-}Xe^+$, $FO_2SN(H)\text{-}Xe^+$, $F_4S{=}N\text{-}Xe^+$ and $F_5SN(H)\text{-}Xe^+$ may be considered as compounds of the form R-Xe-F, where the Xe-F bond is completely ionic. Ionization of the Xe-F bonds therefore results from the relatively low electronegativity of the nitrogen ligands and largely accounts for the highly shielded ^{129}Xe NMR resonances.

Since the ^{129}Xe NMR chemical shifts for xenon(II) compounds are directly related to the covalent character of the xenon-ligand bonds, it is possible to qualitatively estimate the relative electronegativities of the $F_5TeN(H)$- and $FO_2SN(H)$- ligands. The ^{129}Xe NMR chemical shifts of $F_5TeN(H)\text{-}Xe^+$ (-2902 ppm) and $FO_2SN(H)\text{-}Xe^+$ (-2660 ppm) indicate that $FO_2SN(H)$- is more electronegative than $F_5TeN(H)$-. This is in accordance with the greater electronegativity of FO_2SO- than F_5TeO-, as indicated in a ^{129}Xe NMR study of the mixed derivatives XeL_2 and FXeL (L = *cis*-$OIOF_4$, *trans*-$OIOF_4$, -$OTeF_5$, -OSO_2F).[42]

(B) CONCLUSIONS

Significant progress has been made in noble-gas chemistry by preparing and

investigating the spectroscopic properties of xenon(II) compounds containing novel xenon-nitrogen and xenon-oxygen bonds. The first ionization potential of $CF_3C(O)NH_2$ has been used as a measure of its resistence to oxidation by the XeF^+ cation. Bases whose first adiabatic ionization potentials are equal to or greater than the estimated electron affinity of XeF^+ are potentially resistent to oxidation by XeF^+. The successful preparation of $CF_3C(OXeF)NH_2^+AsF_6^-$ at low temperature further illustrates the utility of this method of selecting appropriate bases for preparing adduct cations of XeF^+ which are stable at low temperatures.

The overall significance and impact of this work is summarized below:

(1) The preparation of $CF_3C(OXeF)NH_2^+AsF_6^-$ represents the second example of an adduct cation containing the O-Xe-F linkage, thus contributing to a rare class of compounds.

(2) The use of the two-dimensional heteronuclear (^1H-^{19}F) NOESY technique to determine the assignments for the amido protons in the ^1H NMR spectrum of $CF_3C(OXeF)NH_2^+AsF_6^-$ represents the first use of this well-established technique to facilitate the characterization of a thermally unstable noble-gas compound.

(3) The preparation of $F_5TeNH_3^+AsF_6^-$ and $FO_2SNH_3^+AsF_6^-$ represents the first attempts to protonate the electronegative amines, F_5TeNH_2 and FO_2SNH_2, and the Raman spectroscopic study of these amines and their ammonium salts has improved the vibrational characterization of the previously reported amines, and has probed the effect of protonation on the bonding in the F_5TeN- and FO_2SN-groups.

(4) The preparation of $F_5TeN(H)\text{-}Xe^+AsF_6^-$ and $FO_2SN(H)\text{-}Xe^+AsF_6^-$ has provided two new examples of xenon(II)-nitrogen compounds in which the nitrogen center is sp^3-hybridized. Previous to this work, only one example of this class of compounds was known, namely, $F_5SN(H)\text{-}Xe^+AsF_6^-$.

(5) The nucleophilic fluorination of $F_5TeN(H)\text{-}Xe^+$ to give F_5TeNF_2 represents a mode of decomposition not previously observed for compounds containing xenon(II)-nitrogen bonds.

(6) The preparation of F_5TeNF_2 from the decomposition of $F_5TeN(H)\text{-}Xe^+AsF_6^-$ is significant in that it represents the first report of this difluoramino compound, although the sulfur analog, F_5SNF_2, has been known since 1963.[307] The decomposition of F_5TeNF_2 in AsF_5-acidified HF solvent indicates that the chemical behavior of this compound is similar to other known difluoramino compounds.

(C) DIRECTIONS FOR FURTHER RESEARCH

(i) Preparation of New Amines from the Reaction of $F_5TeN(H)\text{-}Xe^+AsF_6^-$ with Nucleophiles

The decomposition of $F_5TeN(H)\text{-}Xe^+AsF_6^-$ resulted in the formation of F_5TeNF_2 in HF and BrF_5 solvents. The decomposition of $F_5TeN(H)\text{-}Xe^+AsF_6^-$ necessarily increases the AsF_5 concentration in solution, which probably catalyzes the decomposition of F_5TeNF_2 (see Chapter 6). Isolation of the novel monofluoramine, $F_5TeN(H)F$, may be

possible by preparing $F_5TeN(H)\text{-}Xe^+AsF_6^-$ in a non-acidic solvent such as $CH_3C{\equiv}N$ or CH_2Cl_2. Addition of an excess of a fluoride source such as $N(CH_3)_4^+F^-$ may facilitate the nucleophilic fluorination of $F_5TeN(H)\text{-}Xe^+AsF_6^-$ without generation of AsF_5 [equation (9.3)]. In the absence of AsF_5, the ionization of XeF_2 to give the powerful oxidative

$$F_5TeN(H)\text{-}Xe^+AsF_6^- + N(CH_3)_4^+X^- \longrightarrow F_5TeN(H)X + Xe + N(CH_3)_4^+AsF_6^- \quad (X = F, Br, I) \qquad (9.3)$$

fluorinator XeF^+ will not occur, and $F_5TeN(H)F$, which was assumed to be oxidatively fluorinated by XeF^+ in Chapter 6, may be observable by ^{19}F and ^1H NMR spectroscopy. Addition of $(CH_3)_4N^+I^-$ or $(CH_3)_4N^+Br^-$ may also result in nucleophilic attack on the nitrogen center, by analogy with the analogous reactions of these halide sources with $[C_6F_5Xe^+][C_6F_5BF_3^-]$ to give C_6F_5X (X = Br, I) and xenon gas.[95] In this way it may be possible to prepare the hitherto unknown compounds, $F_5TeN(H)Br$ and $F_5TeN(H)I$.

(ii) <u>Preparation of Substituted Hydrazines and/or Diazenes</u>

The decomposition of F_5TeNF_2 in the presence of an excess of $F_5TeNH_3^+AsF_6^-$ in AsF_5-acidified HF solvent (Chapter 6) is postulated to involve the nucleophilic attack of F_5TeNF_2 by $F_5TeNH_3^+$, with AsF_5 acting as a catalyst. While the decomposition of the difluoramino compounds, RNF_2 (R = CF_3, F_5S, Cl, F_5SO, CF_3O), in AsF_5-acidified HF has been investigated,[275] the reaction of these difluoramines with primary amines has

not been investigated. As discussed in Chapter 6, reductive deamination of primary and secondary amines results upon reaction with HNF_2 [equations (6.16) and 6.17)]. It would be interesting to attempt the same reactions with the series of difluoramino compounds mentioned above [equation (9.4)]. In the absence of an oxidative fluorinating agent (e.g., XeF^+), $[R\text{-}NH_2\text{-}N(F)\text{-}R']^+AsF_6^-$ may be isolable. Elimination of HF [equations (9.5) and (9.6)] may result in the diazenes, R-N=N-R'. Although the compounds, R-N=N-H (R =

$$R\text{-}NH_2 + R'\text{-}NF_2 + AsF_5 \longrightarrow [R\text{-}NH_2\text{-}N(F)\text{-}R']^+AsF_6^- \qquad (9.4)$$

(R = alkyl, fluoroalkyl; R' = CF_3, F_5S, Cl, etc.)

$$[R\text{-}NH_2\text{-}N(F)\text{-}R']^+AsF_6^- \rightleftharpoons R\text{-}N(H)\text{-}N(F)\text{-}R' + H^+AsF_6^- \qquad (9.5)$$

$$R\text{-}N(H)\text{-}N(F)\text{-}R' \longrightarrow R\text{-}N{=}N\text{-}R' + HF \qquad (9.6)$$

alkyl), are not stable, decomposing to give R-H and N_2, the electronegative substituents in R-N=N-R' above may stabilize the diazene in the same way that fluorine stabilizes F-N=N-F, whereas H-N=N-H is not an isolable species.

(iii) <u>Further Characterization of $FO_2SN(H)\text{-}Xe^+AsF_6^-$ by ^{129}Xe and ^{15}N NMR</u>

The ^{129}Xe, ^1H and ^{19}F NMR parameters for natural abundance and 99.5% ^{15}N-enriched $FO_2SN(H)\text{-}Xe^+$ have been obtained at low temperatures (see Chapter 8). Only the one-bond scalar coupling $^1J(^{129}Xe\text{-}^{15}N)$ was observed in the ^{129}Xe NMR spectrum

using an external magnetic field strength of 11.7440 T. Similarly, only $^{1}J(^{129}Xe\text{-}^{15}N)$ was observed in the ^{129}Xe NMR spectrum of $F_5TeN(H)\text{-}Xe^+$ at 11.7440 T. Obtaining the ^{129}Xe NMR spectrum at 7.4630 T significantly reduced the linewidths of $F_5TeN(H)\text{-}Xe^+$ resulting from SA broadening (see Chapter 5), and all possible scalar couplings were observed except $^{3}J(^{129}Xe\text{-}^{19}F_{ax.})$, the scalar coupling of ^{129}Xe with the axial fluorine bonded to tellurium(VI). By analogy it may be possible to reduce the line width of the ^{129}Xe NMR resonance for $FO_2SN(H)\text{-}Xe^+$ by performing the NMR experiment at 7.4630 T, enabling the scalar couplings, $^{2}J(^{129}Xe\text{-}^{1}H)$ and $^{3}J(^{129}Xe\text{-}^{19}F)$ to be resolved.

Conditions must be optimized so that the ^{15}N NMR spectrum of $FO_2SN(H)\text{-}Xe^+$ can be obtained. Due to the low concentration of this species in BrF_5 solvent at *ca.* -60 °C and the thermal instability of $FO_2SN(H)\text{-}Xe^+$ upon warming samples above this temperature, it was not possible to obtain a satisfactory ^{15}N NMR spectrum. Since the magnitude of the one-bond coupling, $^{1}J(^{1}H\text{-}^{15}N)$, is known from the ^{1}H NMR spectrum, it should be possible to perform an INEPT experiment with ^{15}N as the observed nucleus; polarization transfer from ^{1}H to ^{15}N will significantly improve the signal-to-noise and the rate of acquisition of the ^{15}N NMR spectrum, thus enabling the ^{15}N NMR spectrum of 99.5% ^{15}N-enriched $FO_2SN(H)\text{-}Xe^+$ to be obtained.

(iv) <u>Proposed Preparation of $F_2P(O)N(H)\text{-}Xe^+AsF_6^-$</u>

The ligand $F_2P(O)O$- was shown to stabilize xenon(II) in the compounds $FXeOP(O)F_2$ and $Xe[OP(O)F_2]_2$ from the reaction of μ-oxo-bis(phosphoryl difluoride), $P_2O_3F_4$, and XeF_2 at 22 °C in $CFCl_3$ solution.[43] By analogy with FO_2SNH_2 and

F_5TeNH_2, the amine, $F_2P(O)NH_2$, may also stabilize xenon(II) in the form of a cation at low temperature [equation (9.7)] in BrF_5 or HF solvents. The compound, $F_2P(O)NH_2$, has

$$F_2P(O)NH_3^+AsF_6^- + XeF_2 \longrightarrow F_2P(O)N(H)\text{-}Xe^+AsF_6^- + 2\ HF \qquad (9.7)$$

been prepared from the reaction of NH_3 with $F_2P(O)\text{-}O\text{-}P(O)F_2$ [equation (9.8)],[308] and it may be possible to protonate $F_2P(O)NH_2$ as well [equation (9.9)] in AsF_5-acidified HF.

$$F_2P(O)\text{-}O\text{-}P(O)F_2 + 2\ NH_3 \longrightarrow NH_4^+PO_2F_2^- + F_2P(O)NH_2 \qquad (9.6)$$

$$F_2P(O)NH_2 + HF + AsF_5 \longrightarrow F_2P(O)NH_3^+AsF_6^- \qquad (9.7)$$

The method of synthesis of $F_2P(O)NH_2$ will allow for a relatively simple synthesis of the ^{15}N-enriched analog, which will probably be required to observe the scalar Xe-N coupling in the ^{129}Xe NMR spectrum.

REFERENCES

1. P. Laszlo and G.J. Schrobilgen, Angew. Chem., Int. Ed. Engl., 27, 479 (1988).
2. H. Moissan, Bull. Soc. Chim. Fr., 13, 976 (1895).
3. M. Berthelot, Ann. Chim. Phys., 11, 15 (1897).
4. R.J. Strutt, Proc. Roy. Soc. London (A), 87, 381 (1913).
5. G. Oddo, Gazz. Chim. Ital., 63, 380 (1933).
6. A. von Antropoff, Z. Angew. Chem., 37, 217 (1924).
7. W. Kossel, Ann. Phys. (Leipzig) Serie 4, 49, 229 (1916).
8. L. Pauling, J. Am. Chem. Soc., 55, 1895 (1933).
9. D.M. Yost and A.L. Kaye, J. Am. Chem. Soc., 55, 3891 (1933).
10. G.N. Lewis, J. Am. Chem. Soc., 38, 762 (1916).
11. N. Bartlett and D.H. Lohmann, Proc. Chem. Soc., 115 (1962).
12. N. Bartlett and D.H. Lohmann, J. Chem. Soc., 5253 (1962).
13. R. Hoppe, W. Dahne, H. Mattauch and K.M. Rodder, Angew. Chem., Int. Ed. Engl., 1, 599 (1962).
14. H.H. Claassen, H. Selig and J.G. Malm, J. Am. Chem. Soc., 84, 3593 (1962).
15. J. Slivnik, B.S. Brčić, B. Volavšek, J. Marsel, V. Vrščaj, A. Šmalc, B. Frlec and A. Zemljič, Croat. Chem. Acta., 34, 253 (1962).
16. D.F. Smith, J. Am. Chem. Soc., 85, 816 (1963).
17. D.F. Smith, Science, 140, 899 (1963).
18. J.L. Huston, J. Phys. Chem., 71, 3339 (1967).
19. R.J. Gillespie and G.J. Schrobilgen, J. Chem. Soc., Chem. Commun., 595 (1977).

20. K. Seppelt and D. Lentz, In "Progress in Inorganic Chemistry", S.J. Lippard, Ed.; John Wiley & Sons, Inc.: New York, 1982, Vol. 29, pp. 167 - 202.

21. H. Selig and J.H. Holloway, In "Topics in Current Chemistry", F.L. Bosche, Ed.; Springer-Verlag: New York, 1984, pp. 33 - 90.

22. H.H. Claassen, "The Noble Gases", D.C. Heath and Company: Boston, 1966.

23. J.H. Holloway, "Noble-Gas Chemistry", Methuen & Co.: Bungay, Suffolk, 1968.

24. "Noble-Gas Compounds", H.H. Hyman, Ed.; The University of Chicago Press: Chicago, 1963.

25. N. Bartlett and F.O. Sladky, In "Comprehensive Inorganic Chemistry", J.C. Bailar, H.J. Emeleus, R. Nyholm and A.F. Trotman-Dickenson, Eds.; Pergamon Press: New York, 1973, Vol. 1, Chapt. 6.

26. G.J. Schrobilgen, In "Synthetic Fluorine Chemistry", G.A. Olah, R.D. Chambers and G.K.S. Prakash, Eds.; John Wiley & Sons, New York, 1992, pp. 1 - 30.

27. R.S. Berry and C.W. Reimann, J. Chem. Phys., 38, 1540 (1963).

28. M. Wechsberg, P.A. Bulliner, F.O. Sladky, R. Mews and N. Bartlett, Inorg. Chem., 11, 3063 (1972).

29. M. Karplus, C.W. Kern and D. Lazdins, J. Chem. Phys., 40, 3738 (1964).

30. J. Berkowitz and J. Chupka, Chem. Phys. Lett., 7, 447 (1970).

31. J.G. Perlow and H. Yoshida, J. Chem. Phys., 49, 1474 (1968).

32. B. Jaselskis and J.P. Warriner, Anal. Chem., 38, 563 (1966).

33. H. Meinert, Z. Chem., 6, 71 (1966).

34. W.F. Howard, and L. Andrews, J. Am. Chem. Soc., 96, 7864 (1974).

35. (a) Nat. Bur. Stand. (U.S.), Tech. Note, No. 270-3 (1968). (b) Nat. Bur. Stand. (U.S.),

Tech. Note, No. 270-4 (1969).

36. L. Pauling, "Nature of the Chemical Bond", Cornell University Press: Ithaca, N.Y.; 3rd Edition, 1960.

37. N. Bartlett, M. Wechsberg, F.O. Sladky, P.A. Bulliner, G.R. Jones and R.D. Burbank, J. Chem. Soc., Chem. Commun., 703 (1969).

38. N. Bartlett, M. Wechsberg, G.R. Jones and R.D. Burbank, Inorg. Chem., 11, 1124 (1972).

39. M. Eisenberg and D.D. DesMarteau, Inorg. Chem., 6, 29 (1970).

40. J.I. Musher, J. Am. Chem. Soc., 90, 7371 (1968).

41. F. Sladky, Monatsh. Chem., 101, 1571 (1970).

42. R.G. Syvret and G.J. Schrobilgen, Inorg. Chem., 28, 1564 (1989).

43. M. Eisenberg and D.D. DesMarteau, Inorg. Chem., 11, 1901 (1972).

44. K. Seppelt, Angew. Chem. Int. Ed. Engl., 11, 723 (1972).

45. K. Seppelt, Chem. Ber., 106, 157 (1973).

46. F.O. Sladky, Angew. Chem., Int. Ed. Engl., 8, 373 (1969).

47. F.O. Sladky, Angew. Chem., Int. Ed. Engl., 8, 523 (1969).

48. F.O. Sladky, Monatsh. Chem., 101, 1559 (1970).

49. D. Lentz and K. Seppelt, Angew. Chem., Int. Ed. Engl., 15, 66 (1976).

50. D. Lentz and K. Seppelt, Angew. Chem., Int. Ed. Engl., 17, 356 (1978).

51. E. Jacob, D. Lentz, K. Seppelt and A. Simon, Z. Anorg. Allg. Chem., 472, 7 (1981).

52. K. Seppelt, Angew. Chem., Int. Ed. Engl., 21, 877 (1982).

53. D. Lentz and K. Seppelt, Angew. Chem., Int. Ed. Engl., 18, 66 (1979).

54. N. Keller and G.J. Schrobilgen, Inorg. Chem., 20, 2118 (1981).

55. F. Sladky, Monatsh. Chem., 101, 1578 (1970).

56. R.D. LeBlond and D.D. DesMarteau, J. Chem. Soc., Chem. Commun., 555 (1974).

57. J.F. Sawyer, G.J. Schrobligen and S.J. Sutherland, Inorg. Chem., 21, 4064 (1982).

58. D.D. DesMarteau, R.D. LeBlond, S.F. Hossain and D. Nöthe, J. Am. Chem. Soc., 103, 7734 (1981).

59. G.A. Schumacher and G.J. Schrobilgen, Inorg. Chem., 22, 2178 (1983).

60. R. Faggiani, D.K. Kennepohl, C.J.L. Lock, and G.J. Schrobilgen, Inorg. Chem., 25, 563 (1986).

61. J. Foropoulos and D.D. DesMarteau, J. Am. Chem. Soc., 104, 4260 (1982).

62. C.A. Coulson, J. Chem. Soc., 1442 (1964).

63. G.C. Pimentel, J. Chem. Phys., 19, 446 (1951).

64. N. Bartlett, M. Gennis, D.D. Gibler, B.K. Morrell and A. Zalkin, Inorg. Chem., 12, 1717 (1973).

65. V.M. McRae, R.D. Peacock and D.R. Russell, J. Chem. Soc., Chem. Commun., 62 (1969).

66. J. Burgess, C.J.W. Fraser, V.M. McRae, R.D. Peacock and D.R. Russell, J. Inorg. Nucl. Chem., Suppl., 183 (1976).

67. F.O. Sladky, P.A. Bulliner and N. Bartlett, J. Chem. Soc. (A), 2179 (1969).

68. R.J. Gillespie and B. Landa, Inorg. Chem., 12, 1383 (1973).

69. R.J. Gillespie and G.J. Schrobilgen, Inorg. Chem., 15, 22 (1976).

70. V.H. Dibeler and S.K. Liston, J. Chem. Phys., 48, 4765 (1968).

71. G.J. Schrobilgen, J. Chem. Soc., Chem. Commun., 1506 (1988).

72. A.A.A. Emara and G.J. Schrobilgen, J. Chem. Soc., Chem. Commun., 1644 (1987).

73. A.A.A. Emara and G.J. Schrobilgen, Inorg. Chem., 31, 1323 (1992).

74. A.A.A. Emara, Ph.D. Thesis, McMaster University, Hamilton, Ontario, Canada (1991).

75. A.A.A. Emara and G.J. Schrobilgen, J. Chem. Soc., Chem. Commun., 257 (1988).

76. C.R. Brundle, M.B. Robin and N.A. Keubler, J. Am. Chem. Soc., 94, 1466 (1972).

77. D.B. Beach, W.L. Jolly, R. Mews and A. Waterfield, Inorg. Chem., 23, 4080 (1984).

78. G.J. Schrobilgen, J. Chem. Soc., Chem. Commun., 863 (1988).

79. N. Bartlett and F.O. Sladky, Chem. Commun., 1046 (1968).

80. R. Minkwitz and G. Nowicki, Inorg. Chem., 30, 4426 (1991).

81. R. Minkwitz, G. Nowicki and H. Preut, Z. Anorg. Allg. Chem., 611, 23 (1992).

82. R. Minkwitz and A. Werner, Z. Naturforsch., 43b, 403 (1988).

83. A.M. Forster and A.J. Downs, J. Chem. Soc., Dalton Trans., 2827 (1984).

84. R. Minkwitz and G. Nowicki, Inorg. Chem., 31, 225 (1992).

85. R. Minkwitz and W. Molsbeck, Z. Anorg. Allg. Chem., 612, 35 (1992).

86. R. Minkwitz and G. Nowicki, Z. Naturforsch., 44b, 1343 (1989).

87. R. Minkwitz and G. Nowicki, Angew. Chem., Int. Ed. Engl., 29, 688 (1990).

88. R. Minkwitz, G. Nowicki, B. Bäck and W. Sawodny, Inorg. Chem., 32, 787 (1993).

89. H.M. Rosenstock, K. Draxl, B.W. Steiner and J.T. Herron, J. Phys. Ref. Data, Suppl. No. 1, 6 (1977).

90. R. Minkwitz and W. Molsbeck, Z. Anorg. Allg. Chem., 607, 175 (1992).

91. L.J. Turbini, R.E. Aikman and R.J. Lagow, J. Am. Chem. Soc., 101, 5833 (1979).

92. D. Holtz and J.L. Beauchamp, Science, 173, 1238 (1971).

93. J.K. Hovey and T.B. McMahon, J. Am. Chem. Soc., 108, 528 (1986).

94. Reference (25), p. 254.

95. H.J. Frohn and S. Jakobs, J. Chem. Soc. Chem. Commun., 625 (1989).

96. H.J. Frohn, S. Jakobs, and C. Rossbach, Eur. J. Solid State Inorg. Chem., 29, 729 (1992).

97. H.J. Frohn and A. Klose, J. Fluorine Chem., 64, 201 (1993).

98. H. Butler, D. Naumann, and W. Tyrra, Eur. J. Solid State Inorg. Chem., 29, 739 (1992).

99. D. Naumann and W. Tyrra, J. Chem. Soc., Chem. Commun., 47 (1989).

100. H.J. Frohn, S. Jakobs and G. Henkel, Angew. Chem. Int. Ed. Engl., 28, 1506 (1989).

101. V.V. Zhdankin, P. Stang, and N.S. Zefirov, J. Chem. Soc., Chem. Commun., 578 (1992).

102. Reference (25), p. 226.

103. G.J. Schrobilgen, In "NMR and the Periodic Table", R.K. Harris and B.E. Mann, Eds.; Academic Press: London, 1978, Chapter 14, pp. 439 - 475.

104. C.J. Jameson, In "Multinuclear NMR", J. Mason, Ed.; Plenum Press: New York, 1987, Chapter 18, pp. 463 - 475.

105. J.E. Huheey, In "Inorganic Chemistry, Principles of Structure and Reactivity", Harper & Row: New York, 1983, 3rd Edition, Chapter 3.

106. U.H. Mölder, I.A. Koppel, R.J. Pikver and J.J. Tapfer, Organic Reactivity, 25, 255 (1988).

107. T.R.G. Syvret, Ph.D. Thesis, McMaster University, Hamilto ntario, Canada (1987).

108. G.J. Schrobilgen, J.H. Holloway, P. Granger and C. Brevard, Inorg. Chem., 17, 980 (1978).

109. K.O. Christe and W.W. Wilson, J. Fluorine Chem., 47, 117 (1990).

110. H.P.A. Mercier, J.C.P. Sanders and G.J. Schrobilgen, J. Am. Chem. Soc., 116, 2921 (1994).

111. R.J. Gillespie, A. Netzer and G.J. Schrobilgen, Inorg. Chem., 13, 1455 (1974).

112. H.P.A. Mercier, J.C.P. Sanders, G.J. Schrobilgen and S.S. Tsai, Inorg. Chem., 32, 386 (1993).

113. C.J. Hoffman, Inorg. Synth., 4, 150 (1953).

114. K. Seppelt, Inorg. Synth., 20, 33 (1980).

115. F. Sladky, Inorg. Synth., 24, 33 (1986).

116. H. Kropshofer, O. Leitzke, P. Peringer and F. Sladky, Chem. Ber., 114, 2644 (1981).

117. M. J. Collins and G.J. Schrobilgen, Inorg. Chem., 24, 2608 (1985).

118. L. Chun-Hsu, H. Selig, M. Rabinowitz, I. Agranat and S. Sarig, Inorg. Nucl. Chem. Lett., 11, 601 (1975).

119. V. Munch and H. Selig, J. Fluorine Chem., 15, 253 (1980).

120. Obtained from K.O. Christe, Rocketdyne Int., Canoga Park, California.

121. J.H. Noggle and J.D. Baldeschweiler, J. Chem. Phys., 37, 182 (1962).

122. P.W. Schenk, In "Handbook of Preparative Inorganic Chemistry", G. Brauer, Ed.; Academic Press: New York, 1963, Vol. 1, 2nd Ed., pp. 451 - 463.

123. R.O. Sauer and R.H. Hasek, J. Am. Chem. Soc., 66, 1706 (1944).

124. A.H. Cowley and J.R. Schweiger, J. Am. Chem. Soc., 95, 4179 (1973).

125. H. Hartl, P. Huppmann, D. Lentz and K. Seppelt, Inorg. Chem., 22, 2183 (1983).

126. M. Schmidt and W. Siebert, In "Comprehensive Inorganic Chemistry", J.C. Bailar, Jr., H.J. Emeléus, R. Nyholm and A.F. Trotman-Dickenson, Eds.; Pergamon Press: New York, Volume 2, Chapter 23, 1973.

127. R.J. Gillespie and R.A. Rothenbury, Can. J. Chem., 42, 416 (1964).

128. R.J. Gillespie and E.A. Robinson, Can. J. Chem., 39, 2179 (1961).

129. R. Appel and G. Eisenhauser, Z. Anorg. Allg. Chem., 310, 90 (1961).

130. A. Semmoud and P. Vast, Rev. Chim. Min., 16, 80 (1979).

131. F.F. Bentley, L.D. Smithson and A.L. Rozek, "Infrared Spectra and Characteristic

Frequencies", John Wiley & Sons: New York, 1968, p. 337.

132. "Sadtler Standard Spectra", Stadtler Research Laboratories: Philadelphia, 1969, p. 1333.

133. R. Appel and W. Senkpiel, Angew. Chem., 70, 572 (1958).

134. H. Jonas and D. Voigt, Angew. Chem., 70, 572 (1958).

135. R.B. Bohn and L. Andrews, J. Phys. Chem., 93, 5684 (1989).

136. C. Yu and G.C. Levy, J. Am. Chem. Soc., 106, 6533 (1984).

137. D.P. Strommen and K. Nakamoto, "Laboratory Raman Spectroscopy", John Wiley & Sons: New York, 1984.

138. V.H. Dibeler and S.K. Liston, J. Chem. Phys., 48, 4765 (1968).

139. B. Cremer-Lober, H. Butler, D. Naumann and W. Tyrra, Z. Anorg. Allg. Chem., 607, 34 (1992).

140. M. Wechsberg, P.A. Bulliner, F.O. Sladky, R. Mews and N. Bartlett, Inorg. Chem., 11, 3063 (1972).

141. K. Seppelt and H.H. Rupp, Z. Anorg. Allg. Chem., 409, 338 (1974).

142. K. Seppelt and D. Nothe, Inorg. Chem., 12, 2727 (1973).

143. W.E. Stewart, and T.H. Siddall, III, Chem. Rev., 70, 517 (1970).

144. T. Birchall and R.J. Gillespie, Can. J. Chem., 41, 2642 (1963).

145. R.J. Gillespie and T. Birchall, Can. J. Chem., 41, 148 (1963).

146. G. Fraenkel, and C. Franconi, J. Am. Chem. Soc., 82, 4478 (1960).

147. C.L. Perrin and E.R. Johnston, Can. J. Chem., 59, 2527 (1981).

148. M. Liler, J. Chem. Soc., Perkin II, 71 (1974).

149. G.A. Olah, J. Nishimura and P. Kreienbühl, J. Am. Chem. Soc., 95, 7672 (1973).

150. H. Akiyama, M. Tachikawa, T. Furuya and K. Ouchi, J. Chem. Soc., Perkin II, 771

(1973).

151. J.S. Hartman and G.J. Schrobilgen, Can. J. Chem., 51, 99 (1972).

152. J.S. Hartman and R.R. Yetman, Can. J. Chem., 54, 1130 (1976).

153. Hindered rotation was observed in the ^1H NMR spectra of O-protonated carbamyl fluoride, $FC(OH)NH_2^+$, in HSO_3F/SO_2 solution, resulting in two unassigned resonances for the chemically inequivalent NH protons at $\delta(^1H) \approx 8.5$ ppm [reference (149)]. The ^1H NMR spectrum of ^{15}N-enriched O-protonated benzamide in HSO_3F or 100% H_2SO_4 solvent shows two peaks of equal intensity at 8.36 and 7.94 ppm, at temperatures below 65 °C. The high-frequency peak was assigned to the proton trans to the protonated carbonyl group [reference (148)]. Birchall and Gillespie [reference (145)] reported proton-on-nitrogen resonances at 8.36 and 8.24 ppm for O-protonated acetamide in HSO_3F solvent at -80 °C; the high-frequency resonance was assigned to the proton cis to the protonated carbonyl group. Using the nOe difference technique, the proton cis to the carbonyl group was assigned to the high-frequency ^1H NMR resonance in the structurally related protonated trichloroacetimidate cation, $CCl_3C(OCH_3)NH_2^+$, in 95% H_2SO_4 solution [reference (147)].

154. D. Neuhaus and M.P. Williamson, In "The Nuclear Overhauser Effect in Structural and Conformational Analysis"; VCH Publishers, Inc.: New York, 1989.

155. H. Akiyama, F. Yamauchi and K. Ouchi, J. Chem. Soc. (B), 1014 (1971).

156. H.-O. Kalinowski, S. Berger and S. Braun, "Carbon-13 NMR Spectroscopy"; John Wiley and Sons: New York, 1988; pp. 1[illegible]00.

157. The errors associated with integration of NMR resonances are estimated to be ± 10%.

158. R.J. Gillespie and B. Landa, Inorg. Chem., 12, 1383 (1973).

159. C. Naulin and R. Bougon, J. Chem. Phys., 64, 4155 (1976).

160. P.J. Krueger and D.W. Smith, Can. J. Chem., 45, 1611 (1967).

161. E.K. Murthy and G.R. Rao, J. Raman Spectrosc., 19, 359 (1988).

162. W. Kutzelnigg and R. Mecke, Spectrochim. Acta, 18, 549 (1962).

163. W. Gerrard, M.F. Lappert, H. Pyszora and J.W. Wallis, J. Chem. Soc., 2144 (1960).

164. R.B. Bohn and L. Andrews, J Phys. Chem., 93, 5684 (1989).

165. D. Cook, Can. J. Chem., 42, 2721 (1964).

166. R. Merenyi, In "Advances in Organic Chemistry"; H. Böhme and G.E. Viehe, Eds.; John Wiley and Sons: New York, 1976; Vol. 9, pp. 23-105.

167. D. Cook, Can. J. Chem., 40, 2362 (1962).

168. R.L. Jones, J. Mol. Spectrosc., 11, 411 (1963).

169. W. Maringgele and A. Meller, Chem. Ber., 112, 1595 (1979).

170. K. Nakamoto, "Infrared and Raman Spectra of Inorganic and Coordination Compounds"; John Wiley and Sons: New York, 1986, 4th ed.; pp. 147-148.

171. K.O. Christe, C.J. Schack and R.D. Wilson, Inorg. Chem., 2224, 14 (1975).

172. K.O. Christe, Inorg. Chem., 14, 2230 (1975).

173. K.O. Christe, Inorg. Chem., 14, 2821 (1975).

174. J. Terpiński, In "Laser Raman Spectroscopy - Analytical Applications"; H. Barańska, A. Labudzińska and J. Terpiński, Eds.; John Wiley and Sons: New York, 1987; p. 81.

175. (a) ν_{sym}(Xe-F) = 495 cm^{-1} in the Raman spectrum measured at -165 °C; this work. (b) D.F. Smith, In "Noble Gas Compounds"; H.H. Hyman, Ed.; University of Chicago Press: Chicago and London, 1963; p. 295. (c) Ibid., J.J. Turner and G.C. Pimentel, p. 101.

176. A. Zalkin, D.L. Ward, R.N. Biagioni, D.H. Templeton and N. Bartlett, Inorg. Chem., 17, 1318 (1978).

177. B. Žemva, A. Jesih, D.H. Templeton, A. Zalkin, A.K. Cheetham and N. Bartlett, J. Am. Chem. Soc., 109, 7420 (1987).

178. Examples of molecular adducts containing symmetric XeF_2 ($D_{\infty h}$ point symmetry) include $XeF_2 \cdot IF_5$ [G.R. Jones *et al.*, Inorg. Chem., 9, 2264 (1970)], $XeF_2 \cdot XeOF_4$ [N. Bartlett and M. Wechsberg, Z. Anorg. Allg. Chem., 385, 5 (1971)], $XeF_2 \cdot 2XeF_6 \cdot 2AsF_5$ [reference (177)], $XeF_2 \cdot XeF_4$ [J.H. Burns, *et al.*, Acta Cryst., 18, 11 (1965)] and $Ag(XeF_2)_2AsF_6$ [R. Hagiwara, *et al.*, Eur. J. Solid State Inorg. Chem., 28, 855 (1991)].

The Raman spectra of these adducts are essentially reproduced by summing the spectra of the starting materials and are consistent with negligible changes in the bonding of the constituent molecules in the adducts. The adducts $XeF_2 \cdot 2XeF_6 \cdot 2AsF_5$ and $Ag(XeF_2)_2AsF_6$ are the only previously reported examples of symmetrical XeF_2 coordinated to cations. The Raman spectrum of the former shows a prominent peak at 498 cm^{-1} that is assigned to ν_{sym}(Xe-F) for XeF_2 in the adduct, which is not significantly different from that observed for crystalline XeF_2, at 496 cm^{-1} [reference (175b)]. The bands attributed to ν_{sym}(Xe-F) in $Ag(XeF_2)_2AsF_6$ occur at 501 and 508 cm^{-1}, indicating an average increase of 8 cm^{-1} relative to crystalline XeF_2. The crystal structures of $XeF_2 \cdot 2XeF_6 \cdot 2AsF_5$ and $Ag(XeF_2)_2AsF_6$ indicate that the fluorine ligands of XeF_2 are weakly coordinated to the cations (central Xe atom of XeF_5^+ and Ag^+, respectively), and the Xe-F bond lengths are 2.01(2) and 1.979(3) Å that are not significantly different from the Xe-F bond length in crystalline XeF_2 (2.00(1) Å) [H.A. Levy and P.A. Agron, J. Am. Chem. Soc., 85, 241 (1963)]. This is consistent with little alteration of the bonding of XeF_2 in these adducts; the intermolecular bonding in these adducts may be attributed primarily to the electrostatic interaction of the cation and the fluorine atoms of XeF_2, which contain partial negative charge due to a high degree of Xe-F bond polarity [also see reference (25), p. 259].

179. Reference (25), pp. 223 - 228.

180. J.C.P. Sanders and G.J. Schrobilgen, unpublished work.

181. T. Birchall, R.D. Myers, H. deWaard and G.J. Schrobilgen, Inorg. Chem., 21, 1068 (1982).

182. R.R. Ernst, G. Bodenhausen and A. Wokaun, In "Principles of Nuclear Magnetic Resonance in One and Two Dimensions"; Clarendon Press: Oxford, 1987; p. 288.

183. A. Engelbrecht, F. Sladky, Adv. Inorg. Chem. Radiochem., 24, 189 (1981).

184. K. Seppelt, Acc. Chem. Res., 12, 211 (1979).

185. F.B. Dudley, G.H. Cady, and D.F. Eggers, Jr., J. Am. Chem. Soc., 78, 1553 (1956).

186. G. Mitra and G.H. Cady, J. Am. Chem. Soc., 81, 2646 (1959).

187. R.B. Harvey and S.H. Bauer, J. Am. Chem. Soc., 76, 859 (1954).

188. A. Engelbrecht, W. Loreck and W. Nehoda, Z. Anorg. Allg. Chem., 360, 88 (1968).

189. A. Engelbrecht, and F. Sladky, Angew. Chem. Int. Ed. Engl., 3, 383 (1964).

190. A. Engelbrecht and B. Stoll, Z. Anorg. Allg. Chem., 292 20 (1957).

191. K. Seppelt, Angew. Chem. Int. Ed. Engl., 11, 630 (1972).

192. K. Seppelt, Angew. Chem. Int. Ed. Engl., 44, 15, (1976).

193. K. Seppelt, Z. Anorg. Allg. Chem., 428, 35 (1977).

194. P. Huppmann, J. Labischinski, D. Lentz, H. Pritzkow and K. Seppelt, Z. Anorg. Allg. Chem., 487, 7 (1982).

195. K. Seppelt, Chem. Ber., 109, 1046 (1976)

196. L.K. Templeton, D.H. Templeton, N. Bartlett and K. Seppelt, Inorg. Chem., 15, 2720 (1976).

197. J.C.P. Sanders and G.J. Schrobilgen, J. Chem. Soc., Chem. Commun., 1576 (1989).

198. P. Huppmann, D. Lentz and K. Seppelt, Z. Anorg. Allg. Chem., 472, 26 (1981).

199. F. Sladky and H. Kropshofer, Inorg. Nucl. Chem. Lett., 8, 195 (1972).

200. W. Porcham and A. Engelbrecht, Monatsh. Chem., 102, 333 (1971).

201. A. Engelbrecht and A. Sladky, Inorg. Nucl. Chem. Lett., 1, 15 (1965).

202. P.K. Miller, K.D. Abney, A.K. Rappé, O.P. Anderson and S.H. Strauss, Inorg. Chem., 27, 2255 (1988).

203. S.H. Strauss, K.D. Abney and O.P. Anderson, Inorg. Chem., 25, 2806 (1986).

204. K. Seppelt, Chem. Ber., 105, 243 (1972).

205. K.O. Christe, D.A. Dixon, J.C.P. Sanders, G.J. Schrobilgen and W.W. Wilson, Inorg. Chem., 32, 4089 (1993).

206. E. Mayer and F. Sladky, Inorg. Chem., 14, 589 (1975).

207. K. Seppelt, Z. Anorg. Allg. Chem., 406, 287 (1974).

208. K. Seppelt, Chem. Ber., 106, 1920 (1973).

209. J.S. Thrasher and K. Seppelt, Z. Anorg. Allg. Chem., 529, 85 (1985).

210. K.O. Christe, C.J. Schack, D. Pilipovich, E.C. Curtis and W. Sawodny, Inorg. Chem., 12, 620 (1973).

211. O. Linquist and M.C. Lehman, Acta. Chem. Scand., 27, 85 (1973).

212. M. Lustig and J.K. Ruff, Inorg. Chem., 6, 2115 (1967).

213. W.C. Smith and V.A. Englehardt, J. Am. Chem. Soc., 82, 3838 (1960).

214. K. Seppelt, Z. Anorg. Allg. Chem., 399, 65 (1973).

215. K. Seppelt, Z. Anorg. Allg. Chem., 399, 87 (1973).

216. H. Oberhammer and K. Seppelt, Inorg,. Chem., 17, 1435 (1978).

217. A.E. Reed and P. Schleyer, J. Am. Chem. Soc., 112, 1434 (1990).

218. J. Mason, Adv. Inorg. Chem. Radiochem., 18, 197 (1976).

219. J. Mason, Adv. Inorg. Chem. Radiochem., 22, 199 (1979).

220. H. Bürger, Z. Anorg. Allg. Chem., 360, 97 (1968).

221. O. Ruff and W. Willenburg, Chem. Ber., 73, 724 (1940).

222. D.A. Barr, and R.N. Hazeldine, J. Chem. Soc., 2533 (1955).

223. J.A. Young, S.N. Tsoukalas and R.D. Dresdner, J. Am. Chem. Soc., 80, 3604 (1958).

224. R.E. Banks, W.M. Cheng, and R.N. Hazeldine, J. Chem. Soc., 2485 (1964).

225. C.W. Tullock, D.D. Coffman and E.L. Muetterties, J. Am. Chem. Soc., 86, 359 (1964).

226. A.F. Clifford and L.C. Duncan, Inorg. Chem., 5, 692 (1966).

227. A.F. Clifford and G.R. Zeilenga, Inorg. Chem., 8, 1789 (1969).

228. G.W. Fraser, R.D. Peacock and P.M. Watkins, Chem. Commun., 1248 (1967).

229. G.W. Fraser, R.D. Peacock and P.M. Watkins, J. Chem. Soc. (A), 1125 (1971).

230. K. Seppelt, Inorg. Chem., 12, 2837 (1973).

231. R.J. Gillespie and J. Liang, J. Am. Chem. Soc., 110, 6053 (1988).

232. M. Tsuboi, Spectrochim. Acta, 16, 505, (1960).

233. C.J. Schack, W.W. Wilson, and K.O. Christe, Inorg. Chem., 22, 18 (1983).

234. W.V.F. Brooks, M. Eshaque, L. Clement, J. Passmore, Can. J. Chem., 54, 817, (1976).

235. E.B. Wilson, Jr., J.C. Decius and P.C. Cross, "Molecular Vibrations", Dover Publications: New York, 1955, pp. 333 - 340.

236. D.F. Smith and G.M. Begun, J. Chem. Phys., 43, 2001 (1965).

237. T. Ottersen, Acta. Chem. Scand., 29A, 939 (1975).

238. P. Schleyer and A.J. Kos, Tetrahedron, 39, 1141, (1983).

239. R. Minkwitz and R. Naß, Z. Naturforsch., 43b, 1478, (1988).

240. G. Binsch, J.B. Lambert, B.W. Roberts and J.D. Roberts, J. Am. Chem. Soc., 86, 5564 (1964).

241. A.J.R. Bourn and E.W. Randall, Mol. Phys., 8, 567 (1964).

242. J.A. Pople and D.P. Santry, Mol. Phys., 8, 1 (1964).

243. G.A. Olah and T.E. Kiovsky, J. Am. Chem. Soc., 90, 4666 (1968).

244. J. Mason and K.O. Christe, Inorg. Chem., 22, 1849 (1983).

245. P. Lazzeretti, E. Rossi, F. Taddei and R. Zanasi, J. Chem. Phys., 77, 408 (1982).

246. L. Burnett and A.H. Zeltmann, J. Chem. Phys., 56, 4695 (1972).

247. G. Balimann, P.S. Pregosin, J. Magn. Res., 26, 283 (1977).

248. W. Tötsch, P. Peringer and F. Sladky, J. Chem. Soc., Chem. Commun., 16, 841 (1981).

249. L.J. Bellamy, "Infrared Spectra of Complex Molecules", John Wiley & Sons: New York, 1954, p. 202.

250. Reference (249), p. 213.

251. G.A. Webb, In "NMR and the Periodic Table", R.K. Harris and B.E. Mann, Eds.; Academic Press: New York, 1978, Chapter 3, pp. 49 - 84.

252. J.K.M. Sanders and B.K. Hunter, "Modern NMR Spectroscopy, A Guide for Chemists"; Oxford University Press: 1990, Chapt. 3, pp. 81 - 84.

253. D. Naumann, H. Butler, R. Gnann and W. Tyrra, Inorg. Chem., 32, 861 (1993).

254. R.K. Harris, "Nuclear Magnetic Resonance Spectroscopy", John Wiley & Sons: New York, 1991, p. 236.

255. G.J. Schrobilgen, unpublished results.

256. H.E. Dubb, R.C. Greenough and E.C. Curtis, J. Chem. Phys., 38, 461 (1963).

257. G.E. Moore and R.M. Badger, J. Am. Chem. Soc., 74, 6076 (1952).

258. Reference (249), p. 215 - 216.

259. J.H.B. George, J.A. Rolfe and L.A. Woodward, Trans. Faraday Soc., 49, 375 (1953).

260. (a) C.J. Jameson, In "Multinuclear NMR", J. Mason, Ed.; PLenum Press: New York, 1987, Chapter 4, pp. 116-118. (b) C.J. Jameson and H.S. Gutowsky, J. Chem. Phys, 51, 2790 (1969). (c) R.W. Kunz, Helv. Chim. Acta, 63, 2054 (1980). (d) J. Mason, Polyhedron, 8, 1657 (1989). (e) B. Wrackmeyer and K. Horschler, In "Annual Reports on NMR Spectroscopy", G.A. Webb, Ed.; Academic Press, London, 1989; Vol. 22, p.261.

261. H.A. Bent, Chem. Rev., 61, 276 (1961).

262. H.J. Frohn, A. Klose and V.V. Bardin, J. Fluorine Chem., 64, 201 (1993).

263. H.J. Frohn, S. Jakobs and C. Rossbach, J. Fluorine Chem., 54, 8 (1991).

264. H.J. Frohn and S. Jakobs, J. Fluorine Chem., 45, 11 (1989).

265. N. Bartlett, B.G. DeBoer, F.J. Hollander, F.O. Sladky, D.H. Templeton and A. Zalkin, Inorg. Chem., 13, 780 (1974).

266. E.C. Stump, Jr., C.D. Padjett and W.S. Brey, Jr., Inorg. Chem., 2, 648 (1963).

267. C.B. Colburn, F.A. Johnson and C. Haney, J. Chem. Phys., 43, 4526 (1965).

268. R.J. Harris and K.J. Packer, J. Chem. Soc., 4736 (1961).

269. A. Saika and C.P. Slichter, J. Chem. Phys., 22, 26 (1954).

270. J.A. Pople, Mol. Phys., 7, 301 (1964).

271. A.M. Qureshi, J.A. Ripmeester and F. Aubke, Can. J. Chem., 47, 4247 (1969).

272. (a) D. Moy and A.R. Young, II, J. Am. Chem. Soc., 87, 1889 (1965). (b) K.O. Christe and D.A. Dixon, J. Am. Chem. Soc., 114, 2978 (1992).

273. K.O. Christe, R.D. Wilson, W.W. Wilson, R. Bau, S. Sukumar and D.A. Dixon, J. Am. Chem. Soc., 113, 3795 (1991).

274. W. Witanowski, L. Stefaniak and G.A. Webb, In "Annual Reports on NMR Spectroscopy", G.A. Webb, Ed.; Academic Press: New York, 1977, p. 211.

275. K.O. Christe, W.W. Wilson, C.J. Schack and R.D. Wilson, Inorg. Chem., 24, 303 (1985).

276. "Gmelin Handbook of Inorganic Chemistry, Fluorine"; Springer-Verlag: Berlin, 1986, Volume 4, Supplement F, pp. 385 - 403.

277. D.L. Klopotek and B.G. Hobrock, Inorg. Chem., 6, 1750 (1967).

278. A.V. Pankrotov and O.M. Sokolov, Russ. J. Inorg. Chem., 11, 943 (1966).

279. D.L. Klopotek, B.G. Hobrock, P. Kovacic and M.B. Jones, J. Org. Chem., 45, 1665 (1980).

280. C.L. Bumgardner, K.J. Martin, J.P. Freeman, J. Am. Chem. Soc., 85, 97 (1963).

281. R.S. Atkinson, In "Azides and Nitrenes, Reactivity and Utility", E.F. Scriven, Ed.; Academic Press: Orlando, 1984, pp. 247 - 295.

282. C.L. Bumgardner and J.F. Liebman, J. Fluorine Chem., 65, 7 (1993).

283. D.D. DesMarteau, W.Y. Lam, B.A. O'Brien and S. Chang, J. Fluorine Chem., 25, 387 (1984).

284. M. Becke-Goehring, In "Advances in Inorganic Chemistry and Radiochemistry", H.J. Emeléus and A.G. Sharpe, Eds., Academic Press: New York, Vol. 2, 1960, p.159.

285. G.A. Jeffrey and H.P. Stadler, J. Chem. Soc., 1467 (1951).

286. J. Brunvoll, M. Kolonits, C. Bliefert, K. Seppelt and I. Hargittai, J. Mol. Struct., 78, 307 (1982).

287. J.W. Bats, P. Coppens and T.F. Koetzle, Acta. Cryst. B33, 37 (1977).

288. D.J.W. Cruickshank, J. Chem. Soc., 5486 (1961).

289. C.H. Dungan and J.R. van Wazer, "Compilation of Reported F^{19} NMR Chemical Shifts", John Wiley & Sons: New York, 1970.

290. J.C.P. Sanders and G.J. Schrobilgen, In "A Methodological Approach to Multinuclear Magnetic Resonance in Liquids and Solids - Chemical Applications"; P. Granger and R.K. Harris. Eds., Kluwer Academic Publishers: Dordrecht, 1990, pp. 157 - 186.

291. A. Kennedy and C.B. Colburn, J. Am. Chem. Soc., 81, 2906 (1959).

292. T.T. Crow and R.T. Lagemann, Spectrochim. Acta, 12, 143 (1958).

293. K. Nakamoto, "Infrared and Raman Spectra of Inorganic and Coordination Compounds", John Wiley & Sons: New York, 1978, 3rd Ed., 1978, p. 126.

294. R. Minkwitz, A. Liedtke and R. Naß, J. Fluorine Chem., 35, 307 (1987).

295. R. Minkwitz and R. Naß, Z. Naturforsch., 37b, 1558 (1982).

296. A.J. Barnes, J. Chem. Soc., Faraday Trans. II 69, 738 (1973).

297. G.M. Begun and A.C. Rutenberg, Inorg. Chem., 6, 2212 (1967).

298. A.M. Qureshi and F. Aubke, Can. J. Chem., 48, 3117 (1970).

299. Reference (293), p. 145.

300. Reference (293), p. 144.

301. R.J. Gillespie and E.A. Robinson, Can. J. Chem., 41, 2074 (1963).

302. D.R. Lide and R.M. Fristrom, J. Chem. Phys., 26, 734 (1957).

303. R. Prietzold, K. Dosteil and A. Ruzieka, Z. Anorg. Allg. Chem., 348, 1 (1966).

304. R.A. Abramovitch and R. Jeyaraman, In "Azides and Nitrenes, Reactivity and Utility", E.F.V. Scriven, Ed.; Academic Press, 1984, Chapter 6, p.297.

305. L. Pauling, "Nature of the Chemical Bond", 3rd Edition; Cornell University Press: Ithaca, New York, 1960, p.255.

306. G.A. Olah, G.K.S. Prakash and J. Sommer, In "Superacids", John Wiley & Sons: New York, 1985, p. 35.

307. A.L. Logothetis, G.N. Sausen and R.J. Schozda, Inorg. Chem., 2, 173, (1963).

308. S. Kongpricha and W.C. Preusse, Inorg. Chem., 6, 1915 (1967).